A speciation study of various Pt(II) and Pt(IV) complexes including hexaaquaplatinum(IV) by means of ^{195}Pt NMR spectroscopy, in support of a preliminary study of the oxidation mechanism of various Pt(II) complexes.

By

Pieter Murray

Thesis presented for the degree of Doctor of Philosophy

at the

University of Stellenbosch

Promoter: Professor Klaus R. Koch

F gego dgt'2012

Declaration

By submitting this thesis electronically, I declare that the entirety of the work contained herein is my own, original work, that I am the owner of the copyright thereof (unless to the extent explicitly otherwise stated) and that I have not previously in its entirety or in part submitted it for obtaining any qualification.

Date: F gego dgt '2012

ii

"Our greatest weakness lies in giving up. The most certain way to succeed is always to try just one more time." – Thomas A. Edison

Acknowledgements

I would sincerely like to thank:

- My supervisor, prof. Klaus Koch, for his believe in me, and the *carte blanche* and freedom to often pursue whatever experiment I thought necessary, making it a truly exciting and enriching study. I thank him for his enthusiasm, encouragement and for being a true mentor not only academically but also in other areas of life.

- Prof. Rudi van Eldik for hosting and supervising me in Erlangen, Germany to carry out the kinetic experiments in this study. It was special being able to discuss intimate aspects of the oxidation mechanism in the middle of Germany in Afrikaans! I thank him for his contribution to make it a fruitful and unforgettable experience.

- Dr. Wilhelmus Gerber, always willing to assist and listen to my newest hypothesis, although often shot down diplomatically!

- Dr. Jurjen Kramer, especially during the early stages of this study, for his guidance and for showing me "the way" in the lab.

- AngloAmerican, National Research Foundation, Deutscher Akademischer Austausch Dienst and the University of Stellenbosch for funding.

- The staff from the NMR lab, Jean McKenzie, Elsa Malherbe and Jaco Brand.

- The technical staff and the Analytical Chemistry department, Shafiek Mohammed, Deidre Williams, Lisinda Bailey and Roger Lawrence.

- The PGM group for their entertainment and *comradery*. I would especially like to thank Eugene "Terblanche" Lakay and Izak "Langarm" Kotze for being true friends from whom I have learnt much.

- My family and friends who has always supported and encouraged me throughout my studies.

- My wife Carlien Murray, for believing in me always, patiently supporting me in all my endeavours and for loving me unconditionally. I am truly fortunate to have her in my life.

- Jesus Christ, in whom I have salvation and find meaning for life.

Conference Proceedings

RSC SACI-Inorganic Conference 2007, Club Mykonos, Western Cape, South Africa.
Poster presentation and best poster prize

ICCC (International Conference on Coordination Chemistry) **2008,** Jerusalem, Israel.
Poster presentation

SACI Young Chemists Mini Symposium 2008, Stellenbosch, South Africa.
Oral presentation

COS (Cape Organometallic Symposium) **2008**, Cape Town, South Africa.
Oral presentation

RSC 39th SACI Convention 2008, Stellenbosch, South Africa
Poster presentation and best poster prize (this work was presented in part in an oral presentation by Klaus R. Koch)

RSC SACI Inorganic Conference 2009, Bloemfontein, South Africa.
Poster presentation

WWMR (World Wide Magnetic Resonance) Conference **2010**: joint **EUROMAR** (European Magnetic Resonance Meeting) and 17th **ISMAR** (International Society of Magnetic Resonance) conferences **2010**, Florance, Italy.
Poster presentation (this work was presented in part in an oral presentation by Klaus R. Koch).

RSC 40th SACI Convention 2011, WITS University, Johannnesburg, South Africa.

Publications

- ^{195}Pt *NMR isotopologue and isotopomer distributions of* $[PtCl_n(H_2O)_{6-n}]^{4-n}$ *(n = 6-4) species as a fingerprint for unambiguous assignment of isotopic stereoisomers*

  W. J. Gerber, P. Murray and K. R. Koch, *Dalton Transactions*, 2008, 4113-4117.

- *A* ^{195}Pt *NMR study of the oxidation of* $[PtCl_4]^{2-}$ *with chlorate, bromate, and hydrogen peroxide in acidic aqueous solution.*

  Pieter Murray; Klaus R. Koch, *Journal of Coordination Chemistry*, 2010, 63, 2561-2577.

Manuscripts are being prepared for publication under the titles:

- ^{195}Pt *NMR isotopologue and isotopomer distributions of* $[PtX_nY_{6-n}]^{4-n}$ *(n = 2–6, X =* $^{35}Cl/^{37}Cl$*, Y =* $H_2^{16}O/H_2^{18}O$*) complexes.*

  P. Murray, W. J. Gerber and K. R. Koch

- *Oxidation of* $[PtCl_4]^{2-}$ *with hydrogen peroxide in hydrochloric acid: interplay between reaction orders.*

  P. Murray, K. R. Koch and R. van Eldik

Abstract

A ^{195}Pt NMR spectroscopy study of the speciation of Pt(II)-aqua-bromido-chlorido complexes, after chloride/bromide anation of $[Pt(H_2O)_4]^{2+}$ or aquation of a $[PtCl_4]^{2-}$/$[PtBr_4]^{2-}$ mixture was carried out. All of the 21 possible $[PtCl_nBr_m(H_2O)_{4-n-m}]^{2-n-m}$ (n, m = 0-4) complex ions are observed by the relative chemical shifts $\delta(^{195}Pt)$ of which 9 of these have not been reported before. Systematic $\delta(^{195}Pt)$ increments result from substitution of H_2O with chloride and bromide, to facilitate assignment of the Pt(II) species. The $\delta(^{195}Pt)$ increments resulting from substitution of H_2O by Cl^- *trans* to Cl^- is bigger than substitution of Cl^- *trans* to H_2O and allow assignment of stereoisomers. The same proportionalities are valid for substitution of H_2O by Br^-. ^{195}Pt NMR "chemical shift trend analysis" as demonstrated here, is a relatively robust method for the rapid assignment of $[PtCl_nBr_m(H_2O)_{4-n-m}]^{2-n-m}$ (n, m = 0-4) complexes in solution.

A detailed analysis of the $^{35}Cl/^{37}Cl$ isotope shifts induced in the 128.8 MHz ^{195}Pt NMR resonances of $[PtCl_n(H_2O)_{6-n}]^{4-n}$ (n = 1-5) and $[PtCl_n(OH)_{6-n}]^{2-}$ (n = 1-5) complex ions were carried out. The $[PtCl_5(H_2O)]^-$, *cis*-$[PtCl_4(H_2O)_2]$ and *mer*-$[PtCl_3(H_2O)_3]^+$ complexes exhibit unique *isotopologue* signals in addition to *isotopomer* signals, facilitated by the chloride *trans* influence resulting in $Pt–OH_2$ bond lengthening. Analysis of $^{35}Cl/^{37}Cl$ induced isotope shifts serve as a fingerprint for the unambiguous identification and assignment of all the $[PtCl_n(H_2O)_{6-n}]^{4-n}$ (n = 1-5) ions in solution, including isotopic stereoisomers. The *trans* influence of -OH counteracts the chloride *trans* influence in the $[PtCl_n(OH)_{6-n}]^{2-}$ (n = 1-5) *hydroxido* complexes, resulting in only *isotopologue* signals. Analysis of ^{195}Pt resonance signals for the $[PtCl_n(H_2O)_{6-n}]^{4-n}$ (n = 1-5) complex ions enriched with $H_2^{18}O$ confirms that the splitting hierarchy of $^{35}Cl/^{37}Cl$ and $^{16}O/^{18}O$ induced *isotopologue* and *isotopomer* signals is in accord with that predicted by an isotope mass factor.

Synthesis of the $[Pt(H_2O)_6]^{4+}$ complex has not been reported before, even though the existence of this complex is possible according to molecular orbital theory. Synthesis of $[Pt(H_2O)_6]^{4+}$ and possible characterization by ^{195}Pt NMR were investigated. All of the $[PtCl_n(H_2O)_{6-n}]^{4-n}$ (n = 1-5) *aqua* ions are formed by driving aquation of $[PtCl_6]^{2-}$ *via*

addition of $AgClO_4$ to an aqueous solution of $[PtCl_6]^{2-}$. The $[Pt(H_2O)_6]^{4+}$ complex is not detected by ^{195}Pt NMR due to the high thermodynamic stability of $[Pt(Cl(H_2O)_5]^{3+}$. Treating an aqueous $[Pt(OH)_6]^{2-}$ solution with 6 M $HClO_4$, or oxidation of $[Pt(H_2O)_4]^{2+}$ with $NaXO_3$ (X = Cl or Br) in 6 M $HClO_4$ give $\delta(^{195}Pt)$ values close to -3324 ppm, the estimated $\delta(^{195}Pt)$ of $[Pt(H_2O)_6]^{4+}$. The $\delta(^{195}Pt)$ values of $[Pt(OH)_6]^{2-}$ as a function of $[HClO_4]$ indicate an inflection point at ~2.5 M $HClO_4$, and suggest protonation of the *hydroxido* ligand in $[Pt(OH)(H_2O)_5]^{3+}$, forming $[Pt(H_2O)_6]^{4+}$. Exchange of H_2O on putative $[Pt(H_2O)_6]^{4+}$ as measured by $H_2^{18}O$ enrichment and ^{195}Pt NMR is extremely slow, while Cl^-/Br^- anation is relatively fast, implying an I_a mechanism as envisaged for $[Pt(H_2O)_6]^{4+}$. These results are the first support for the existence of the $[Pt(H_2O)_6]^{4+}$ complex in strong acidic solution.

Oxidation of $[PtCl_4]^{2-}$, $[Pt(CN)_4]^{2-}$ and $[Pt(H_2O)_4]^{2+}$ with H_2O_2, $NaClO_3$ and $NaBrO_3$ were studied by ^{195}Pt NMR spectroscopy. Oxidation of $[PtCl_4]^{2-}$ with H_2O_2 reveals one product *trans*-$[PtCl_4(OH)_2]^{2-}$ in *water* while all the $[PtCl_n(H_2O)_{6-n}]^{4-n}$ (n = 1-6) complex ions are observed in 1 M $HClO_4$. It is demonstrated that *trans*-$[PtCl_4(H_2O)_2]$ is formed as the oxidation product in *acidic* solution, but is rapidly redistributed into the $[PtCl_n(H_2O)_{6-n}]^{4-n}$ (n = 1-6) complexes as a result of Pt(II) associations with Pt(IV). Oxidation of $[PtCl_4]^{2-}$ with $NaXO_3$ (X = Cl or Br) and electron transfer takes place *via* a Pt(II)–oxygen bond, and essentially results in the same speciation as oxidation with H_2O_2. Formation of some $[PtCl_nBr_m(H_2O)_{6-n-m}]^{4-n}$ (n, m = 1-6) species indicates reduction of BrO_3^- and subsequent oxidation of Pt(II) with reduced forms of BrO_3^-. The speciation after oxidation of $[Pt(CN)_4]^{2-}$ and $[Pt(H_2O)_4]^{2+}$ support the idea of a Pt(II)–oxygen bonded intermediate and *trans* oxidative addition reaction with H_2O_2, $NaClO_3$ and $NaBrO_3$ and is fundamental in understanding the oxidation mechanism.

A UV-visible kinetic study of the oxidation of $[PtCl_4]^{2-}$ with H_2O_2 in hydrochloric acid was carried out. Oxidation proceeds *via* two parallel mechanisms, while the main mechanism depends on the reagent concentrations. High Pt(II) concentration ($\geq$ 0.2 mM) and low H_2O_2 concentration ($\leq$ 300 mM) favour a first-order mechanism with respect to Pt(II) with pseudo-first order rate constant 1.52 x 10^{-2} $M^{-1}s^{-1}$ due to oxidation with H_2O_2. Low Pt(II)

concentration ($\leq$ 0.07 mM) and high H_2O_2 concentration ($\geq$ 40 mM) favour a zero-order mechanism with pseudo-zero order rate constant $k_0 = (7.0 \pm 0.8) \times 10^{-7}$ s^{-1} due to the steady-state catalytic formation and oxidation with HOCl which forms *via* reaction H_2O_2 + Cl$^-$ + H$^+$ $\leftrightarrows$ HClO + H_2O. Oxidation of $[PtCl_4]^{2-}$ with HOCl is rapid compared to oxidation with H_2O_2, so that HOCl formation is the rate determining step and the reaction appear zero-order with respect to Pt(II). Activation parameters $\Delta H^{\ddagger} = 52 \pm 1$ kJ mol^{-1}; 84 ± 3 kJ mol^{-1} and $\Delta S^{\ddagger} = -121 \pm 4$ JK^{-1}mol^{-1}; -104 ± 10 JK^{-1}mol^{-1} were calculated for the zero- and first-order mechanisms respectively and support an inner-sphere one step two-electron transfer mechanism for oxidation with both HOCl and H_2O_2. Activation volumes $\Delta V^{\ddagger} = -7.6 \pm 0.4$ cm^{3}mol^{-1} and -7.9 ± 1.9 cm^{3}mol^{-1} for the zero- and first-order mechanisms indicate similar activation states as expected for oxidation with HOCl and H_2O_2. These results provide a new perspective for the oxidation of Pt(II) complexes in hydrochloric acid and is fundamental to help understand the oxidation mechanism of Pt(II) with $NaClO_3$ and $NaBrO_3$.

x

Opsomming

'n ^{195}Pt NMR spektroskopie studie is onderneem van Pt(II)-aqua-bromied-chloried komplekse, verkry deur chloried/bromied anasie van $[Pt(H_2O)_4]^{2+}$ en $[PtCl_4]^{2-}/[PtBr_4]^{2-}$ akwasie. Al 21 van die moontlike $[PtCl_nBr_m(H_2O)_{4-n-m}]^{2-n-m}$ (n, m = 0-4) kompleks ione is observeer, waarvan 9 nog nie voorheen gerapporteer is nie. Sistematiese verhoudings tussen die $\delta(^{195}Pt)$ waardes is sigbaar as gevolg van die substitusie van H_2O met chloried en bromied en fasiliteer identifikasie van Pt(II) species. Identifikasie van stereoisomere is moontlik aangesien die $\delta(^{195}Pt)$ verskuiwings wat ontstaan vanweë die substitusie van H_2O deur Cl$^-$ *trans* van Cl$^-$ groter is as substitusie van Cl$^-$ *trans* van H_2O. Dieselfde verhoudings is geldig teenoor substitusie van H_2O deur Br$^-$. Hierdie "chemiese verskuiwing tendens analiese" is 'n relatiewe robuste metode vir die vinnige identifikasie van Pt(II) komplekse.

'n Omvattende analise is uitgevoer op die $^{35}C/^{37}Cl$ isotoop verskuiwings wat geinduseer word in die 128.8 MHz ^{195}Pt KMR resonans van $[PtCl_n(H_2O)_{6-n}]^{4-n}$ (n = 1-5) en $[PtCl_n(OH)_{6-n}]^{2-}$ (n = 1-5) komplekse. Die $[PtCl_5(H_2O)]^-$, *cis*-$[PtCl_4(H_2O)_2]$ en *mer*-$[PtCl_3(H_2O)_3]^+$ komplekse het unieke *isotopoloog* en *isotopomeer* pieke, as gevolg van die chloried *trans* invloed wat Pt–OH$_2$ bindings verlenging veroorsaak. Analise van $^{35}C/^{37}Cl$ geïnduseerde isotoop verskuiwings dien as vingerafdruk vir die identifikasie van al die $[PtCl_n(H_2O)_{6-n}]^{4-n}$ (n = 1-5) komplekse in oplossing. Die *trans* invloed van –OH werk die *trans* invloed van Cl$^-$ teë in die $[PtCl_n(OH)_{6-n}]^{2-}$ (n = 1-5) *hidroksied* komplekse, wat slegs *isotopoloog* pieke tot gevolg het. Analise van ^{195}Pt resonans pieke vir die $[PtCl_n(H_2O)_{6-n}]^{4-n}$ (n = 1-5) kompleks ione verryk met $H_2^{18}O$ bevestig die split hiërargie van $^{35}Cl/^{37}Cl$ en $^{16}O/^{18}O$ geïnduseerde *isotopoloog* en *isotopomeer* pieke soos voorspel deur 'n isotoop massa faktor.

Sintese van die $[Pt(H_2O)_6]^{4+}$ kompleks is nooit voorheen gerapporteer nie, alhoewel Molekulêre Orbitale teorie bepaal dat dit moontlik is. Sintese van $[Pt(H_2O)_6]^{4+}$ en karakterisering deur middel van ^{195}Pt KMR is ondersoek. Al die $[PtCl_n(H_2O)_{6-n}]^{4-n}$ (n = 1-5) *aqua* komplekse is gevorm deur akwasie van $[PtCl_6]^{2-}$ te dryf *via* toevoeging van AgClO$_4$ by 'n waterige oplossing van $[PtCl_6]^{2-}$. Die $[Pt(H_2O)_6]^{4+}$ kompleks is nie opgespoor deur ^{195}Pt KMR nie, vanweë die hoë termodinamiese stabiliteit van $[Pt(Cl(H_2O)_5]^{3+}$.

Behandeling van 'n waterige $[Pt(OH)_6]^{2-}$ oplossing met 6 M $HClO_4$, of oksidasie van $[Pt(H_2O)_4]^{2+}$ met $NaXO_3$ (X = Cl or Br) in 6 M $HClO_4$, gee 'n $\delta(^{195}Pt)$ waarde na aan die -3324 ppm voorspel vir $[Pt(H_2O)_6]^{4+}$. Die relatiewe ^{195}Pt chemiese verskuiwing van $[Pt(OH)_6]^{2-}$ as 'n funksie van die $HClO_4$ konsentrasie wys 'n draaipunt by ~2.5 M $HClO_4$, en stel protonasie van die *hydroksied* ligand in $[Pt(OH)(H_2O)_5]^{3+}$ voor, om $[Pt(H_2O)_6]^{4+}$ te vorm. Uitruiling van H_2O soos gemeet deur $H_2^{18}O$ verryking en ^{195}Pt KMR is uitermatig stadig, terwyl Cl^-/Br^- anasie relatief vinnig is, en impliseer 'n I_a meganisme soos voorgestel vir $[Pt(H_2O)_6]^{4+}$. Hierdie resultate is die eerste ondersteuning wat die bestaan van die $[Pt(H_2O)_6]^{4+}$ kompleks motiveer.

Oksidasie van $[PtCl_4]^{2-}$, $[Pt(CN)_4]^{2-}$ en $[Pt(H_2O)_4]^{2+}$ met H_2O_2, $NaClO_3$ en $NaBrO_3$ is bestudeer met ^{195}Pt KMR spektroskopie. Oksidasie van $[PtCl_4]^{2-}$ met H_2O_2 gee slegs *trans*-$[PtCl_4(OH)_2]^{2-}$ as produk in *water* terwyl $\delta(^{195}Pt)$ waardes van al die $[PtCl_n(H_2O)_{6-n}]^{4-n}$ (n = 1-6) komplekse waargeneem word in 1 M $HClO_4$. Dit word gedemonstreer dat *trans*-$[PtCl_4(H_2O)_2]$ gevorm word as oksidasie produk in *suur* oplossing, maar vinnig herverdeel word in die $[PtCl_n(H_2O)_{6-n}]^{4-n}$ (n = 1-6) komplekse as gevolg van Pt(II) assosiasies met Pt(IV). Oksidasie van $[PtCl_4]^{2-}$ met $NaXO_3$ (X = Cl of Br) en elektron oordrag vind plaas *via* 'n Pt(II)–suurstof binding en veroorsaak basies dieselfde spesies as oksidasie met H_2O_2. Vorming van sommige van die spesies in die reeks $[PtCl_nBr_m(H_2O)_{6-n-m}]^{4-n}$ (*n, m* = 1-6) dui op reduksie van BrO_3^- en gevolglik oksidasie van Pt(II) met gereduseerde vorms van BrO_3^-. Oksidasie van $[Pt(CN)_4]^{2-}$ en $[Pt(H_2O)_4]^{2+}$ ondersteun die idee van 'n Pt(II)–suurstof gebinde tussenproduk en 'n *trans* oksidatiewe addisie reaksie vir oksidasie met H_2O_2, $NaClO_3$ en $NaBrO_3$ en is fundamenteel om die oksidasie meganisme te verstaan.

'n UV-sigbare kinetiese studie van die oksidasie van $[PtCl_4]^{2-}$ met H_2O_2 is uitgevoer in soutsuur. Oksidasie vind plaas *via* twee parallele meganismes terwyl die hoof meganisme afhang van die reagens konsentrasies. Hoë Pt(II) konsentrasie ($\geq$ 0.2 mM) en lae H_2O_2 konsentrasie ($\leq$ 300 mM) bevoordeel 'n eerste-orde meganisme ten opsigte van Pt(II) met pseudo-eerste orde tempo konstante 1.52 x 10^{-2} $M^{-1}s^{-1}$ as gevolg van oksidasie met H_2O_2. Lae Pt(II) konsentrasie ($\leq$ 0.07 mM) en hoë H_2O_2 konsentrasie ($\geq$ 40 mM) bevoordeel 'n zero-orde meganisme met pseudo-zero orde tempo konstante k_0 = (7.0 $\pm$ 0.8) x 10^{-7} s^{-1} as

gevolg van die bestendige katalitiese vorming en oksidasie met HOCl *via* die reaksie H_2O_2 + Cl^- + H^+ ⇆ HClO + H_2O. Oksidasie van $[PtCl_4]^{2-}$ met HOCl is vinnig in vergelyking met oksidasie deur H_2O_2, sodat HOCl vorming die tempo bepalende stap is en die reaksie lyk zero-orde met respek tot Pt(II). Aktiverings parameters $\Delta H^{\ddagger}$ = 52 ± 1 kJ mol^{-1}; 84 ± 3 kJ mol^{-1} en $\Delta S^{\ddagger}$ = -121 ± 4 $JK^{-1}mol^{-1}$; -104 ± 10 $JK^{-1}mol^{-1}$ is bereken vir die zero- and eerste-orde meganismes onderskeidelik en ondersteun 'n binne-sfeer een stap twee-elektron oordrags meganisme vir oksidasie met beide HOCl en H_2O_2. Aktiverings volumes $\Delta V^{\ddagger}$ = -7.6 ± 0.4 cm^3mol^{-1} en -7.9 ± 1.9 cm^3mol^{-1} vir die zero- and eerste-orde meganismes dui op soortgelyke aktiverings toestande soos verwag vir oksidasie met HOCl en H_2O_2. Hierdie resultate gee 'n nuwe perspektief vir die oksidasie van Pt(II) komplekse in soutsuur en is fundamenteel om die oksidasie van Pt(II) met $NaClO_3$ en $NaBrO_3$ te verstaan.

Table of Content

List of Figures

List of Tables

Chapter 1

Brief introduction and overview of the study

The catalytic properties of the platinum group metals (PGMs) are utilized in several industrial processes. Hydrogenation, dehydrogenation and reforming reactions in the petroleum refining industry as well as organic/inorganic oxidation reactions such as the Wacker and Ostwald processes are just some of the applications.[1, 2] Platinum (Pt) have long been known to efficiently catalyze the reduction of harmful automotive exhaust emissions like carbon monoxide, hydrocarbons and oxides of nitrogen and are used on a large scale for this application in the developed world.[1] Due to the brilliant appearance and corrosion resistant properties, PGMs are also used extensively in jewellery manufacturing and electroplating applications. The discovery that *cis*-[PtCl$_2$(NH$_3$)$_2$] (*cis*-platin) inhibit tumour growth has sparked interest in the coordination chemistry of both Pt(II)[3-5] and Pt(IV)[3, 6, 7] and a lot of effort has been directed towards finding more effective derivatives for anti-cancer applications. A diagram of the platinum demand by application for 2009 is shown in Figure 1.1.
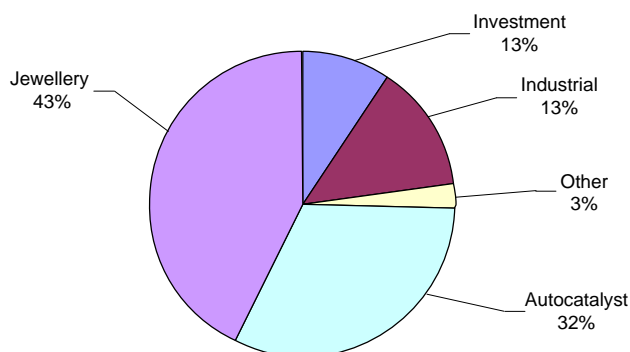
Figure 1.1: Platinum demand by application (total: 7.04 million oz) for 2009.[8]

Depending on the source, PGM deposits are found as mixtures of platinum (Pt), palladium (Pd), gold (Au), ruthenium (Ru), rhodium (Rh), iridium (Ir) and osmium (Os) intertwined with various base metal and amphoteric elements.[9] The low natural abundance of the PGMs (estimated to be ~0.005 mg/kg in the earth's crust) and intricate extraction/refining process have led to an ever increasing demand, especially in the light of increasing strict legislation on automotive emission control, putting more pressure on platinum refining companies to increase production.[8] South Africa exports a large quantity of PGMs and in 2009, 77 % of the world's platinum was produced here.[8] A diagram of the platinum supply by country for 2009 is shown in Figure 1.2.
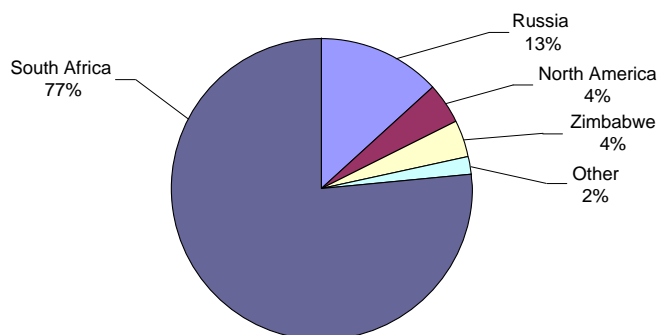
Figure 1.2: Platinum supply by country (total: 5.92 million oz) for 2009.[8]

Downstream PGM separation was originally achieved by froth flotation precipitation techniques.[1] This is however costly and time consuming, and has since been replaced by more efficient methods that include a combination of classical methods (e.g. selective precipitation), more modern solvent extraction (SX) techniques[1] and to a lesser extent ion-exchange chromatography.[10, 11] Dissolution of PGMs by chlorine oxidation in acidic chloride rich solution is a cost-effective method by which PGMs can be concentrated into the anionic chlorido complexes $[MCl_6]^{x-}$ (where M is the metal ion and x the formal charge).[1] Although the PGMs often share characteristics, they display very different properties which can be exploited to assist separation.[12] These differences include: (*i*) The oxidation state as it influences the geometry of the complex, e.g. the liquid-liquid and ion-exchange extraction properties of the $[PtCl_6]^{2-}$ anion are significantly more favourable compared to the square-planar $[PtCl_4]^{2-}$ anion.[13] (*ii*) The extent of aquation, since $[PtCl_6]^{2-}$ extracts much better than $[PtCl_5(H_2O)]^{-}$ [1] and (*iii*) the effective charge of the complex is of significance e.g. for $[RhCl_6]^{3-}$ the hydration energy $\Delta G_{hydration}$ is comparable to the phase transfer $\Delta G_{phase\ transfer}$ which can decrease extraction efficiency.[1] Large-scale separation and refining of the PGMs is thus based predominantly on the favourable properties of their anionic chloro-complexes such as $[PtCl_6]^{2-}$, $[PdCl_4]^{2-}$, $[RhCl_6]^{3-}$ and $[IrCl_6]^{2-/3-}$, while Ru, and Os are generally separated by means of oxidative distillation.[1, 12] Efficient oxidation is therefore critical in the refining process.

Oxidation of $[PtCl_4]^{2-}$ with sodium chlorate (NaClO$_3$) and sodium bromate (NaBrO$_3$) are used on a large scale in the refining industry to oxidize PGMs to facilitate separation and efficient refining. The use of NaClO$_3$ and NaBrO$_3$ as oxidants in the commercial refining of

PGMs has been reported in the patent literature,[14] although no detailed study of the oxidation of Pt(II) square-planar complexes with $NaClO_3$ and/or $NaBrO_3$ has been reported. Since the separation of platinum from other PGMs is dependent, amongst other factors, on the efficient oxidation of Pt(II) to Pt(IV), one of the objectives in this study was to study the oxidation mechanism of Pt(II) with H_2O_2, $NaClO_3$ and $NaBrO_3$. As will be shown, oxidation of $[PtCl_4]^{2-}$ with these oxidants are complicated and oxidation with $NaBrO_3$ results in more than 20 Pt(IV) species in perchloric acid! Some aspects of the oxidation mechanism may be inferred from the speciation after oxidation. For this reason it was first necessary to find a method for the speciation of Pt(II)- and Pt(IV)-aqua-bromido-chlorido complexes before mechanistic interpretations can be made.

The chemical speciation of the chlorido-complexes in solution at different stages of the actual separation process is of critical importance and the efficiency of these methods can be improved considerably by a detailed understanding of the *speciation*† at the different stages of separation.[1] It was previously shown, that ^{195}Pt NMR 'chemical-shift-trend' analysis is a powerful method as a means of rapid assignment of for example the entire series of $[PtCl_{6-n}(OH)_n]^{2-}$ (n = 0-6) and $[PtCl_{6-m-n}Br_m(OH)_n]^{2-}$ (m, n = 0-6) complexes in solutions.[16] In the context of PGM refining process solutions, it was of interest to establish if the same principles of ^{195}Pt NMR chemical-shift-trend analysis applies to Pt(II) species, particularly in *acidic* solution. **Chapter 2** thus deals with the synthesis of the $[PtCl_n(H_2O)_{4-n}]^{2-n}$ (n = 0-4), $[PtBr_n(H_2O)_{4-n}]^{2-n}$ (n = 0-4) and the mixed $[PtCl_nBr_m(H_2O)_{4-n-m}]^{2-n-m}$ (n, m = 0-4) series of complex ions, and species assignment by ^{195}Pt NMR chemical-shift-trend analysis.

While this method provides for the rapid identification of such species in solution with considerable certainty, the sensitivity of the ^{195}Pt chemical shift ($\delta(^{195}$Pt)) to other factors such as concentration, solvent composition, temperature and ionic strength (e.g. HCl concentration) makes an additional spectroscopic technique for unambiguous identification

---

†The term *speciation* can be used in a number of ways. In order to avoid confusion in the discussion, the analytical activity of identifying and/or determining the quantity of one or more chemical species will be referred to as *speciation analysis*. The distribution of a specific element between chemical species will be referred to as *speciation of an element* or simply *speciation* as defined by IUPAC.[15]

of Pt(II) and Pt(IV) complex species desirable. It was previously demonstrated[17] that small $^{35}Cl/^{37}Cl$ isotope induced ^{195}Pt NMR shifts at higher magnetic fields (9.4 T) are well resolved for the $[Pt^{35}Cl_n{}^{37}Cl_{6-n}]^{2-}$ (n = 0-6) complex. In **Chapter 3**, such effects are investigated in detail for the $[PtCl_n(H_2O)_{6-n}]^{4-n}$ (n = 1-6) and $[PtCl_n(OH)_{6-n}]^{2-}$ (n = 1-6) complexes as a means to assign these complexes by ^{195}Pt NMR, from the unique isotope distribution.

The $[Pt(H_2O)_6]^{4+}$ complex which is anticipated to be one of the oxidation products of $[Pt(H_2O)_4]^{2+}$ with $NaClO_3$ or $NaBrO_3$ could not been obtained and characterized before. This complex is not only significant in the context of oxidation and a mechanistic study but ligand exchange studies on this hexa-aqua complex will reveal fundamental properties of the Pt(IV) nucleus. In **Chapter 4**, different pathways are investigated to obtain the elusive $[Pt(H_2O)_6]^{4+}$ complex. Characterization of $[Pt(H_2O)_6]^{4+}$ by ^{195}Pt is tricky and necessitates calculation of solvent exchange rates. ^{195}Pt NMR and $H_2{}^{18}O$ enrichment are utilized to estimate exchange rates and motivate the existence of $[Pt(H_2O)_6]^{4+}$.

After the methods for Pt(II)- and Pt(IV)-aqua-bromido-chlorido speciation is established in *Chapter 2* and *3*, oxidation of $[PtCl_4]^{2-}$ is investigated. As will be seen in **Chapter 5**, the distribution of product Pt(IV) species particularly in acidic solutions is far from simple, and thus for comparison we have used the relatively well studied oxidation of $[PtCl_4]^{2-}$ by H_2O_2 as a benchmark, to elucidate this chemistry particularly in *acidic* solutions. Although speciation of the oxidation products with ^{195}Pt NMR may reveal some aspects of the oxidation mechanism, intimate properties of the oxidation mechanism or the rate law remains unknown. A kinetic high-pressure UV-visible spectrophotometry study was undertaken at the University of Erlangen-Nürnberg to determine the rate determining parameters. In **Chapter 6**, the oxidation of $[PtCl_4]^{2-}$ with hydrogen peroxide is studied in hydrochloric acid, to mimic refining process solutions and serve as benchmark for the oxidation with sodium chlorate and sodium bromate.

1. F. L. Bernardis, R. A. Grant, D. C. Sherrington, React. Funct. Polym., 2005, *65*, 205-217.

2. M. R. Pitts, *Platinum Metals Rev.,* 2008, *52 (2),*

3. Y. Jung, S. J. Lippard, *Chem. Rev.,* 2007, *107*, 1387-1407.

4. J. Reedijk, Proc. Natl. Acad. Sci. U. S. A., 2003, *100*, 3611-3616.

5. M. A. Fuertes, C. Alonso, J. M. Perez, *Chem. Rev.,* 2003, *103*, 645-662.

6. R. Kuroda, S. Neidle, I. M. Ismail, P. J. Sadler, *Inorg. Chem.,* 1983, *22*, 3620-3624.

7. S. Al-Baker, J. C. Dabrowiak, *Inorg. Chem.,* 1987, *26*, 613-617.

8. D. Jollie, in *Platinum 2010*, Johnson Matthey, 2010.

9. J. D. Edwards, D. F. Colton, R. K. Lea, Patent No. 49567, EP, 1982.

10. G. Schmuckler, Patent No. 4885143, US, 1989.

11. R. A. Grant, Y. Taylor, Patent No. 756013, EP, 1997.

12. N. N. Greenwood, A. Earnshaw, *Chemistry of the Elements. Second Edition. Butterworth-Heineman, Oxford, UK.*, 1984.

13. K. R. Koch, M. R. Burger, J. Kramer, A. N. Westra, *Dalton Trans.,* 2006, 3277-3284.

14. W. H. Pittie, G. Overbeek, K. F. Doig, Patent No. 1418060, ZA, 1973.

15. D. M. Templeton, F. Ariese, R. Cornelis, L.-G. Danielsson, H. Muntau, H. P. Van Leeuwen, R. Łobiński, *Pure Appl. Chem.,* 2000, *72*, 1453-1470.

16. J. Kramer, K. R. Koch, *Inorg. Chem.,* 2007, *46*, 7466-7476.

17. I. M. Ismail, S. J. S. Kerrison, P. J. Sadler, *Chem. Commun.,* 1980, 1175-1176.

Chapter 2

Speciation of Pt(II) aqua-bromido-chlorido complex species by ^{195}Pt NMR chemical-shift-trend analysis

2.1   Introduction

In the context of speciation of an element and speciation analysis, high resolution [195]Pt NMR is a powerful tool to measure and characterize Pt(II) and (IV) species in solution.[1-4] Since NMR is a direct non-invasive analytic technique, speciation of an element can be determined without changing the dynamics of the solution, which is not possible with separation/fractionation analytic techniques such as chromatography. The [195]Pt nucleus is the only Pt isotope with spin $I = \frac{1}{2}$ and has a natural abundance of 33.8 % with relative sensitivity of 9.94 x 10^{-3} ensuring relative good [195]Pt NMR sensitivity.[3-5] These properties of the [195]Pt nucleus as well as short spin-lattice relaxation times T_1 (most values are less than 2 s), allows rapid acquisition of [195]Pt NMR spectra since no waiting time between pulses is required. The [195]Pt NMR chemical shift, δ([195]Pt), covers a wide range of approximately 13000 ppm so that different spectral "windows" is often needed to observe all complex species in a solution. The [195]Pt nucleus is extremely sensitive to changes in solution as is reflected by changes in the δ([195]Pt) value with changes of the oxidation state,[3] coordinated ligands,[6] solvent,[3, 7] ionic strength[8, 9] and temperature.[10] The sensitivity of the Pt nucleus towards coordinated ligands is utilized here to allow assignment of Pt(II) complex species in solution.

Goggin and Goodfellow[11] measured the [195]Pt NMR δ([195]Pt) values for various Pt(II) species and showed that substitution of a coordinated Cl$^-$ at a position *cis* to another Cl$^-$ with Br$^-$ results in a bigger difference in δ([195]Pt) value ($\Delta\delta$([195]Pt)), than in the case of substitution at a position *trans* to another Cl$^-$. This observation was utilized by Von Zelewsky[12] and later by Kerrison and Sadler,[13] who reported the δ([195]Pt) of all species in the [PtBr$_n$Cl$_{4-n}$]$^{2-}$ (n = 0-4) series and extended the general rules: (*i*) successive substitutions of Cl$^-$ for Br$^-$ causes the δ([195]Pt) value to shift in the same direction (i.e. downfield or up-field) and (*ii*) differences in geometric isomers result in a much smaller $\Delta\delta$([195]Pt) than those between the number of substituents.[11, 13] While this methodology is correct and useful, in more complicated systems (*vide infra*) a systematic method for species assignment is required.

In this context, Kramer and Koch[14, 15] recently showed that ^{195}Pt NMR chemical-shift-trend analysis is a powerful method for rapid assignment of all the *hydroxido* $[PtCl_nBr_m(OH)_{6-n-m}]^{2-}$ (*m, n* = 0-6) species and *mono-aqua* $[PtCl_nBr_m(H_2O)_{6-n-m}]^{2-}$ (*m, n* = 5-6) species. Burger *et al.*[16] used the experimental $\delta(^{195}Pt)$ values obtained in this study to show that Density Functional Theory (DFT) calculations can successfully predict experimental $\delta(^{195}Pt)$ values of the $[PtCl_nBr_{6-n}]^{2-}$ (*n* = 0-6) complexes. Large deviations from the calculated values were obtained for the OH$^-$ complexes, presumably as a result of a more complicated hydration and solvation network not accounted for successfully by DFT calculations. It is therefore anticipated that the deviation will be more pronounced in the *aqua* ligand system, especially since the formal charge of the complex changes within a series as H_2O is substituted by Cl$^-$ or Br$^-$.

This study therefore extended the work of Kramer and Koch[14] to determine experimental $\delta(^{195}Pt)$ values of Pt(II)-*aqua-bromido-chlorido* complexes. The first objective in this study was to obtain the $[PtCl_n(H_2O)_{4-n}]^{2-n}$ (*n* = 0-4) and $[PtBr_m(H_2O)_{4-m}]^{2-m}$ (*m* = 0-4) complex species respectively and secondly to ascertain if ^{195}Pt NMR chemical-shift-trend analysis can be applied successfully to assign the complexes. The principles of chemical shift trend analysis are then applied to more complicated solutions, containing all of the $[PtCl_nBr_m(H_2O)_{4-n-m}]^{2-n-m}$ (*n, m* = 0-4) complexes to assign the $\delta(^{195}Pt)$ values not previously reported using ^{195}Pt NMR spectroscopy.

2.2   Experimental

2.2.1   Reagents

Potassium tetrachloroplatinate(II) (99.9+%, K_2PtCl_4, Aldrich), potassium tetrabromo-platinate(II) (99.99%, K_2PtBr_4, Aldrich), sodium hexachloroplatinate(IV) hexahydrate (98%, $Na_2PtCl_6{\cdot}6H_2O$, Aldrich), were all of reagent grade quality and used without further purification. Silver perchlorate hydrate (99%, $AgClO_4$, Aldrich), sodium chloride (99+%, NaCl, Aldrich), sodium bromide (NaBr, Holpro Analytics) potassium bromide (99.5%, KBr, N.T. Laboratory Supplies), sodium hydroxide pellets (NaOH, MERCK) were also of reagent grade quality and used as is. Deuterium oxide (99.9%, D_2O, Aldrich) was used as solvent to obtain a lock signal for NMR measurements. Perchloric acid (70% w/w $HClO_4$, 1 L = 1.68 kg, MERCK) was used as stock for $HClO_4$ dilutions. All aqueous solutions were made with ultra pure Milli-Q water (MQ > 18 MΩ) and degassed with Ar to remove O_2 for at least 1 h prior to use.

2.2.2 Instrumentation

^{195}Pt NMR Spectroscopy

^{195}Pt NMR spectra were recorded at various temperatures (± 0.1 K) using a Varian INOVA 600 MHz spectrometer operating at 128.8 MHz with a 5 mm broad-band probe. All spectra were recorded at 30°C relative to a 1 mm coaxial insert tube containing $[PtCl_6]^{2-}$ as reference solution ($\delta^{195}Pt$ = 0 ppm at 500 mg cm^{-3} $H_2PtCl_6{\cdot}2H_2O$ in 30 % v/v D_2O /1 M HCl). Spectra were recorded under conditions of optimal resolution using an excitation pulse of 2.0 μs, with an acquisition time 1.016 s, and no relaxation delay was applied in order to ensure homogeneous and complete excitation over the full spectral window. The T_1 relaxation times of most Pt species were measured as < 2 s in solution and ensure complete relaxation of all species. Broad band ^{1}H-decoupling was applied in all measurements. A line-broadening factor of 20 Hz was applied in processing the experimental FID data, resulting in an effective line-width at half height. The relative peak intensities of some

species may not accurately reflect the concentration at a certain period in time. The large spectral windows used here (up to 2000 ppm), ensure that homogeneous excitation isn't possible over the whole spectral range, and species far from the transmitter offset may not accurately reflect the concentration, but may serve as a relative indication. In order to observe all species in solution, [195]Pt NMR spectra were recorded in some cases in a dynamic-state, before any steady-state was reached, which is necessary due to the thermodynamic stability of certain species.

2.2.3   Methods of Pt(II/IV) complex preparation

Synthesis of the Pt(II)-aqua-chlorido series

The Pt(II)-*aqua-chlorido* species of complexes with general formula $[PtCl_n(H_2O)_{4-n}]^{2-n}$ ($n =$ 0-4) were obtained in two different ways. The series could be synthesized either by stepwise adding fractions of $AgClO_4$ to a solution of $[PtCl_4]^{2-}$ or by adding ~3 mol equivalents NaCl (with regards to Pt(II)) to 0.15 M $[Pt(H_2O)_4]^{2+}$. In the first method, 0.207 g K_2PtCl_4 was dissolved in 1.5 mL 2 M $HClO_4$ to give an initial concentration of 0.33 M $[PtCl_4]^{2-}$. The solution was heated under reflux at 70°C while adding 0.1 mL portions of 3.13 M $AgClO_4$ over a 6 h time period. Samples were extracted from the reaction flask between additions, filtered and analyzed with [195]Pt NMR spectroscopy. The reaction flask was covered with tin foil to prevent light induced reduction of Ag^+. The solution was kept under constant Ar gas flow to exclude air from the reaction flask. In the second method, $[Pt(H_2O)_4]^{2+}$ was prepared prior to the reaction according to the method of Elding[17] as this complex is not commercially available. The synthesis and concentration of $[Pt(H_2O)_4]^{2+}$ is a long and tedious process as described in the literature and was characterized by UV-visible spectrophotometry ($\varepsilon_{273} = 56.5$ cm^{-1}M^{-1}) and [195]Pt NMR spectroscopy ($\delta(^{195}Pt) = $ ~30 ppm in 1 M $HClO_4$, relative to external $[PtCl_6]^{2-}$).

Synthesis of the Pt(II)-aqua-bromido series

The Pt(II)-*aqua-bromido* species of complexes with general formula $[PtBr_m(H_2O)_{4-m}]^{2-m}$ (m = 0-4) were obtained by adding 3 mol equivalents NaBr to 0.1 M $[Pt(H_2O)_4]^{2+}$. The solution changed from bright yellow to yellow-orange on addition of NaBr after which a [195]Pt NMR

spectrum was recorded. Another 0.54 mol equivalents of NaBr was added to the above solution and stirred until the salt dissolved. The yellow-orange coloured solution changed to bright orange and a second ^{195}Pt NMR spectrum was recorded 24 h after the initial NaBr addition.

Synthesis of the Pt(II)-aqua-bromido-chlorido series

The Pt(II)-*aqua-bromido-chlorido* species of complexes with general formula $[PtBr_mCl_n(H_2O)_{4-m-n}]^{2-m-n}$ (*m*, *n* = 0-4) were obtained *via* two different methods, to ensure formation of all species in the series at adequately high concentrations to allow detection with ^{195}Pt NMR spectroscopy. The first ^{195}Pt NMR spectrum which represents the species with a higher degree of aquation (*n*, *m* ≤ 2) in the spectral range 200 to -1000 ppm, was obtained after adding 2 mol equivalents NaBr and 2 mol equivalents NaCl simultaneously to 0.15 M $[Pt(H_2O)_4]^{2+}$. The solution was stirred until all the salt dissolved and a ^{195}Pt NMR spectrum was recorded immediately after dissolution. The second ^{195}Pt NMR spectrum representing the species with a lower degree of aquation (*n*, *m* ≥ 2) in the spectral range -1000 to -3000, was obtained after mixing 0.2 M K_2PtBr_4 with 0.2 M K_2PtCl_4 in 1 M $HClO_4$. The solution was stirred for 30 min and a ^{195}Pt NMR spectrum was recorded directly thereafter.

2.3   Results and discussion

2.3.1   Formation of the $[PtCl_n(H_2O)_{4-n}]^{2-n}$ (n = 0-4) complex species and assignment with ^{195}Pt NMR chemical-shift-trend analysis

The $[PtCl_n(H_2O)_{4-n}]^{2-n}$ (n = 0-4) series was obtained from two different starting compounds as described in the experimental section and both reaction methods resulted in formation of all six possible complexes of interest. Addition of Cl$^-$ to $[Pt(H_2O)_4]^{2+}$ results in formation of all complexes due to consecutive Cl$^-$ anation reactions as illustrated in Figure 2.1A.[18] For simplicity the labelling system proposed by Drew and Preetz[19] for Pt(IV) complexes are adopted and applied to our system of Pt(II) complexes for better clarity, where the 1st digit = no. coordinated Cl$^-$, 2nd = no. Br$^-$, 3rd = no. H$_2$O, c = *cis* and t = *trans*.
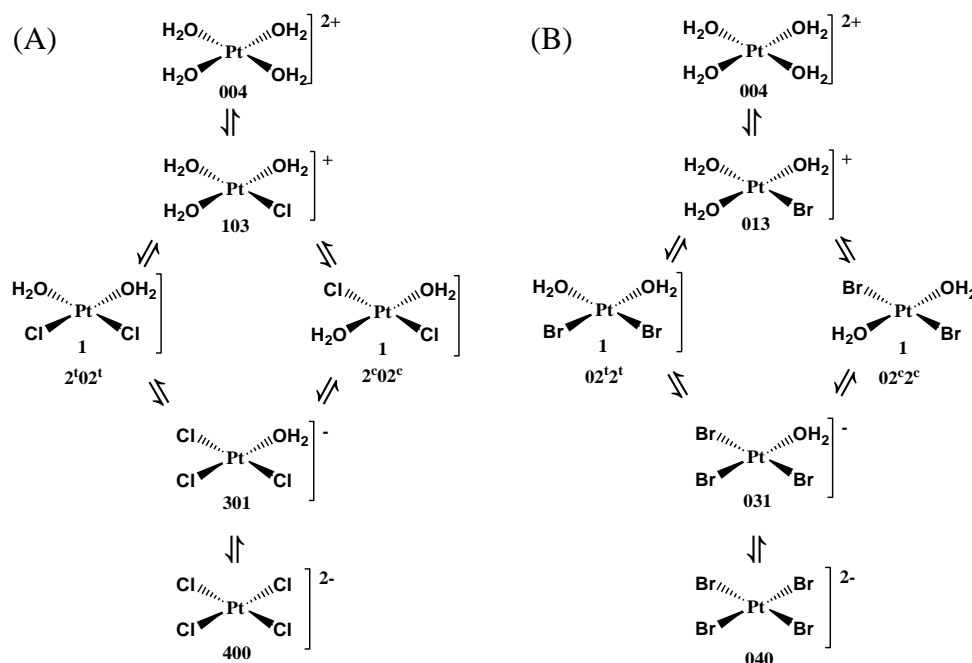
Figure 2.1: (A) Reaction scheme illustrating the stepwise substitution of H$_2$O by Cl$^-$ ions and **(B)** Br$^-$ ions. The formal complex charge is shown after the parenthesis and the statistical expected isomer ratio is indicated below each entry. The nomenclature code is adapted from Drew and Preetz and used as cross reference.[19]

A ^{195}Pt NMR spectrum of all six expected $[PtCl_n(H_2O)_{4-n}]^{2-n}$ (n = 0-4) species obtained *via* Cl$^-$ addition to $[Pt(H_2O)_4]^{2+}$ is shown in Figure 2.2. According to the principles of Goggin and Goodfellow,[11] as H$_2$O is substituted by a Cl$^-$ ion a systematic shielding of the Pt(II) nucleus and consequent systematic up-field shift increment is observed. A remarkable

systematic decrease in the $\delta(^{195}Pt)$ value is obtained, defined by a second-order function $\delta(^{195}Pt) = 26.1 - 342.4n - 17.4n^2$; $R^2 > 0.999$ obtained in a plot of $\delta(^{195}Pt)$ as a function of n (Figure 2.3A). This correlation allows for the assignment of all the complexes except for the stereoisomers $trans$-$[PtCl_2(H_2O)]_2$ and cis-$[PtCl_2(H_2O)]_2$. Although the $\delta(^{195}Pt)$ of these species were reported by different authors before,[3, 9, 20, 21] Gröning and Elding[22] first noted that consistent changes in the $\delta(^{195}Pt)$ values are obtained depending on the position where the ligand exchange takes place on a specific stereoisomer within the Pt(II) coordination sphere. This principle of ^{195}Pt NMR chemical-shift-trend analysis was confirmed and utilized by Kramer and Koch[14] to study and assign all the $[PtBr_mCl_n(OH)_{6-m-n}]^{4-m-n}$ (m, n = 0-6) complexes in solution. The authors concluded that the systematic change in $\delta(^{195}Pt)$ value, for a specific series is consistently larger when a coordinated Cl^- ligand is substituted by an OH^- at a position $trans$ to another Cl^- ligand, compared to at a position $trans$ to a OH^- ligand.
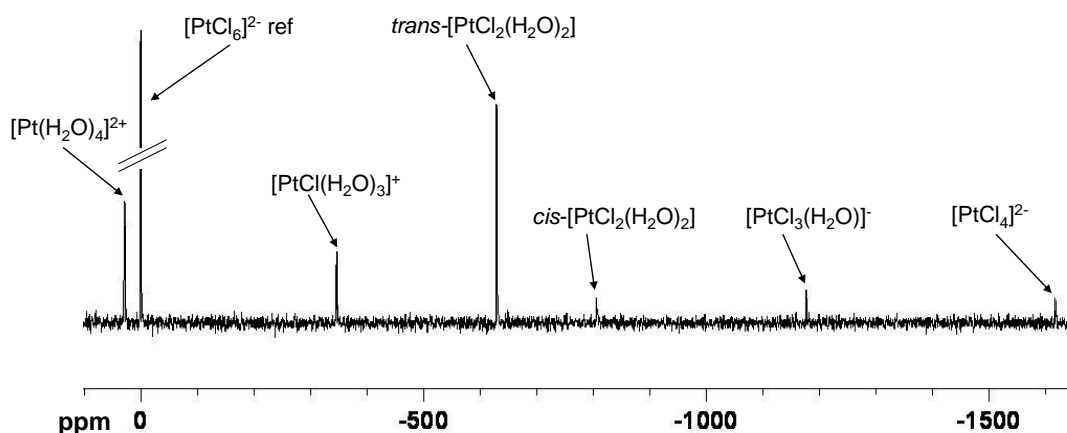
Figure 2.2: ^{195}Pt NMR spectrum of the $[PtCl_n(H_2O)_{4-n}]^{2-n}$ (n = 0-4) series in 1 M $HClO_4$ obtained by addition of NaCl to $[Pt(H_2O)_4]^{2+}$.

Applying the same principle here, the chemical shift increment $\Delta\delta(^{195}Pt)$, for the substitution of H_2O by a Cl^- ion at a position $trans$ to a coordinated Cl^- ligand is therefore correlated by a different linear trend line $\Delta\delta(^{195}Pt) = -127 - 79n$; $(R^2 > 0.99)$ compared to that resulting from the substitution of H_2O by a Cl^- ion at a position $trans$ to a H_2O $\Delta\delta(^{195}Pt) = -287.6 - 86.4n$; $(R^2 > 0.9999)$ as indicated in Figure 2.3B.
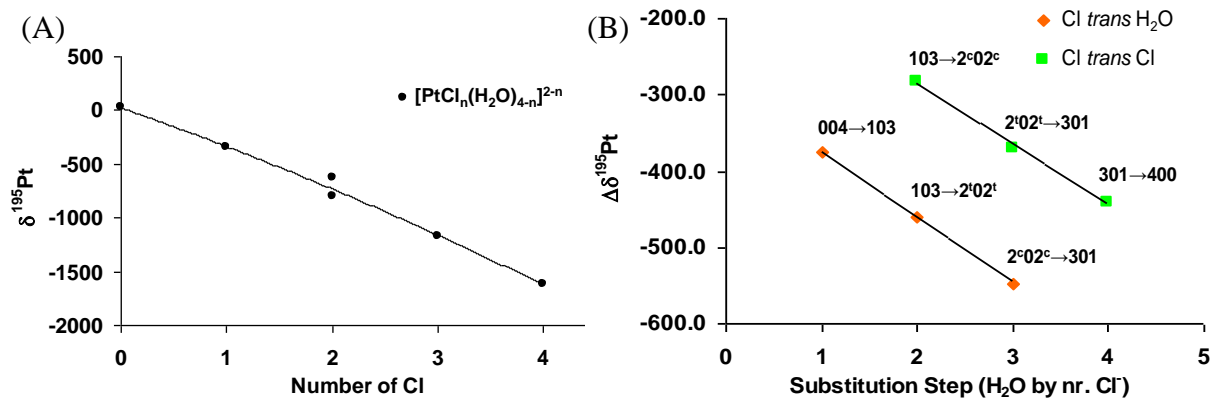
Figure 2.3: **(A)** Second-order correlations of $\delta(^{195}Pt)$ values for $[PtCl_n(H_2O)_{4-n}]^{2-n}$ ($n = 0\text{-}4$) complexes as a function of substituted Cl^-. **(B)** *Linear* correlation of substitutions for ◆ Cl^- *trans* to H_2O and ■ Cl^- *trans* to Cl^-.

The respective *trans* substitutions in Figure 2.3B are correlated with entries in Figure 2.1A by making use of the nomenclature code of Drew and Preetz.[19] In this case substitution of a H_2O ligand by a Cl^- ion *trans* to another H_2O ligand, causes a 92 - 106 ppm larger $\Delta\delta(^{195}Pt)$ compared to substitution of H_2O by a Cl^- ion *trans* to a Cl^- and allows discrimination between the stereoisomers. From this method of assignment, the $\delta(^{195}Pt)$ values at -629 and -805 ppm are assigned to the *trans*- and *cis*-$[PtCl_2(H_2O)_2]$ stereoisomers respectively along with the rest of the observed species and agrees well with assignments made previously.[20, 22] The assignments are indicated in Figure 2.2 and the specific values obtained are listed in Table 2.1 for comparison with literature values. The spectrum shown in Figure 2.2 was obtained ~1 h after the initial Cl^- addition was made. Detailed kinetic studies on Cl^- anation of $[Pt(H_2O)_4]^{2+}$ revealed that the first anation step is slow[18] while the subsequent second step is fast as a result of the kinetic Cl^- *trans* effect. The final speciation at equilibrium depends on the Cl^- concentration, temperature and ionic strength. For this reason ^{195}Pt NMR spectra were acquired at different times after the initial Cl^- addition in order to observe as many species possible in the solution. After ~2 hours no more $[Pt(H_2O)_4]^{2+}$ was observed as the species distribution approached equilibrium by forming the presumably thermodynamically more stable species in the order $n = 0\rightarrow4$ of the $[PtCl_n(H_2O)_{4-n}]^{2-n}$ series.

Table 2.1: $\delta(^{195}\text{Pt})$ data of the $[\text{PtCl}_n(\text{H}_2\text{O})_{4-n}]^{2-n}$ (n = 0-4) species compared to literature values. All values were obtained at 30°C in this study while the listed literature values were recorded between 18 and 28°C.

Complex species	Nomenclature code	$\delta(^{195}\text{Pt})$ (this work)	$\delta(^{195}\text{Pt})$ (previously reported values)
$[\text{Pt}(\text{H}_2\text{O})_4]^{2+}$	004	29	31 [21]
$[\text{PtCl}(\text{H}_2\text{O})_3]^+$	103	-346	-350 [20]
$trans\text{-}[\text{PtCl}_2(\text{H}_2\text{O})_2]$	2^t02^t	-629	-630 [21]
$cis\text{-}[\text{PtCl}_2(\text{H}_2\text{O})_2]$	2^c02^c	-805	-811 [20]
$[\text{PtCl}_3(\text{H}_2\text{O})]^-$	301	-1176	-1180 [9]
$[\text{PtCl}_4]^{2-}$	400	-1617	-1614 [3]

From Figure 2.3B it is clear that the principles which applies to the Pt(IV) complexes of $[\text{PtBr}_m\text{Cl}_n(\text{OH})_{6-m-n}]^{4-m-n}$ (m, n = 0-6) [14] also apply to the $[\text{PtCl}_n(\text{H}_2\text{O})_{4-n}]^{2-n}$ (n = 0-4) series of complexes even if the effective charge changes from 2+ to 2-. If all species can be obtained within the same solution i.e. under the same accurately defined reaction conditions, ^{195}Pt NMR chemical-shift-trend analysis appears to be a relatively robust method for the quick identification of complexes within a series. This method is consequently applied more confidently to the Pt(II)-*aqua-bromido* series in which the $\delta(^{195}\text{Pt})$ values have not been reported in the literature before, with $[\text{PtBr}_4]^{2-}$ the only exception.

2.3.2 Formation of the $[\text{PtBr}_m(\text{H}_2\text{O})_{4-m}]^{2-m}$ (m = 0-4) complex species and assignment with ^{195}Pt NMR chemical-shift-trend analysis

The $[\text{PtCl}_n(\text{H}_2\text{O})_{4-n}]^{2-n}$ (n = 0-4) complexes have been investigated in much more detail compared to the $[\text{PtBr}_m(\text{H}_2\text{O})_{4-m}]^{2-m}$ (m = 0-4) series of complexes as is reflected by the amount of literature dealing with these species. Although the Br⁻ anation of $[\text{Pt}(\text{H}_2\text{O})_4]^{2+}$ and aquation of $[\text{PtBr}_4]^{2-}$ have previously studied by UV-visible spectroscopy[23-26] no associated ^{195}Pt NMR studies have been reported. Apart from $[\text{PtBr}_4]^{2-}$, the $\delta(^{195}\text{Pt})$ values of the rest of the species in the series remains unknown and for this reason a ^{195}Pt NMR speciation study was of particularly interest. Addition of NaBr to a solution of $[\text{Pt}(\text{H}_2\text{O})_4]^{2+}$ (according to the method described in the experimental section) results in the formation of six signals, possibly correlating to the expected six $[\text{PtBr}_m(\text{H}_2\text{O})_{4-m}]^{2-m}$ (m = 0-4) complex species illustrated in Figure 2.1B. Due to the large $\Delta\delta(^{195}\text{Pt})$ between $[\text{Pt}(\text{H}_2\text{O})_4]^{2+}$ and $[\text{PtBr}_4]^{2-}$ it was necessary to acquire two different spectral windows 200 to -1800 and -1000

to -3000 ppm, in order to observe all complex species as shown in Figure 2.4 (the ^{195}Pt NMR spectra are joined as indicated below).
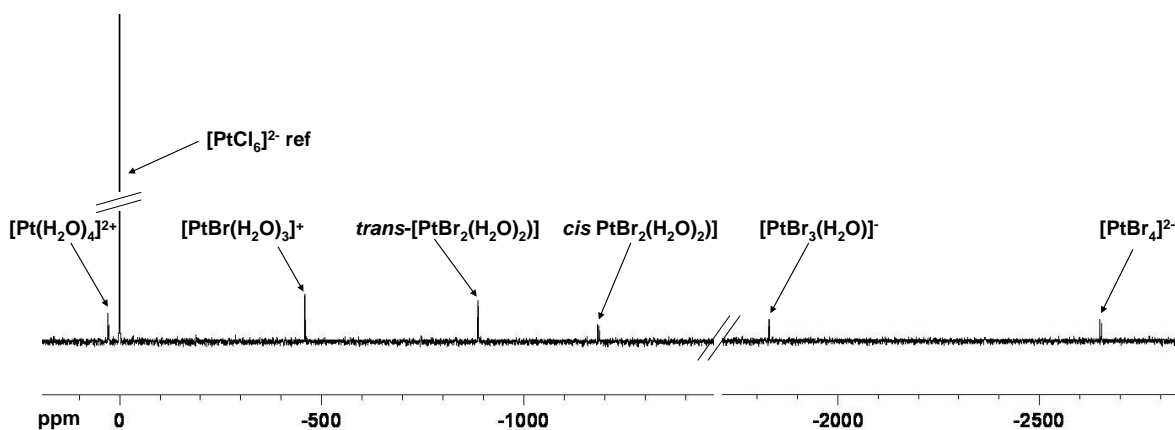
Figure 2.4: ^{195}Pt NMR spectra of the $[PtBr_m(H_2O)_{4-m}]^{2-m}$ (m = 0-4) complexes in 1 M HClO$_4$ obtained by adding NaBr to $[Pt(H_2O)_4]^{2+}$. Due to the large $\delta(^{195}$Pt$)$ range of this series, the ^{195}Pt NMR spectra were recorded in two different windows, linked as indicated.

A plot of the observed $\delta(^{195}$Pt$)$ value as a function of the number of coordinated Br$^-$ ligands, produces a systematic $\Delta\delta(^{195}$Pt$)$ value defined by the second-order correlation $\delta(^{195}$Pt$)$ = 27.3 - 418.2n - 63.3n^2; R^2 > 0.999 in Figure 2.5A.
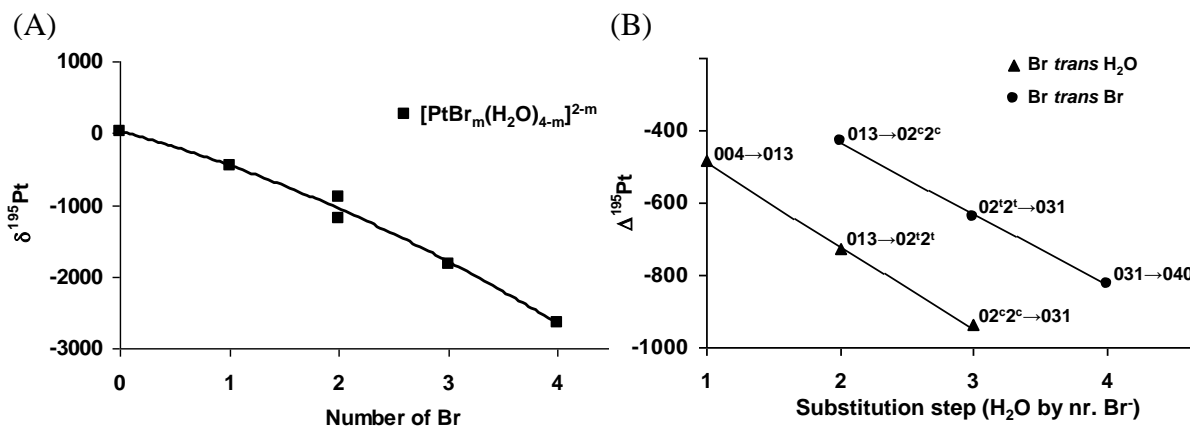
Figure 2.5: (A) Correlation of $\delta(^{195}$Pt$)$ NMR values of the $[PtBr_m(H_2O)_{4-m}]^{2-m}$ (m = 0-4) series as a function of the substituted ligand (H$_2$O with Br$^-$). **(B)** Correlations of substitutions for ▲ Br$^-$ *trans* to H$_2$O and ● Br$^-$ *trans* to Br$^-$

To assign the *trans*- and *cis*-$[PtBr_2(H_2O)_2]$ stereoisomers, the same principles were used as described for the *trans*- and *cis*-$[PtCl_2(H_2O)_2]$ stereoisomers. The substitution of a H$_2$O ligand with a Br$^-$ ion *trans* to another H$_2$O is defined by the linear trend line $\delta(^{195}$Pt$)$ = -

263.1 - 227.1n; $R^2 > 0.99$ compared to the substitution of a H_2O ligand with a Br^- ion *trans* to another Br^- coordinated ligand that is defined by the linear trend line $\delta(^{195}Pt) = -37.0 - 197.4n$; $R^2 > 0.99$. These plots are shown in Figure 2.5B and confirm that the $\delta(^{195}Pt)$ values at -887 and -1187 ppm are assigned to the *trans-* and *cis-*[PtBr$_2$(H$_2$O)$_2$] complex species respectively. The respective substitution reactions in Figure 2.5B are also illustrated in Figure 2.1B for better clarity and the respective substitution reactions are indicated by the correlating nomenclature codes. The $\delta(^{195}Pt)$ values of [PtBr$_3$(H$_2$O)]$^+$, *trans/cis-*[PtBr$_2$(H$_2$O)$_2$] and [PtBr$_3$(H$_2$O)]$^-$ have not been reported in the literature before and is listed in Table 2.2.

Table 2.2: $\delta(^{195}Pt)$ values of the [PtBr$_m$(H$_2$O)$_{4-m}$]$^{2-m}$ (m = 0-4) species compared to available literature values. All values were obtained at 30°C in this study while the listed literature value was recorded at 28°C.

Complex species	Nomenclature code	$\delta(^{195}Pt)$ (this work)	$\delta(^{195}Pt)$ (previously reported values)
[Pt(H$_2$O)$_4$]$^{2+}$	004	26	31 [21]
[PtBr(H$_2$O)$_3$]$^+$	013	-459	
trans-[PtBr$_2$(H$_2$O)$_2$]	02^{t}2^t	-887	
cis-[PtBr$_2$(H$_2$O)$_2$]	02^{c}2^c	-1187	Not reported
[PtBr$_3$(H$_2$O)]$^-$	031	-1825	
[PtBr$_4$]$^{2-}$	040	-2648	-2690 [12]

The above results and associated correlations show that the principles of ^{195}Pt NMR chemical-shift-trend analysis is also valid for the [PtBr$_m$(H$_2$O)$_{4-m}$]$^{2-m}$ (m = 0-4) complex species, suggesting that it may be valid for more complex distributions of Pt(II) complexes. These principles are consequently applied to solutions containing the [PtCl$_n$Br$_m$(H$_2$O)$_{4-n-m}$]$^{2-n-m}$ (n, m = 0-4) species.

2.3.3   Formation of the [PtCl$_n$Br$_m$(H$_2$O)$_{4-n-m}$]$^{2-n-m}$ (n, m = 0-4) complex species and assignment with chemical-shift-trend analysis

Although Kerrison and Sadler[13] reported the $\delta(^{195}Pt)$ values for the [PtCl$_n$Br$_{4-n}$]$^{2-}$ (n = 0-4) complexes, the mixed *Pt(II)-aqua-bromido-chlorido* species has not been studied and almost no related literature can be found concerned with the [PtCl$_n$Br$_m$(H$_2$O)$_{4-n-m}$]$^{2-n-m}$ (n, m = 0-3) complexes. It was attempted to generate all 21 possible Pt(II) complexes [PtCl$_n$Br$_m$(H$_2$O)$_{4-n-m}$]$^{2-n-m}$ (n, m = 0-4) in one solution by adding equal quantities of NaCl and NaBr to a [Pt(H$_2$O)$_4$]$^{2+}$ solution. All the species could not be generated in one solution

via Cl⁻ and Br⁻ anation of $[Pt(H_2O)_4]^{2+}$ under one set of conditions. The large number of possible species compared to the relatively low starting concentration of $[Pt(H_2O)_4]^{2+}$, in addition to the expected variable thermodynamic stabilities of these mixed halide complexes may account for why some of the aquated species are not observed when employing this synthetic approach. As a consequence two different methods of synthesis were used to generate the species in this series at concentrations sufficient to detect by [195]Pt NMR spectroscopy in a reasonable time period (as described in the experimental section).

Addition of NaCl and NaBr to a 0.15 M $[Pt(H_2O)_4]^{2+}$ solution in 1 M HClO₄ resulted in the formation of the complex species observed in the left part of the [195]Pt NMR spectrum shown in Figure 2.6. The species observed in the right part of the spectrum were obtained from another solution by mixing 0.2 M $[PtCl_4]^{2-}$ with 0.2 M $[PtBr_4]^{2-}$ in 1 M HClO₄. For this reason the signal/noise ratio is better in the spectrum on the right hand side. [195]Pt NMR spectra were collected continuously after initial mixing the solutions in order to observe as many complexes as possible. For this reason the relative intensities of the observed complexes do not present the concentrations at equilibrium.
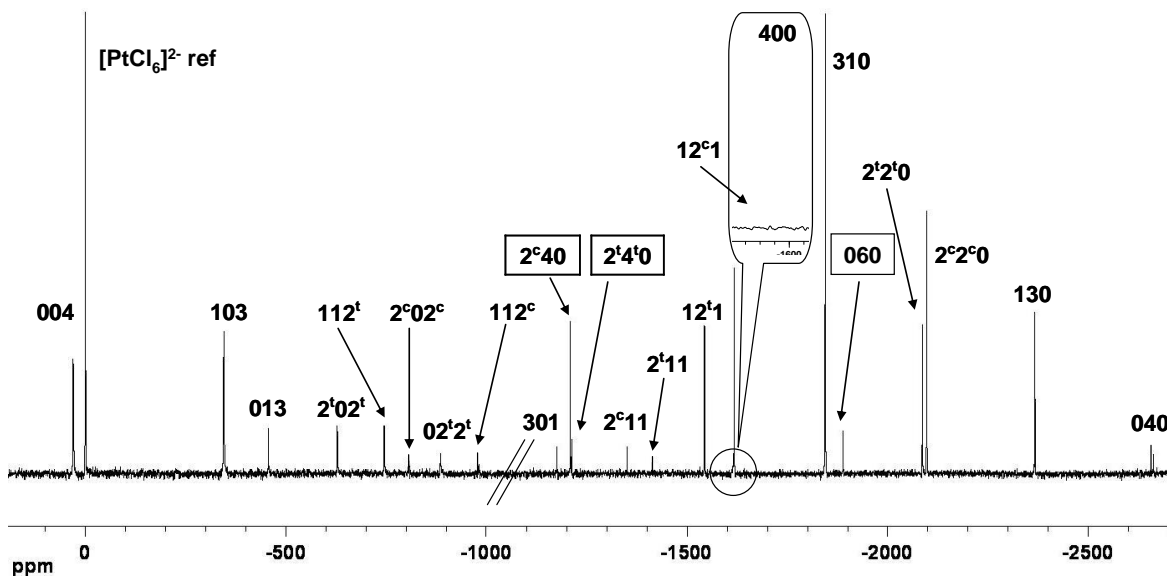
Figure 2.6: [195]Pt NMR spectra of the $[PtBr_mCl_n(H_2O)_{4-m-n}]^{2-m-n}$ (*m, n* = 0-4) complexes observed in 1 M HClO₄. These complexes were generated in two different solutions and acquired in two different spectral windows and linked as indicated above. The Pt(IV) species 2^{c}40, 2^{t}4^{t}0 and 060 were detected in the solution which originates from a $[PtBr_6]^{2-}$ impurity in the $[PtBr_4]^{2-}$ salt (obtained from Aldrich).

19

A plot of all the observed $\delta(^{195}Pt)$ values as a function of coordinated Br^- ions (0-4) reveals five distinctly different groups of complexes correlated by systematic $\Delta\delta(^{195}Pt)$ values and defined by different second-order functions as shown in Figure 2.7.
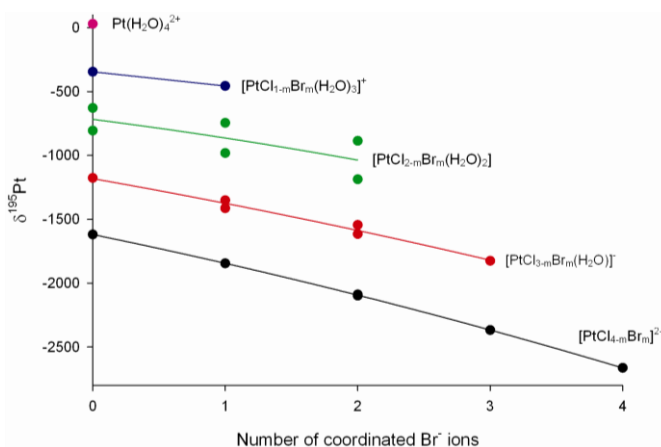
Figure 2.7: All the $[PtBr_mCl_n(H_2O)_{4-m-n}]^{2-m-n}$ (*m, n* = 0-4) complexes are shown and grouped as five distinct groups of $[PtCl_n(H_2O)_{4-n}]^{2-n}$ (*n* = 0-4) showing increased Br^- coordination and substitution of Cl^- which results in five groups with the same formal charge.

All the possible $[PtCl_nBr_m(H_2O)_{4-n-m}]^{2-n-m}$ (*n, m* = 0-4) species are illustrated in Figure 2.8 for comparison to the experimental result. The arrows do not necessarily represent the only pathways of formation but is shown merely to illustrate the different possible complexes. Formation of all species in the series can be envisaged by Cl^- substitution of the Br^- ligands in the $[PtBr_m(H_2O)_{4-m}]$ (*m* = 0-4) series, resulting in five different groups with the same formal charge.

A comparison of the experimental values in Figure 2.7 with the different group of complexes in Figure 2.8 reveals a similar pattern of number of complexes for each group. From previously reported values for the $[PtCl_nBr_{4-n}]^{2-}$ (*n* = 0-4) complexes, it is evident that the most up-field second-order correlation must correspond to the six $\delta(^{195}Pt)$ values of this series. According to the principles defined earlier for the $[PtCl_n(H_2O)_{4-n}]^{2-n}$ (*n* = 0-4) and $[PtBr_m(H_2O)_{4-m}]^{2-m}$ (*m* = 0-4) series, the second most up-field set of $\delta(^{195}Pt)$ values in Figure 2.7 must be associated with complex species that contains one coordinated H_2O ligand i.e. the six possible complex species of the $[PtCl_{4-m}Br_m(H_2O)]^-$ (*m* = 0-3) series. By the same analogy, the species which forms part of the third and fourth graphs are assigned to the six possible $[PtCl_{4-m}Br_m(H_2O)_2]$ (*m* = 0-2) complexes and the two possible $[PtCl_{4-m}Br_m(H_2O)_3]^+$

(m = 0-1) complexes. Finally the most downfield $\delta(^{195}\text{Pt})$ value is assigned to the known value of $[\text{Pt}(\text{H}_2\text{O})_4]^{2+}$.
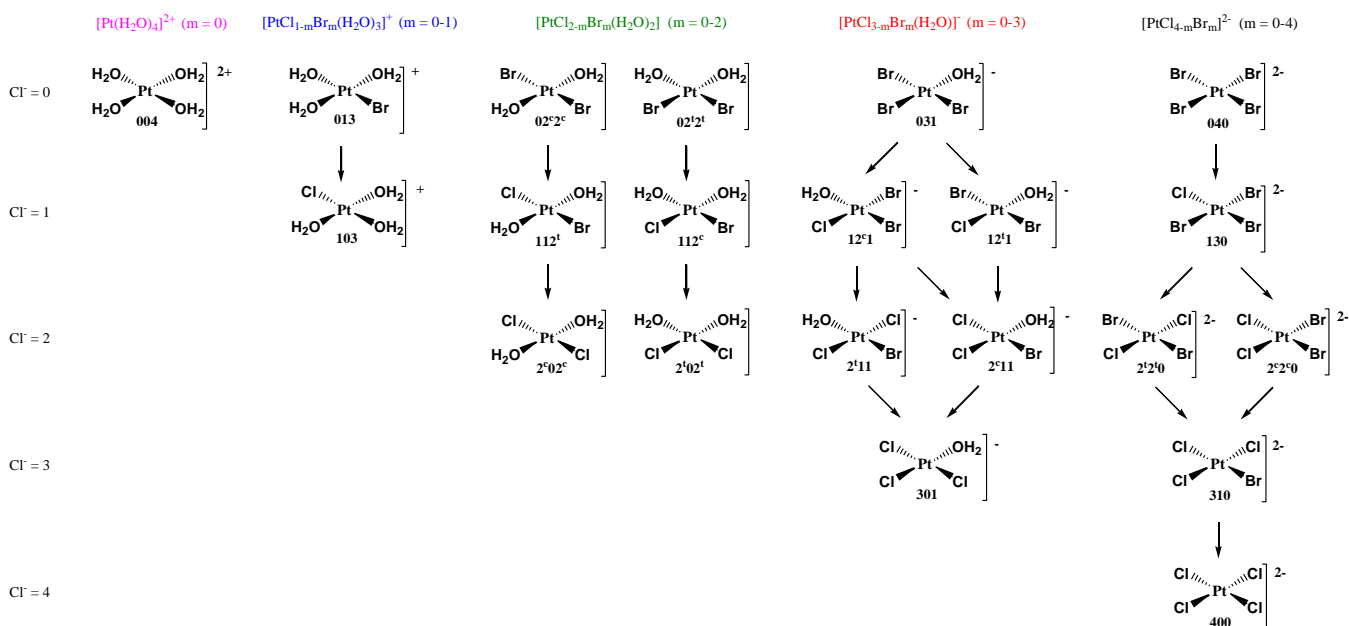
Figure 2.8: Reaction scheme illustrating the stepwise substitution of coordinated Br$^-$ with Cl$^-$ ions in the $[\text{PtBr}_m(\text{H}_2\text{O})_{4-m}]^{2-m}$ (m = 0-4) series. Arrows do not represent the only mechanistic pathways of formation but is shown merely to illustrate the different possible complexes.

In order to assign the stereoisomers, $\Delta\delta(^{195}\text{Pt})$ values for specific substitution reactions were evaluated as previously described. For the $[\text{PtCl}_n\text{Br}_{4-n}]^{2-}$ (n = 0-4) series, the $\Delta\delta(^{195}\text{Pt})$ value for substitution of a coordinated Cl$^-$ by Br$^-$ *trans* to another Cl$^-$ ligand is consistently 10 ppm smaller than substitution of Cl$^-$ *trans* to Br$^-$. Plotting $\Delta\delta(^{195}\text{Pt})$ values for the respective *trans* substitution reactions thus presents two different linear trends as shown in Figure 2.9A and allow assignment of *trans*- and *cis*-[PtCl$_2$Br$_2$]. The $[\text{PtCl}_{4-m}\text{Br}_m(\text{H}_2\text{O})]^-$ (m = 0-3) series contains two sets of stereoisomers i.e. *trans*- and *cis*-[PtCl$_2$Br(H$_2$O)]$^-$ and *trans*- and *cis*-[PtClBr$_2$(H$_2$O)]$^-$. Substitution of a coordinated Cl$^-$ ligand by Br$^-$ *trans* to another Cl$^-$ ligand is consistently 60 ppm smaller than substitution of Cl$^-$ *trans* to Br$^-$ so that the stereoisomers can be assigned from the respective substitution reactions illustrated here in Figure 2.9B. Finally substitution of a coordinated Cl$^-$ ligand by a Br$^-$ ion *trans* to another Cl$^-$ ligand is consistently 130 ppm smaller (not shown here) than substitution of Cl$^-$ *trans* to Br$^-$ in the $[\text{PtCl}_{4-m}\text{Br}_m(\text{H}_2\text{O})_2]$ (m = 0-2) series and allow identification of the six stereoisomers in this series. Unfortunately the [PtBr$_3$(H$_2$O)]$^-$ (031) and *cis*-[PtBr$_2$(H$_2$O)$_2$] (02^{c}2^c) species could not be observed in either of the ^{195}Pt NMR spectra in Figure 2.9.

21

Hence $\delta(^{195}\text{Pt})$ values obtained for these complexes in Figure 2.6 were used to complete the trend analysis curves, which resulted in excellent $\delta(^{195}\text{Pt})$ *vs.* number of Cl⁻/Br⁻ ligand substitution correlations as is illustrated in Figure 2.9B.

(A)

(B)
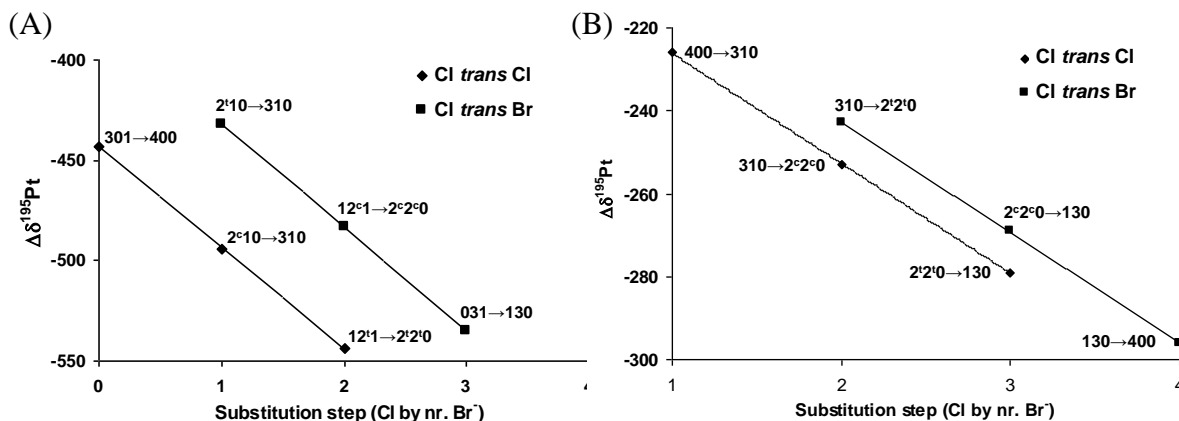
Figure 2.9: (A) Chemical shift difference $\Delta\delta(^{195}\text{Pt})$, between $[\text{PtBr}_m\text{Cl}_{4-m}]^{2-}$ (*m, n* = 0-4) species in which ◆ Cl⁻ *trans* to Cl⁻ and ■ Cl⁻ *trans* to Br⁻ is substituted by Br⁻. **(B)** Chemical shift difference $\Delta\delta(^{195}\text{Pt})$, between $[\text{PtCl}_{3-m}\text{Br}_m(\text{H}_2\text{O})]^-$ (*m* = 0-3) species in which ◆Cl⁻ *trans* to Cl⁻ and ■ Cl⁻ *trans* to Br⁻ is substituted by Br⁻.

Interestingly, the commercially obtained K_2PtBr_4 salt obtained from Aldrich, appears to contain $[\text{PtBr}_6]^{2-}$ impurities, and consequently some mixed Pt(IV)-*bromido-chlorido* species are observed (2ᶜ40, 2ᵗ4ᵗ0 and 060) and indicated in Figure 2.6. These can be identified from the $^{35}\text{Cl}/^{37}\text{Cl}$ isotopic shifts which is effectively eliminated in the Pt(II) species due to the NMR chemical shift anisotropy effect. A detailed discussion of $^{35}\text{Cl}/^{37}\text{Cl}$ isotopic effects in Pt(IV)-*aqua-chlorido* complexes are deferred to Chapter 3. The $\delta(^{195}\text{Pt})$ values of all the $[\text{PtBr}_m\text{Cl}_n(\text{H}_2\text{O})_{4-m-n}]^{2-m-n}$ (*m, n* = 0-4) complexes observed in solution are listed in Table 2.3. Ten of these complexes are reported here for the first time.

Table 2.3: The $\delta(^{195}\text{Pt})$ values of all the $[\text{PtBr}_m\text{Cl}_{m-4}(\text{H}_2\text{O})]^-$ (*m* = 0-4) complexes is listed and compared to available literature values. These values were obtained at 30°C in 1 M HClO_4.

Code	Number of H_2O	Complex species	$\delta(^{195}\text{Pt})$ ppm	Literature values
040	0	$[\text{PtBr}_4]^{2-}$	-2663	-2690 [12]
130	0	$[\text{PtClBr}_3]^{2-}$	-2367	-2380 [13]
2ᶜ2ᶜ0	0	c-$[\text{PtCl}_2\text{Br}_2]$	-2098	-2111 [13]
2ᵗ2ᵗ0	0	t-$[\text{PtCl}_2\text{Br}_2]$	-2088	-2101 [13]
310	0	$[\text{PtCl}_3\text{Br}]^{2-}$	-1845	-1858 [13]

Table 2.3 continued from the previous page.

031	1	$[PtBr_3(H_2O)]^-$	-1825	Not reported
400	0	$[PtCl_4]^{2-}$	-1619	-1614 [3]
12^c1	1	c-$[PtClBr_2(H_2O)]$	-1616	
12^t1	1	t-$[PtClBr_2(H_2O)]$	-1544	
2^t11	1	t-$[PtCl_2Br(H_2O)]$	-1413	Not reported
2^c11	1	c-$[PtCl_2Br(H_2O)]$	-1351	
02^c2^c	2	c-$[PtBr_2(H_2O)_2]$	-1187	
301	1	$[PtCl_3(H_2O)]^-$	-1177	-1180 [9]
112^c	2	c-$[PtClBr(H_2O)_2]$	-982	Not reported
02^t2^t	2	t-$[PtBr_2(H_2O)_2]$	-886	
2^c02^c	2	c-$[PtCl_2(H_2O)_2]$	-806	-811 [20]
112^t	2	t-$[PtClBr(H_2O)_2]$	-746	Not reported
2^t02^t	2	t-$[PtCl_2(H_2O)_2]$	-629	-630 [21]
013	3	$[PtBr(H_2O)_3]^+$	-457	Not reported
103	3	$[PtCl(H_2O)_3]^+$	-346	-350 [20]
004	4	$[Pt(H_2O)_4]^{2+}$	29	31 [21]

2.4   Conclusions

All of the $[PtCl_n(H_2O)_{4-n}]$ (n = 0-4) complexes could be obtained in solution *via* chloride anation of $[Pt(H_2O)_4]^{2+}$ or $[PtCl_4]^{2-}$ aquation, driven by the precipitation of AgCl with addition of AgClO_4. The $[PtBr_m(H_2O)_{4-m}]$ (m = 0-4) series of complexes was only obtained *via* bromide anation of $[Pt(H_2O)_4]^{2+}$. Formation of these complexes *via* $[Pt(H_2O)_4]^{2+}$ anation is possible as a result of the presumed thermodynamic stability increase of complexes with a decreasing number of coordinated H_2O (thermodynamic stability increase n, m = 0→4). Systematic up-field shifts result from coordination of chloride or bromide to $[Pt(H_2O)_4]^{2+}$. The complexes $[PtCl_4]^{2-}$ and $[PtBr_4]^{2-}$ are therefore the most shielded in the respective series, whereas $[Pt(H_2O)_4]^{2+}$ is the least shielded. A plot of the observed $\delta(^{195}Pt)$ as a function of the number of coordinated chloride or bromide ions can be defined by a second-order correlation and allow assignment between complex species where n, m = 0-4. Substitution of H_2O by Cl^- *trans* to another Cl^-, give the same $\delta(^{195}Pt)$ value, while substitution of H_2O *trans* to another H_2O give a different value. The same principle is also valid for substitution of H_2O by Br^-. This property of the $[PtCl_n(H_2O)_{4-n}]$ (n = 0-4) and $[PtBr_m(H_2O)_{4-m}]$ (m = 0-4) series of complexes allow assignment of *cis*/*trans*-$[PtCl_2(H_2O)_2]$ and *cis*/*trans*-$[PtBr_2(H_2O)_2]$ stereoisomers in the respective series. The value of this method is demonstrated in the rapid assignment of all 21 possible $[PtCl_nBr_m(H_2O)_{4-n-m}]^{2-n-m}$ (n, m =

0-4) complexes, showing that ^{195}Pt NMR chemical-shift-trend analysis as carried out here, is a relatively robust method to quickly identifying Pt(II)-*aqua-bromido-chlorido* complexes in complicated solutions. The $\delta(^{195}$Pt$)$ of nine of the $[PtCl_nBr_m(H_2O)_{4-n-m}]^{2-n-m}$ (*n, m* = 0-4) complexes are reported here for the first time. This method of analysis is accurate even though the formal charge of the species changes from -2→+2 within the series and successfully account for the anticipated more complicated hydration network and possible electrostatic effects. The principles of ^{195}Pt NMR chemical-shift-trend analysis established here for Pt(II)-*aqua-bromido-chlorido* species is also valid for Pt(IV)-*aqua-bromido-chlorido* complexes as will be shown in *Chapter 3* and *4*, and is applied throughout this thesis to validate the assignment of Pt(II) and Pt(IV) complexes in solution.

2.5   References

1. C. Carr, P. L. Goggin, R. J. Goodfellow, *Inorg. Chim. Acta,* 1984, *81*, L25-L26.

2. J. Duvigneau, G. Peters, W. Preetz, *Z. Anorg. Allg. Chem.,* 1993, *619*, 2043-2049.

3. J. J. Pesek, W. R. Mason, *J. Magn. Reson.,* 1977, *25*, 519-529.

4. B. M. Still, P. G. A. Kumar, J. R. Aldrich-Wright, W. S. Price, *Chem. Soc. Rev.,* 2007, *36*, 665-686.

5. P. S. Pregosin, *Coord. Chem. Rev.,* 1982, *44*, 247-291.

6. J. R. L. Priqueler, I. S. Butler, F. D. Rochon, *Appl. Spectrosc. Rev.,* 2006, *41*, 185-226.

7. K. R. Koch, M. R. Burger, J. Kramer, A. N. Westra, *Dalton Trans.,* 2006, 3277-3284.

8. S. J. S. Kerrison, P. J. Sadler, *Dalton Trans.: Inorg. Chem.,* 1982, 2363-2369.

9. W. Freeman, P. S. Pregosin, S. N. Sze, L. M. Venanzi, *J. Magn. Reson.,* 1976, *22*, 473-478.

10. S. M. Cohen, T. H. Brown, *J. Chem. Phys.,* 1974, *61*, 2985-2986.

11. P. L. Goggin, R. J. Goodfellow, S. R. Haddock, B. F. Taylor, I. R. H. Marshall, *Dalton Trans.: Inorg. Chem.,* 1976, 459-467.

12. A. Von Zelewsky, *Helv. Chim. Acta,* 1968, *51*, 803-807.

13. S. J. S. Kerrison, P. J. Sadler, *J. Magn. Reson.,* 1978, *31*, 321-325.

14. J. Kramer, K. R. Koch, *Inorg. Chem.,* 2007, *46*, 7466-7476.

15. J. Kramer, K. R. Koch, *Inorg. Chem.,* 2006, *45*, 7843-7855.

16. M. R. Burger, J. Kramer, H. Chermette, K. R. Koch, *Magn. Reson. Chem.,* 2010, *48*, S38-S47.

17. L. I. Elding, *Inorg. Chim. Acta,* 1976, *20*, 65-69.

18. L. I. Elding, *Inorg. Chim. Acta,* 1978, *28*, 255-262.

19. W. Preetz, G. Peters, D. Bublitz, *Chem. Rev.,* 1996, *96*, 977-1025.

20. T. G. Appleton, J. R. Hall, S. F. Ralph, C. S. M. Thompson, *Inorg. Chem.,* 1984, *23*, 3521-3525.

21. O. Groning, T. Drakenberg, L. I. Elding, *Inorg. Chem.,* 1982, *21*, 1820-1824.

22. O. Groning, L. I. Elding, *Inorg. Chem.,* 1989, *28*, 3366-3372.

23. L. I. Elding, *Acta Chem. Scand.,* 1970, *24*, 2546-2556.

24. L. I. Elding, *Acta Chem. Scand.,* 1970, *24*, 2557-2564.

25. L. I. Elding, L. F. Olsson, *J. Phys. Chem.,* 1978, *82*, 69-74.

26. J. E. Teggins, D. S. Martin, Jr., *Inorg. Chem.,* 1967, *6*, 1003-1007.

Chapter 3

Isotope effects in high-resolution ^{195}Pt NMR: a fingerprint for the unambiguous assignment of Pt(IV)-aqua-chlorido and Pt(IV)-chlorido-hydroxido complexes in aqueous solution.

3.1   Introduction

The use of high-resolution ^{195}Pt NMR spectroscopy to examine the speciation of platinum complexes in chloride ion-rich acidic solutions, has shown the utility of ^{195}Pt 'chemical-shift-trend' analysis as a means to rapidly assign various Pt(II)-aqua-bromido-chlorido (*Chapter 2*) and Pt(IV)-bromido-chlorido-hydroxido[1] complexes in solutions of well defined origin. While this method allows for the rapid identification of such species with considerable certainty, the sensitivity of $\delta(^{195}$Pt) to other factors such as concentration, solvent composition,[2] temperature[3] and ionic strength,[4] demand an additional spectroscopic method for the unambiguous identification of Pt(II) and Pt(IV) complexes. Another limitation of ^{195}Pt NMR chemical-shift-trend analysis is that several species in a specific series needs to be present in solution in order to make accurate assignments, which is not always possible.

Almost 3 decades ago, Ismail *et al.*[5] demonstrated that at high magnetic field (9.4 T), ^{35}Cl/^{37}Cl isotope shifts can be resolved for the $[PtCl_6]^{2-}$ complex into an approximate five signal pattern recognized as "isotopomers" (Figure 3.1). The peak height ratios were correlated with the expected signal intensities of the $[Pt^{35}Cl_n^{37}Cl_{6-n}]^{2-}$ (n = 0-6) isotope signals due to the natural abundance of the ^{35}Cl (75.4 %) and ^{37}Cl (24.6 %) isotopes. Although seven isotope signals are statistically possible, $[Pt^{35}Cl^{37}Cl_5]^{2-}$ and $[Pt^{37}Cl_6]^{2-}$ were not observed due to the low statistical probability of these isotope signals (0.38 and 0.02 % respectively).
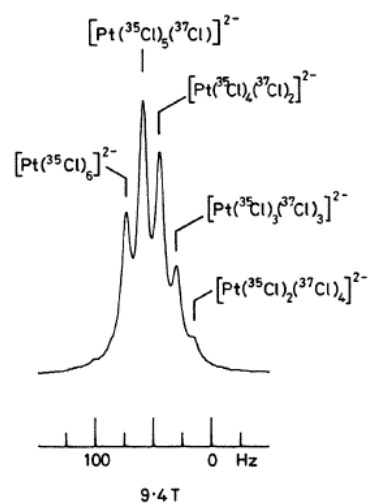
Figure 3.1: ^{195}Pt NMR resolved spectrum of $[PtCl_6]^{2-}$ reported by Ismail *et al.*[5] revealing $[Pt^{35}Cl_n^{37}Cl_{6-n}]^{2-}$ (n = 2-6) isotope shifts.

There is some confusion regarding the terms *isotopologue* and *isotopomer* in the NMR literature. Generally the term *isotopomer* has been used when in fact *isotopologues* were at hand. The term *isotopologue* is used to refer to a chemical species that differ only in isotopic composition of their molecules or ions e.g. $[Pt^{35}Cl_6]^{2-}$ and $[Pt^{35}Cl_5^{37}Cl]^{2-}$. *Isotopomers* are isomers with the same number of isotopic atoms, differing in their position in the molecule or ion e.g. *trans*-$[Pt^{35}Cl_4^{37}Cl_2]^{2-}$ where both ^{37}Cl isotopes are *trans* to each other *vs.* *cis*-$[Pt^{35}Cl_4^{37}Cl_2]^{2-}$ where both ^{37}Cl isotopes are *trans* to ^{35}Cl isotopes. In Figure 3.1 the signals were therefore referred to incorrectly as *isotopomers* by Ismail *et al.*[5] since only *isotopologues* are observed.

Based on the work of Ismail *et al.*[5] it was anticipated that the isotope effect may be a new way to characterize $[PtCl_n(H_2O)_{6-n}]^{4-n}$ (n = 1-5) *aqua* and $[PtCl_n(OH)_{6-n}]^{2-}$ (n = 1-5) *hydroxido* complexes. Since for $[PtCl_6]^{2-}$ seven $^{35}Cl/^{37}Cl$ isotopologues are expected, six signals are expected for $[PtCl_5(H_2O)]^-$, five for *cis/trans*-$[PtCl_4(H_2O)_2]$ and so on. However, the situation is more perplexing, since *isotopologue* and *isotopomer* effects are observed for the Pt(IV)-*aqua*-chlorido complexes while only *isotopologue* effects are observed for Pt(IV)-chlorido-*hydroxido* complexes.

In this chapter the $^{35}Cl/^{37}Cl$ isotope shifts for all of the $[PtCl_n(H_2O)_{6-n}]^{4-n}$ (n = 1-5) *aqua* and $[PtCl_n(OH)_{6-n}]^{2-}$ (n = 1-5) *hydroxido* complexes are resolved with high resolution ^{195}Pt NMR. Least-squares analysis of the $^{35}Cl/^{37}Cl$ isotope shifts is applied as an alternative to peak intensities for calculation of peak ratios. The hierarchy of isotope splitting is investigated in more detail as a means for additional spectroscopic confirmation of isotope effects that arise when both $^{16}O/^{18}O$ and $^{35}Cl/^{37}Cl$ isotopes are present in $H_2^{18}O$ enriched solution containing the $[PtCl_n(H_2O)_{6-n}]^{4-n}$ (n = 1-5) complex species.

3.2   Experimental

3.2.1   Reagents

The platinum salts potassium tetrachloroplatinate(II) (99.9+ %, K_2PtCl_4, Aldrich), were of reagent grade quality and used without further purification and stored in a desiccator. Oxidizing agents hydrogen peroxide (30%, H_2O_2, Riedel-de Haën) and sodium chlorate (99+ %, Sigma-Aldrich, $NaClO_3$), were of reagent grade quality and used as is. Deuterium oxide (99.9 %, D_2O, Aldrich) was used as solvent to obtain a lock signal for NMR measurements. Perchloric acid (70 %, $HClO_4$, 1L = 1.68 kg, MERCK) was used as stock for $HClO_4$ dilutions and $H_2^{18}O$ (97% $H_2^{18}O$, Isotec) was used for isotopic enrichment. All aqueous solutions were made with ultra pure de-ionized water (Milli-Q > 18 MΩ) and degassed with Ar to remove O_2 for at least 1 h prior to use.

3.2.2   Instrumentation

^{195}Pt NMR spectroscopy

128.8 MHz ^{195}Pt NMR spectra were recorded at various temperatures (278 – 303 K) using a Varian INOVA 600 MHz spectrometer, with a 5 mm broad-band probe. Essensially the same parameters described in Chpater 2 were used. In order to observe the best resolved ^{195}Pt NMR isotopologue and isotopomer spectra, careful magnetic field shimming and thermally equilibration of solutions (which typically takes 15-20 minutes) is essential. It is also important to avoid ^1H – decoupling which induces large temperature fluctuations. Chemical shifts (ppm) are reported relative to $[PtCl_6]^{2-}$ at $\delta(^{195}Pt) = 0$ ppm where applicable. Since no absolute referencing was necessary and better resolved spectra were obtained by shimming with internal D_2O (30 % v/v), no external reference solution was used in most cases. Typical resonance line-widths ($\nu_{1/2}$) at optimum temperatures ranged from 9-12 Hz, and ^{195}Pt NMR spectra were processed with a line broadening factor of 1-2 Hz to observe $^{35}Cl/^{37}Cl$ isotope shifts. A line broadening factor of 10 Hz was sufficient to observe $^{16}O/^{18}O$ isotope effects.

3.2.3   Preparation of solutions used to observe $^{35}Cl/^{37}Cl$ and $^{16}O/^{18}O$ isotopic shifts

Three 0.25 M $[PtCl_6]^{2-}$ solutions (I –III) prepared under subdued lighting by dissolving 102 mg $H_2PtCl_6 \cdot 2H_2O$ in 1000 μL 42 % (v/v) D_2O containing the appropriate quantity of concentrated $HClO_4$ and concentrated HCl (I = 1 M $HClO_4$, II = 1 M $HClO_4$ + 1 M HCl and III = 1 M $HClO_4$ + 6M HCl) were examined.

The $[Pt^{35/37}Cl_n(H_2O)_{6-n}]^{4-n}$ (n = 1-6) complexes were obtained to observe $^{35}Cl/^{37}Cl$ isotope shifts by dissolving 83 mg K_2PtCl_4 in 1000 μL of 1 M $HClO_4$ containing 30 % (v/v) D_2O. This solution was oxidized with five mol equivalents of $NaClO_3$ (with respect to Pt(II)) by stirring the solution at 60°C for five minutes as indicated by a change in color from red-orange to bright yellow. No Pt(II) remained in the deshielded region relative to the $[PtCl_6]^{2-}$ reference as confirmed by ^{195}Pt NMR.

The $[Pt^{35/37}Cl_n(H_2{}^{16/18}O)_{6-n}]^{4-n}$ (n = 2-6) series was obtained to observe $^{16}O/^{18}O$ istope shifts by dissolving 168 mg K_2PtCl_4 in 1000 μl 2 M $HClO_4$ containing 30 % (v/v) D_2O and 30 % $H_2{}^{18}O$ (v/v). This solution was also oxidized with five mol equivalents of $NaClO_3$ (with respect to Pt(II)) at 60°C for five minutes and coincided with the same color change observed above. In order to obtain high concentrations of the $[PtCl_n(OH)_{6-n}]^{2-}$ (n = 1-5) *hydroxido* complexes, two different methods of synthesis were used. The $[PtCl_n(OH)_{6-n}]^{2-}$ (n = 1-3) complexes were obtained by adding six mol equivalents of NaOH (with respect to Pt(IV)) to a 0.2 M $[PtCl_6]^{2-}$ solution in water. The $[PtCl_n(OH)_{6-n}]^{2-}$ (n = 4-5) complexes were obtained in high concentration by oxidation of 0.2 M $[PtCl_4]^{2-}$ in 0.5 M $HClO_4$ with five mol equivalents $NaClO_3$ (with respect to Pt(II)) and subsequent treatment with 2 M NaOH to adjust the pH to 9.

3.3   Results and discussion

3.3.1 ^{195}Pt NMR chemical shifts of $[Pt^{35}Cl_n{}^{37}Cl_{6-n}]^{2-}$ (n = 1-6) isotopologues and temperature effect on the resonance

A ^{195}Pt NMR spectrum of 0.25 M $[PtCl_6]^{2-}$ in 1 M $HClO_4$ and 6 M HCl was recorded at the optimal temperature of 20°C (*vide infra*). Under these reaction conditions, one large resonance signal of $[PtCl_6]^{2-}$ can be observed at *ca.* -12 ppm. The ^{195}Pt NMR FID was processed by applying an exponential line broadening factor of 2 Hz, which clearly resolves the signal into six different $[Pt^{35}Cl_n{}^{37}Cl_{6-n}]^{2-}$ (n = 1-6) isotopologues (Figure 3.2A), comparable with the spectrum shown in Figure 3.1. The relative statistical probability, $P(n)$, for each of the $[Pt^{35}Cl_n{}^{37}Cl_{6-n}]^{2-}$ (n = 0-6) isotopologues at the fractional natural abundance[6] (α) of ^{35}Cl (0.7553 %) and ^{37}Cl (0.2447 %) were calculated from Equation 3.1 where n, r = no. of coordinated ^{35}Cl and ^{37}Cl ions.

$$P(n) = \sum_{n=0}^{n=\frac{(n+r)!}{n!r!}} (\alpha_{35Cl}^{n}\alpha_{37Cl}^{r}) \qquad (3.1)$$

The ^{195}Pt chemical shifts of the respective ^{35}Cl/^{37}Cl isotopologues, $\delta_{itl}(^{195}Pt)$ were then simulated from the sum of seven Lorentzian peaks of equal peak width at half height (v½ = 8.1 Hz) and fixed isotope chemical shift spacing per ^{35}Cl/^{37}Cl isotopologue. The non-linear least-squares fit between the experimental and simulated ^{195}Pt spectrum of $[Pt^{35}Cl_n{}^{37}Cl_{6-n}]^{2-}$ (n = 1-6) (Figure 3.2A *vs*. B) with a 0.171 ppm up-field isotope shift per ^{35}Cl/^{37}Cl isotopologue ($\Delta\delta_{itl}(^{195}Pt)$) is excellent, confirming the isotopologue model (Table 3.1).
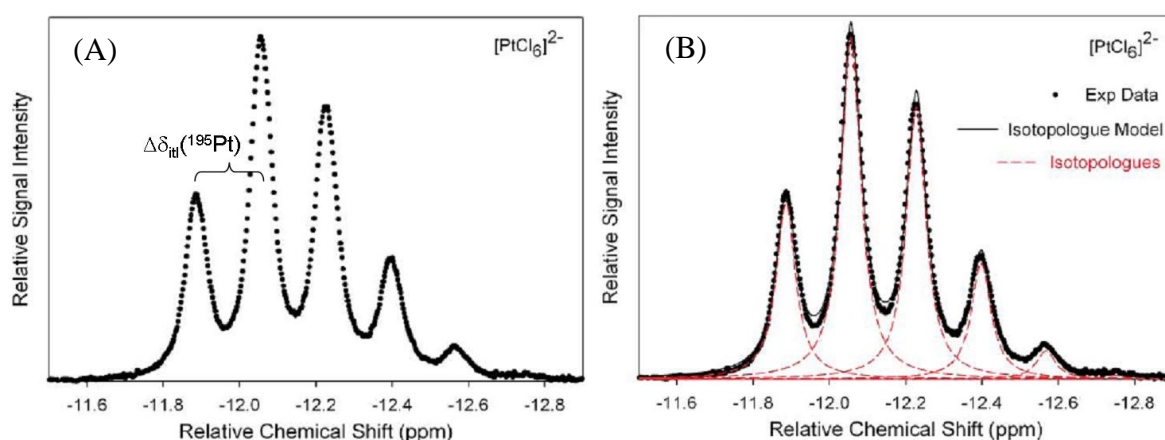
Figure 3.2: (**A**) Experimental ^{195}Pt NMR spectrum of $[PtCl_6]^{2-}$ in 1 M $HClO_4$ and 6 M HCl at 20°C. The difference bewteen respective ^{35}Cl/^{37}Cl isotopologues ($\Delta\delta_{itl}(^{195}Pt)$) is indicated. (**B**) Excellent least-squares fit between the experimental isotopic spectrum of $[PtCl_6]^{2-}$ and the isotopologue model.

Both Ismail *et al.*[5] and Preetz *et al.*[7] used peak intensities to compare with the statistical probability of the isotopologues – which showed poorer agreement. As can be seen from Table 3.1, within experimental error, our agreement between the observed and statistially expected isotopologue distribution (as percentage of total) using resonance areas, is significantly better than those previously estimated from relative peak intensities.[5, 7]

Table 3.1: ^{195}Pt NMR experimental (Expt.) and statistical $[PtCl_6]^{2-}$ isotopologue distribution, obtained by a least-square fit of the experimental spectrum, Figure 3.2B.

	Percent $[PtCl_6]^{2-}$ isotopologue distribution			
	Expt.^{a}	Statistical	Expt.(ref. 5)	Expt.(ref. 7)^b.
$[Pt^{35}Cl_6]^{2-}$	18.78 ($\pm$ 0.1)	18.92	18.6	21.2
$[Pt^{35}Cl_5^{37}Cl]^{2-}$	36.47 ($\pm$ 0.1)	36.31	36.1	36.0
$[Pt^{35}Cl_4^{37}Cl_2]^{2-}$	29.03 ($\pm$ 0.1)	29.03	29.2	29.1
$[Pt^{35}Cl_3^{37}Cl_3]^{2-}$	12.36 ($\pm$ 0.1)	12.38	12.6	14.4
$[Pt^{35}Cl_2^{37}Cl_4]^{2-}$	2.97 ($\pm$ 0.1)	2.97	3.1	5.0
$[Pt^{35}Cl^{37}Cl_5]^{2-}$	0.39	0.38	-	-
$[Pt^{37}Cl_6]^{2-}$	*n.o.*	0.02	-	-

^{a} Errors estimated from spectra with high signal/noise ratio obtained for solution III with 100 000 FID's; $[PtCl_6]^{2-}$ = 0.25 M at 293 K. Relatively good agreement with theory can also be obtained for only 256 FID's, with solution III at 293 K, for which relative error below 2-3 % for the main peaks, can be obtained. ^{b} Estimated values from peak heights.

From the relative concentration ratios, it is clear that the $[Pt^{35}Cl_5^{37}Cl]^{2-}$ isotopologue resonates just up-field from the $[Pt^{35}Cl_6]^{2-}$ isotopologue. The $\Delta\delta_{itl}(^{195}Pt)$ value between subsequent $^{35}Cl/^{37}Cl$ isotopologues is remarkably consistent (0.16 ppm) and a plot of $\delta_{itl}(^{195}Pt)$ *vs.* number of coordinated ^{37}Cl isotopes gives a straight line (R^2 = 1; Figure 3.3). The consistent $\Delta\delta_{itl}(^{195}Pt)$ increments allows accurate prediction of the $[Pt^{37}Cl_6]^{2-}$ isotopologue $\delta_{itl}(^{195}Pt)$ value as illustrated in Figure 3.3, since it is not observed in Figure 3.2 due to insufficient signal/noise ratio. The consistency in the increment between $\delta_{itl}(^{195}Pt)$ values as an ^{35}Cl isotope is replaced by an ^{37}Cl isotope assist accurate least-squares analysis and is critical for the assignment of the respective isotopologue signals. As will be shown, small differences in the $\Delta\delta_{itl}(^{195}Pt)$ values may reveal significant properties of the isotopic species to assist in assigment between stereoisomers and $\delta_{itl}(^{195}Pt)$ values are therefore very significant in the context of this discussion. These $\delta_{itl}(^{195}Pt)$ values are discussed in more detail in the next section 3.3.2.
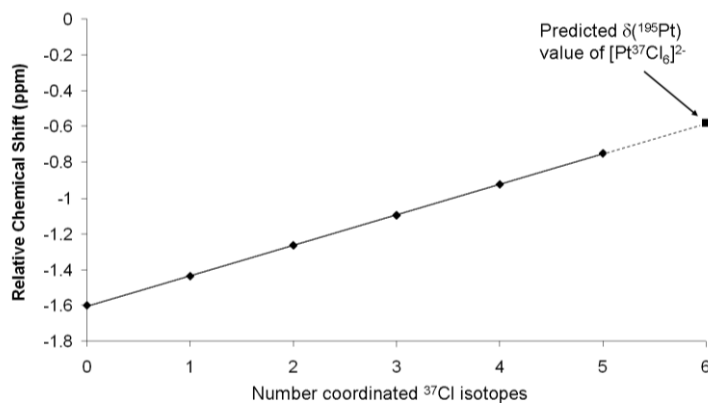
Figure 3.3: Experimental $\delta_{itl}(^{195}Pt)$ values of the respective $[Pt^{35}Cl_n^{37}Cl_{6-n}]^{2-}$ ($n = 0$-6) isotopologues as a function of coordinated ^{37}Cl isotopes. The $\delta_{itl}(^{195}Pt)$ value of the $[Pt^{37}Cl_6]^{2-}$ isotopologue can be predicted from the consistent $\Delta\delta_{itl}(^{195}Pt)$ value between consecutive $^{35}Cl/^{37}Cl$ isotopologues.

In the pursuit of optimizing the $^{35}Cl/^{37}Cl$ isotopologue resolution, it was found that the solution temperature at which the ^{195}Pt NMR spectrum was recorded significantly affects the resolution. Thus, it should be emphasized that in order to achieve a 'best-fit' between experimental and simulated ^{195}Pt spectra, it is important to record ^{195}Pt spectra from solutions which were allowed to temperature equilibrate inside the spectrometer for at least 20 min at the desired temperature under conditions in which the magnetic field homogeneity is carefully optimized. In order to find the optimum temperature at which the best resolution of ^{195}Pt NMR spectra is obtained, a temperature dependence experiment was carried out in the temperature range 5-30°C. The observed line-widths of the $[Pt^{35}Cl_n^{37}Cl_{6-n}]^{2-}$ ($n = 1$-6) isotopologue signals show an interesting, but perplexing temperature dependence, displaying a minimum line-width of ~8 Hz for ^{195}Pt resonances at 20°C. At temperatures below 18°C, and above 22°C, loss of resolution is observed, resulting in generally a poorer least-squares fit between the simulated and experimental ^{195}Pt NMR spectra. This relatively narrow optimum temperature range, suggests that different temperature dependent effects may be operative leading to line-broadening of the set of isotopologue resolved ^{195}Pt NMR resonances. In order to examine whether ligand/solvent exchange processes may account for this trend, a temperature dependence experiment of ^{195}Pt NMR using three separate 0.25 M $[PtCl_6]^{2-}$ solutions with increasing Cl^- concentrations (I = 1 M $HClO_4$, II = 1 M $HClO_4$, 1 M HCl and III = 1 M $HClO_4$, 6 M HCl) were examined over the temperature range 5-30°C. The spectra and temperature dependence of the ^{195}Pt NMR resolution for samples I-III are very similar, so that it is only necessary to show the results for solution II, illustrating

the change in line-width and resolution of the ^{195}Pt resonance. Note that the $\delta(^{195}$Pt$)$ is very sensitive towards changes in temperature resulting in a downfield shift of the ^{195}Pt NMR resonance signal by ~ 1 ppm/°C [3] as seen in Figure 3.4.
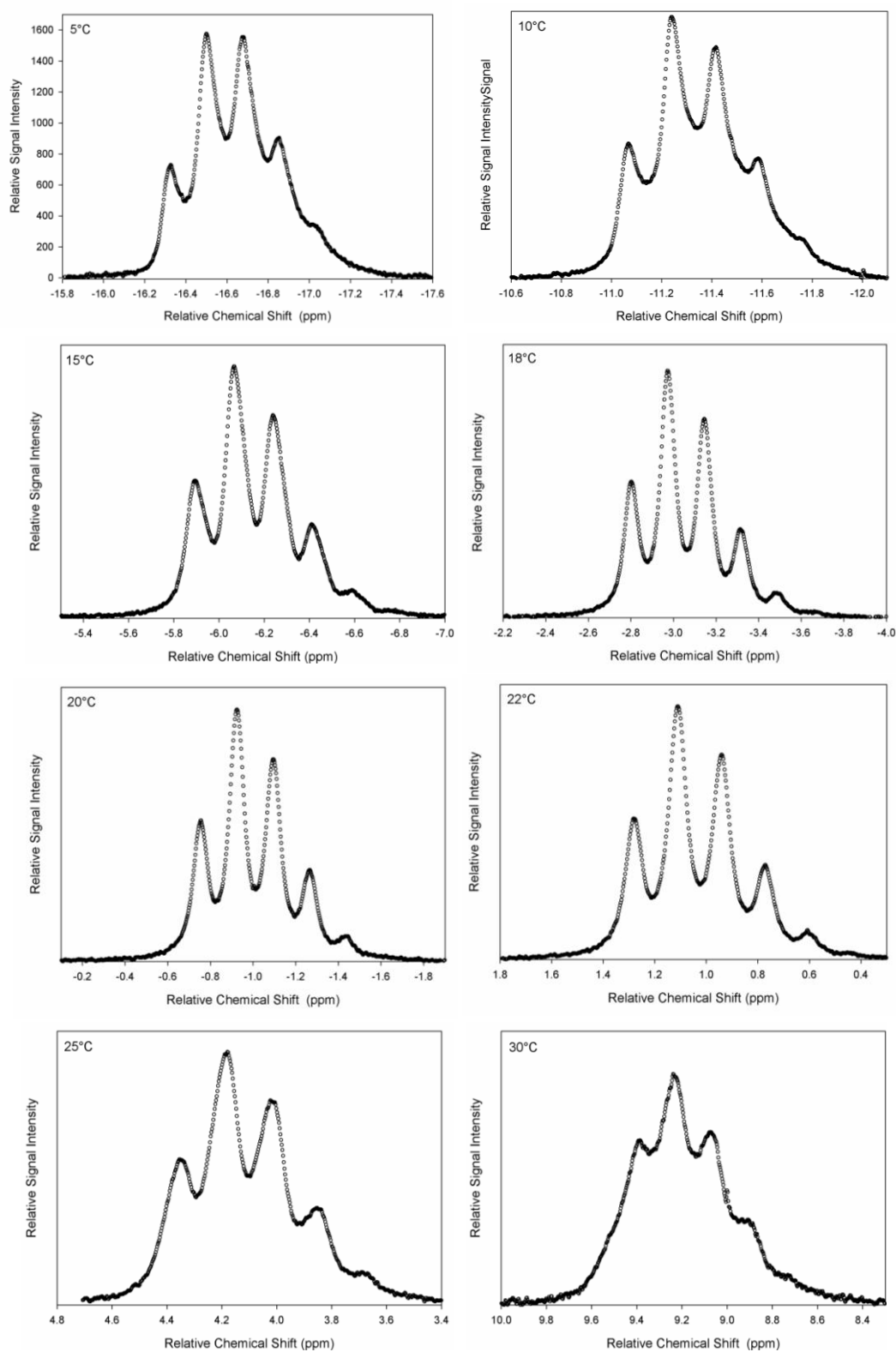
Figure 3.4: The ^{35}Cl/^{37}Cl isotopologue resolution of 0.25 M [PtCl$_6$]$^{2-}$ in 1 M HClO$_4$ and 1 M HCl as a function of temperature (5-30°C).

The resolution of $[PtCl_6]^{2-}$ becomes marginally better as the Cl^- concentration is increased in solutions I-III. Preliminary inter-molecular Cl^- exchange rates estimated by doping $[PtCl_6]^{2-}$ solutions with $Na^{35}Cl$, show that Cl^- exchange is slow on the NMR time-scale and thus can not account for the observed line-broadening. This is consistent with another study in which the Cl^- exchange rate was measured by a different technique.[8] The reason for the narrow temperature range within which optimally resolved ^{195}Pt NMR spectra of octahedral Pt(IV) complexes are obtained is not fully understood, but is likely to relate to the vibrational structure of the Pt–Cl bond for these isotopologues. Although an exhaustive study of the temperature dependence phenomenon was not carried out, several contributory factors could include both *intra*- and *inter*-molecular Cl^- exchange, solvent viscosity effects at lower temperature affecting processes dependent on molecular correlation times (τ_c), in addition to *inter alia* the temperature dependent spin-rotation relaxation mechanism, thought to be important for such complexes.[11] The ^{195}Pt NMR spectra of the rest of the $[PtCl_n(H_2O)_{6-n}]^{4-n}$ (n = 2-5) complexes were subsequently aqcuired at 20ºC to ensure optimum resolution.

3.3.2 $^{35}Cl/^{37}Cl$ isotope effects of the *aqua* complex species $[PtCl_n(H_2O)_{6-n}]^{4-n}$ (n = 2-5) as observed with ^{195}Pt NMR.

Due to the presumably high thermodynamic stability of $[PtCl_6]^{2-}$, aquation thereof is not a practical method to obtain high concentrations of the $[PtCl_n(H_2O)_{6-n}]^{4-n}$ (n = 1-5) complexes.[9-11] A 0.2 M $[PtCl_4]^{2-}$ solution was therefore "aged" in 1 M $HClO_4$ prior to oxidation with $NaClO_3$ as a means to synthesize the species of interest. The ratio of $[PtCl_4]^{2-}$ to $[PtCl_3(H_2O)]^-$ species after 12 h in 1 M $HClO_4$ was determined with ^{195}Pt NMR to be 79 : 21 %. Oxidation of the latter solution at 50°C with five mol equivalents of $NaClO_3$ (as described in the experimental section) is evident from a colour change from red-orange to bright yellow and result in the formation of eight new Pt(IV) complexes as shown in the ^{195}Pt NMR spectra of Figure 3.5. The $\delta(^{195}Pt)$ values are listed in Table 3.4.
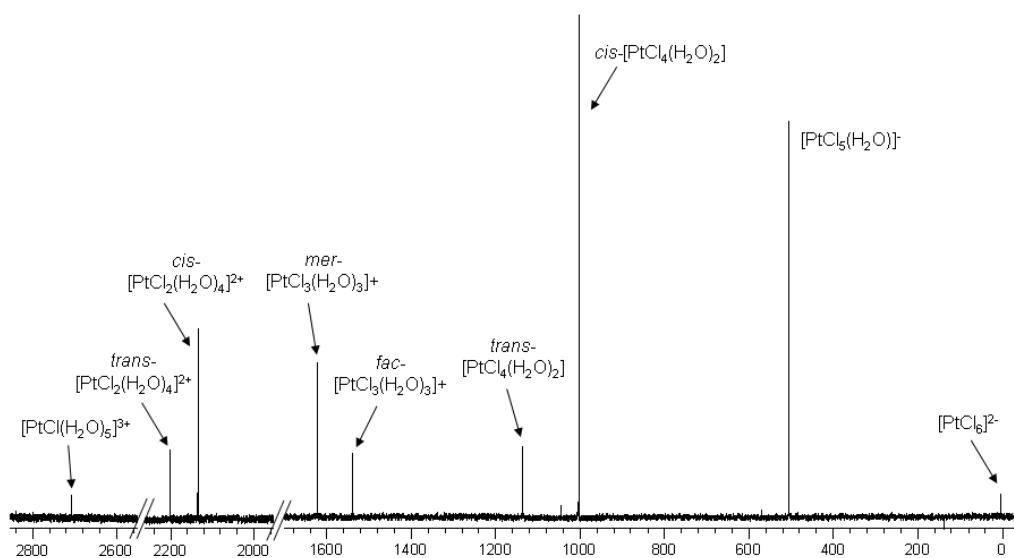
Figure 3.5: ^{195}Pt NMR spectra of 0.35 M [PtCl$_4$]$^{2-}$ in 1 M HClO$_4$ oxidized with five mol equivalents of NaClO$_3$, resulting in formation of the[PtCl$_n$(H$_2$O)$_{6-n}$]$^{4-n}$ (n = 1-5) species.

Quantitative oxidation of Pt(II) was confirmed by ^{195}Pt NMR in the spectral range of 200 to -1800 ppm. Initial assignments of the complexes were made with ^{195}Pt NMR chemical-shift-trend analysis according to the same principles discussed earlier for Pt(II) complexes (*Chapter 2*). A plot of the δ(^{195}Pt) values *vs.* number of coordinated H$_2$O results in a slight positive deviation from a non-linear trend (Figure 3.6A; δ(^{195}Pt) = $5.2n^2 + 518n$ -1.9; R^2 > 0.99) and allow assignment of the Pt(IV)-*aqua-chlorido* species.

(A)   (B)
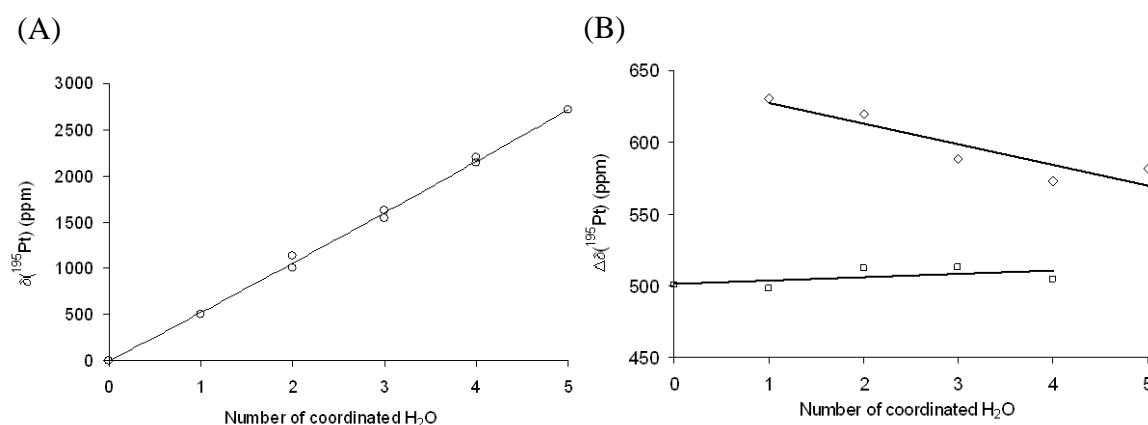
Figure 3.6: (A) Second-order correlation of the δ(^{195}Pt) values observed in Figure 3.5 with number of coordinated H$_2$O. **(B)** Different linear correlations resulting from $\Delta\delta$(^{195}Pt) values obtained from different *trans* substitutions of H$_2$O with Cl$^-$.

The stereoisomers were assigned by plotting the $\Delta\delta$(^{195}Pt) value between respective *trans* substitutions. Substitution of H$_2$O by Cl$^-$ *trans* to H$_2$O is consistently smaller

37

than substitution of H_2O by Cl^- trans to Cl^- which result in different linear fits (Figure 3.6B) which displays a converging trend. The $[PtCl_n(H_2O)_{6-n}]^{4-n}$ (n = 1-5) species assigned with ^{195}Pt NMR chemical-shift-trend analysis correlate very well with previously assigned values.[10] Although this method of synthesis produced relatively small quantities of some complexes in the $[PtCl_n(H_2O)_{6-n}]^{4-n}$ (n = 2−5) series, all are present at high enough concentration so that a ^{195}Pt NMR spectrum acquired with 10000 FID's gave satisfactory signal/noise ratios to allow for detailed least-squares analysis of the resulting ^{195}Pt NMR isotopic effects.

3.3.2.1 Least-squares analysis of the $[Pt^{35}Cl_n^{37}Cl_{5-n}(H_2O)]^-$ (n = 2-5) isotopic ^{195}Pt NMR shifts.

An expansion of the $[PtCl_5(H_2O)]^-$ ^{195}Pt NMR signal observed in Figure 3.5 reveals additional isotopic shifts shown in Figure 3.7A. The expected statistical isotopologue distribution of the $[PtCl_5(H_2O)]^-$ complex was calculated from Equation 3.1 and simulated as shown in Figure 3.7B, by using fixed peak widths and $\Delta_{itl}\delta(^{195}Pt)$ values. Surprisingly, the experimental lineshape of the $[PtCl_5(H_2O)]^-$ signal is notably different from the simulated isotopologue distribution as anticipated from the $^{35}Cl/^{37}Cl$ isotopologue model that is valid for $[PtCl_6]^{2-}$. The experimental spectrum of the *cis*-$[PtCl_5(H_2O)]^-$ complex was acquired as well and compared to the statistical simulated isotopologue distribution (Figure 3.7C *vs*. D), and also show a significantly different spectrum. After carefull consideration of the experimental result it was realized that the experimental lineshape of $[PtCl_5(H_2O)]^-$ can be rationalized by taking into account the statistical *isotopomer* distribution for a given $^{35}Cl/^{37}Cl$ *isotopologue* in which either a ^{35}Cl or a ^{37}Cl is *trans* to coordinated H_2O in the complex. It is obvious that the $[Pt^{35}Cl_5(H_2O)]^-$ isotopologue can exist as one possible isotopomer only giving rise to one signal. However, the $[Pt^{35}Cl_4^{37}Cl(H_2O)]^-$ isotopologue can exist as two different isotopomers; in four positions the ^{37}Cl isotope can be *cis* to H_2O and in only one position the ^{37}Cl isotope can be *trans* to H_2O as illustrated in Figure 3.8A. The $[Pt^{35}Cl_4^{37}Cl(H_2O)]^-$ *isotopologue* with an overall statistical abundance of 39.93 % (calculated from Equation 3.1), therefore consists of two groups of *isotopomers* with a statistical probability of 4:1.
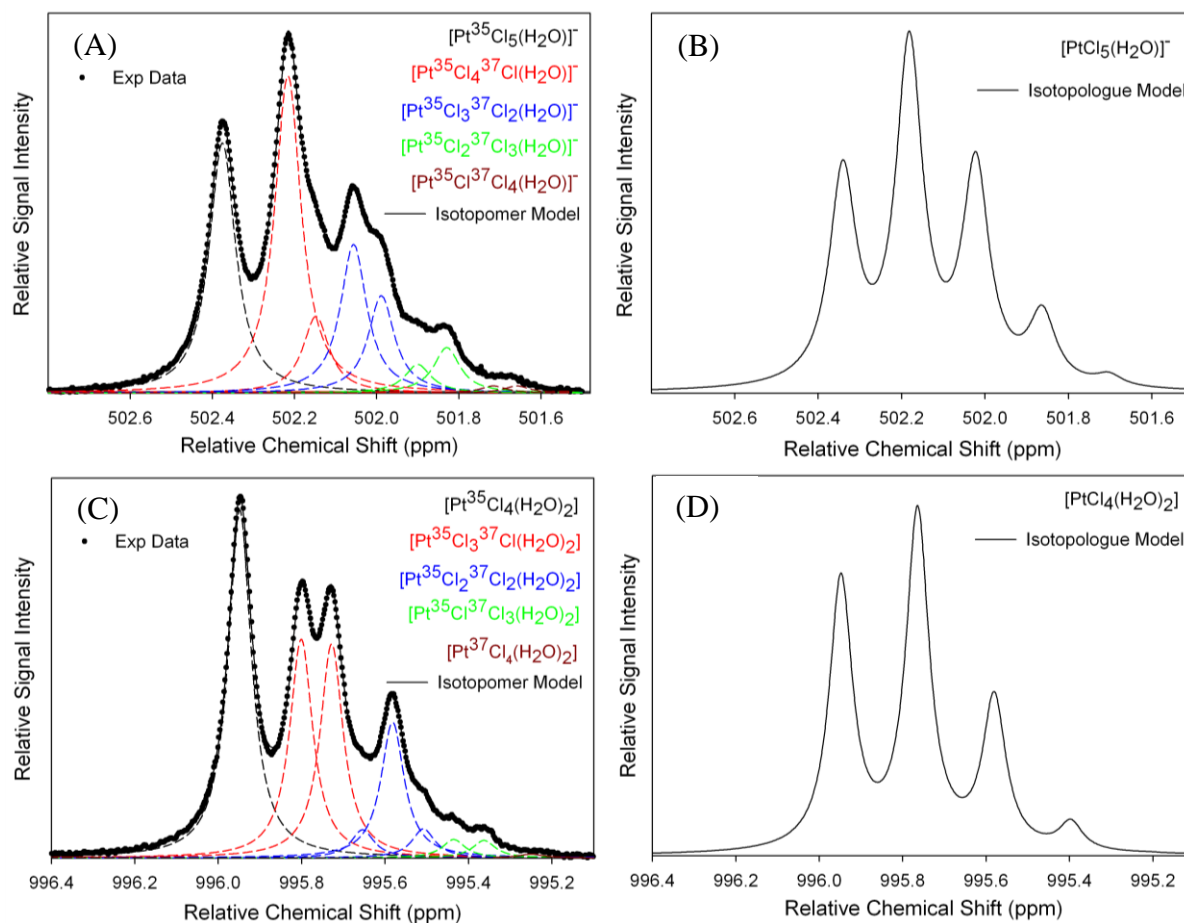
Figure 3.7: Experimental ^{195}Pt spectra of $[PtCl_5(H_2O)]^-$ and *cis*-$[PtCl_4(H_2O)_2]$ are traced by symbols in (C) and (E) for solutions containing these species. Excellent least-squares fit between the experimental spectra of the isotopologues including isotopomers for $[PtCl_5(H_2O)]^-$ **(A)** and simulated spectra using only an isotopologue model for $[PtCl_5(H_2O)]^-$ **(B),** *cis*-$[PtCl_4(H_2O)_2]$ **(C)** and *cis*-$[PtCl_4(H_2O)_2]$ neglecting isotopomers **(D)**.

By following this line of argument, the $[Pt^{35}Cl_3^{37}Cl_2(H_2O)]^-$ isotopologue, consists of two isotopomers, where either a ^{35}Cl isotope or a ^{37}Cl isotope is *trans* to H_2O with statistical probability 3:2. Similarly the $[Pt^{35}Cl_2^{37}Cl_3(H_2O)]^-$ isotopologue has two isotopomers with a statistical probability of 2:3. Finally, the $[Pt^{35}Cl^{37}Cl_4(H_2O)]^-$ isotopologue can exist as two isotopomers with a statistaical probability of 1:4. The $[Pt^{37}Cl_5(H_2O)]^-$ isotopologue only have one possible isotopic configuration and thus no isotopomers are possible, but is not observed in Figure 3.7A due to the low statistical probability (0.08 %) and insufficient signal/noise ratio.
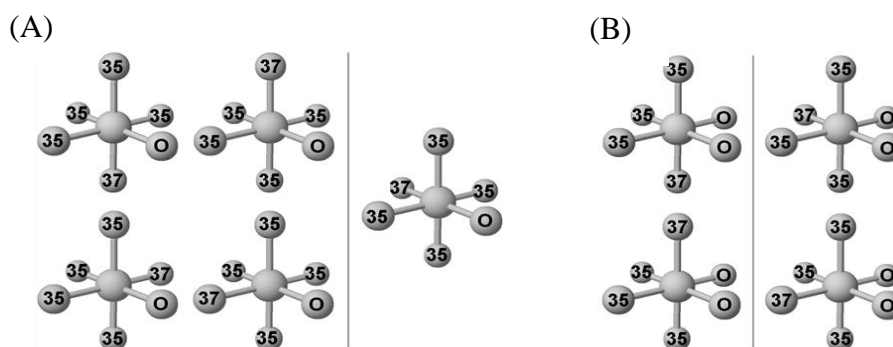
Figure 3.8: Isotopomers associated with $^{35}Cl/^{37}Cl$ isotopologues $[Pt^{35}Cl_4^{37}Cl(H_2O)]^-$ **(A)** and *cis*-$[Pt^{35}Cl_3^{37}Cl(H_2O)_2]$ **(B)** where $^{35}Cl/^{37}Cl$ is coordinated *trans* with respect to water results in a 4:1 and 1:1 ratio respectively (35 = ^{35}Cl, 37 = ^{37}Cl and O = H_2O).

Table 3.2: Comparison the relative amounts (as a percentage) from experimental ^{195}Pt spectra at 293 K of $[PtCl_5(H_2O)]^-$ and *cis*-$[PtCl_4(H_2O)_2]$ with their statistically expected isotopomer distributions for each isotopologue.

$^{35/37}Cl$ *trans* to H_2O	Pt(IV) isotopologue	Percent of $[PtCl_5(H_2O)]^-$ and *cis*-$[PtCl_4(H_2O)_2]$ isotopomers		Sum percent of isotopomers of $[PtCl_5(H_2O)]^-$ and *cis*-$[PtCl_4(H_2O)_2]$ isotopologues	
		Expt.[a]	Statistical[b]	Expt.	Statistical
^{35}Cl	$[Pt^{35}Cl_5(H_2O)]^-$	26.1 ± 0.4	24.97	25.8	24.97
^{35}Cl	$[Pt^{35}Cl_4^{37}Cl(H_2O)]^-$	33.4 ± 0.7	31.94	40.6	39.93
^{37}Cl		7.3 ± 0.6	7.99		
^{35}Cl	$[Pt^{35}Cl_3^{37}Cl_2(H_2O)]^-$	15.6 ± 0.3	15.32	25.3	25.54
^{37}Cl		9.5 ± 0.5	10.22		
^{35}Cl	$[Pt^{35}Cl_2^{37}Cl_3(H_2O)]^-$	3.0 ± 0.1	3.27	7.6	8.17
^{37}Cl		4.4 ± 0.3	4.9		
^{35}Cl	$[Pt^{35}Cl^{37}Cl_4(H_2O)]^-$	0.7 ± 0.2	0.26	1.2	1.31
^{37}Cl		0.4 ± 0.3	1.05		
^{37}Cl	$[Pt^{37}Cl_5(H_2O)]^-$	not reliably measurable	0.08	not reliably measurable	0.08
$^{35}Cl,^{35}Cl$	*cis*-$[Pt^{35}Cl_4(H_2O)_2]$	34.4 ± 0.1	32.96	34.4	32.96
$^{35}Cl,^{35}Cl$	*cis*- $[Pt^{35}Cl_3^{37}Cl(H_2O)_2]$	21.5 ± 0.1	21.08	42.8	42.16
$^{35}Cl,^{37}Cl$		20.9 ± 0.3	21.08		
$^{35}Cl,^{35}Cl$	*cis*- $[Pt^{35}Cl_2^{37}Cl_2(H_2O)_2]$	2.7 ± 0.1	3.37	19.1	20.22
$^{35}Cl,^{37}Cl$		13.3 ± 0.2	13.48		
$^{37}Cl,^{37}Cl$		2.9 ± 0.1	3.37		
$^{35}Cl,^{37}Cl$	*cis*- $[Pt^{35}Cl^{37}Cl_3(H_2O)_2]$	2.0 ± 0.1	2.16	3.6	4.31
$^{37}Cl,^{37}Cl$		2.0 ± 0.2	2.16		
$^{37}Cl,^{37}Cl$	*cis*- $[Pt^{37}Cl_4(H_2O)_2]$	0.3 ± 0.3	0.34	0.3	0.34

[a] From ^{195}Pt NMR spectra with *ca*100 000 FID's for $[PtCl_5(H_2O)]^-$ and *cis*-$[PtCl_4(H_2O)_2]$ at approximately 0.1 M. [b] Calculated from Equation (3.1) and obtained from deconvoluting the ^{195}Pt spectra least-squares fit.

This $^{35}Cl/^{37}Cl$ isotopomer model results in an excellent least-squares fit of the experimental $[PtCl_5(H_2O)]^-$ data (solid black line in Figure 3.7A). To determine the overall isotopologue concentrations it was neccesary to take the sum of individual isotopomers associated with a specific isotopologue. The experimental values calculated by this manner is listed in Table 3.2 and correlates well with the

statistical calculated values. From the least-squares fit the individual isotopologue and isotopomer concentrations as well as the individuel $^{35}Cl/^{37}Cl$ isotopologue ^{195}Pt chemical shift ($\delta_{itl}(^{195}Pt)$) and isotopomer ^{195}Pt chemical shift ($\delta_{itm}(^{195}Pt)$) values can be obtained. These values were subsequently used to simulate the individual *isotopologue* (different coloured dotted lines) and *isotopomer* (same coloured dotted lines) signals as shown in Figure 3.7A. The experimetal data can therefore be envisaged by four ^{195}Pt NMR observable *isotopologues* that are where relevent sub-divided into statistically determined *isotopomers* depending whether ^{35}Cl or ^{37}Cl is *trans* to H_2O. An excellent correlation between experimental and statistical values are obtained, which confirms the $^{35}Cl/^{37}Cl$ isotopomer model to account for the isotopic effects observed for $[Pt^{35}Cl_n Cl_{5-n}(H_2O)]^-$ (n = 0-5).

3.3.2.2 Least-squares analysis of cis- and trans-$[Pt^{35}Cl_n^{37}Cl_{4-n}(H_2O)_2]$ (n = 0-4)

The $^{35}Cl/^{37}Cl$ isotopomer model was also applied to the spectrum of *cis*-$[PtCl_4(H_2O)_2]$ shown in Figure 3.7C, which differs visually even more from the naïve statistically expected *isotopologue* spectrum, in which possible *isotopomers* are ignored (Figure 3.7D). The experimental spectrum can be rationalized if isotopomer effects are considered in addition to isotopologue effects. The *cis*-$[Pt^{35}Cl_4(H_2O)_2]$ isotopologue only has one isotopic configuration so that one signal is observed. The *cis*-$[Pt^{35}Cl_3^{37}Cl(H_2O)_2]$ isotopologue can exist as two different isotopomers; in two positions the ^{37}Cl isotope can be *trans* to H_2O and in the other two positions it can be *cis* to H_2O as illustrated in Figure 3.8B. Two isotopomers with a statistical probability of 2:2 are observed as indicated in Figure 3.7C. For the $[Pt^{35}Cl_2^{37}Cl_2(H_2O)_2]$ isotopologue three different isotopomers are possible. In the first case both ^{35}Cl isotopes can be *trans* to H_2O, in the second one ^{35}Cl and one ^{37}Cl can be *trans* to H_2O and in the third both ^{37}Cl isotopes can be *trans* to H_2O. The satistical probability of these isotopomers is 1:4:1 and is in line with the experimental spectrum (Figure 3.7C). For the $[Pt^{35}Cl^{37}Cl_3(H_2O)_2]$ isotopologue two isotopomers are possible with the same statistical probablity of 2:2. The final $[Pt^{37}Cl_4(H_2O)_2]$ isotopologue can not have a different isotopic configuration and therefore does not have any associated isotopomers. The experimental values obtained from the sum of the individual isotopomers associated with a specific isotopologue compared to the statistical calculated values are included in Table 3.2

and show excellent correlation with the calculated *isotopologue* and *isotopomer* values, further validating the ^{35}Cl/^{37}Cl isotopomer model.

The ^{35}Cl/^{37}Cl isotopic ^{195}Pt NMR spectra of *cis-* and *trans-*[PtCl$_4$(H$_2$O)$_2$] differ significantly (Figure 3.9 A vs. B). It might be anticipated that the ^{195}Pt spectrum of *trans-*[PtCl$_4$(H$_2$O)$_2$] should resemble the spectrum shown in Figure 3.7D, since no ^{35}Cl/^{37}Cl isotopes are coordinated *trans* to H$_2$O and thus no isotopomer signals are possible. Interestingly, the isotopologue distribution of *trans-*[PtCl$_4$(H$_2$O)$_2$] is not fully resolved and inspection alone is not sufficient to verify this complex. The non-linear least-squares fits between the experimental and simulated spectra, are excellent and the relative percentage error obtained between the calculated and that expected is less than 1.5% as shown in Table 3.3. Apart from the magnitude of $\Delta\delta_{itl}$(^{195}Pt) that separate the ^{35}Cl/^{37}Cl isotopologues, the ^{195}Pt NMR spectrum obtained for *trans-*[PtCl$_4$(H$_2$O)$_2$] is identical to the simulated spectrum predicted in Figure 3.7D. The least-squares fit confirms that for a specific Pt(IV) complex each isotopologue has the same peak width at half height ($v\frac{1}{2}$) and the same $\Delta\delta_{itl}$(^{195}Pt) value as ^{37}Cl replaces ^{35}Cl. The presence of *isotopomers* in *cis-*[PtCl$_4$(H$_2$O)$_2$] and the absence thereof in *trans-*[PtCl$_4$(H$_2$O)$_2$] thus allows discrimination between these stereoisomers by means of ^{195}Pt NMR. To the knowledge of the author this is the first reported technique based on ^{195}Pt NMR with which it is clearly possible to discriminate between *isotopomers* with different ^{35}Cl/^{37}Cl isotope stereochemistry. It is interesting to note that apparently it is of little consequence whether the two ^{35}Cl/^{37}Cl isotopes are situated *cis* or *trans* relative to each other, confirming that in such situations the possible isotope induced shifts over two bonds in an octahedral complex are very small (estimated at *ca.* 0.007 ppm < 1 Hz at the magnetic field used[12]). Evidently however, the position of ^{35}Cl/^{37}Cl relative to coordinated H$_2$O in these Pt(IV) complexes induces a larger observable difference in isotopomer shielding, since otherwise the resonances of isotopic species such as [Pt^{35}Cl$_n^{37}$Cl$_{6-n}$]$^{2-}$ (n = 0-6) might also be expected to exhibit additional "fine structure", something not seen in the spectra discussed here at 14.1 Tesla. It might be possible to observe separate resonances for different ^{35}Cl/^{37}Cl isotopes *cis* or *trans* with respect to each other, at even higher magnetic fields.

3.3.2.3 Least-squares analysis of mer/fac-$[Pt^{35}Cl_n{}^{37}Cl_{3-n}(H_2O)_3]^+$ (n = 0-3)

The $^{35}Cl/^{37}Cl$ isotopomer model which explain the isotopic effects of $[PtCl_5(H_2O)]^-$ and $cis/trans$-$[PtCl_4(H_2O)_2]$ also account for the mer/fac-$[PtCl_3(H_2O)_3]^+$ stereoisomer complexes. Similarly to $trans$-$[PtCl_4(H_2O)_2]$, the fac-$[PtCl_3(H_2O)_3]^+$ complex do not contain isotopomers since both ^{35}Cl and ^{37}Cl are always $trans$ to H_2O. The ^{195}Pt NMR resonance signal for this complex therefore only exhibits four $^{35}Cl/^{37}Cl$ isotopologue signals with statistically expected ratios. The non-linear least-squares fit of the experimental data based on this proposal is excellent and the relative percentage error obtained between the calculated and that expected from statistical considerations for an *isotopologue* was always below 1.5 % (Table 3.3).

Table 3.3: Comparison of the experimental (Figures 3.9A–F) and statistically expected isotopologue and isotopomer distributions for the $[Pt^{35/37}Cl_n(H_2O)_{6-n}]^{4-n}$ (n = 2-6) complexes.

$^{35/37}Cl$ *trans* to H_2O	Pt(IV) isotopologue	Percent isotopomers		Sum percent of isotopomers to yield isotopologue amount	
		Expt.	Statistical	Expt.	Statistical
	$trans$-$[Pt^{35}Cl_4(H_2O)_2]$			33.6 ($\pm$ 0.1)	32.96
	$trans$-$[Pt^{35}Cl_3{}^{37}Cl(H_2O)_2]$			42.5 ($\pm$ 0.3)	42.16
	$trans$-$[Pt^{35}Cl_2{}^{37}Cl_2(H_2O)_2]$			19.6 ($\pm$ 0.1)	20.22
	$trans$-$[Pt^{35}Cl^{37}Cl_3(H_2O)_2]$			4.3 ($\pm$ 0.3)	4.31
	$trans$-$[Pt^{37}Cl_4(H_2O)_2]$			0.1 ($\pm$ 0.2)	0.34
^{35}Cl	mer-$[Pt^{35}Cl_3(H_2O)_3]^+$	42.9 ($\pm$ 0.1)	43.50	42.9	43.50
^{35}Cl ^{37}Cl	mer-$[Pt^{35}Cl_2{}^{37}Cl(H_2O)_3]^+$	26.7 ($\pm$ 0.2) 14.9 ($\pm$ 0.2)	27.82 13.91	41.6	41.73
^{35}Cl ^{37}Cl	mer-$[Pt^{35}Cl^{37}Cl_2(H_2O)_3]^+$	5.0 ($\pm$ 0.3) 9.0 ($\pm$ 0.2)	4.45 8.90	14.0	13.35
^{37}Cl	mer-$[Pt^{37}Cl_3(H_2O)_3]^+$	1.4 ($\pm$ 0.3)	1.42	1.4	1.42
$^{35}Cl,^{35}Cl,^{35}Cl$	fac-$[Pt^{35}Cl_3(H_2O)_3]^+$			44.9 ($\pm$ 0.1)	43.50
$^{35}Cl,^{35}Cl,^{37}Cl$	fac-$[Pt^{35}Cl_2{}^{37}Cl(H_2O)_3]^+$			42.0 ($\pm$ 0.2)	41.73
$^{35}Cl,^{37}Cl,^{37}Cl$	fac-$[Pt^{35}Cl^{37}Cl_2(H_2O)_3]^+$			12.2 ($\pm$ 0.2)	13.35
$^{37}Cl,^{37}Cl,^{37}Cl$	fac-$[Pt^{37}Cl_3(H_2O)_3]^+$			0.9 ($\pm$ 0.3)	1.42
$^{35}Cl,^{35}Cl$	cis-$[Pt^{35}Cl_2(H_2O)_4]^{2+}$			57.6 ($\pm$ 0.1)	57.41
$^{35}Cl,^{37}Cl$	cis-$[Pt^{35}Cl^{37}Cl(H_2O)_4]^{2+}$			36.4 ($\pm$ 0.2)	36.72
$^{37}Cl,^{37}Cl$	cis-$[Pt^{37}Cl_2(H_2O)_4]^{2+}$			6.0 ($\pm$ 0.3)	5.87
	$trans$-$[Pt^{35}Cl_2(H_2O)_4]^{2+}$			58.5 ($\pm$ 0.2)	57.41
	$trans$-$[Pt^{35}Cl^{37}Cl(H_2O)_4]^{2+}$			36.5 ($\pm$ 0.1)	36.72
	$trans$-$t^{37}Cl_2(H_2O)_4]^{2+}$			5.1 ($\pm$ 0.3)	5.87
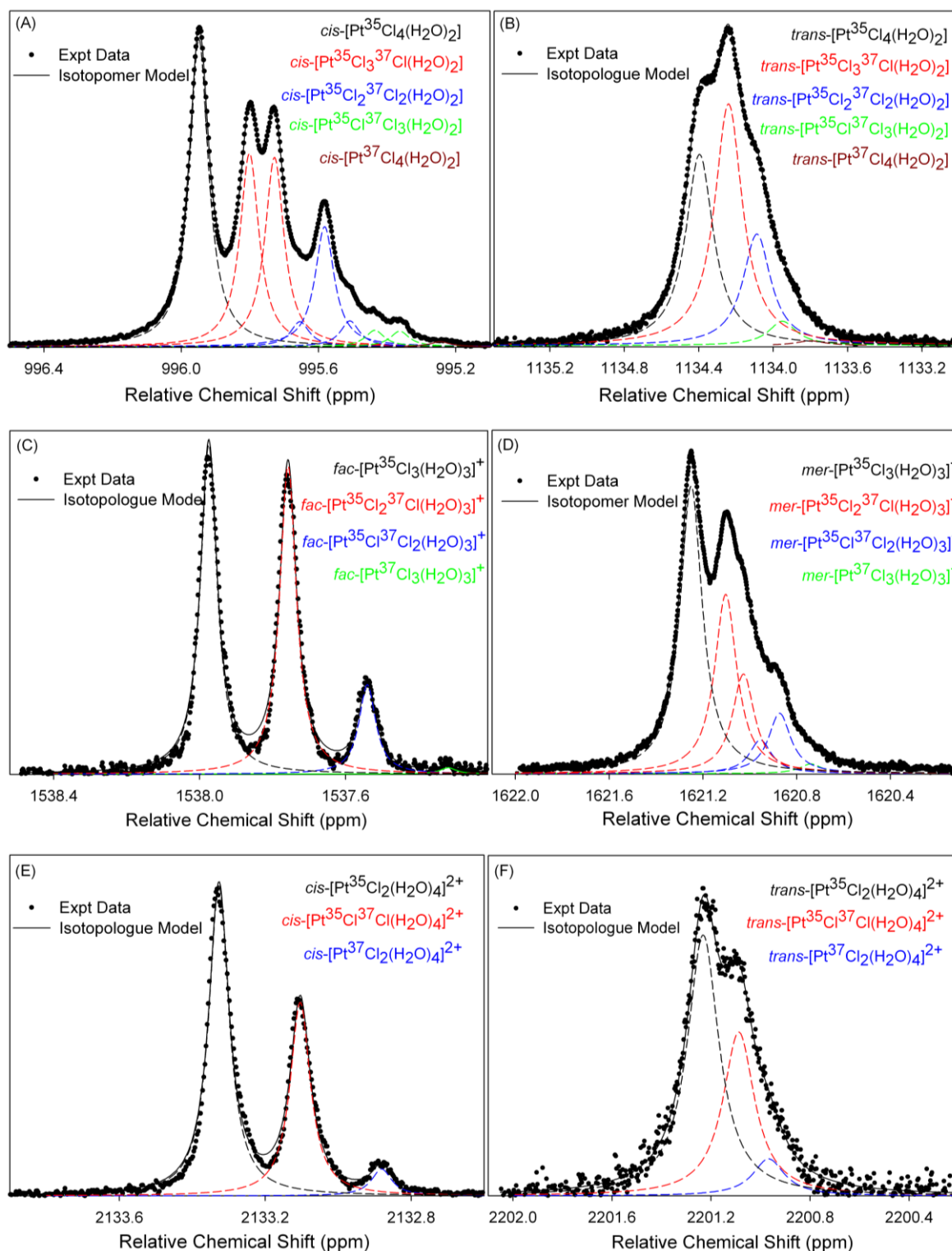
Figure 3.9: Experimental ^{195}Pt NMR spectra of $[Pt^{35/37}Cl_n(H_2O)_{6-n}]^{4-n}$ (n = 2-4) (A–F) are traced by symbols. The solid lines are the non-linear least-squares fits of the isotopic $\delta(^{195}Pt)$ model that incorporates $^{35}Cl/^{37}Cl$ isotopologues and isotopomers.

The isotopic *mer*-$[PtCl_3(H_2O)_3]^+$ signals are not fully resolved (Figure 3.9D) since the signal exhibit isotopomers in addition to isotopologues and inspection alone is not sufficient to verify this complex. For the *mer*-$[Pt^{35}Cl_2^{37}Cl(H_2O)_3]^+$ isotopologue there

44

are two positions where the ^{37}Cl isotope can be *trans* to a ^{35}Cl isotope but only one position where it can be *trans* to H_2O. Two isotopomers are also possible for the *mer*-$[Pt^{35}Cl^{37}Cl_2(H_2O)_3]^+$ isotopologue; in one position ^{35}Cl can be *trans* to H_2O and in two positions ^{35}Cl can be *trans* to ^{37}Cl. By including two isotopomers for the *mer*-$[Pt^{35}Cl_2^{37}Cl(H_2O)_3]^+$ and *mer*-$[Pt^{35}Cl^{37}Cl_2(H_2O)_3]^+$ isotopologues, with 2:1 and 1:2 proportionalities respectively, the non-linear least-squares fit result in excellent agreement with the experimental data (Table 3.3).

3.3.2.4 Least-squares analysis of cis/trans-$[Pt^{35}Cl_n^{37}Cl_{2-n}(H_2O)_4]^{2+}$ (n = 0-2)

Since both *cis*- and *trans*-$[PtCl_2(H_2O)_4]^{2+}$ do not exhibit isotopomers, initial assignments of these two stereoisomers were achieved by ^{195}Pt NMR chemical-shift-trend analysis as shown in Figures 3.6A and B, with *trans*-$[PtCl_2(H_2O)_4]^{2+}$ resonating downfield from *cis*-$[PtCl_2(H_2O)_4]^{2+}$. An expansion of these ^{195}Pt NMR signals reveals that the *cis*-$[PtCl_2(H_2O)_4]^{2+}$ isotopologues are well resolved compared to the poorly resolved *trans*-$[PtCl_2(H_2O)_4]^{2+}$ isotopologue signals (Figure 3.9E *vs*. Figure 3.9F). Least-squares analysis reveals three isotopologue signals for each stereoisomer, which correlates well with the statistical calculated values (Table 3.3). The isotopic ^{195}Pt spectra of these stereoisomers (Figures 3.9E *vs*. F) clearly indicates that the $\Delta\delta_{itl}(^{195}Pt)$ value between respective ^{35}Cl/^{37}Cl isotopologues of *cis*-$[PtCl_2(H_2O)_4]^{2+}$ are considerable larger (0.223 ppm) than that of the *trans* stereoisomer (0.144 ppm). A unique spectrum for each complex therefore exists, which allow discrimination between these complexes even in the absence of isotopomers.

3.3.2.5 Origin of the differences in ^{195}Pt NMR isotopologue values of the Pt(IV)-aqua-chlorido complexes

Although NMR spectroscopy does not measure the mean bond displacements directly, Jameson and coworkers[12-14] have used harmonic/anharmonic force field calculations to show that the $\delta_{itl}(^{195}Pt)$ value of a specific isotopologue (due to temperature or isotopic replacement) can be correlated with how the nuclear shielding changes with the mean M–L bond length. The sensitivity of $\delta_{itl}(^{195}Pt)$, with regards to the $[PtCl_6]^{2-}$ complex, on bond length was estimated with density functional theory (DFT) calculations to be 180 ppm.pm^{-1} and show that contraction or elongation of the mean Pt–Cl bond displacement leads to shielding or deshielding of the Pt nucleus respectively.[15, 16] The fundamental

work on the origin of the isotope shift in ML_6 type molecules,[13, 14, 17] demonstrates a direct proportionality to a *(m'-m)/m'* factor (where *m* and *m'* are the atomic masses of the isotopes of L bonded to M), which in turn depends on the mean M–L bond displacement. However, this mass factor proportionality has only been shown to apply to isotopologues and not when isotopomers[18] are also present.

The average $\Delta\delta_{itl}(^{195}Pt)$ value as ^{37}Cl replaces ^{35}Cl for a specific complex fluctuates in the $[PtCl_n(H_2O)_{6-n}]^{4-n}$ (*n* = 2-6) series (Table 3.4), so that no obvious correlation can be drawn from these values. However, when comparing the $\Delta\delta_{itl}(^{195}Pt)$ values of the stereoisomers, it is clear that stereoisomers where Cl⁻ is always *trans* to H_2O (*cis*-$[PtCl_4(H_2O)_2]$, *fac*-$[PtCl_3(H_2O)_3]^+$ and *cis*-$[PtCl_2(H_2O)_4]^{2+}$) exhibit bigger $\Delta\delta_{itl}(^{195}Pt)$ values compared to the stereoisomers where Cl⁻ is primarily *trans* to Cl⁻. To make such a comparison it was necessary to take the arithmetic mean of the isotopomers (where relevant) to obtain the average $\delta_{itm}(^{195}Pt)$ value of the corresponding "isotopologue". When isotopomers are present in addition to isotopologues i.e. $[PtCl_5(H_2O)]^-$, *cis*-$[PtCl_4(H_2O)_2]$ and *mer*-$[PtCl_3(H_2O)_3]^+$, the respective $\Delta\delta_{itm}(^{195}Pt)$ value are now proportional to the mass factor. For $[PtCl_5(H_2O)]^-$ there are thus two proportionalities to the mass factor. In the first case the $\Delta_{itm}\delta(^{195}Pt)$ value that is obtained for ^{35}Cl *trans* to H_2O and in the second where ^{37}Cl is *trans* to H_2O (Figure 3.10). The excellent agreement between experimental and simulated spectra using regular chemical shift spacing for corresponding isotopomers associated with each isotopologue convincingly supports this model as illustrated in Figure 3.10.

Table 3.4: $^{35}Cl/^{37}Cl$ isotopic shift effects of the $[Pt^{35/37}Cl_n(H_2O)_{6-n}]^{4-n}$ (*n* = 1-6) complexes in 1 M $HClO_4$

Species	$\delta(^{195}Pt)$ in 1 M $HClO_4$ (ppm)	$\delta(^{195}Pt)$ (Literature)	Average $^{35}Cl/^{37}Cl$ $\Delta\delta_{itl}(^{195}Pt)$ (ppm)	$^{35}Cl/^{37}Cl$ $v_{itl}^{1/2}$ (ppm / Hz)
$[PtCl_6]^{2-}$	-12	0 [19]	0.171	0.038 / 3.30
$[PtCl_5(H_2O)]^-$	502	504 [19]	0.194	0.039 / 3.34
cis-$[PtCl_4(H_2O)_2]$	996	1005 [19]	0.184	0.034 / 2.90
trans-$[PtCl_4(H_2O)_2]$	1134	1134 [19]	0.156	0.091 / 7.81
fac-$[PtCl_3(H_2O)_3]^+$	1538	1500 [19]	0.217	0.028 / 2.39
mer-$[PtCl_3(H_2O)_3]^+$	1621	1603 [19]	0.185	0.058 / 4.96
cis-$[PtCl_2(H_2O)_4]^{2+}$	2133	2125 [19]	0.223	0.034 / 2.89
trans-$[PtCl_2(H_2O)_4]^{2+}$	2201	2208 [19]	0.144	0.078 / 6.69
$[PtCl(H_2O)_5]^{3+}$	2695ᵃ	2640 [10]	0.220	0.046 / 3.98

ᵃ This complex was not obtained in sufficiently high enough concentrations in the above experiments, but it was obtained in sufficient concentrations in another experiment discussed in *Chapter 4* from which the values are obtained and reported here for completion.
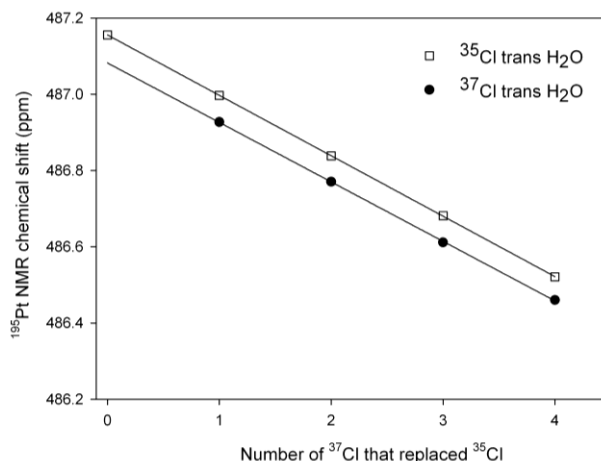
Figure 3.10: ^{195}Pt NMR chemical shift proportionality of the $[Pt^{35}Cl_n^{37}Cl_{5-n}(H_2O)]^-$ (n = 0-5) isotopomers with the ($m'-m$)/m' mass factor.

Since the isotopomers where ^{35}Cl is *trans* to H_2O is more de-shielded compared to where ^{37}Cl is *trans* to H_2O it must imply a shorter bond in the latter cases. When dealing with a 'shorter' Pt–Cl bond, we reasonably assume that upon replacing a ^{35}Cl with a ^{37}Cl ligand, the percentage change in mean bond length will be larger compared to when dealing with a longer Pt–Cl bond in the stereoisomers with higher symmetry (*trans*-$[PtCl_4(H_2O)_2]$, *mer*-$[PtCl_3(H_2O)_3]^+$ and *trans*-$[PtCl_2(H_2O)_4]^{2+}$). If this assumption is valid, a bigger average $\Delta\delta_{itl}(^{195}Pt)$ value is expected for the stereoisomers of lower symmetry i.e. where Cl^- is *trans* to H_2O. This explains qualitatively the trend in the relative magnitudes of the $\Delta\delta_{itl}(^{195}Pt)$ values between stereoisomers evident from Table 3.4, and can be used to discriminate between stereoisomers where no isotopomers are present i.e. *cis*/*trans*-$[PtCl_2(H_2O)_4]^{2+}$.

Interestingly, when the isotopologue peak width at half height (ν_{itl}½) associated with the corresponding stereoisomers of the $[PtCl_n(H_2O)_{6-n}]^{4-n}$ (n = 2-4) complexes are compared, the stereoisomers where Cl^- is *trans* to H_2O, has a much smaller ν_{itl}½ value. This aspect shared with the bigger average $\Delta\delta_{itl}(^{195}Pt)$ value, results in much better resolved isotope signals compared to where Cl^- is primarily *trans* to Cl^-. As all of these Pt(IV) species are present in the same solution the contribution of magnetic field inhomogeneity to peak shape and width can effectively be ignored in the comparison. Since several parameters[4] contribute to the magnitude of T_2 (which determines peak shape) it is difficult to isolate which relaxation mechanism or combination of mechanisms has the major influence on T_2. That these strict proportionalities are observed is perplexing and requires a detailed theoretical study to understand the

47

implications. These proportionalities are however most useful when dealing with more complex resonance signals (*vide infra*) which exhibit severe overlap of isotopologue and isotopomer signals.

3.3.3 ^{195}Pt NMR isotopic signals of the $[Pt^{35/37}Cl_n(H_2^{16/18}O)_{6-n}]^{n-4}$ ($n = 2\text{-}6$) complexes

One of the major objectives of this thesis is the elucidation of the oxidation mechanism of various Pt(II) square-planar complexes (see *Chapter 5*). In this regard, it was of interest to determine how $H_2^{18}O$ enrichment and the resulting $^{16}O/^{18}O$ isotopic signals could assist assignment of oxidation products and mechanistic interpretations. A related study was carried out by Dunham *et al.*[20] who investigated the oxidation of $[PtCl_4]^{2-}$ with H_2O_2 in aqueous solution containing $H_2^{16}O$ and $H_2^{18}O$. It was found *trans*-$[PtCl_4(OH)_2]$ is formed exclusively and from the observed $^{16}O/^{18}O$ isotopologues it was concluded that one OH^- ligand originate from H_2O_2 and the other from solvent H_2O. Gröning *et al.*[10] also employed $^{16}O/^{18}O$ isotopologues to study the oxidation of $[Pt(H_2O)_4]^{2+}$ and *trans*-$[PtCl_2(H_2O)_2]$ with Cl_2. In this experiment, six $^{16}O/^{18}O$ isotopologues were observed which corresponded to $[PtCl(H_2^{16}O)_n(H_2^{18}O)_{5-n}]^{3+}$ ($n = 0$-5) and four $^{16}O/^{18}O$ isotopologues which corresponded to *mer*-$[PtCl_3(H_2^{16}O)_n(H_2^{18}O)_{3-n}]^+$ ($n = 0$-3). Based on the work of these authors, oxidation of $[PtCl_4]^{2-}$ with ClO_3^- in a $H_2^{18}O$ enriched solution was carried out to determine the origin of the coordinated H_2O ligands in the resulting Pt(IV) complexes. $^{16}O/^{18}O$ isotopic effects in addition to $^{35}Cl/^{37}Cl$ isotopic effects were observed which has not been reported before. Gröning *et al.*[10] did mention than additional $^{35}Cl/^{37}Cl$ isotopic effects were observed in their experiments, but these were filtered out to simplify the ^{195}Pt NMR spectra and no discussion of $^{35}Cl/^{37}Cl$ isotope effects was presented. Here, the experimental result is discussed in the context of speciation to confirm the hierarchy of isotopic splitting for the $[PtCl_{6-n}(H_2O)_n]^+$ ($n = 1$-5) complexes if $H_2^{18}O$ is also present in solution. The implications from a mechanistic point of view are discussed in *Chapter 5*.

3.3.3.1 ^{195}Pt NMR signal of $[PtCl_5(H_2^{16/18}O)]^-$, *cis*-$[PtCl_4(H_2^{16/18}O)_2]$, *fac*-$[PtCl_3(H_2^{16/18}O)_3]^+$

A 0.4 M K_2PtCl_4 solution in 2 M $HClO_4$ was enriched with 30 % $H_2^{18}O$ (v/v) prior to oxidation with 3 mol equivalents of $NaClO_3$ (with respect to Pt(II); see experimental

section). Long acquisition times were necessary to obtain sufficient signal/noise ratios and therefore it was critical that the concentration of the species remains constant. In order to prevent changes in the speciation during ^{195}Pt spectra acquisition, the solution was "aged" for two weeks to allow enough time to equilibrate. No change in Pt speciation occurred when the solution was aged for longer periods. All the $[PtCl_n(H_2O)_{6-n}]^{4-n}$ (n = 1-6) complex species are obtained as shown in Figure 3.11 and correlates well with the $\delta(^{195}Pt)$ values observed earlier (Figure 3.5). The $\delta(^{195}Pt)$ values observed are listed in Table 3.6.
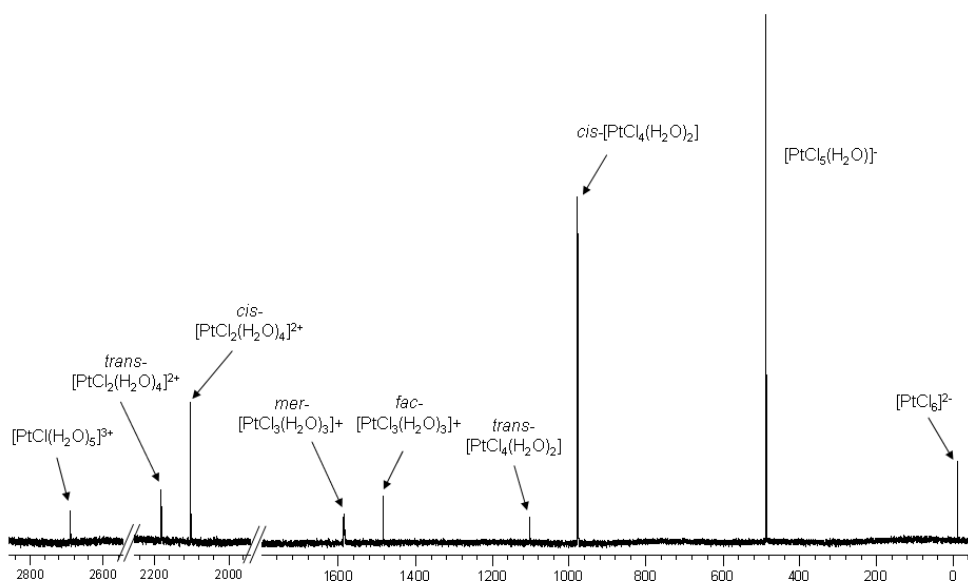
Figure 3.11: ^{195}Pt NMR spectra of the solution resulting from oxidation of 0.4 M $[PtCl_4]^{2-}$ with five mol equivalents $NaClO_3$ in 1 M $HClO_4$ containing 30% $H_2^{18}O$. The ^{195}Pt NMR spectra were obtained after "ageing" the solution for two weeks.

Expansion of each of the signals reveals significant $^{16}O/^{18}O$ isotope effects. Figures 3.12A-C show several additional resonances for $[PtCl_5(H_2O)]^-$, cis-$[PtCl_4(H_2O)_2]$ and fac-$[PtCl_3(H_2O)_3]^+$ due to the presence of $H_2^{16}O$ and $H_2^{18}O$ compared to the corresponding species shown in Figure 3.7 and 3.9 in the absence of added $H_2^{18}O$. It is clear that the additional resonance signals are an identical replicate of the origin signal observed, with the number of replicate sets correlating with the number of possible $^{16}O/^{18}O$ isotopologues.

The $[PtCl_5(H_2O)]^-$ complex display two possible $^{16}O/^{18}O$ isotopologues $[PtCl_5(H_2^{16}O)]^-$ and $[PtCl_5(H_2^{18}O)]^-$ (Figure 3.12A), each sub-divided into the $^{35}Cl/^{37}Cl$ isotopologue and isotopomer signals previously observed for $[PtCl_5(H_2O)]^-$ where only $H_2^{16}O$ is present (Figure 3.7A). For the cis-$[PtCl_4(H_2O)_2]$ complex three possible $^{16}O/^{18}O$

isotopologues are observed (Figure 3.12B), each with the $^{35}Cl/^{37}Cl$ isotopologue and isotopomer signals previously observed for *cis*-$[PtCl_4(H_2O)_2]$ where only $H_2^{16}O$ is present (Figure 3.7C). In the same way *fac*-$[PtCl_3(H_2^{16/18}O)_3]^+$ has four sets of $^{16}O/^{18}O$ isotopologues (Figure 3.12C), each representing the $^{35}Cl/^{37}Cl$ isotopologue distribution previously observed for *fac*-$[PtCl_3(H_2^{16}O)_3]^+$ in Figure 3.9C where only $H_2^{16}O$ is present.
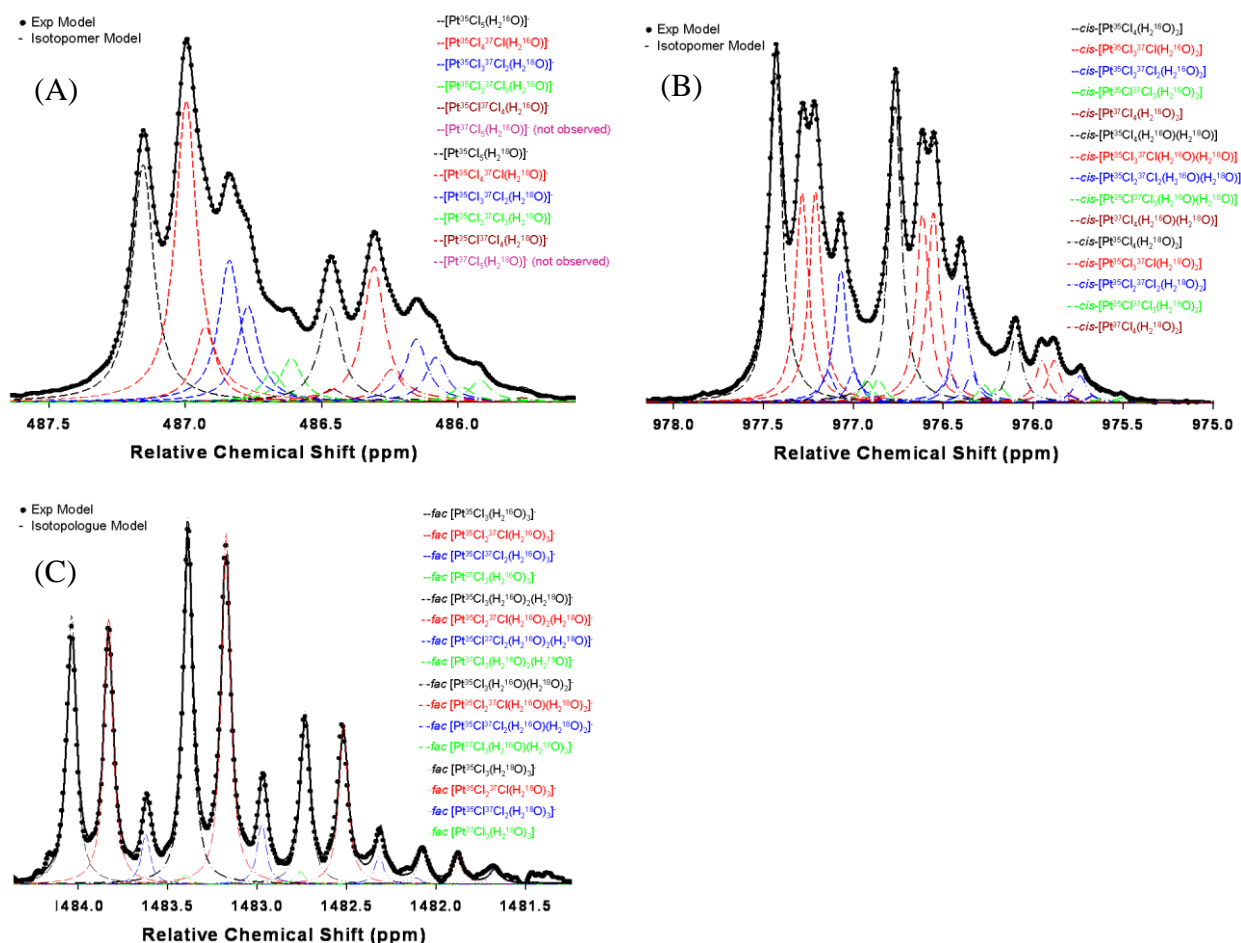
Figure 3.12: Experimental ^{195}Pt NMR spectra of **(A)** $[PtCl_5(H_2^{16/18}O)]^-$, **(B)** *cis*-$[PtCl_4(H_2^{16/18}O)_2]$ and **(C)** *fac*-$[PtCl_3(H_2^{16/18}O)_3]^+$ traced by symbols. The solid lines are the non-linear least-squares fits of the isotopic chemical shift model that incorporates $^{16}O/^{18}O$ and $^{35}Cl/^{37}Cl$ isotopologues and $^{35}Cl/^{37}Cl$ isotopomers. The same dotted lines trace the individual sets of $^{16}O/^{18}O$ isotopologues.

The larger relative mass difference (%) between the $^{16}O/^{18}O$ isotopes (0.111 %), compared to the $^{35}Cl/^{37}Cl$ isotopes (0.054 %) result in bigger $\Delta\delta_{itl}(^{195}Pt)$ values between respective $^{16}O/^{18}O$ isotopologues due to the direct proportionality to the *(m'-m)/m'* mass factor[12-14] previously described. As $H_2^{16}O$ is replaced by $H_2^{18}O$ the Pt(IV) nucleus becomes more shielded, similar to that observed for $^{35}Cl/^{37}Cl$ isotopic replacement.

Table 3.5: Comparison of the experimental (Figures 3.12 A–C) and statistically expected isotopologue and isotopomer distributions for the $[Pt^{35/37}Cl_n(H_2^{16/18}O)_{6-n}]^{4-n}$ (n = 3-5) series of complexes.

$^{35/37}$Cl *trans* to H$_2$O	Pt(IV) isotopologue	Percent isotopomers		Sum percent of isotopomers to yield isotopologue amount	
		Experimental	Statistical	Experimental	Statistical
^{35}Cl	$[Pt^{35}Cl_5(H_2^{16}O)]^-$	25.2 (± 0.3)	24.97	25.2	24.97
^{35}Cl	$[Pt^{35}Cl_4{}^{37}Cl(H_2^{16}O)]^-$	32.0 (± 0.5)	31.94	40.0	39.93
^{37}Cl		8.00 (± 0.4)	7.99		
^{35}Cl	$[Pt^{35}Cl_3{}^{37}Cl_2(H_2^{16}O)]^-$	15.1 (± 0.2)	15.32	25.3	25.54
^{37}Cl		10.2 (± 0.3)	10.22		
^{35}Cl	$[Pt^{35}Cl_2{}^{37}Cl_3(H_2^{16}O)]^-$	3.2 (± 0.2)	3.27	7.8	8.17
^{37}Cl		4.6 (± 0.3)	4.9		
^{35}Cl	$[Pt^{35}Cl^{37}Cl_4(H_2^{16}O)]^-$	0.3 (± 0.2)	0.26	1.7	1.31
^{37}Cl		1.4 (± 0.3)	1.05		
^{37}Cl	$[Pt^{37}Cl_5(H_2^{16}O)]^-$	not reliably measurable	0.08	not reliably measurable	0.08
^{35}Cl	$[Pt^{35}Cl_5(H_2^{18}O)]^-$	23.1 (± 0.3)	24.97	23.1	24.97
^{35}Cl	$[Pt^{35}Cl_4{}^{37}Cl(H_2^{18}O)]^-$	32.8 (± 0.4)	31.94	40.7	39.93
^{37}Cl		7.9 (± 0.4)	7.99		
^{35}Cl	$[Pt^{35}Cl_3{}^{37}Cl_2(H_2^{18}O)]^-$	15.3 (± 0.3)	15.32	26.1	25.54
^{37}Cl		10.8 (± 0.4)	10.22		
^{35}Cl	$[Pt^{35}Cl_2{}^{37}Cl_3(H_2^{18}O)]^-$	3.6 (± 0.2)	3.27	8.9	8.17
^{37}Cl		5.3 (± 0.1)	4.9		
^{35}Cl	$[Pt^{35}Cl^{37}Cl_4(H_2^{18}O)]^-$	0.2 (± 0.2)	0.26	1.2	1.31
^{37}Cl		1.0 (± 0.1)	1.05		
^{37}Cl	$[Pt^{37}Cl_5(H_2^{18}O)]^-$	not reliably measurable	0.08	not reliably measurable	0.08
^{35}Cl,^{35}Cl	*cis*-$[Pt^{35}Cl_4(H_2^{16}O)_2]$	33.7 (± 0.2)	32.96	33.7	32.96
^{35}Cl,^{35}Cl	*cis*-$[Pt^{35}Cl_3{}^{37}Cl(H_2^{16}O)_2]$	21.4 (± 0.1)	21.08	42.9	42.16
^{35}Cl,^{37}Cl		21.5 (± 0.2)	21.08		
^{35}Cl,^{35}Cl	*cis*-$[Pt^{35}Cl_2{}^{37}Cl_2(H_2^{16}O)_2]$	3.1 (± 0.1)	3.37	20.20	20.22
^{35}Cl,^{37}Cl		13.6 (± 0.2)	13.48		
^{37}Cl,^{37}Cl		3.3 (± 0.1)	3.37		
^{35}Cl,^{37}Cl	*cis*-$[Pt^{35}Cl^{37}Cl_3(H_2^{16}O)_2]$	1.4 (± 0.3)	2.16	2.8	4.31
^{37}Cl,^{37}Cl		1.4 (± 0.2)	2.16		
^{37}Cl,^{37}Cl	*cis*-$[Pt^{37}Cl_4(H_2^{16}O)]$	0.6 (± 0.3)	0.34	0.6	0.34
^{35}Cl,^{35}Cl	*cis*-$[Pt^{35}Cl_4(H_2^{16}O)(H_2^{18}O)]$	33.8 (± 0.2)	32.96	33.8	32.96
^{35}Cl,^{35}Cl	*cis*-$[Pt^{35}Cl_3{}^{37}Cl(H_2^{16}O)(H_2^{18}O)]$	21.3 (± 0.1)	21.08	42.8	42.16
^{35}Cl,^{37}Cl		21.5 (± 0.3)	21.08		
^{35}Cl,^{35}Cl	*cis*-$[Pt^{35}Cl_2{}^{37}Cl_2(H_2^{16}O)(H_2^{18}O)]$	3.1 (± 0.1)	3.37	19.9	20.22
^{35}Cl,^{37}Cl		13.5 (± 0.2)	13.48		
^{37}Cl,^{37}Cl		3.3 (± 0.1)	3.37		
^{35}Cl,^{37}Cl	*cis*-$[Pt^{35}Cl^{37}Cl_3(H_2^{16}O)(H_2^{18}O)]$	1.5 (± 0.2)	2.16	2.9	4.31
^{37}Cl,^{37}Cl		1.4 (± 0.1)	2.16		
^{37}Cl,^{37}Cl	*cis*-$[Pt^{37}Cl_4(H_2^{16}O)(H_2^{18}O)]$	0.6 (± 0.3)	0.34	0.6	0.34
^{35}Cl,^{35}Cl	*cis*-$[Pt^{35}Cl_4(H_2^{18}O)_2]$	34.6 (± 0.2)	32.96	34.6	32.96
^{35}Cl,^{35}Cl	*cis*-$[Pt^{35}Cl_3{}^{37}Cl(H_2^{18}O)_2]$	20.8 (± 0.1)	21.08	42.7	42.16
^{35}Cl,^{37}Cl		21.9 (± 0.3)	21.08		
^{35}Cl,^{35}Cl	*cis*-$[Pt^{35}Cl_2{}^{37}Cl_2(H_2^{18}O)_2]$	3.0 (± 0.1)	3.37	19.2	20.22
^{35}Cl,^{37}Cl		13.0 (± 0.2)	13.48		
^{37}Cl,^{37}Cl		3.2 (± 0.1)	3.37		
^{35}Cl,^{37}Cl	*cis*-$[Pt^{35}Cl^{37}Cl_3(H_2^{18}O)_2]$	1.6 (± 0.1)	2.16	3.1	4.32
^{37}Cl,^{37}Cl		1.5 (± 0.2)	2.16		
^{37}Cl,^{37}Cl	*cis*-$[Pt^{37}Cl_4(H_2^{18}O)_2]$	0.5 (± 0.2)	0.34	0.5	0.34
^{35}Cl,^{35}Cl,^{35}Cl	*fac*-$[Pt^{35}Cl_3(H_2^{16}O)_3]^+$			43.1 (± 0.2)	43.50
^{35}Cl,^{35}Cl,^{37}Cl	*fac*-$[Pt^{35}Cl_2{}^{37}Cl(H_2^{16}O)_3]^+$			43.0 (± 0.1)	41.73
^{35}Cl,^{37}Cl,^{37}Cl	*fac*-$[Pt^{35}Cl^{37}Cl_2(H_2^{16}O)_3]^+$			12.9 (± 0.2)	13.35
^{37}Cl,^{37}Cl,^{37}Cl	*fac*-$[Pt^{37}Cl_3(H_2^{16}O)_3]^+$			1.0 (± 0.4)	1.42
^{35}Cl,^{35}Cl,^{35}Cl	*fac*-$[Pt^{35}Cl_3(H_2^{16}O)_2(H_2^{18}O)]^+$			43.9 (± 0.1)	43.50
^{35}Cl,^{35}Cl,^{37}Cl	*fac*-$[Pt^{35}Cl_2{}^{37}Cl(H_2^{16}O)_2(H_2^{18}O)]^+$			42.5 (± 0.3)	41.73
^{35}Cl,^{37}Cl,^{37}Cl	*fac*-$[Pt^{35}Cl^{37}Cl_2(H_2^{16}O)_2(H_2^{18}O)]^+$			12.6 (± 0.2)	13.35
^{37}Cl,^{37}Cl,^{37}Cl	*fac*-$[Pt^{37}Cl_3(H_2^{16}O)_2(H_2^{18}O)]^+$			1.1 (± 0.4)	1.42
^{35}Cl,^{35}Cl,^{35}Cl	*fac*-$[Pt^{35}Cl_3(H_2^{16}O)(H_2^{18}O)_2]^+$			43.4 (± 0.1)	43.50
^{35}Cl,^{35}Cl,^{37}Cl	*fac*-$[Pt^{35}Cl_2{}^{37}Cl(H_2^{16}O)(H_2^{18}O)_2]^+$			41.2 (± 0.1)	41.73
^{35}Cl,^{37}Cl,^{37}Cl	*fac*-$[Pt^{35}Cl^{37}Cl_2(H_2^{16}O)(H_2^{18}O)_2]^+$			14.2 (± 0.3)	13.35
^{37}Cl,^{37}Cl,^{37}Cl	*fac*-$[Pt^{37}Cl_3(H_2^{16}O)(H_2^{18}O)_2]^+$			1.1 (± 0.4)	1.42

Table 3.5 continued from the previous page.

Isotopomer	Species				
^{35}Cl,^{35}Cl,^{35}Cl	fac-[Pt^{35}Cl$_3$(H$_2^{18}$O)$_3$]$^+$			43.1 ($\pm$0.1)	43.50
^{35}Cl,^{35}Cl,^{37}Cl	fac-[Pt^{35}Cl$_2^{37}$Cl(H$_2^{18}$O)$_3$]$^+$			37.5 ($\pm$0.2)	41.73
^{35}Cl,^{37}Cl,^{37}Cl	fac-[Pt^{35}Cl^{37}Cl$_2$(H$_2^{18}$O)$_3$]$^+$			18.3 ($\pm$0.2)	13.35
^{37}Cl,^{37}Cl,^{37}Cl	fac-[Pt^{37}Cl$_3$(H$_2^{18}$O)$_3$]$^+$			1.0 ($\pm$0.3)	1.42
^{35}Cl	cis-[Pt^{35}Cl$_2$(H$_2^{16}$O)$_4$]$^{2+}$			15.76 ($\pm$0.6)	13.78
^{35}Cl, ^{37}Cl	cis-[Pt^{35}Cl^{37}Cl(H$_2^{16}$O)$_4$]$^{2+}$			9.50 ($\pm$0.3)	8.82
^{37}Cl	cis-[Pt^{37}Cl$_2$(H$_2^{16}$O)$_4$]$^{2+}$			1.35 ($\pm$0.3)	1.41
^{35}Cl (H$_2^{16}$O)	cis-[Pt^{35}Cl$_2$(H$_2^{16}$O)$_3$(H$_2^{18}$O)]$^{2+}$	12.47 ($\pm$0.6)	11.82	24.95	23.63
^{35}Cl (H$_2^{16}$O, H$_2^{18}$O)	cis-[Pt^{35}Cl$_2$(H$_2^{16}$O)$_3$(H$_2^{18}$O)]$^{2+}$	12.47 ($\pm$0.6)	11.82		
^{35}Cl,^{37}Cl (H$_2^{16}$O, H$_2^{16}$O)	cis-[Pt^{35}Cl^{37}Cl(H$_2^{16}$O)$_3$(H$_2^{18}$O)]$^{2+}$	7.72 ($\pm$0.4)	7.56	15.45	15.11
^{35}Cl,^{37}Cl (H$_2^{16}$O, H$_2^{18}$O)	cis-[Pt^{35}Cl^{37}Cl(H$_2^{16}$O)$_3$(H$_2^{18}$O)]$^{2+}$	7.72 ($\pm$0.4)	7.56		
^{37}Cl (H$_2^{16}$O, H$_2^{16}$O)	cis-[Pt^{37}Cl$_2$(H$_2^{16}$O)$_3$(H$_2^{18}$O)]$^{2+}$	0.79 ($\pm$0.1)	1.21	1.59	2.42
^{37}Cl (H$_2^{16}$O, H$_2^{18}$O)	cis-[Pt^{37}Cl$_2$(H$_2^{16}$O)$_3$(H$_2^{18}$O)]$^{2+}$	0.79 ($\pm$0.1)	1.21		
^{35}Cl (H$_2^{16}$O)	cis-[Pt^{35}Cl$_2$(H$_2^{16}$O)$_2$(H$_2^{18}$O)$_2$]$^{2+}$	2.56 ($\pm$0.2)	2.53	14.83	15.19
^{35}Cl (H$_2^{16}$O, H$_2^{18}$O)	cis-[Pt^{35}Cl$_2$(H$_2^{16}$O)$_2$(H$_2^{18}$O)$_2$]$^{2+}$	9.70 ($\pm$0.6)	10.13		
^{35}Cl (H$_2^{18}$O, H$_2^{18}$O)	cis-[Pt^{35}Cl$_2$(H$_2^{16}$O)$_2$(H$_2^{18}$O)$_2$]$^{2+}$	2.56 ($\pm$0.2)	2.53		
^{35}Cl,^{37}Cl (H$_2^{16}$O)	cis-[Pt^{35}Cl^{37}Cl(H$_2^{16}$O)$_2$(H$_2^{18}$O)$_2$]$^{2+}$	1.40 ($\pm$0.1)	1.62	9.17	9.72
^{35}Cl,^{37}Cl (H$_2^{16}$O, H$_2^{18}$O)	cis-[Pt^{35}Cl^{37}Cl(H$_2^{16}$O)$_2$(H$_2^{18}$O)$_2$]$^{2+}$	6.37 ($\pm$0.4)	6.48		
^{35}Cl,^{37}Cl (H$_2^{18}$O, H$_2^{18}$O)	cis-[Pt^{35}Cl^{37}Cl(H$_2^{16}$O)$_2$(H$_2^{18}$O)$_2$]$^{2+}$	1.40 ($\pm$0.1)	1.62		
^{37}Cl (H$_2^{16}$O, H$_2^{16}$O)	cis-[Pt^{37}Cl$_2$(H$_2^{16}$O)$_2$(H$_2^{18}$O)$_2$]$^{2+}$	not reliably measurable	0.26	not reliably measurable	
^{37}Cl (H$_2^{16}$O, H$_2^{18}$O)	cis-[Pt^{37}Cl$_2$(H$_2^{16}$O)$_2$(H$_2^{18}$O)$_2$]$^{2+}$	0.90	1.04	0.90	1.56
^{37}Cl (H$_2^{18}$O, H$_2^{18}$O)	cis-[Pt^{37}Cl$_2$(H$_2^{16}$O)$_2$(H$_2^{18}$O)$_2$]$^{2+}$	not reliably measurable	0.26	not reliably measurable	
^{35}Cl (H$_2^{16}$O, H$_2^{18}$O)	cis-[Pt^{35}Cl$_2$(H$_2^{16}$O)(H$_2^{18}$O)$_3$]$^{2+}$	1.68 ($\pm$0.1)	2.17	3.98	4.34
^{35}Cl (H$_2^{18}$O, H$_2^{18}$O)	cis-[Pt^{35}Cl$_2$(H$_2^{16}$O)(H$_2^{18}$O)$_3$]$^{2+}$	2.30 ($\pm$0.1)	2.17		
^{35}Cl,^{37}Cl (H$_2^{16}$O, H$_2^{18}$O)	cis-[Pt^{35}Cl^{37}Cl(H$_2^{16}$O)(H$_2^{18}$O)$_3$]$^{2+}$	0.89 ($\pm$0.1)	1.39	2.52	2.78
^{35}Cl,^{37}Cl (H$_2^{18}$O, H$_2^{18}$O)	cis-[Pt^{35}Cl^{37}Cl(H$_2^{16}$O)(H$_2^{18}$O)$_3$]$^{2+}$	1.63 ($\pm$0.1)	1.39		
^{37}Cl (H$_2^{16}$O, H$_2^{18}$O)	cis-[Pt^{37}Cl$_2$(H$_2^{16}$O)(H$_2^{18}$O)$_3$]$^{2+}$	not reliably measurable	0.22	0.44	
^{37}Cl (H$_2^{18}$O H$_2^{18}$O)	cis-[Pt^{37}Cl$_2$(H$_2^{16}$O)(H$_2^{18}$O)$_3$]$^{2+}$	not reliably measurable	0.22		
^{35}Cl	cis-[Pt^{35}Cl$_2$(H$_2^{18}$O)$_4$]$^{2+}$	not reliably measurable			0.47
^{35}Cl, ^{37}Cl	cis-[Pt^{35}Cl^{37}Cl(H$_2^{18}$O)$_4$]$^{2+}$	not reliably measurable			0.30
^{37}Cl	cis-[Pt^{37}Cl$_2$(H$_2^{18}$O)$_4$]$^{2+}$	not reliably measurable			0.05

The result is a clear-cut image of the ^{35}Cl/^{37}Cl isotopologue and isotopomer signals. The overall intensities of the ^{195}Pt signals of [PtCl$_5$(H$_2^{16}$O)]$^-$ and [PtCl$_5$(H$_2^{18}$O)]$^-$ integrate to a ratio of 71:29 %, close to the statistically expected ratio of 70:30 % confirming the ^{16}O/^{18}O isotopic model. The isotopic model used to fit the data in Figure 3.7 and 3.9 is therefore extended to include isotopologues resulting from the substitution of H$_2^{16}$O by H$_2^{18}$O in the Pt(IV) coordination sphere. The least-square fits based on this model are in excellent agreement with the data as shown in Figures 3.12A–C, and the ^{195}Pt signals ascribed to the various isotopologue and isotopomers agree quantitatively with the theoretical statistical distributions (Table 3.5). In this sample the concentration of cis-[PtCl$_4$(H$_2$O)$_2$] and mer-[PtCl$_3$(H$_2$O)$_3$]$^+$ were not high enough to allow a least-squares analysis of the peak areas and comparison with the respective stereoisomers. Although it may be reasonable to expect a similar hierarchy of $^{35/37}$Cl and $^{16/18}$O isotopic effects, a

different pattern of isotope signals is observed for the *cis*-[PtCl$_2$(H$_2{}^{16/18}$O)$_4$]$^{2+}$ stereoisomer.

3.3.3.2 Isotopologue and isotopomer distribution of cis-[Pt^{35}Cl$_n{}^{37}$Cl^{2-n}(H$_2{}^{16}$O)$_m$(H$_2{}^{18}$O)$^{4-m}$] (n = 0-2; m = 0-4) observed with ^{195}Pt NMR.

Expansion of the *cis*-[PtCl$_2$(H$_2{}^{16/18}$O)$_4$]$^{2+}$ signal reveals a complicated spectrum of ^{195}Pt NMR signals as shown in Figure 3.13.
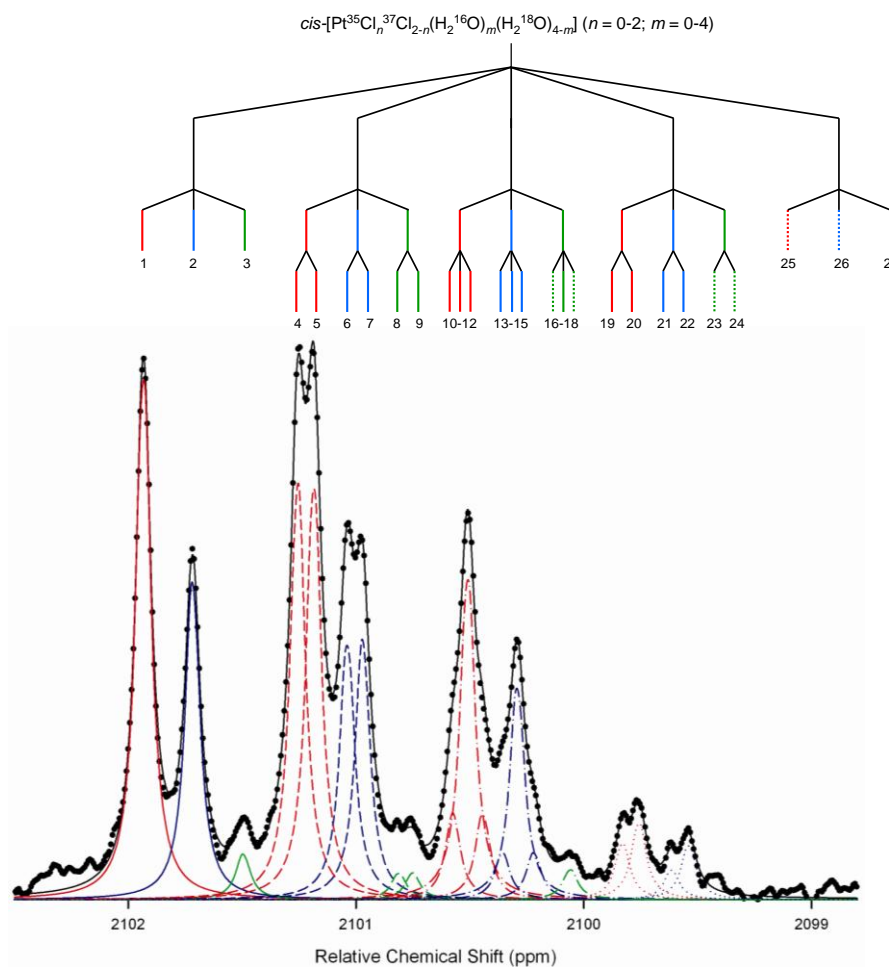
Figure 3.13: ^{195}Pt NMR spectrum of *cis*-[Pt$^{35/37}$Cl$_2$(H$_2{}^{16/18}$O)$_4$]$^{2+}$ defined by a least-squares model that incorporates isotopologues and isotopomers (solid black line). Each signal is simulated individually from the least-squares calculated fit and is correlated to the specific isotopic complex by the numbers 1-27. The dotted lines used in the splitting hierarchy indicate signals not incorporated in the model, due to insufficient signal/noise ratio.

Four different groups of ^{16}O/^{18}O isotopologues are identified as predicted by the number of ^{16}O/^{18}O complexes (the fifth group is not observed due to insufficient signal/noise ratio). Interestingly, the groups of ^{16}O/^{18}O isotopologue signals are different compared to the identical sets of ^{16}O/^{18}O isotopologues found for [PtCl$_5$(H$_2{}^{16/18}$O)]$^-$, *cis*-

$[PtCl_4(H_2{}^{16/18}O)_2]$ and *fac*-$[PtCl_3(H_2{}^{16/18}O)_3]^+$ in Figure 3.12A-C. The first set of $^{35}Cl/^{37}Cl$ isotopologues (labeled as signals 1-3 in Figure 3.13) is assigned to the *cis*-$[PtCl_2(H_2O)_4]^{2+}$ complex where all four coordinated H_2O has the ^{16}O isotope. Since no $^{16}O/^{18}O$ isotopomer configuration is possible in this case, the isotopic distribution is analogous to the isotopologue distribution of *cis*-$[PtCl_2(H_2O)_4]^{2+}$ shown in Figure 3.9E where no additional $H_2{}^{18}O$ is present as. The three isotopologues that correlate with these $^{35}Cl/^{37}Cl$ isotopologue signals are illustrated in Figure 3.14 and are correlated to the signals in Figure 3.13 by the same numbering system and colour scheme.
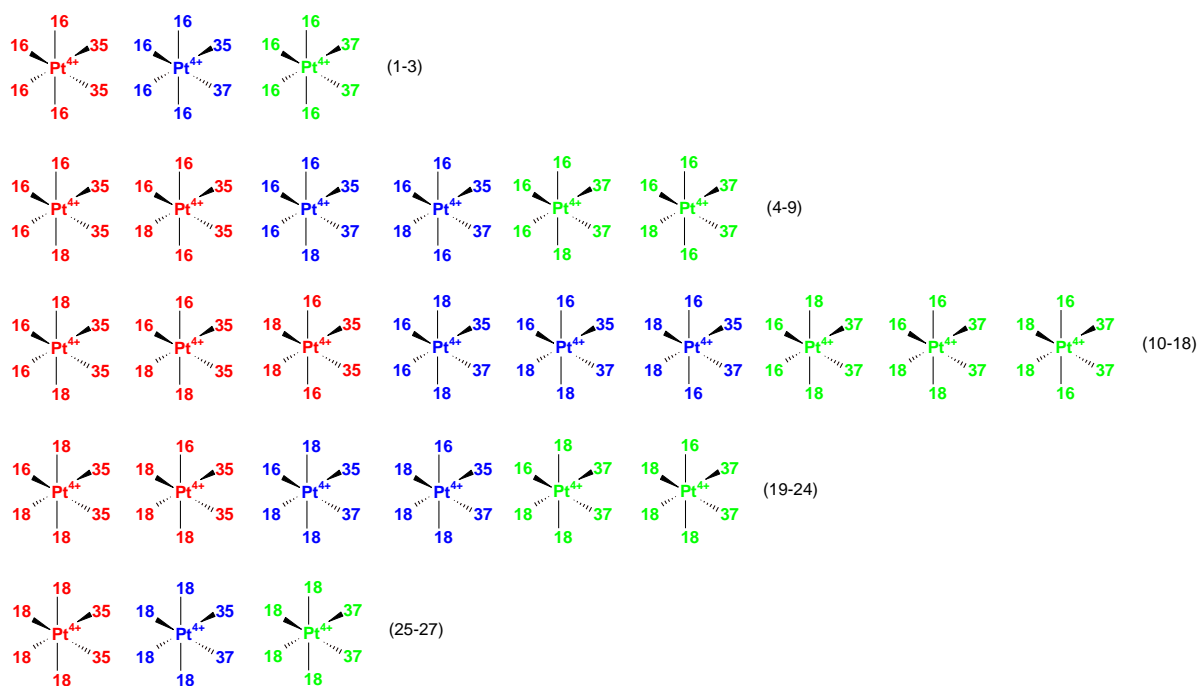
Figure 3.14: Diagram illustrating the statistical probabilities of *cis*-$[PtCl_2(H_2O)_4]^{2+}$ if both $^{35}Cl/^{37}Cl$ and $^{16}O/^{18}O$ isotopes are present where 16 = ^{16}O, 18 = ^{18}O and 35 = ^{35}Cl, 37 = ^{37}Cl.

The second set of $^{16}O/^{18}O$ isotopologues (signals 4-9) correlate with the *cis*-$[PtCl_2(H_2O)_4]^{2+}$ complex which has one coordinated $H_2{}^{18}O$. From Figure 3.9E it is clear than no $^{35}Cl/^{37}Cl$ isotopomers are observed for the *cis*-$[PtCl_2(H_2O)_4]^{2+}$ complex when no $H_2{}^{18}O$ is present. The unique isotopologue/isotopomer distribution pattern observed for *cis*-$[PtCl_2(H_2{}^{16}O)_3(H_2{}^{18}O)]^{2+}$ must therefore originate from the position of the $^{35}Cl/^{37}Cl$ isotopes relative to $H_2{}^{16}O/H_2{}^{18}O$, thereby inducing an $^{16}O/^{18}O$ *isotopomer* effect. For the *cis*-$[Pt^{35}Cl_2(H_2{}^{16}O)_3(H_2{}^{18}O)]^{2+}$ *isotopologue* one *isotopomer* is thus observed if both ^{35}Cl are *trans* to $H_2{}^{16}O$ and the other if one ^{35}Cl is *trans* to $H_2{}^{18}O$ (signals 4 and 5; in Figure 3.14). The *cis*-$[Pt^{35}Cl^{37}Cl(H_2{}^{16}O)_3(H_2{}^{18}O)]^{2+}$ *isotopologue* is also divided into

two *isotopomers* (signals 6 and 7), where both $^{35}Cl/^{37}Cl$ is *trans* to $H_2^{16}O$ and where ^{35}Cl or ^{37}Cl is *trans* to $H_2^{18}O$. It seems that only one signal is observed for the *cis*-$[Pt^{35}Cl^{37}Cl(H_2^{16}O)_3(H_2^{18}O)]^{2+}$ *isotopomer* where ^{35}Cl or ^{37}Cl is *trans* to $H_2^{18}O$ (species 7 in Figure 3.15). This is merely a property of the unique configuration of this isotopologue since in the first possibility if the ^{35}Cl isotope is *trans* to $H_2^{18}O$, the ^{37}Cl isotope will always be *trans* to $H_2^{16}O$. In the other possibility, if the ^{37}Cl isotope is *trans* to $H_2^{18}O$, the ^{35}Cl isotope will always be *trans* to $H_2^{16}O$, resulting in what seems to be the same $\delta_{itm}(^{195}Pt)$ value. The *cis*-$[Pt^{37}Cl_2(H_2^{16}O)_3(H_2^{18}O)]^{2+}$ *isotopologue* is also sub-divided into two $^{16}O/^{18}O$ *isotopomers* (signals 8 and 9). Signals 4-9 is thus seen as a single $^{16}O/^{18}O$ *isotopologue*, divided into three $^{35}Cl/^{37}Cl$ *isotopologues*, which is finally divided into two $^{16}O/^{18}O$ *isotopomers* each. The $^{16}O/^{18}O$ *isotopologue* has a statistical value contributing to the fraction of $H_2^{18}O$ present in solution, while the ratio of the three $^{35}Cl/^{37}Cl$ *isotopologues* are determined by the natural abundance of $^{35}Cl/^{37}Cl$ (Equation 3.1), and finally the six $^{16}O/^{18}O$ *isotopomers* are divided according to the statistical probability purely based on the number of possible orientations.

The third set of $^{16}O/^{18}O$ isotopologues corresponds to the *cis*-$[PtCl_2(H_2O)_4]^{2+}$ complex with two coordinated $H_2^{18}O$ molecules (signals 10-18 in Figure 3.13). According to the $^{16}O/^{18}O$ isotopomer model discussed above, three $^{16}O/^{18}O$ isotopomers are possible for each of the three $^{35}Cl/^{37}Cl$ isotopologues. For the $^{35}Cl/^{37}Cl$ isotopologue *cis*-$[Pt^{35}Cl_2(H_2^{16}O)_2(H_2^{18}O)_2]^{2+}$, the first $^{16}O/^{18}O$ isotopomer is observed when both $H_2^{16}O$ are *trans* to ^{35}Cl (signal 10), the second where one $H_2^{18}O$ is *trans* to ^{35}Cl (signal 11) and the third where both $H_2^{18}O$ is *trans* to ^{35}Cl (signal 12). For the second $^{35}Cl/^{37}Cl$ isotopologue *cis*-$[Pt^{35}Cl^{37}Cl(H_2^{16}O)_2(H_2^{18}O)_2]^{2+}$ the first $^{16}O/^{18}O$ isotopomer is observed when both $H_2^{16}O$ are *trans* to $^{35}Cl/^{37}Cl$ (signal 13), the second where one $H_2^{18}O$ is *trans* to ^{35}Cl or ^{37}Cl (signal 14) and the third where both $H_2^{18}O$ is *trans* to $^{35}Cl/^{37}Cl$ (signal 15). Finally for the third $^{35}Cl/^{37}Cl$ isotopologue *cis*-$[Pt^{37}Cl_2(H_2^{16}O)_2(H_2^{18}O)_2]^{2+}$ the first $^{16}O/^{18}O$ isotopomer is expected where both $H_2^{16}O$ are *trans* to ^{37}Cl (signal 16), the second is observed where one $H_2^{18}O$ is *trans* to ^{37}Cl (signal 17) and the third where both $H_2^{18}O$ is *trans* to ^{37}Cl (signal 18). Signals 16 and 18 was not analyzed by least-squares analysis due to an insufficient signal/noise ratio. Signals 10-18 are thus seen as one $^{16}O/^{18}O$ isotopologue, divided into three $^{35}Cl/^{37}Cl$ isotopologues, which is finally divided into three $^{16}O/^{18}O$ isotopomers each.

The fourth set of $^{16}O/^{18}O$ isotopologues corresponds to cis-$[PtCl_2(H_2O)_4]^{2+}$ with three coordinated $H_2^{18}O$ molecules (signals 19-24). Each of the $^{35}Cl/^{37}Cl$ isotopologues must display two $^{16}O/^{18}O$ isotopomers as predicted by the model according to the same hierarchy discussed for species 4-9. The experimental result confirms these predictions although signals 23 and 24 are not observed due to an insufficient signal/noise ratio. The fifth set of $^{16}O/^{18}O$ isotopologues contributing to cis-$[PtCl_2(H_2^{18}O)_4]^{2+}$ is not observed due to the low concentration of this species but is expected to have the same $^{35}Cl/^{37}Cl$ isotopologue distribution as cis-$[PtCl_2(H_2^{16}O)_4]^{2+}$ without any $^{16}O/^{18}O$ isotopomers present. The experimental values are listed in Table 3.5 and correlate well with the statistically calculated values, confirming the $^{16}O/^{18}O$ isotopomer model.

Although the signal/noise ratio is insufficient for $trans$-$[PtCl_4(H_2O)_2]$, mer-$[PtCl_3(H_2O)_3]^+$, $trans$-$[PtCl_2(H_2O)_4]^{2+}$ and $[PtCl(H_2O)_5]^{3+}$ to do a least-squares analysis, it was possible to measure the $\Delta\delta_{itl}(^{195}Pt)$ value between respective $^{16}O/^{18}O$ isotopologues. The $\Delta\delta_{itl}(^{195}Pt)$ values between respective $^{16}O/^{18}O$ isotopologues (Table 3.7) are considerably bigger compared to $\Delta\delta_{itl}(^{195}Pt)$ values between respective $^{35}Cl/^{37}Cl$ isotopologues (Table 3.4) as a result of the bigger percentage mass difference between $^{16}O/^{18}O$ (11.11 %) compared to $^{35}Cl/^{37}Cl$ (5.41 %).

Table 3.6: $^{16}O/^{18}O$ isotopic shift increments of the $[Pt^{35/37}Cl_n(H_2^{16/18}O)_{6-n}]^{4-n}$ (n = 1-6) complexes in 2 M $HClO_4$.

Species	$\delta(^{195}Pt)$ in 2 M $HClO_4$ (ppm)	Average $^{16}O/^{18}O$ $\Delta\delta_{itl}(^{195}Pt)$ (ppm)
$[PtCl_6]^{2-}$	-10.5	not applicable
$[PtCl_5(H_2O)]^-$	487	0.686
cis-$[PtCl_4(H_2O)_2]$	977	0.664
$trans$-$[PtCl_4(H_2O)_2]$	1103	0.950
fac-$[PtCl_3(H_2O)_3]^+$	1484	0.648
mer-$[PtCl_3(H_2O)_3]^+$	1586	0.910
cis-$[PtCl_2(H_2O)_4]^{2+}$	2102	0.716
$trans$-$[PtCl_2(H_2O)_4]^{2+}$	2181	0.830
$[PtCl(H_2O)_5]^{3+}$	2690	0.750

A clear trend is evident from the $\Delta\delta_{itl}(^{195}Pt)$ values in Table 3.6 between respective stereoisomers. The $\Delta\delta_{itl}(^{195}Pt)$ value between $^{16}O/^{18}O$ isotopologues where Cl^- is always $trans$ to H_2O (cis-$[PtCl_4(H_2O)_2]$, fac-$[PtCl_3(H_2O)_3]^+$ and cis-$[PtCl_2(H_2O)_4]^{2+}$) is considerably smaller compared to $^{16}O/^{18}O$ isotopologues where Cl^- is always $trans$ to Cl^-. As expected this trend is opposite from that observed for $^{35}Cl/^{37}Cl$

56

isotopologues in Table 3.4, and is consistent with the *trans* influence model. The Pt–O bond is expected to be shorter in complexes where H_2O is *trans* to H_2O compared to the case where H_2O is *trans* to Cl^-, so that bigger $\Delta\delta_{itl}(^{195}Pt)$ values between $^{16}O/^{18}O$ isotopologues are expected for *trans*-$[PtCl_4(H_2O)_2]$, *mer*-$[PtCl_3(H_2O)_3]^+$ and *trans*-$[PtCl_2(H_2O)_4]^{2+}$.

3.3.4 ^{195}Pt NMR $^{35}Cl/^{37}Cl$ isotopologue distribution of the $[PtCl_n(OH)_{6-n}]^{2-}$ (*n* = 1-5) *hydroxido* complexes.

The $[PtCl_n(OH)_{6-n}]^{2-}$ (*n* = 1-5) *hydroxido* complexes were obtained by two different methods of synthesis as described in the experimental section. Some of the species were obtained in relatively low concentrations, resulting in low signal/noise ratios. Initial assignments were made by ^{195}Pt NMR chemical-shift-trend analysis, according to the principles stipulated in *Chapter 2*. The $\delta(^{195}Pt)$ values and assignments agrees well with that found by Kramer and Koch.[1] Expansion of the $[PtCl_n(OH)_{6-n}]^{2-}$ (*n* = 1-5) ^{195}Pt NMR signals reveals well resolved $^{35}Cl/^{37}Cl$ isotopologue signals, while no isotopomers are observed. The experimental ^{195}Pt NMR spectra of the $[PtCl_n(OH)_{6-n}]^{2-}$ (*n* = 1-5) species are shown in Figure 3.15.

It is remarkable that no *isotopomer* signals are observed for $[PtCl_5(OH)]^{2-}$, *cis*-$[PtCl_4(OH)_2]^{2-}$ and *mer*-$[PtCl_3(OH)_3]^{2-}$ *hydroxido* species. The *isotopologue* distributions of the respective stereoisomers *cis/trans*-$[PtCl_4(OH)_2]^{2-}$, *fac/mer*-$[PtCl_3(OH)_3]^{2-}$ and *cis/trans*-$[PtCl_4(OH)_2]^{2-}$ are well resolved and looks almost identical. Least-squares analysis results in the expected statistical $^{35}Cl/^{37}Cl$ isotopologue concentrations and confirms the assignments (Table 3.8), but discrimination between stereoisomers are not possible based on the $^{35}Cl/^{37}Cl$ isotopologue concentrations.

Isotopomers of the $[PtCl_5(H_2O)]^-$, *cis*-$[PtCl_4(H_2O)_2]$ and *mer*-$[PtCl_3(H_2O)_3]^+$ *aqua* complexes are observed depending on whether a ^{35}Cl or ^{37}Cl isotope is *trans* to H_2O, resulting different Pt–Cl bond lengths. Studies by Kuroda *et al.*[21] on the crystal structures of three stereoisomers of $[PtCl_2(NH_3)_2(OH)_2]$ have shown that the Pt–Cl bond is slightly longer when *trans* to OH^- compared to when Cl^- is *trans* to another Cl^-. Since OH^- have a stronger *trans* influence than H_2O,[22, 23] it seems that the Cl^- *trans* influence is counteracted by the OH^- *trans* influence so that no *isotopomers* are observed.

57
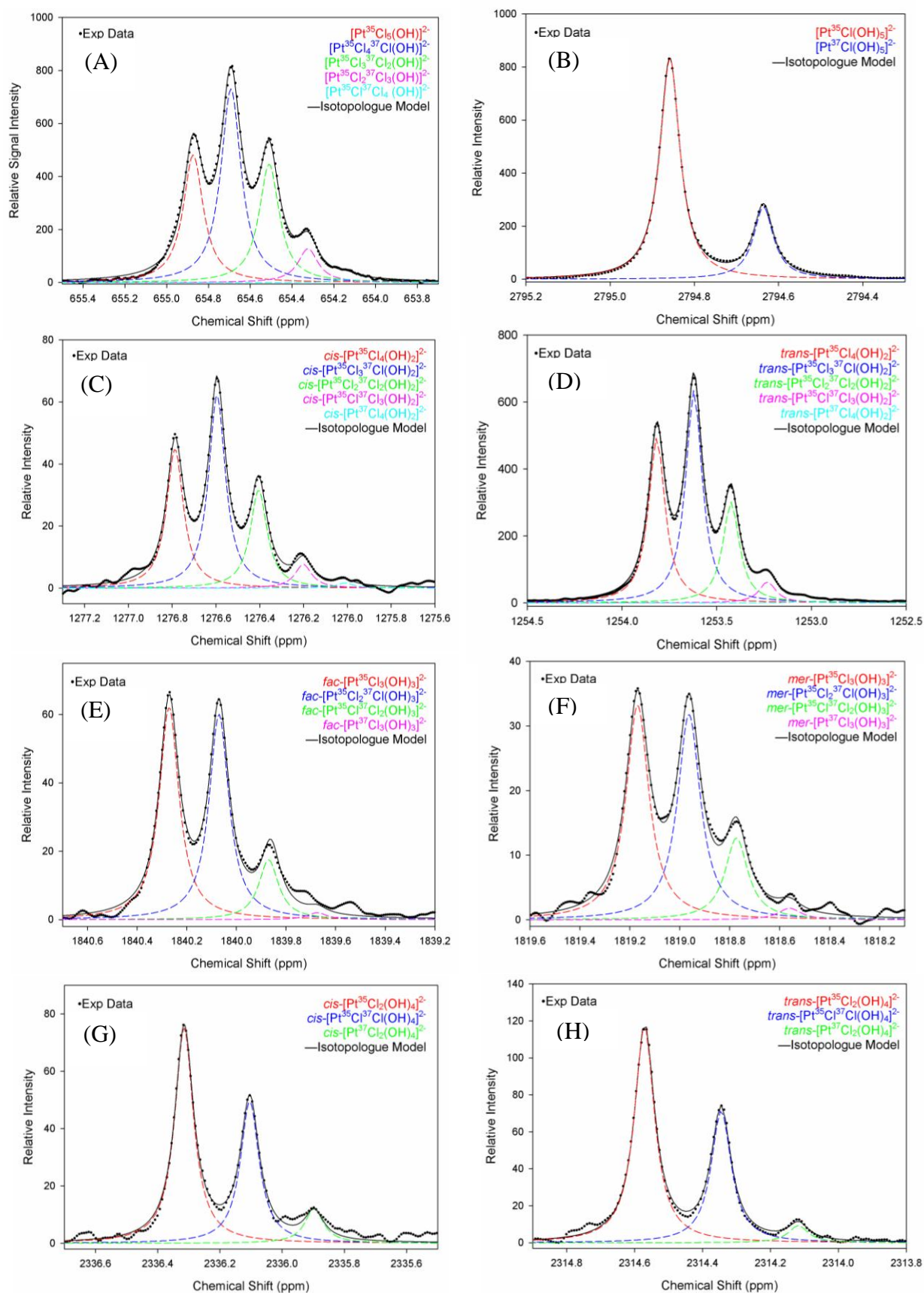
Figure 3.15: ^{195}Pt NMR spectrum (•) of the $[PtCl_n(OH)_{6-n}]^{2-}$ (*n* = 1-6) *hydroxido* complexes (A-H). The least-squares fit (solid line) between the experimental spectra and the ^{35}Cl/^{37}Cl isotopologue model (coloured dashed lines) are shown.

Table 3.8: Comparison of the experimental (Figures 3.15A–H) and statistically expected isotopologue and isotopomer distributions for the $[Pt^{35/37}Cl_n(OH)_{6-n}]^{2-}$ (n = 1-6) complexes.

Pt(IV) isotopologue	Sum percent of isotopomers to yield isotopologue amount		Pt(IV) isotopologue	Sum percent of isotopomers to yield isotopologue amount	
	Expt.	Statistical		Expt.	Statistical
$[Pt^{35}Cl_5(OH)]^{2-}$	26.78	24.97			
$[Pt^{35}Cl_4^{37}Cl(OH)]^{2-}$	40.60	39.93			
$[Pt^{35}Cl_3^{37}Cl_2(OH)]^{2-}$	24.83	25.54			
$[Pt^{35}Cl_2^{37}Cl_3(OH)]^{2-}$	7.11	8.17			
$[Pt^{35}Cl^{37}Cl_4(OH)]^{2-}$	0.68	1.31			
$[Pt^{37}Cl_5(OH)]^{2-}$	not observed	0.08			
$trans$-$[Pt^{35}Cl_4(OH)_2]^{2-}$	32.97	32.96	cis-$[Pt^{35}Cl_4(OH)_2]^{2-}$	29.90	32.96
$trans$-$[Pt^{35}Cl_3^{37}Cl(OH)_2]^{2-}$	42.35	42.16	cis-$[Pt^{35}Cl_3^{37}Cl(OH)_2]^{2-}$	42.81	42.16
$trans$-$[Pt^{35}Cl_2^{37}Cl_2(OH)_2]^{2-}$	20.11	20.22	cis-$[Pt^{35}Cl_2^{37}Cl_2(OH)_2]^{2-}$	21.10	20.22
$trans$-$[Pt^{35}Cl^{37}Cl_3(OH)_2]^{2-}$	4.23	4.31	cis-$[Pt^{35}Cl^{37}Cl_3(OH)_2]^{2-}$	5.11	4.31
$trans$-$[Pt^{37}Cl_4(OH)_2]^{2-}$	0.34	0.34	cis-$[Pt^{37}Cl_4(OH)_2]^{2-}$	1.08	0.34
mer-$[Pt^{35}Cl_3(OH)_3]^{2-}$	44.04	43.50	fac-$[Pt^{35}Cl_3(OH)_3]^{2-}$	44.47	43.50
mer-$[Pt^{35}Cl_2^{37}Cl(OH)_3]^{2-}$	41.29	41.73	fac-$[Pt^{35}Cl_2^{37}Cl(OH)_3]^{2-}$	43.01	41.73
mer-$[Pt^{35}Cl^{37}Cl_2(OH)_3]^{2-}$	14.67	13.35	fac-$[Pt^{35}Cl^{37}Cl_2(OH)_3]^{2-}$	12.52	13.35
mer-$[Pt^{37}Cl_3(OH)_3]^{2-}$	not observed	1.42	fac-$[Pt^{37}Cl_3(OH)_3]^{2-}$	not observed	1.42
$trans$-$[Pt^{35}Cl_2(OH)_4]^{2-}$	54.98	57.41	cis-$[Pt^{35}Cl_2(OH)_4]^{2-}$	59.22	57.41
$trans$-$[Pt^{35}Cl^{37}Cl(OH)_4]^{2-}$	36.19	36.72	cis-$[Pt^{35}Cl^{37}Cl(OH)_4]^{2-}$	36.11	36.72
$trans$-$[Pt^{37}Cl_2(OH)_4]^{2-}$	8.83	5.87	cis-$[Pt^{37}Cl_2(OH)_4]^{2-}$	4.67	5.87
$[Pt^{35}Cl(OH)_5]^{2-}$	75.36	75.77			
$[Pt^{37}Cl(OH)_5]^{2-}$	24.64	24.23			

The stronger OH$^-$ *trans* influence is also reflected by the similar $^{35}Cl/^{37}Cl$ isotopologue $\Delta\delta_{itl}(^{195}Pt)$ values obtained for two specific stereoisomers (Table 3.9). It implies that where Cl$^-$ is *trans* to OH$^-$, the Pt–Cl bond is not contracted since the $\Delta\delta_{itl}(^{195}Pt)$ value is the same where Cl$^-$ is *trans* to Cl$^-$. Small differences in the peak shape originate from different $\nu_{itl}^{½}$ values, although no systematic trend is observed between stereoisomers (Table 3.9).

Table 3.9: $^{35}Cl/^{37}Cl$ isotopic shift effects of the $[Pt^{35/37}Cl_n(OH)_{6-n}]^{2-}$ (n = 1-6) complexes in 2 M HClO$_4$.

Species	$\delta(^{195}Pt)$ (ppm)	$^{35}Cl/^{37}Cl\ \Delta\delta_{itl}(^{195}Pt)$ (ppm)	$\nu_{itl}^{½}$ (ppm/Hz)
$[PtCl_6]^{2-}$	-6	0.171	0.038 / 3.30
$[PtCl_5(OH)]^{2-}$	655	0.184	0.058 / 5.00
$trans$-$[PtCl_4(OH)_2]^{2-}$	1253	0.195	0.053 / 4.57
cis-$[PtCl_4(OH)_2]^{2-}$	1276	0.194	0.047 / 4.05
mer-$[PtCl_3(OH)_3]^{2-}$	1819	0.201	0.048 / 4.14
fac-$[PtCl_3(OH)_3]^{2-}$	1840	0.203	0.056 / 4.83
$trans$-$[PtCl_2(OH)_4]^{2-}$	2314	0.209	0.037 / 3.19
cis-$[PtCl_2(OH)_4]^{2-}$	2336	0.227	0.036 / 3.10
$[PtCl(OH)_5]^{2-}$	2795	0.222	0.029 / 2.50

An increase of $\Delta\delta_{itl}(^{195}Pt)$ and decrease of $\nu_{itl}\frac{1}{2}$ values are seen as a function of n in the $[PtCl_n(OH)_{6-n}]^{2-}$ (n = 1-5) series. Since the *trans* influence cannot adequately account for these relations, other factors such as the ^{195}Pt nuclei relaxation mechanism and thus interaction with the second coordination sphere[4, 24-27] may also contribute to these dependencies. Such trends are not observed for the *aqua* series, where solvation will be greatly influenced by the differently charged complex as a function of n, causing possible erratic chemical shift changes. These trends are perplexing yet interesting and require a detailed theoretical study to understand the implications.

3.4   Conclusions

Well resolved $^{35}Cl/^{37}Cl$ isotope shifts are observed for the $[PtCl_n(H_2O)_{6-n}]^{4-n}$ (n = 1-5) complex species at high magnetic field under conditions of well defined origin in the temperature range 18-22°C. Only $^{35}Cl/^{37}Cl$ *isotopologue* signals are observed for $[PtCl_6]^{2-}$, *trans*-$[PtCl_4(H_2O)_2]$, *fac*-$[PtCl_3(H_2O)_3]^+$, *trans*-$[PtCl_4(H_2O)_2]^{2+}$ and $[PtCl(H_2O)_5]^{3+}$ while $^{35}Cl/^{37}Cl$ *isotopomers* are also observed for $[PtCl_5(H_2O)]^-$ *cis*-$[PtCl_4(H_2O)_2]$ and *mer*-$[PtCl_3(H_2O)_3]^+$. Isotopomer signals originate from the *trans* orientation of $^{35}Cl/^{37}Cl$ isotopes with respect to H_2O, causing the isotopologues to "split" into isotopomers. The ratio of the respective isotopolgues are in line with that calculated from the natural abundance of the $^{35}Cl/^{37}Cl$ isotopes, while the ratio of the isotopomers are calculated from the number of possible orientations for each isotopomer. Least-squares analysis allow accurate deconvolution of the respective signals and estimation of peak ratios. This method of isotopic anaylsis serve as a unique fingerprint for the unambiguous identification of these species in acidic solutions, which is not reliant on chemical-shift-trend analysis. Moreover, the isotopomer/isotopologue distribution observed in the ^{195}Pt NMR resonances of $[PtCl_5(H_2O)]^-$, *cis*-$[PtCl_4H_2O)_2]$ and *mer*-$[PtCl_3(H_2O)_3]^+$ complexes serves as a means to distinguish between isotopic stereoisomers in solution.

The fact that the isotopomer where ^{37}Cl is *trans* to H_2O is observed up-field from ^{35}Cl *trans* to H_2O, implies a shorter Pt–Cl bond in the former case as a result of a stronger *trans* influence. Stereoisomers where Cl^- is always *trans* to H_2O display bigger chemical shift difference between respective $^{35}Cl/^{37}Cl$ isotopologues, and is ascribed to bigger

differences in the Pt–Cl bond length in these stereoisomers. The ^{195}Pt NMR signal of $[PtCl_5(OH)^{2-}$, *cis*-$[PtCl_4(OH)_2]^{2-}$ and *fac*-$[PtCl_3(OH)_3]^{2-}$ display only isotopologue signals due to the stronger *trans* influence of OH$^-$ which counterbalance the *trans* influence induced by Cl$^-$. Oxygen-18 enriched $[PtCl_n(H_2O)_{6-n}]^{4-n}$ (n = 1-5) complex species demonstrate that the resonance signal splitting pattern hierarchy is in accord with the $(m'-m)/m'$ mass factor[12-14] (mean bond length difference) when more than one element (e.g. ^{35}Cl/^{37}Cl and ^{16}O/^{18}O) bound to the ^{195}Pt nucleus has isotope induced effects. The presence of ^{16}O/^{18}O in addition to ^{35}Cl/^{37}Cl coordinated isotopes, thus cause splitting of the ^{16}O/^{18}O isotopologues into ^{35}Cl/^{37}Cl isotopologues and/or isotopomer signals as predicted by the mass factor. The *cis*-$[PtCl_2(H_2O)_4]^{2+}$ complex species also exhibits ^{16}O/^{18}O isotopomer effects due to the unique configuration of this complex.

3.5 References

1. J. Kramer, K. R. Koch, *Inorg. Chem.,* 2007, *46*, 7466-7476.

2. A. N. Westra, PhD Thesis, Stellenbosch University, 2005.

3. S. M. Cohen, T. H. Brown, *J. Chem. Phys.,* 1974, *61*, 2985-2986.

4. P. S. Pregosin, *Coord. Chem. Rev.,* 1982, *44*, 247-291.

5. I. M. Ismail, S. J. S. Kerrison, P. J. Sadler, *Chem. Commun.,* 1980, 1175-1176.

6. *CRC Handbook of Chemistry and Physics*, 64th ed., CRC Press Inc., Boca Raton, Florida, 1984.

7. W. Preetz, J. G. Uttecht, G. Peters, *Z. Anorg. Allg. Chem.,* 2003, *629*, 410-414.

8. R. Dreyer, K. Koenig, H. Schmidt, *Z. Phys. Chem.,* 1964, *227*, 257-271.

9. L. I. Elding, L. Gustafson, *Inorg. Chim. Acta,* 1976, *19*, 31-38.

10. O. Groning, L. I. Elding, *Inorg. Chem.,* 1989, *28*, 3366-3372.

11. Y.-T. Yu, J. Wang, J.-H. Zhang, H.-J. Yang, B.-Q. Xu, J.-C. Sun, *J. Phys. Chem.,* 2007, *111*, 18563-18567.

12. C. J. Jameson, *J. Am. Chem. Soc.,* 1987, *109*, 2586-2588.

13. C. J. Jameson, A. K. Jameson, *J. Chem. Phys.,* 1986, *85*, 5484-5492.

14. C. J. Jameson, D. Rehder, M. Hoch, *J. Am. Chem. Soc.,* 1987, *109*, 2589-2594.

15. E. Penka Fowe, P. Belser, C. Daul, H. Chermette, *Phys. Chem. Chem. Phys.,* 2005, *7*, 1732-1738.

16. M. R. Burger, PhD Thesis, Stellenbosch University, 2008.

17. C. J. Jameson, A. K. Jameson, D. Oppusunggu, *J. Chem. Phys.,* 1986, *85*, 5480 - 5483.

18. W. J. Gerber, P. Murray, K. R. Koch, *Dalton Trans.,* 2008, 4113-4117.

19. C. Carr, P. L. Goggin, R. J. Goodfellow, *Inorg. Chim. Acta,* 1984, *81*, L25-L26.

20. S. O. Dunham, R. D. Larsen, E. H. Abbott, *Inorg. Chem,* 1993, *32*, 2049-2055.

21. R. Kuroda, I. M. Ismail, P. J. Sadler, *J. Inorg. Biochem.,* 1984, *22*, 103-117.

22. D. R. Armstrong, R. Fortune, P. G. Perkins, *Inorg. Chim. Acta,* 1976, *17*, 73-79.

23. T. G. Appleton, H. C. Clark, L. E. Manzer, *Coord. Chem. Rev.,* 1973, *10*, 335-422.

24. J. J. Pesek, W. R. Mason, *J. Magn. Reson.,* 1977, *25*, 519-529.

25. B. M. Still, P. G. A. Kumar, J. R. Aldrich-Wright, W. S. Price, *Chem. Soc. Rev.,* 2007, *36*, 665-686.

26. J. R. L. Priqueler, I. S. Butler, F. D. Rochon, *Appl. Spectrosc. Rev.,* 2006, *41*, 185-226.

27. P. L. Goggin, R. J. Goodfellow, S. R. Haddock, B. F. Taylor, I. R. H. Marshall, *Dalton Trans.: Inorg. Chem.,* 1976, 459-467.

Chapter 4

Synthesis and characterization of putative hexa-aqua-platinum(IV) by means of ^{195}Pt NMR

4.1   Introduction

Water exchange on hexa-aqua metal ions is the simplest reaction in aqueous solution and fundamental in understanding the reactivity of the metal ion in chemical and biological systems. Preparation of octahedral hexa-aqua metal ions, and related water exchange studies has received much attention over the last few decades as is reflected by the large amount of literature on this topic.[1-5] Unlike the Pt(II) square-planar $[Pt(H_2O)_4]^{2+}$ complex,[6] the Pt(IV) octahedral $[Pt(H_2O)_6]^{4+}$ complex has not been reported in the literature.

Kinetic and high-pressure studies revealed that a dissociative interchange (I_d) mechanism are not necessarily valid for the low-spin t_{2g}^5 $[Ru(H_2O)_6]^{3+}$ and t_{2g}^6 $[Ru(H_2O)_6]^{2+}$, $[Rh(H_2O)_6]^{3+}$ and $[Ir(H_2O)_6]^{3+}$ complexes as anticipated from Ligand Field Activation Energies (LFAEs). Although H_2O exchange on $[Ru(H_2O)_6]^{2+}$ for instance tends to proceed *via* an interchange (I) mechanism,[7] exchange on $[Rh(H_2O)_6]^{3+}$ [8] and $[Ir(H_2O)_6]^{3+}$ [9] proceed primarily *via* an associative interchange (I_a) mechanism. Since mechanistic studies regarding H_2O exchange on the heavier second and third row octahedral hexa-aqua metal ions are limited to above mentioned complexes, H_2O exchange on $[Pt(H_2O)_6]^{4+}$ is of particular interest as it will add to the fundamental understanding of Pt(IV) lability toward ligand exchange especially in terms of Molecular Orbitals (MO) theory.

This $[Pt(H_2O)_6]^{4+}$ complex is also of interest in the context of this thesis as it is a potential oxidation product obtained from oxidation of $[Pt(H_2O)_4]^{2+}$ with various oxidants which is investigated in *Chapter 5*. The main objective in this chapter is to prepare the $[Pt(H_2O)_6]^{4+}$ complex and to characterize it with ^{195}Pt NMR, a venture which pose several challenges (*vida infra*). The $[Pt(H_2O)_6]^{4+}$ complex is unique from other t_{2g}^6 hexa-aqua metal ions (the $[Pd(H_2O)_6]^{4+}$ complex also remains uncharacterized), since it may facilitate a 4+ charged complex which will be extremely electron deficient. As a result it may exhibit mechanistic properties and/or reaction kinetics not accounted for by LFAEs according to MO theory.

The highly charged $[Pt(H_2O)_6]^{4+}$ metal ion has partly added to the inability to stabilize and characterize this complex in solution, as it is anticipated to be extremely acidic and coordinated H_2O may hydrolyze even in strong acidic solution. The extent to which the coordinated hydroxido ligands of the $[Pt(OH)_6]^{2-}$ ion can be protonated has been the subject of previous investigation. Tschugajeff[10] found that the *hydoxido* $[Pt(NH_3)_5(OH)]Cl_3$ salt crystallizes from concentrated HCl solution and not the *aqua* $[Pt(NH_3)_5(H_2O)]Cl_4$ salt as expected. Richens[4] argued that this may indicate a very low pK_a value (< 1) for $[Pt(H_2O)_6]^{4+}$. Formation of the $[Pt(H_2O)_5(OH)]^{3+}$ complex may therefore be favourable, thereby counteracting the highly charged electron deficient complex, so that formation of $[Pt(H_2O)_6]^{4+}$ is not necessarily guaranteed even in 10 M $HClO_4$. On the other hand it may be argued, that the fact that $[Pt(NH_3)_5(OH)]Cl_3$ crystallizes from solution rather indicates favourable electrostatic interactions in the solid state for the 3+ charged species, and do not necessarily indicate that $[Pt(NH_3)_5(H_2O)]^{4+}$ do not exist in solution. In this regard such a comparison is risky. Furthermore, a large positive formal charge of 4+ is not known for Pt(IV) and complexes such as $[Pt(NH_3)_6]Cl_4$[11-13] or $[Pt(en)_3]Cl_4$ (en = ethylenediamine)[14] are well characterized and dissociates completely in solution to form formally 4+ charged complexes.

It was recently shown that Density Functional Theory (DFT) calculations can give relatively good $\delta(^{195}Pt)$ predictions for Pt(II)- and Pt(IV)-*chlorido-bromido* complex species.[15, 16] However, $\delta(^{195}Pt)$ predictions of species that contain coordinated *hydroxido* or *aqua* ligands deviate largely from experimental results, possibly due to hydrogen bonding affects not accounted for by this method.[17] DFT predictions of a $\delta(^{195}Pt)$ value is therefore of limited help to validate the existence of $[Pt(H_2O)_6]^{4+}$ in solution and an experimental approach was undertaken to obtain $[Pt(H_2O)_6]^{4+}$ in solution. Three different methods can be envisaged to prepare the $[Pt(H_2O)_6]^{4+}$ complex: (1) Removal of the coordinated Cl^- ligands of $[PtCl_6]^{2-}$ *via* precipitation with Ag^+ in aqueous solution; (2) Protonation of the coordinated *hydroxido* ligands of $[Pt(OH)_6]^{2-}$; and (3) Oxidation of $[Pt(H_2O)_4]^{2+}$ in acidic solution with H_2O_2 or other oxygen donating oxidants such as ClO_3^- or BrO_3^-. The nature of the putative $[Pt(H_2O)_6]^{4+}$ complex is investigated in more detail by

monitoring the rate of H_2O exchange in oxygen-18 enriched solution, and the rate of halide anation (Cl^- and Br^-) with ^{195}Pt NMR.

4.2   Experimental

4.2.1   Reagents

Sodium hexachloroplatinate(IV) hexahydrate (98%, $Na_2PtCl_6 \cdot 6H_2O$, Aldrich) and sodium hexahydroxyplatinate(IV) (99%, $Na_2Pt(OH)_6$, Aldrich) were of reagent grade quality, stored in a desiccator and used without further purification. Silver perchlorate hydrate (99%, $AgClO_4$, Aldrich), sodium chloride (99+%, NaCl, Aldrich), sodium bromide (NaBr, Holpro Analytics), sodium hydroxide pellets (NaOH, MERCK) were also of reagent grade quality and used as is. Hydrogen peroxide (30% (w/w), H_2O_2, Riedel-de Haën), sodium chlorate (99+ %, Sigma-Aldrich, $NaClO_3$) and sodium bromate (99+ %, Sigma, $NaBrO_3$) were of reagent grade quality and used as is. Oxygen-18 enriched water (97 %) was obtained from Isotec and used for enriching Pt(IV) solutions. Deuterium oxide (99.9%, D_2O, Aldrich) was used as solvent to obtain a lock signal for NMR measurements. Perchloric acid (70% w/w $HClO_4$, 1 L = 1.68 kg, MERCK) was used as stock for $HClO_4$ dilutions. All aqueous solutions were made with ultra pure Milli-Q water (MQ > 18 MΩ) and degassed with Ar to remove O_2 for at least 1 h prior to use.

4.2.2 Instrumentation

^{195}Pt NMR Spectroscopy

The same ^{195}Pt NMR parameters described in *Chapters 2* are applicable. For measurements of $^{35}Cl/^{37}Cl$ and $^{16}O/^{18}O$ isotopic signals, the same parameters described in *Chapter 3* were used. ^{195}Pt NMR data were collected at 20 or 30°C, and is indicated in text. Analysis of certain solutions required very long acquisition times (up to 48 h) due to low Pt concentrations in solution. In such cases it is essential that the species in the solution is at equilibrium or that changes in speciation are extremely slow.

4.2.3   Methods of Pt(II/IV) complex preparation

The experimental details form part of the discussion. For this reason all the experimental details are discussed in text at the relevant topic.

4.3   Results and discussion

4.3.1   Attempted synthesis of $[Pt(H_2O)_6]^{4+}$ *via* AgClO$_4$ addition to $[PtCl_6]^{2-}$ in acidic solution

The presumably higher thermodynamic stability of the $[PtCl_n(H_2O)_{6-n}]^{4-n}$ (n = 0-6) complexes in the order n = 0→6 ensures that only $[PtCl_6]^{2-}$ and minor quantities of $[PtCl_5(H_2O)]^-$ are formed in solution if the Na$_2$PtCl$_6$ salt (0.2 M) is dissolved in 1 M HClO$_4$ and allowed to "age" for a few days at room temperature in the dark. It was therefore attempted to generate $[Pt(H_2O)_6]^{4+}$ *via* the stepwise addition of small quantities of AgClO$_4$ to a $[PtCl_6]^{2-}$ solution, thereby removing Cl$^-$ ions by precipitation of AgCl, thus driving aquation of the Pt(IV) complex. Aliquots of 100 μL 4.7 M AgClO$_4$ were added to a 0.36 M H$_2$PtCl$_6$ solution kept at 50°C. Samples were extracted periodically from the reaction flask between additions of AgClO$_4$, filtered, and analyzed with ^{195}Pt NMR in an effort to observe formation of the $[PtCl_n(H_2O)_{6-n}]^{4-n}$ (n = 0-6) complexes. The reaction flask was covered with tin foil to prevent light induced reduction of Ag$^+$ and kept under a constant flow of Ar gas to exclude air from the reaction. The ^{195}Pt NMR spectra shown in Figure 4.1 were obtained after addition of 1.25 mol equivalents of AgClO$_4$ (with respect to Cl$^-$), and display nine of the possible ten complexes in the $[PtCl_n(H_2O)_{6-n}]^{4-n}$ (n = 0-6) series.
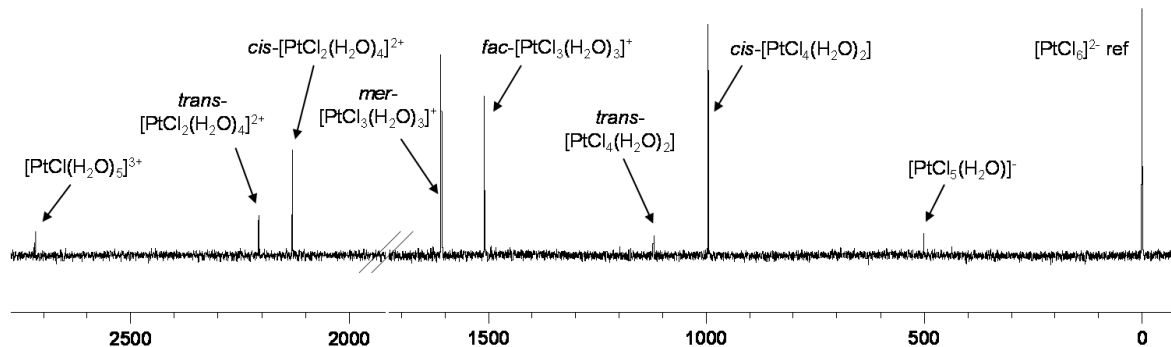
Figure 4.1: ^{195}Pt NMR spectra (30°C) of the $[PtCl_n(H_2O)_{6-n}]^{4-n}$ (n = 1-6) complexes obtained after addition of 1.25 mol equivalents of AgClO$_4$ (with respect to Cl$^-$) to $[PtCl_6]^{2-}$. The ^{195}Pt NMR spectra were obtained in two separate windows as indicated.

The species observed in Figure 4.1 were assigned by using ^{195}Pt NMR chemical-shift-trend analysis as described in *Chapter 2* for Pt(II) complexes. A plot of the observed $\delta(^{195}$Pt) values *vs.* number of coordinated H_2O ligands results in a slight positive deviation from a linear trend (Figure 4.2A; $\delta(^{195}$Pt$) = 8.8n^2 + 501n + 2.2$; $R^2 > 0.999$). Substitution of Cl$^-$ by H_2O *trans* to Cl$^-$, give $\Delta\delta(^{195}$Pt) values between 590-620 ppm, consistently bigger than values obtained for substitution of Cl$^-$ by H_2O *trans* to another H_2O ligand (495-520 ppm) as indicated in Figure 4.2B.

(A)　　　　　　　　　　　　　　　　(B)
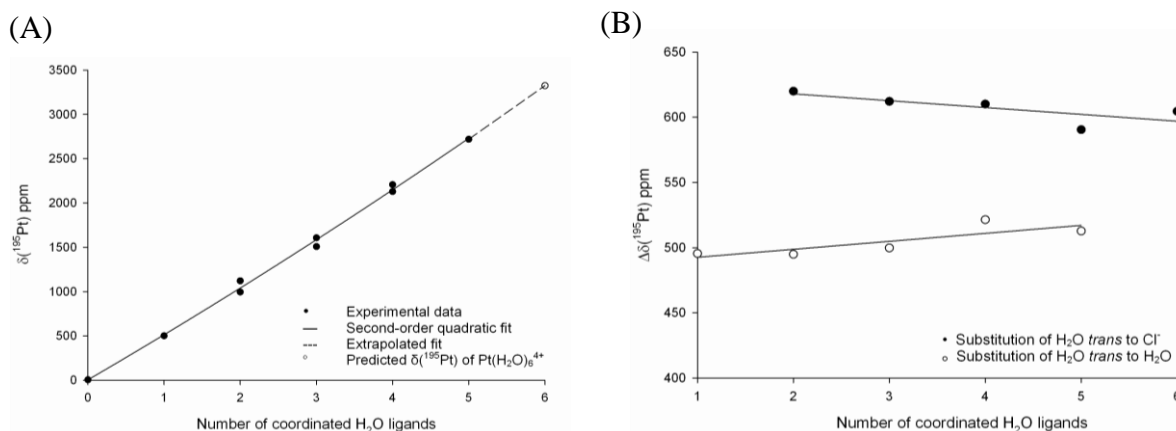
Figure 4.2: **(A)** *Second*-order correlation of $[PtCl_n(H_2O)_{6-n}]^{4-n}$ (n = 1-6) complexes as a function of number coordinated H_2O. The $\delta(^{195}$Pt) value of $[Pt(H_2O)_6]^{4+}$ is predicted by extrapolation of the *second*-order correlation. **(B)** *Linear* correlations of Cl$^-$ substituted by ● H_2O *trans* to Cl$^-$ and ■ H_2O *trans* to H_2O. The estimated $\delta(^{195}$Pt) value calculated for $[Pt(H_2O)_6]^{4+}$ from (A) was used in the plot (B) for substitution of H_2O *trans* to Cl$^-$.

The $\Delta\delta(^{195}$Pt) values in Figure 4.2B shows a lot of scatter and the two linear trends converge as the number of H_2O ligands per Pt(IV) complex increase (these same trends were observed in *Chapter 3*, Figure 3.6). These deviations from that observed for the $[PtCl_n(OH)_{6-n}]^{2-}$ (n = 0-6) series[17] may originate from the differences in formal charge (2$^-$ →3$^+$) for the Pt(IV)-*aqua-chlorido* complex species. The highly charged hydrated complexes (1 M HClO$_4$) may partake in hydrogen bonding with the solvent, forming possible ion-pairs to stabilize the hydrated complexes. Such interactions are anticipated to be different not only for species with different formal charges, but also for the stereoisomers with the same charge, especially in the highly hydrated complexes where electrostatic interactions and hydrogen bonding effects becomes more important.[18] Nevertheless, assignment of the $[PtCl_n(H_2O)_{6-n}]^{4-n}$ (n = 2-4) stereoisomers are possible from those trends and the assignments made here correlates well with that assigned in *Chapter 3*

(Table 3.4). These assignments are also indicated in Figure 4.1, although no more $[PtCl_6]^{2-}$ is observed at the stage when the [195]Pt NMR spectra shown were taken.

Table 4.1: Comparison of $\delta(^{195}Pt)$ values for the $[PtCl_n(H_2O)_{6-n}]^{2-}$ ($n = 0\text{-}6$) complexes obtained in different acid concentrations (1 M and 6 M $HClO_4$) and compared to literature values.

Nomenclature code	No. of H_2O	Pt(IV) complex	$\Delta(^{195}Pt)$ Ag^+ addition (1 M $HClO_4$)	$\Delta(^{195}Pt)$ Cl^- anation (6 M $HClO_4$)	Literature values
600	0	$[PtCl_6]^{2-}$	6	28	0 [20]
501	1	$[PtCl_5(H_2O)]^{1-}$	501	496	504 [20]
4c02c	2	*cis* $[PtCl_4(H_2O)_2]$	996	982	1005 [20]
4t02t	2	*trans* $[PtCl_4(H_2O)_2]$	1121	1119	1134 [20]
3f03f	3	*fac* $[PtCl_3(H_2O)_3]^+$	1508	Not observed	1500 [20]
3m03m	3	*mer* $[PtCl_3(H_2O)_3]^+$	1608	1573	1603 [20]
2c04c	4	*cis* $[PtCl_2(H_2O)_4]^{2+}$	2129	Not observed	2125 [20]
2t04t	4	*trans* $[PtCl_2(H_2O)_4]^{2+}$	2207	2200	2208 [20]
105	5	$[PtCl(H_2O)_5]^{3+}$	2720	Not observed	2640 [19]
006	6	$[Pt(H_2O)_6]^{4+}$	3324 [b]	3329	Not reported before

[a] $\delta(^{195}Pt)$ values were obtained at 30°C; [b] Predicted value from extrapolation of the trend in Figure 2.13

A plot of the observed $\delta(^{195}Pt)$ values of the $[PtCl_n(H_2O)_{6-n}]^{4-n}$ ($n = 0\text{-}6$) complexes (as a function of the number coordinated *water* ligands) on the same graph as the $[PtCl_n(OH)_{6-n}]^{2-}$ ($n = 0\text{-}6$) complexes (as a function of the number coordinated *hydroxide* ligands; experimental data points were taken from Table 3.9; Pt(IV) = 0.2 M, ~1 M NaOH), gives a positive and negative deviation from a linear trend respectively (Figure 4.3). The $\delta(^{195}Pt)$ of $[PtCl_6]^{2-}$ does not differ significantly in 1 M NaOH and 1 M $HClO_4$ so that both trends have similar $\delta(^{195}Pt)$ values at $n = 0$.
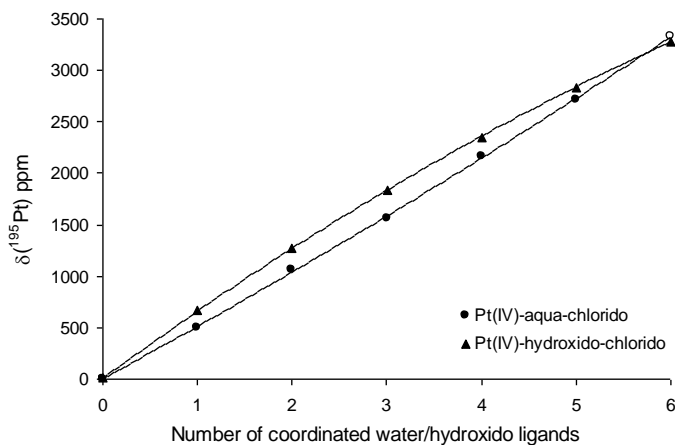
Figure 4.3: [195]Pt NMR chemical shifts of the series ▲ $[PtCl_n(OH)_{6-n}]^{2-}$ ($n = 0\text{-}6$) in 1 M NaOH and ■ $[PtCl_n(H_2O)_{6-n}]^{4-n}$ ($n = 0\text{-}6$) in 1 M $HClO_4$ illustrating negative and positive deviations from a linear trend respectively.

Since the Pt(IV)-*hydroxido*-chlorido complexes are generally more de-shielded compared to the Pt(IV)-*aqua*-chlorido complexes (maximum $\delta(^{195}Pt)$ difference where $n = 3$), it is possible to distinguish whether the coordinated ligands are mainly protonated or de-protonated i.e. *aqua* or *hydroxido* ligands. Unfortunately, as the number of coordinated H_2O or OH^- ligands increase, the $\delta(^{195}Pt)$ values for both series converges so that where $n = 6$, assignment between the *aqua* and *hydroxido* complex is ambiguous. This raises the question that even if an experimental $\delta(^{195}Pt)$ value for $[Pt(H_2O)_6]^{4+}$ is obtained, if it will be possible to distinguished from amphoteric *aqua-hydroxido*-mixed $[Pt(H_2O)_n(OH)_{6-n}]^{n-2}$ ($n = $ 1-5) signals. To investigate this problem more systematically, a ^{195}Pt NMR titration type experiment was carried out by treating $[Pt(OH)_6]^{2-}$ with $HClO_4$, in an attempt to observe six protonation steps of coordinated OH^- correlating with $[Pt(H_2O)_6]^{4+}$ formation.

4.3.2   Synthesis of tentative $[Pt(H_2O)_6]^{4+}$ *via* protonation of OH^- coordinated on $[Pt(OH)_6]^{2-}$

It is clear that an acidic solution should favour formation of the cationic $[Pt(HO)_n$-$(H_2O)_{6-n}]^{4-n}$ ($n = $ 0-3) complexes so that in principle $[Pt(H_2O)_6]^{4+}$ must form. A titration type experiment was carried out by measuring the $\delta(^{195}Pt)$ of $[Pt(OH)_6]^{2-}$ as a function of $[HClO_4]$, thereby attempting to illustrate the stepwise change of the $\delta(^{195}Pt)$ value as a result of the stepwise OH^- protonation presented in equilibrium reactions 4.1-4.6:

$$[Pt(OH)_6]^{2-} + H_3O^+ \leftrightharpoons [Pt(OH)_5(H_2O)]^- + H_2O \qquad (4.1)$$

$$[Pt(OH)_5(H_2O)]^- + H_3O^+ \leftrightharpoons [Pt(OH)_4(H_2O)_2] + H_2O \qquad (4.2)$$

$$[Pt(OH)_4(H_2O)_2] + H_3O^+ \leftrightharpoons [Pt(OH)_3(H_2O)_3]^+ + H_2O \qquad (4.3)$$

$$[Pt(OH)_3(H_2O)_3]^+ + H_3O^+ \leftrightharpoons [Pt(OH)_2(H_2O)_4]^{2+} + H_2O \qquad (4.4)$$

$$[Pt(OH)_2(H_2O)_4]^{2+} H_3O^+ \leftrightharpoons [Pt(OH)(H_2O)_5]^{3+} + H_2O \qquad (4.5)$$

$$[Pt(OH)(H_2O)_5]^{3+} + H_3O^+ \leftrightharpoons [Pt(H_2O)_6]^{4+} + H_2O \qquad (4.6)$$
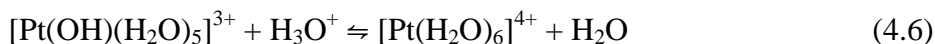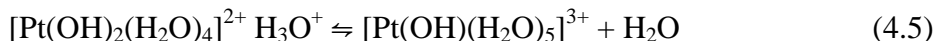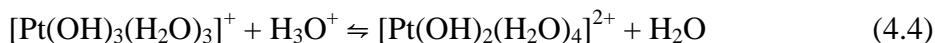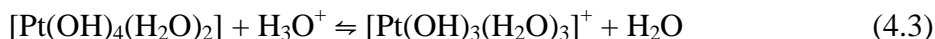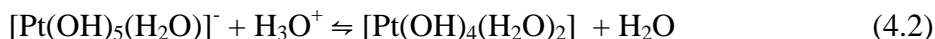
Various nuclei including ^{195}Pt, ^{15}N, ^{31}P and ^1H have been used successfully to acquire NMR titration curves for calculating pK_a values of various Pt(II) and (IV)-*aqua-hydroxido* complexes in moderate pH ranges.[19-22] As a proof of principle, a similar titration type experiment for the acid-base equilibrium reaction 4.7 was generated first.

$$[PtCl_5(OH)]^{2-} + H_3O^+ \rightleftharpoons [PtCl_5(H_2O)]^- + H_2O \qquad (4.7)$$

The $[PtCl_5(H_2O)]^-$ complex is suitable for this purpose, as it is a monoprotic acid in the Brønsted–Lowry sense, and should simplify interpretation of the result. The $[PtCl_5(H_2O)]^-$ complex can be easily obtained *via* $[PtCl_6]^{2-}$ aquation and demonstrate a large $\delta(^{195}Pt)$ difference between the *aqua* and *hydroxido* analogues (Figure 4.3), so that a change in the $\delta(^{195}Pt)$ value can be easily detected with ^{195}Pt NMR as a function of pH.

4.3.2.1 Protonation of the OH⁻ ligand of [PtCl₅(OH)]⁻ as monitored by ^{195}Pt NMR

A solution containing both $[PtCl_5(H_2O)]^-$ and $[PtCl_6]^{2-}$ was obtained by preparing a 0.2 M Na_2PtCl_6 solution in H_2O and "aging" it for a few hours in ambient light. The pH of the solution was first adjusted from 6 to 13 by adding aliquots of diluted 0.1 M NaOH to ensure conversion to the *hydroxido* $[PtCl_5(OH)]^{2-}$ complex. A ^{195}Pt NMR spectrum was collected at pH 13 where after the pH was decreased stepwise by adding aliquots of 0.1 M $HClO_4$. From pH 7→0 additions of concentrated $HClO_4$ was made. A ^{195}Pt NMR spectrum was taken close to every pH integer value in the pH range 7→0. No significant change in the $\delta(^{195}Pt)$ value is observed in the pH range 13→5, but in the range 5→1 there is a sharp drop of 152 ppm in the $\delta(^{195}Pt)$ value indicating protonation of the coordinated *hydroxido* ligand. If the acid-base reaction is slow on the NMR time scale, two signals corresponding to each complex species are expected. The fact that only one signal is observed, indicates fast proton exchange between $[PtCl_5(H_2O)]^-$ and $[PtCl_5(OH)]^{2-}$ according to reaction scheme 4.7 and the observed signal is the concentration-weighted average of the two complexes.

The $\delta(^{195}Pt)$ value can be related to the pK_a value by Equation 4.8:[19]

$$\delta = (\delta_A[H^+] + \delta_B K_a)/([H^+] + K_a) \qquad (4.8)$$

where K_a is the dissociation constant of the coordinated water molecule of $[PtCl_5(H_2O)]^-$ and δ_A and δ_B are the limiting chemical shifts of $[PtCl_5(H_2O)]^-$ and $[PtCl_5(OH)]^{2-}$ at the

equilibration points of the curve, in excess [H$^+$] or [OH$^-$] solutions respectively. A pK$_a$ value of 3.31 ± 0.04 with correlation coefficient R^2 > 0.99 was estimated by a least-squares fit of Equation 4.8 to the experimental data and agrees well with the literature value of 3.48 ± 0.04 reported previously by Shelimov et al.[22] (also determined with ^{195}Pt NMR) and the pK$_a$ value of 3.8 calculated by Davidson et al.[20] (by use of fast microtitration with NaOH). This titration type experiment demonstrate that ^{195}Pt NMR can be utilized to determine pK$_a$ values for Pt(IV) monoprotic acids and the technique is subsequently extended to investigate the hexaprotic acid [Pt(H$_2$O)$_6$]$^{4+}$.
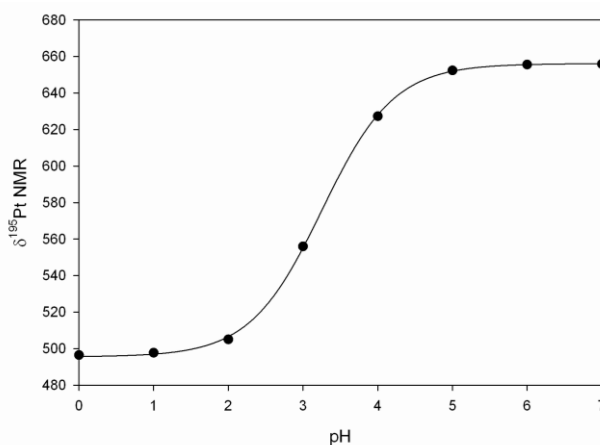
Figure 4.4: Least-squares fit of the experimental δ(^{195}Pt) values of [PtCl$_5$(OH)$_n$(H$_2$O)$_{1-n}$]$^{-1-n}$ (n = 0-1) as a function of pH.

Interestingly, when the HClO$_4$ concentration of the solution is increased further ([HClO$_4$] ≥ 1) the δ(^{195}Pt) value start to decreases again. Since this trend can not be indicative of further protonation reactions, the effect must be related to electrostatic interactions such as ion-pairing and corresponding solvent effects. In contrast to the up-field shift observed here, Appleton et al.[23] reported an exponential downfield shift when the HClO$_4$ concentration of a [Pt(H$_2$O)$_4$]$^{2+}$ solution was increased from 0.5-10 M, even though coordinated water on this complex is considered to be fully protonated at [HClO$_4$] ≥ 0.5 M.[6, 24] On the other hand a linear downfield shift for [Pt(H$_2$O)$_4$]$^{2+}$ was observed in 0.5 M HClO$_4$, when the ionic strength was increased as a function of NaClO$_4$ from 0.5-10 M. Some rationalization in terms of hydrogen bonding and ionic strength effects were expressed by the authors[23] but more detailed studies concerning this behaviour is still outstanding. With respect to interpretation of a possible δ(^{195}Pt) value of [Pt(H$_2$O)$_6$]$^{4+}$, it is important to consider such

influences given the presumably strong acidic conditions required to form and stabilize this complex.

4.3.2.2 Treatment of a $[Pt(OH)_6]^{2-}$ solution with different concentrations of $HClO_4$ in a titration type experiment as monitored by ^{195}Pt NMR

Maltese *et al.*[25] reported that a yellow solid precipitates from solution when aqueous $[Pt(OH)_6]^{2-}$ (originating from hydrolysis of H_2PtCl_6 in a NaOH solution) is treated with acetic acid. The precipitate was identified as hydrogen hexahydroxyplatinate(IV)[25] by elemental analysis and has been reported as $PtO_2^.4H_2O$, $Pt(OH)_4^.2H_2O$ or more commonly, $H_2Pt(OH)_6$ by different authors.[26] Dou *et al.*[27] confirmed the results of Maltese *et al.*[25] by X-ray diffraction (XRD) analysis and found that the yellow insoluble $H_2Pt(OH)_6$ precipitates in the pH region 5→3, when acetic acid is added to a $Na_2[Pt(OH)_6]$ solution. The authors suggested that formation of $H_2Pt(OH)_6$ can be envisaged as two *hydroxido* ligands being protonated according to equilibrium Equations 4.1 and 4.2 (in the *cis* or *trans* position).[27] The authors also stipulated that the remaining four *hydroxido* ligands of $H_2Pt(OH)_6$ can be protonated with nitric acid, but results in formation of a $Pt[\mu\text{-}O(H)]_2Pt$ ring based polynuclear species.[27] In diluted nitric acid a reddish precipitate $PtO_2^.xH_2O$ started forming after 4-8 hours. Drying of this precipitate at 70°C formed a red solid characterized as $PtO_2^.3H_2O$, the same product found by Appleton *et al.*[23] for the oxidation of a $[Pt(H_2O)_4]^{2+}$ solution with concentrated H_2O_2 in 1 M $HClO_4$. XRD analysis of $PtO_2^.3H_2O$ revealed an amorphous compound while $PtO_2^.4H_2O$ is crystalline.[27] Nabivanets[28] determined the solubility of $H_2Pt(OH)_6$ in $HClO_4$ (pH range 11→0), by measuring solubility constants with comparative dialysis and electro dialysis techniques. A minimum in the solubility curve of $H_2Pt(OH)_6$ was observed in the pH range 6→3 and according to the author suggests formation of an amphoteric Pt(IV) hydroxide. It was found that the solubility increase in the pH range 2→0 and it was concluded, that cationic $[Pt(HO)_n(H_2O)_{6-n}]^{4-n}$ (n = 0-3) complexes predominate in this pH range in $HClO_4$ solutions, while additional polynuclear Pt(IV) species also forms in very low concentrations.[28]

Here, a series of 0.04 M $[Pt(OH)_6]^{2-}$ solutions in water (prepared from the $Na_2[Pt(OH)_6]$ salt), were investigated by ^{195}Pt NMR in the pH range 12.7→0.3, by adjusting the pH with

aliquots of $HClO_4$ or $NaOH$ solutions. In this experiment, a similar trend for the solubility of $Na_2[Pt(OH)_6]$ as found by above mentioned authors[25, 27, 28] for $H_2Pt(OH)_6$ was observed. A 0.04 M $Na_2[(Pt(OH)_6]$ solution in water is light yellow and has a pH of 9.3. ^{195}Pt NMR analysis of the solution shows a $\delta(^{195}Pt)$ signal at 3284 ppm. Although some $Na_2Pt(OH)_6$ remains un-dissolved in water, the solubility is relatively good so that a high signal/noise ratio is obtained within ~20 min of acquiring a ^{195}Pt NMR spectrum. When the pH is adjusted to 12.7, the remaining $Na_2Pt(OH)_6$ dissolves completely and no precipitation is evident. When the pH is adjusted from 12.7→7.0 by addition of aliquots 0.1 M $HClO_4$, most of the Pt(IV) precipitates as a yellow solid, presumably $H_2Pt(OH)_6$,[25, 27, 28] and below pH 7.0 the solution is visually clear and no ^{195}Pt signal is observed. When the pH is decreased further, the precipitate eventually re-dissolves and at pH 0.3 a small ^{195}Pt NMR signal is observed at 3270 ppm in the solution. Although the $\delta(^{195}Pt)$ value shifts up-field with ~14 ppm by decreasing the pH from 12.7→0.3, a titration curve could not be obtained in this pH range due to precipitation of $H_2Pt(OH)_6$ in the pH range 7→0.3.

In another experiment, solutions of 0.04 M $[Pt(OH)_6]^{2-}$ were prepared in 0.5, 1, 2, 3, 4, 6, 8 and 10 M $HClO_4$ respectively by adding the appropriate amount of water to the $Na_2Pt(OH)_6$ salt and stirring the solution at ambient temperature for 10 min. Thereafter the appropriate amount of concentrated $HClO_4$ was added to obtain the indicated $HClO_4$ concentrations. Some of the $Na_2Pt(OH)_6$ salt remains un-dissolved in water, 0.5, 1 and 2 M $HClO_4$, but the solubility increases as the $HClO_4$ acid concentration becomes higher: for concentrations ≥ 3 M $HClO_4$ the solution quickly turns into a clear dark yellow-orange colour as the $Na_2Pt(OH)_6$ salt dissolves. This effect is more dramatic as the $HClO_4$ concentration increases so that essentially no precipitate is observed in 6 M $HClO_4$ and a single peak with excellent signal/noise ratio is observed at 3315 ppm with ^{195}Pt NMR. The ^{195}Pt NMR spectra obtained from these solutions are shown in Figure 4.5A and a plot illustrating the change in $\delta(^{195}Pt)$ as a function of $[HClO_4]$ is shown in Figure 4.5B for the concentration range 0.5 - 10 M $HClO_4$ and corresponds to a total $\delta(^{195}Pt)$ upfield shift of ~92 ppm.

(A)

(B)
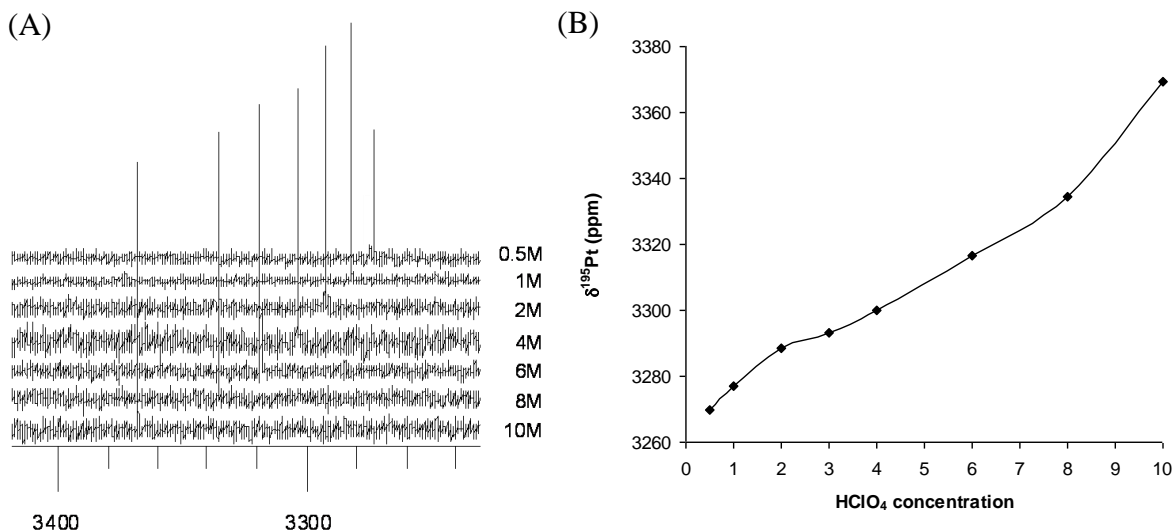
Figure 4.5: (A) [195]Pt NMR spectra of $Na_2Pt(OH)_6$ dissolved in different concentrations of [$HClO_4$] (0.5-10 M), illustrating an up-field shift of the δ([195]Pt) value with increase of [$HClO_4$]. **(B)** A plot of the δ([195]Pt) values obtained in (A) as a function of [$HClO_4$].

At high concentrations of $HClO_4$ ($\geq$ 0.5 M, pH $\leq$ 0.3), the $Na_2Pt(OH)_6$ salt and the amphoteric precipitate $H_2Pt(OH)_6$ is very soluble if the Pt(IV) concentration is 0.04 M. This was not necessarily expected considering the reported insolubility of $H_2Pt(OH)_6$ and precipitation in moderate acid solution,[25, 27] but could have been anticipated from the solubility at lower pH reported by Nabivanets.[28] From Figure 4.5B it is evident that no clear sigmoidal type "titration curve" that illustrates the stepwise protonation of the six *hydroxido* ligands coordinated on [Pt(OH)$_6$]$^{2-}$ (Equations 4.1 - 4.6) can be observed as monitored by [195]Pt NMR. However, a shallow inflection point at ~2.5 M $HClO_4$ is observed. It is significant that the observed δ([195]Pt) value shifts downfield in the pH range 12.3→0.3 but starts to shift upfield when the $HClO_4$ concentration is increased beyond that. All species in the [PtCl$_n$(OH)$_{6-n}$]$^{2-}$ (*n* = 0-6) series shifts downfield with protonation of the coordinated *hydroxido* ligands (Figure 4.3), with [Pt(OH)$_6$]$^{2-}$ the only exception as anticipated from the predicted δ([195]Pt) value for [Pt(H$_2$O)$_6$]$^{4+}$ (from Figure 4.2A). As previously discussed for [PtCl$_5$(OH)]$^{2-}$, the δ([195]Pt) value changes even after protonation in high concentration of $HClO_4$. At high concentrations of $HClO_4$, electrostatic effects like ion-pairing and cation-anion interactions may become increasingly dominant and compete with protonation/hydrolysis effects. The δ([195]Pt) values observed in Figures 4.5 must therefore be viewed as a contribution from both change in the coordinated ligand i.e. (OH$^-$

$\rightarrow H_2O$) and electrostatic effects. To better understand the experimental result of Figures 4.5 the extent of the contribution to the overall $\delta(^{195}Pt)$ value of both factors under these reaction conditions needs to be considered.

Protonation of the coordinated OH^- on $[PtCl_n(OH)_{6-n}]^{2-}$ (n = 0-6) complexes result in an upfield shift (Figure 4.3). The difference in $\delta(^{195}Pt)$ between the *hydroxido* and *aqua* species is small initially (where $n = 0$), but diverge to a maximum $\delta(^{195}Pt)$ difference where $n = 3$, only to converge again to similar values where $n = 6$. This implies the contribution to change in the $\delta(^{195}Pt)$ value (Figure 4.5B) from protonation $OH^-\rightarrow H_2O$ is expected to be minimal. The fact that the pH increase to 9.3 when 0.04 M $Na_2Pt(OH)_6$ is dissolved in water, already indicate that the coordinated OH^- ligands in the $[Pt(OH)_6]^{2-}$ complex must consume protons, thereby acting as a weak base. At low ionic strength, the $\delta(^{195}Pt)$ value of $[Pt(OH)_6]^{2-}$ changes from 3284 ppm in water (pH 9.3) to 3270 ppm in 0.5 M $HClO_4$ (pH 0.3), therefore probably indicating further protonation reactions similar to the $[PtCl_n(HO)_{6-n}]^{2-}$ (n = 1-6) complexes when OH^- ligands are protonated. This view is supported by the findings of Nabivanets,[28] that the cationic $[Pt(H_2O)_{6-n}(HO)_n]^{4-n}$ (n = 0-3) complexes dominate in the pH range (2$\rightarrow$0).

An increase of the $HClO_4$ concentration should therefore result in further protonation reactions and a subsequent up-field shift. However, an overall downfield shift is observed for $[HClO_4] \geq 0.5$, with an inflection point at ~2.5 M $HClO_4$, and an exponential increase in the $\delta(^{195}Pt)$ value thereafter. An exponential increase of ~250 ppm in the $\delta(^{195}Pt)$ value was also observed for $[Pt(H_2O)_4]^{2+}$ in 0.5-10 M $HClO_4$ by Appleton *et al.*[23] opposed to a linear increase of ~65 ppm in 0.5-10 M $NaClO_4$. The result was rationalized in terms of electrostatic interactions becoming more important at high $HClO_4$ concentrations and not due to hydrolysis reactions, since all coordinated OH^- ligands in $[Pt(H_2O)_4]^{2+}$ is regarded to be fully protonated in $HClO_4 \geq 0.5$ M.[6, 24] The negative exponential increase in $\delta(^{195}Pt)$ value from 0.5 M $HClO_4$ (Figure 4.5B) to the inflection point (~2.5 M $HClO_4$) is thus indicative of a competing reaction contributing to an upfield $\delta(^{195}Pt)$ value i.e. $OH^- \rightarrow H_2O$. For $[HClO_4] \geq$ ~2.5 M the positive exponential increase indicates the competing reaction ceased, implying complete protonation.

It is expected that under no conditions, $[Pt(H_2O)_6]^{4+}$ will exist exclusively in solution, but rather in equilibrium with small quantities of $[Pt(H_2O)_5(OH)]^{3+}$ according to equilibrium reaction 4.6. Since only one ^{195}Pt NMR signal is observed in these acidic solutions, it is clear that the acid-base equilibrium between $[Pt(H_2O)_6]^{4+}$ and $[Pt(H_2O)_5(OH)]^{3+}$ is fast on the NMR time scale. The ^{195}Pt NMR signals observed in Figure 4.5A ($[HClO_4] \geq 3$ M) are relatively stable an in 6 M $HClO_4$ the signal persists in solution for days. An orange colloidal like compound, forms in the solution after a few days. After a few weeks, the solution becomes clear while an orange solid precipitates.

4.3.3 Oxidation of $[Pt(H_2O)_4]^{2+}$ with hydrogen peroxide, sodium chlorate and sodium bromate in search of $[Pt(H_2O)_6]^{4+}$

In the third method that was pursued to obtain $[Pt(H_2O)_6]^{4+}$, $[Pt(H_2O)_4]^{2+}$ was oxidized in acidic solution. Since formation of $[Pt(H_2O)_6]^{4+}$ requires Pt(II)−O bond formation with the oxidant prior to electron transfer, hydrogen peroxide, sodium chlorate and sodium bromate were used as oxidants possibly fulfilling the criteria.[29, 30] The results are discussed in the context of $[Pt(H_2O)_6]^{4+}$ formation. A discussion of the mechanistic implications of $[Pt(H_2O)_4]^{2+}$ oxidation with the oxidants are postponed to *Chapter 5*, where the oxidation of various Pt(II) complexes are discussed in more detail with regards to the mechanism.

4.3.3.1 Oxidation of $[Pt(H_2O)_4]^{2+}$ with hydrogen peroxide

Oxidation of $[Pt(H_2O)_4]^{2+}$ with H_2O_2 was previously carried out by Appleton *et al.*[23] It was reported that no reaction occurred at room temperature when 1 mL of 30 % (w/w) H_2O_2 was added to 3 mL of 0.2 M $[Pt(H_2O)_4]^{2+}$ (in 1 M $HClO_4$). After increasing the temperature to 70ºC effervescence occurred and a bright orange precipitate formed.[23] Analysis with ^{195}Pt NMR showed only one small signal at 3274 ppm which was assigned to $[Pt(OH)_6]^{2-}$ by the authors.[23] The precipitate was characterized as $PtO_2 \cdot 3H_2O$ by elemental analysis and is different from yellow $PtO_2 \cdot 4H_2O$ (or $H_2Pt(OH)_6$) which forms if a $K_2Pt(OH)_6$ solution is treated with acetic acid.[25, 27] When the bright orange $PtO_2 \cdot 3H_2O$ precipitate was dissolved in 1 M NaOH, a resonance signal was observed at 3568 ppm. The authors proposed that this precipitate could be a $(HO)_4Pt(\mu\text{-}OH)_2Pt(OH)_4^{2-}$ dimer or a derivative

thereof due to the fact that four member $Pt(OH)_2Pt$ rings typically resonate at this frequency.[23]

Oxidation of $[Pt(H_2O)_4]^{2+}$ with H_2O_2 was reinvestigated by adding 10 mol equivalents of H_2O_2 directly to 0.2 M $[Pt(H_2O)_4]^{2+}$ in 1 M $HClO_4$ and stirring the solution for five minutes at 50ºC. The light yellow solution turns orange while a lot of effervescence takes place as a result of hydrogen peroxide reduction and subsequent oxygen formation. The effervescence continues for an hour, which prevents shimming of the NMR instrument and acquisition of a ^{195}Pt NMR spectrum. A ^{195}Pt NMR spectrum could only be acquired at least 1 h after oxidation was initiated. By the time effervescence ceased the solution turned almost completely clear, while an orange precipitate formed similarly to that described by Appleton *et al.*[23] A small signal was observed at 3275 ppm, which correlates very well with the $\delta(^{195}Pt)$ at 3274 ppm reported by Appleton *et al.*[23] and assigned to $[Pt(OH)_6]^{2-}$.

The reaction conditions used for oxidation of $[Pt(H_2O)_4]^{2+}$ with H_2O_2 do not support formation of $[Pt(H_2O)_6]^{4+}$. Oxidation of Pt(II) with H_2O_2 in acid consumes protons so that the final acid concentration is less than 1 M which is well below the concentration of ~2.5 M required for formation of $[Pt(H_2O)_6]^{4+}$ as suggested by Figure 4.5B. Formation of polynuclear Pt species and subsequent Pt precipitation is relatively slow, but effervescence generated by H_2O_2 reduction prevents ^{195}Pt NMR analysis of the solution. Formation of $[Pt(H_2O)_6]^{4+}$ *via* oxidation of $[Pt(H_2O)_4]^{2+}$ with H_2O_2 does not seem feasible in these reaction conditions. In subsequent oxidation reactions of $[Pt(H_2O)_4]^{2+}$ with $NaClO_3$ and $NaBrO_3$ a acid concentration of 6 M $HClO_4$ was used to prevent $[Pt(H_2O)_6]^{4+}$ hydrolysis.

4.3.3.2 Oxidation of $[Pt(H_2O)_4]^{2+}$ with sodium chlorate

A 0.35 M $[Pt(H_2O)_4]^{2+}$ solution was oxidized with five mol equivalents $NaClO_3$ (with respect to Pt(II)) in 6 M $HClO_4$. Initially no oxidation was noticed and the solution was heated to 50ºC. The light yellow $[Pt(H_2O)_4]^{2+}$ solution turns dark yellow while a chlorine like scent is generated as the oxidation proceeds. At 50ºC the oxidation is complete within five minutes as confirmed by the disappearance of the $[Pt(H_2O)_4]^{2+}$ $\delta(^{195}Pt)$ signal and formation of various new $\delta(^{195}Pt)$ signals in the spectral window 2000 - 4000 ppm. Two

major species are observed in this window at 3310 and 2722 ppm respectively (Figure 4.6). The $\delta(^{195}Pt)$ signal at 3310 ppm is in the range expected for $[Pt(H_2O)_6]^{4+}$ while the signal at 2722 ppm is close to that previously observed for $[PtCl(H_2O)_5]^{3+}$ (Figure 4.1). As expected, expansion of the signal at 2722 ppm reveals the two $^{35}Cl/^{37}Cl$ isotopologues $[Pt^{35}Cl(H_2O)_5]^{3+}$ and $[Pt^{37}Cl(H_2O)_5]^{3+}$ (expansion Figure 4.6).
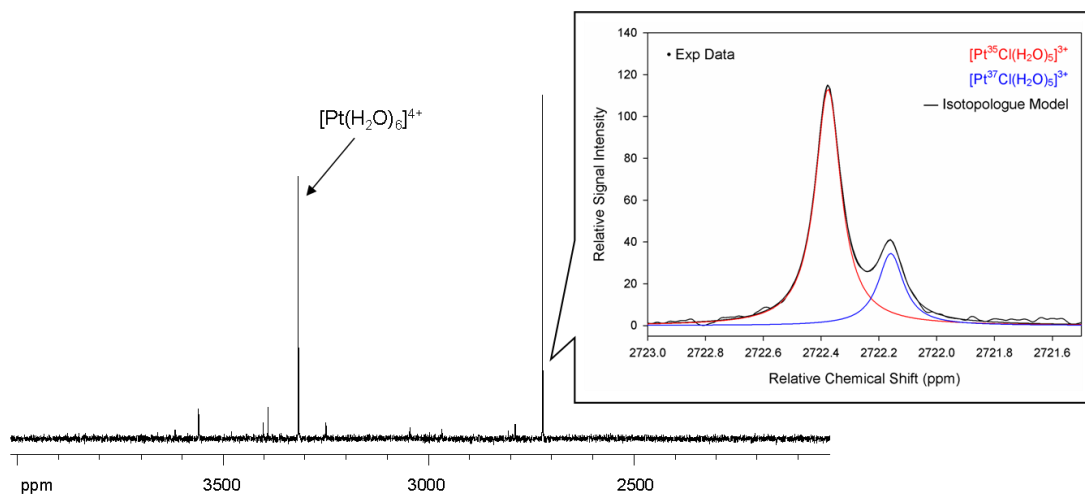
Figure 4.6: ^{195}Pt NMR spectrum (20ºC) of 0.35 M $[Pt(H_2O)_4]^{2+}$ in 6 M $HClO_4$, oxidized by $NaClO_3$.

Least-squares analysis of these signals correlates well the statistical expected $^{35}Cl/^{37}Cl$ isotopologue ratios (Table 4.6) and confirms the $[PtCl(H_2O)_5]^{3+}$ complex. No $^{35}Cl/^{37}Cl$ isotopologues are observed for the signal at 3310 ppm, which implies that no chlorides are coordinated in the complex and supports formation of the $[Pt(H_2O)_6]^{4+}$ complex. In addition to $[PtCl(H_2O)_5]^{3+}$ and $[Pt(H_2O)_6]^{4+}$ various small signals are observed, possibly polynuclear in origin. The $[Pt(H_2O)_6]^{4+}$ signal obtained in these reaction conditions are stable and persist in solution for a few days. Eventually an unknown yellow-orange precipitate forms and the solution becomes clear. This solid is reminiscent of the precipitate described by Appleton *et al*.[23] which was identified as $PtO_2 \cdot 3H_2O$, obtained if $[Pt(H_2O)_4]^{2+}$ is oxidized with H_2O_2.

Table 4.6: Experimentally obtained $^{35}Cl/^{37}Cl$ isotopologue ratios of $[PtCl(H_2O)_5]^{3+}$ compared to the statistically expected $^{35}Cl/^{37}Cl$ isotopologue ratios.

Pt(IV) isotopologue	Percentage of the $[Pt^{35}Cl_n^{37}Cl_{1-n}(H_2O)_5]^-$ (n = 0-1) isotopologues	
	Expt.	**Observed**
$[Pt^{35}Cl(H_2O)_5]^{3+}$	75.93	75.77
$[Pt^{37}Cl(H_2O)_5]^{3+}$	24.07	24.23

4.3.3.3 Oxidation of [Pt(H₂O)₄]²⁺ with sodium bromate

A 0.35 M $[Pt(H_2O)_4]^{2+}$ solution was oxidized with six mol equivalents $NaBrO_3$ (with respect to Pt(II)) in 6 M $HClO_4$. Oxidation is rapid and completed in seconds as indicated by the generation of bromine fumes and colour change from light yellow to dark brown. The ^{195}Pt NMR spectrum recorded after oxidation reveals various Pt(IV) signals in the spectral window 4000 – 2000 ppm. Similar to oxidation with $NaClO_3$, two major $\delta(^{195}Pt)$ signals are observed. The ^{195}Pt signal at 3313 ppm is close to that expected for $[Pt(H_2O)_6]^{4+}$ and to that observed in Figure 4.6. The signal at 2453 ppm is more upfield relative to $[PtCl(H_2O)_5]^{3+}$ and correlates well with the $\delta(^{195}Pt)$ observed for $[PtBr(H_2O)_5]^{3+}$ (*vida infra*). Similar to oxidation of $[Pt(H_2O)_4]^{2+}$ with $NaClO_3$, various small signals are observed in Figure 4.7. The $[Pt(H_2O)_6]^{4+}$ signal obtained in these reaction conditions are stable and persists in solution for days before an orange precipitate forms resulting in a decrease in the Pt(IV) concentration in solution.
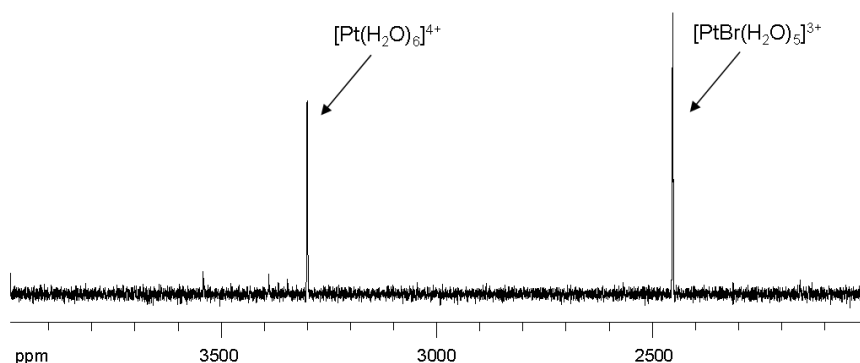
Figure 4.7: ^{195}Pt NMR spectrum (20ºC) of 0.35 M $[Pt(H_2O)_4]^{2+}$ in 6 M $HClO_4$, oxidized by $NaBrO_3$.

Three different methods were investigated in search of $[Pt(H_2O)_6]^{4+}$. Formation of this species *via* precipitation of Cl^- with Ag^+ addition to $[PtCl_6]^{2-}$ is not successful. Although relative high concentration of tentative $[Pt(H_2O)_6]^{4+}$ can be obtained by oxidation of $[Pt(H_2O)_4]^{2+}$ with $NaClO_3$ or $NaBrO_3$ in 6 M $HClO_4$, large concentrations of associated $[PtX(H_2O)_5]^{3+}$ (X = Cl or Br) is formed. Treatment of $[Pt(OH)_6]^{2-}$ with high concentrations of $HClO_4$ ($\geq$ ~2.5 M) results in tentative $[Pt(H_2O)_6]^{4+}$ exclusively and does not introduce halides in the solution which compete with H_2O for Pt(IV) coordination. Since the

$Na_2[Pt(OH)_6]$ salt can be obtained commercially it could be an ideal starting point towards $[Pt(H_2O)_6]^{4+}$ formation. To reveal more about the reactivity of the tentative $[Pt(H_2O)_6]^{4+}$ complex obtained in this manner, H_2O exchange as well as halide anation (Cl^- and Br^-) experiments were carried out.

4.3.4   Ligand exchange of coordinated H_2O on tentative $[Pt(H_2O)_6]^{4+}$ with H_2O, Cl^- and Br^-

Water exchange on octahedral metal ions takes place either *via* a dissociative (D), associative (A) or interchange (I) mechanism as classified by [†]Langford and Grey.[31] The I mechanism is applicable in cases where no definite intermediate can be identified and is sub-divided into Dissociative Interchange (I_d) and Associative Interchange (I_a) mechanisms. Solvent exchange on the first-row 3d hexa-aqua metal ions, has been studied in detail and reviewed by various authors.[1-4, 32] These studies revealed that the solvent exchange mechanism changes from I_a to I_d as the number of d electrons increases and the ionic radius decreases. The change in mechanism has been rationalized by a combination of three effects as stipulated by Helm and Merbach[2] on the subject: (1) "increase of the t_{2g} orbital occupancy disfavour approach of the entering nucleophilic solvent molecule on a trigonal face of the octahedron and rather favour an d-activated mechanism; (2) e_g* electron occupancy increases, which favours breaking of the metal–solvent bond in a dissociative-activated mechanism; and (3) to a lesser extent, the decrease of metal ion radius (r_M) favours dissociation over association due to steric crowding".

Based on the results for the first-row 3d metal ions (hindered nucleophilic attack), a dissociative activated complex was anticipated for the heavier second- and third-row hexa-aqua metal ions. However, as it appears an I mechanism was determined for H_2O exchange on $[Ru(H_2O)_6]^{2+}$ while an I_a mechanism was found for $[Ru(H_2O)_6]^{3+}$, $[Rh(H_2O)_6]^{3+}$ and $[Ir(H_2O)_6]^{3+}$, defying what is predicted by MO theory.[2, 3] It is in the context of these studies that the rate of H_2O exchange on tentative $[Pt(H_2O)_6]^{4+}$ was measured.

[†]This convention of classifying exchange mechanisms has been challenged by Swaddle as it restricts the interpretation of the mechanism to the sensitivity or insensitivity of the entering ligand but in the absence of a more comprehensive classification system, this method is still in use by most authors in discussions on this topic and will be employed here also.[33]

4.3.4.1 $^{16}O/^{18}O$ isotopologue signals of $[Pt(OH)_6]^{2-}$ and the relative solvent exchange rate of H_2O as measured by ^{195}Pt NMR

Water exchange on hexa-aqua metal ions is often measured with the now standard method of ^{17}O enrichment and ^{17}O NMR analysis.[7, 9] The method of speciation analysis discussed in *Chapter 3 via* $H_2^{18}O$ enrichment and measuring the $^{16}O/^{18}O$ isotopic shifts with ^{195}Pt NMR presents another method to measure H_2O exchange as demonstated by Gröning *et al*.[34] for H_2O exchange on $[Pt(H_2O)_4]^{2+}$. As preciously discussed a $^{16}O/^{18}O$ isotopologue is defined as a chemical species that differs in isotopic composition of their molecules or ions e.g. $[Pt(H_2^{16}O)_6]^{4+}$ and $[Pt(H_2^{16}O)_5(H_2^{18}O)]^{4+}$. Since H_2O exchange on Pt(IV) are generally slow (*Chapter 3* and ref. [34]), well resolved ^{195}Pt NMR $^{16}O/^{18}O$ isotopologue signals are anticipated. Enriching $[Pt(H_2O)_6]^{4+}$ is of particular interest since it will confirm six coordinated oxygen ligands, something that has not been verified in solution with NMR before.

A solution of 0.04 M $[Pt(OH)_6]^{2-}$ (obtained from the $Na_2Pt(OH)_6$ salt) was prepared in water. All the salt do not dissolve at room temperature and the solution was filtered to give a clear light-yellow solution (pH = 9.3). A large ^{195}Pt signal is observed at 3285 ppm relative to an external $[Pt(OH)_6]^{2-}$ reference solution kept in a capillary insert (3270 ppm in 1 M NaOH). Both $[Pt(OH)_6]^{2-}$ signals are seen in water and 1 M NaOH (reference) in Figure 4.8A. A small signal is observed at 3284.1 ppm, upfield from the main $[Pt(OH)_6]^{2-}$ signal and is not to be confused with the reference solution. The $\Delta_{itl}\delta(^{195}Pt)$ value of 0.765 ppm indicated by the expansion Figure 4.8A is typical for Pt(IV) $^{16}O/^{18}O$ isotopologues (*Chapter 3*, *Table 3.6*), and is possibly the $[Pt(^{16}OH)_5(^{18}OH)]^{2-}$ isotopologue formed from natural abundant ^{18}O (0.20 %). The low concentration and overlap with $[Pt(^{16}OH)_6]^{2-}$ prevent accurate peak integration, and a relative ratio of 98.5 : 1.5 % is obtained.
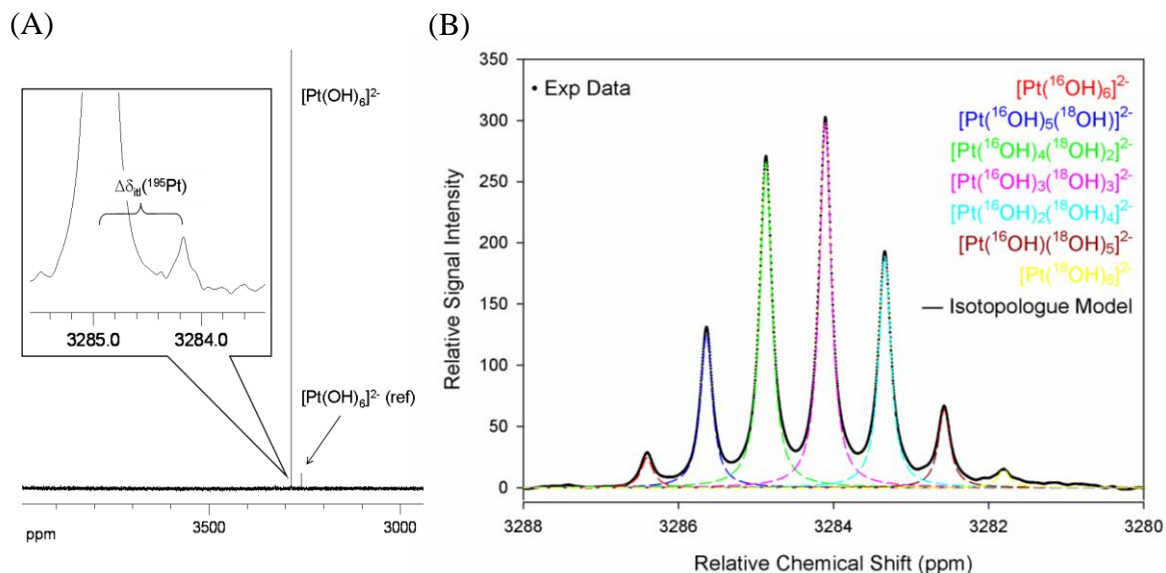
Figure 4.8: **(A)** ^{195}Pt NMR spectrum of $[Pt(OH)_6]^{2-}$ in water, showing the $[Pt(^{16}OH)_6]^{2-}$ and $[Pt(^{16}OH)_5(^{18}OH)]^{2-}$ isotopologues. **(B)** ^{195}Pt NMR spectrum of $[Pt(OH)_6]^{2-}$ in 45% $H_2^{18}O$ after 59 h exposure to light, showing all seven $[Pt(^{16}OH)_n(^{18}OH)_{6-n}]^{2-}$ (n = 0-6) $^{16}O/^{18}O$ isotopologues.

A fraction of $H_2^{18}O$ (97 %) was added to the solution shown in Figure 4.8A to give a 55:45 % ratio of ^{16}O:^{18}O. After "ageing" the solution for 12 h at room temperature in the dark, no additional signals are observed in the ^{195}Pt NMR spectrum, but the small signal observed at 3284.1 ppm has grown slightly to relative integration values of 97 : 3 %, which confirms the $[Pt(^{16}OH)_5(^{18}OH)]^{2-}$ isotopologue signal. Due to the apparent slow ligand exchange of $[Pt(OH)_6]^{2-}$ with solvent $H_2^{16}O/H_2^{18}O$, the solution was exposed to light from a standard slide projector in order to speed up H_2O exchange. After 20 h of exposure the $[Pt(^{16}OH)_5(^{18}OH)]^{2-}$ isotopologue signal grew considerable while three new signals also appeared. After exposing the solution to light for a total of 59 hours, all seven $[Pt(^{16}OH)_{6-n}(^{18}OH)_n]^{2-}$ (n = 0-6) isotopologues formed as shown in Figure 4.8B. Since H_2O exchange is extremely slow and effectively quenched during acquisition in the ^{195}Pt NMR spectrophotometer, well resolved Lorentzian shaped signals are obtained. Least-squares analysis of these signals indicates $^{16}O/^{18}O$ isotopologue ratios consistent with the fraction of $H_2^{18}O$ added (Table 4.7).

Table 4.7: $^{16}O/^{18}O$ isotopologue concentrations obtained from a least-squares fit of the $[Pt(^{16}OH)_{6-n}(^{18}OH)_n]^{2-}$ (n = 0-6) signals. The good correlation between experimentally obtained values and the statistical values calculated from the $^{16}O:^{18}O$ ratio (55:45 %) indicates that equilibrium has been reached.

Pt(IV) isotopologue	Percentage $[Pt(^{16}OH)_{6-n}(^{18}OH)_n]^{2-}$ (n = 0-6) isotopologues	
	Expt.	Statistical
$[Pt(^{16}OH)_6]^{2-}$	2.49	2.48
$[Pt(^{16}OH)_5(^{18}OH)]^{2-}$	12.70	12.67
$[Pt(^{16}OH)_4(^{18}OH)_2]^{2-}$	27.08	26.99
$[PtBr(^{16}OH)_3(^{18}OH)_3]^{2-}$	30.43	30.65
$[Pt(^{16}OH)_2(^{18}OH)_4]^{2-}$	19.29	19.58
$[Pt(^{16}OH)(^{18}OH)_5]^{2-}$	6.49	6.67
$[Pt(^{18}OH)_6]^{2-}$	1.52	0.95

Although the H_2O exchange rate of $[Pt(OH)_6]^{2-}$ is too slow to measure with conventional NMR techniques, the relative exchange rate indicate that H_2O exchange is extremely slow. Only after irradiating the solution for a total of 59 hours, the $^{16}O/^{18}O$ isotopologue ratios seem to have reached equilibrium. That seven $^{16}O/^{18}O$ isotopologues are observed, confirms six oxygen coordinated ligands in the $[Pt(OH)_6]^{2-}$ complex, and has not been confirmed with NMR before.

4.3.4.2 Formation of tentative $[Pt(H_2{}^{16}O)_n(H_2{}^{18}O)_{6-n}]^{4-n}$ (n = 0-6) via protonation of OH⁻ on $[Pt(^{16}OH)_n(^{18}OH)_{6-n}]^{2-}$ (n = 0-6): slow H_2O exchange as measured by ^{195}Pt NMR

A portion of the solution shown in Figure 4.8B (230 µL) was treated with concentrated $HClO_4$ (230 µL) to result in a final $HClO_4$ concentration of ~5.8 M. The total Pt(IV) concentration is thus halved by the volume of $HClO_4$ added and changes the total $^{16}O : ^{18}O$ ratio to 77.4 : 22.6 % in the solution. The low concentration of Pt(IV) necessitated long ^{195}Pt NMR acquisition times to obtain satisfactory signal/noise ratios. Acquisition of a ^{195}Pt NMR spectrum was started ~30 min after addition of concentrated $HClO_4$ and continued for 48 h at 20°C. Addition of $HClO_4$ to the $[Pt(OH)_6]^{2-}$ solution causes a ~29 ppm downfield shift close to the $\delta(^{195}Pt)$ value observed previously in 6 M $HClO_4$ (Figures 4.5 – 4.7). One signal is observed at ~3314 ppm in the ^{195}Pt NMR spectrum, in the region expected for $[Pt(H_2O)_6]^{4+}$. Expansion of this signal reveals several $^{16}O/^{18}O$ isotopologues as shown in Figure 4.9.
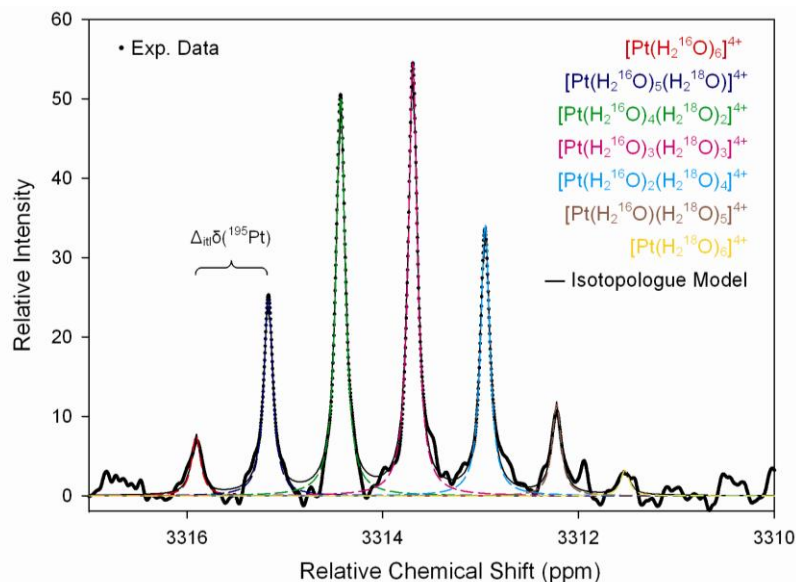
Figure 4.9: ^{195}Pt NMR spectrum of the tentative [Pt(H$_2$^{16}O)$_n$(H$_2$^{18}O)$_{6-n}$] (n = 0-6) *aqua* isotopologues obtained after 48 hours of acquisition after adding concentrated HClO$_4$ (final [H$^+$] = 5.8 M) to a [Pt(^{16}OH)$_n$^{18}(OH)$_{6-n}$]$^{2-}$ (n = 0-6) solution.

A visual comparison between the ^{16}O/^{18}O isotopologue ratios in Figures 4.9 and 4.8 is almost identical and a least-squares analysis confirms only 1% change in the coordinated H$_2$^{16}O : H$_2$^{18}O ratio (Table 4.8) Due to the relative low concentration of Pt(IV) and small signal/noise ratio only six of the seven possible ^{16}O/^{18}O isotopologues are observed.

Table 4.8: Experimentally obtained values of the least-squares fit of observed ^{16}O/^{18}O isotopologues in the alleged [Pt(H$_2$^{16}O)$_{6-n}$(H$_2$^{18}O)$_n$]$^{2-}$ (n = 0-6) series, contributing to a ratio of 54 : 46 %.

Pt(IV) isotopologue	Percentage of the [Pt(H$_2$^{16}O)$_{6-n}$(H$_2$^{18}O)$_n$]$^{2-}$ (n = 0-6) isotopologues		
	Expt.	†Statistical before acid	‡Statistical after acid
[Pt(H$_2$^{16}O)$_6$]$^{4+}$	4.08	2.48	21.67
[Pt(H$_2$^{16}O)$_5$(H$_2$^{18}O)]$^{4+}$	13.41	12.67	37.74
[Pt(H$_2$^{16}O)$_4$(H$_2$^{18}O)$_2$]$^{4+}$	26.96	26.99	27.39
[Pt(H$_2$^{16}O)$_3$(H$_2$^{18}O)$_3$]$^{4+}$	29.26	30.65	10.60
[Pt(H$_2$^{16}O)$_2$(H$_2$^{18}O)$_4$]$^{4+}$	18.39	19.58	2.31
[Pt(H$_2$^{16}O)(H$_2$^{18}O)$_5$]$^{4+}$	6.18	6.67	0.27
[Pt(H$_2$^{18}O)$_6$]$^{4+}$	-	0.95	0.01

†Statistical ^{16}O/^{18}O ratio in the solution calculated before addition of concentrated HClO$_4$. ‡Statistical ^{16}O/^{18}O ratio in the solution calculated at equilibrium after addition of concentrated HClO$_4$.

The constant $\Delta_{itl}\delta(^{195}Pt)$ value between respective $^{16}O/^{18}O$ isotopologues give a remarkable consistent value of 0.74 ppm as a function of coordinated ^{18}O isotopes (resulting in a straight line; $R^2 = 1$) as shown in Figure 4.10. The $\delta(^{195}Pt)$ value of the $[Pt(H_2{}^{18}O)_6]^{4+}$ isotopologue is predicted by extrapolating the linear trend in the Figure 4.10. The concentration of the $[Pt(H_2{}^{18}O)_6]$ isotopologue is calculated from the least-squares fit of the signals so that the $[Pt(H_2{}^{18}O)_6]$ signal could be simulated in Figure 4.9. The $\Delta_{itl}\delta(^{195}Pt)$ value between respective $[Pt(^{16}OH)_{6-m}(^{18}OH)_m]^{2-}$ (m = 0-6) isotopologues are consistently 0.77 ppm, slightly bigger than the corresponding $^{16}O/^{18}O$ isotopologues observed in acidic solution and is also plotted in Figure 4.10 for comparison. Jameson[30] proposed that a bigger isotopic mass difference of a specific ligand coordinated to a metal centre, results in bigger $\Delta_{itl}\delta(^{195}Pt)$ value, due to different M–L bond lengths. With regards to *aqua* and *hydroxido* complexes, a direct comparison between the $\Delta_{itl}\delta(^{195}Pt)$ values are not necessarily related to a stronger and shorter Pt(IV)–OH bond. The root cause for these effects needs to be investigated in detail to better understand the contributing factors of such effects.
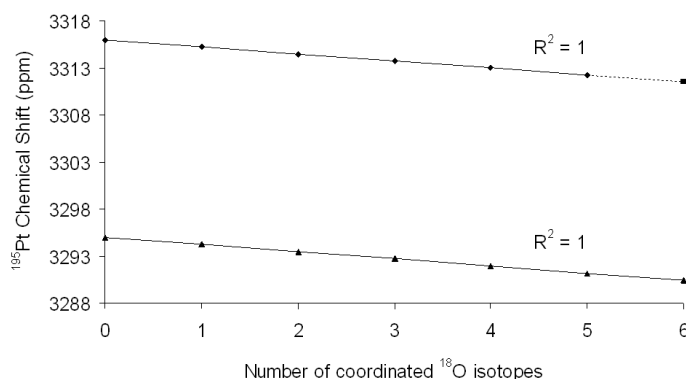
Figure 4.10: $\delta_{itl}(^{195}Pt)$ values of the tentative $[Pt(H_2{}^{16}O)_n(H_2{}^{18}O)_{6-n}]$ (n = 0-5) *aqua* $^{16}O/^{18}O$ isotopologues, allowing prediction of the $\delta_{itl}(^{195}Pt)$ value of $[Pt(H_2{}^{18}O)_6]^{4+}$ (■). The $\delta_{itl}(^{195}Pt)$ values of all the possible *hydroxido* $[Pt(^{16}OH)_n(^{18}OH)_{n-6}]^{2-}$ (n = 0-6) $^{16}O/^{18}O$ isotopologues are also shown (▲).

Due to the slow kinetics, it was not practical to quantify the H_2O exchange rate in these reaction conditions. After addition of concentrated $HClO_4$, the ratio of $^{16}O/^{18}O$ isotopologues changes only ~1 % during the 48 h of acquisition (Table 4.8 *vs.* 4.7), even though the ^{16}O : ^{18}O ratio in the solution changes from 55:45 % to 77.5:22.5 %. The $^{16}O/^{18}O$ isotopologue ratio therefore almost remains unchanged, implying extremely slow H_2O exchange of tentative $[Pt(H_2O)_6]^{4+}$ in 5.8 M $HClO_4$.

4.3.4.3 The relative ligand exchange rate of tentative $[Pt(H_2O)_6]^{4+}$ with chloride and bromide

The reactivity of tentative $[Pt(H_2O)_6]^{4+}$ towards Cl^- anation is illustrated with two experiments. For the first experiment, 6 mol equivalents of NaCl (with respect to Pt(IV)) was added to a $[Pt(OH)_6]^{2-}$ solution in water (prepared from the $Na_2Pt(OH)_6$ salt; pH = 9.3). No Pt(IV)–Cl coordination is observed even after "ageing" the solution for 24 h at ambient temperature, confirming that the $[Pt(OH)_6]^{2-}$ complex is kinetically inert towards Cl^- substitution. In the second experiment six mol equivalents of NaCl (with respect to Pt(IV)) was added to a $[Pt(OH)_6]^{2-}$ solution treated with 6 M $HClO_4$ (also prepared from the $Na_2Pt(OH)_6$ salt). After ~30 min of ^{195}Pt NMR analysis, two signals are observed in addition to the original signal of tentative $[Pt(H_2O)_6]^{4+}$ (left part of the ^{195}Pt NMR spectrum in Figure 4.11). These species are assigned to *trans*-$[PtCl_2(H_2O)_4]^{2+}$ (2205 ppm) and *fac*-$[PtCl_3(H_2O)_3]^+$ (1577 ppm) and closely matches the $\delta(^{195}Pt)$ values reported for these complexes in Table 4.1, if the difference in $HClO_4$ concentration is considered. The spectral window 1800 to -200 ppm was acquired after ~60 min showing four signals correlating to *trans*/*cis*-$[PtCl_4(H_2O)_2]$ (1119 and 982 ppm), $[PtCl_5(H_2O)]^-$ (496 ppm) and $PtCl_6^{2-}$ (28 ppm) respectively as shown in Figure 4.11. All these values are listed in Table 4.1 for comparison to values obtained in 1 M $HClO_4$.
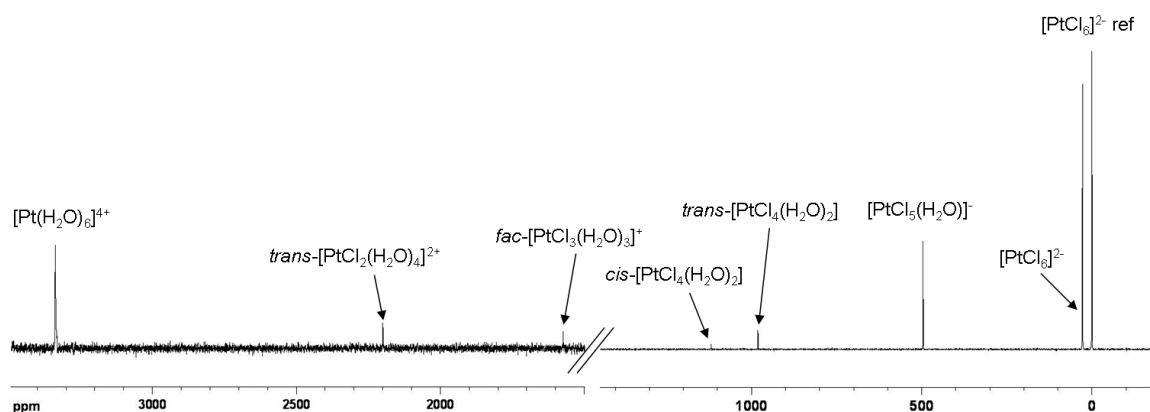
Figure 4.11: ^{195}Pt NMR spectra obtained after addition of six mol equivalents NaCl to $[Pt(OH)_6]^{2-}$ treated with 6 M $HClO_4$.

In a related study Swaminathan and Harris[35] reported that $[Rh(H_2O)_5Cl]^{2+}$ is not detected by UV-visible spectroscopy when Cl^- is added to $[Rh(H_2O)_6]^{3+}$ but only *trans-*

[Rh(H$_2$O)$_4$Cl$_2$]. The authors[35] ascribed this to the strong kinetic *trans* effect of Cl$^-$ which promotes fast substitution of H$_2$O *trans* of Cl$^-$ in the [Rh(H$_2$O)$_5$Cl]$^{2+}$ complex. The dynamic nature of the solution shown in Figure 4.11 is illustrated by the absence of [PtCl(H$_2$O)$_5$]$^{3+}$, *cis*-[PtCl$_2$(H$_2$O)$_4$]$^{2+}$ and *mer*-[PtCl$_3$(H$_2$O)$_3$]$^+$, which are presumably not favoured kinetic products. It may be reasonably expected that formation of *trans*-[PtCl$_4$(H$_2$O)$_2$]$^{2+}$ should be kinetically favoured above the *cis* isomer in view of a strong Cl$^-$ *trans* effect in [PtCl(H$_2$O)$_5$]$^{3+}$. By a similar argument the *fac*-[PtCl$_3$(H$_2$O)$_3$]$^+$ isomer is expected to form instead of the *mer* isomer, which is confirmed in the experimental result.

It is expected that the tentative [Pt(H$_2$O)$_6$]$^{4+}$ complex should display similar reactivity towards Br$^-$ anation as observed for Cl$^-$. Dissolution of 0.2 M H$_2$PtBr$_6$ in 1 M HClO$_4$, results in only small quantities of [PtBr$_5$(H$_2$O)]$^-$ compared to [PtBr$_6$]$^{2-}$ (concentration ratio of 1:5 by peak integration) due to the presumably high thermodynamic stability of [PtBr$_6$]$^{2-}$. A [Pt(OH)$_6$]$^{2-}$ solution was treated with 6 M HClO$_4$ similar to the Cl$^-$ anation experiment. In this case only three mol equivalents of NaBr (with respect to (Pt(IV)) were added to the Pt(IV) solution in an attempt to prevent the equilibrium from shifting too much towards formation of [PtBr$_6$]$^{2-}$. Immediately after adding NaBr, the orange coloured solution turns orange-brown and only a fraction of the original signal at 3312 ppm remains (as perceived from the signal/noise ratio). No other signals are observed between 3400 and 0 ppm. Analysis of the ^{195}Pt spectral window between 0 and -3000 ppm revealed large quantities of [PtBr$_6$]$^{2-}$ (-1913 ppm) and minor quantities of [PtBr$_5$(H$_2$O)]$^-$ (1047 ppm) with respect to the external [PtCl$_6$]$^{2-}$ reference. After "ageing" the solution for two weeks in the dark at room temperature, four additional ^{195}Pt NMR signals formed as shown in Figure 4.12. Due to the large $\Delta\delta$(^{195}Pt) value between respective [PtBr$_m$(H$_2$O)$_{6-m}$]$^{4-m}$ (*m* = 0-6) species, it was necessary to collect ^{195}Pt NMR spectra in four different spectral windows to ensure that the full frequency range is monitored where these species may resonate. The ^{195}Pt spectra collected are joined as indicated in Figures 4.12A and B.
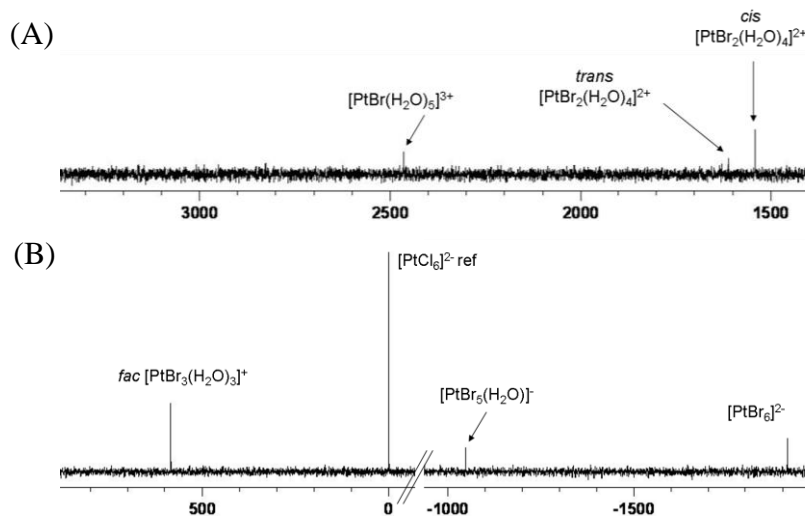
Figure 4.12: ^{195}Pt NMR spectra of $Na_2[Pt(OH)_6]$ dissolved in 6 M $HClO_4$ after adding three mol equivalents NaBr and "ageing" the solution for two weeks **(A)** 3500 to 1500 ppm and **(B)** 1000 to -2000 ppm.

The ^{195}Pt signals observed in Figure 4.12 are assigned to *fac*-[PtBr$_3$(H$_2$O)$_3$]$^+$, *cis/trans*-[PtBr$_2$(H$_2$O)$_4$]$^{2+}$ and [PtBr(H$_2$O)$_5$]$^{3+}$ respectively, by applying the principles of ^{195}Pt NMR chemical-shift-trend analysis. A plot of the observed $\delta(^{195}Pt)$ values as a function of coordinated H$_2$O, results in a linear trend, defined by $\delta(^{195}Pt) = 870 - 1907$; R^2 > 0.999 (Figure 4.13). The ^{195}Pt spectra did not reveal any signals correlating to *mer*-[PtBr$_3$(H$_2$O)$_3$]$^+$ or *cis/trans*-[PtBr$_4$(H$_2$O)$_2$]$^{2+}$. The $\delta(^{195}Pt)$ values of these species were estimated from the $\Delta\delta(^{195}Pt)$ increments expected from Br$^-$ substitution of H$_2$O *trans* to Br$^-$ and H$_2$O *trans* to H$_2$O according to the same principles described in *Chapter 2* for Pt(II) complexes. The predicted and observed $\delta(^{195}Pt)$ values is listed in Table 4.9. Four of these [Pt(H$_2$O)$_{6-m}$-Br$_m$]$^{4-m}$ (*m* = 0-6) experimental $\delta(^{195}Pt)$ values are reported here for the first time.
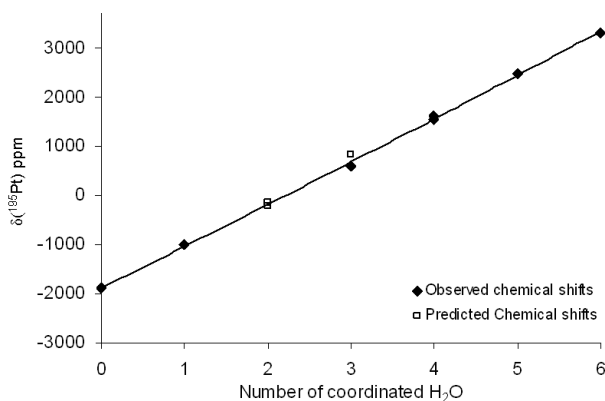
Figure 4.13: Linear plot obtained for the $\delta(^{195}Pt)$ values observed in the [PtBr$_m$(H$_2$O)$_{6-m}$]$^{4-m}$ (*m* = 0-6) series as a function of coordinated H$_2$O. Predicted $\delta(^{195}Pt)$ values are included in the graph for comparison.

Table 4.9: $\delta(^{195}\text{Pt})$ values of the $[\text{Pt}(\text{H}_2\text{O})_{6-m}\text{Br}_m]^{4-m}$ (m = 0-6) species observed in Figure 4.12 compared to available literature values in H_2O. Predicted values are shown for complexes that are not observed.

Correct name	No of H$_2$O	Species	δ ^{195}Pt (ppm) [a]	Literature values [b]
060	0	$[\text{PtBr}_6]^{2-}$	-1913	-1878 [18]
051	1	$[\text{PtBr}_5(\text{H}_2\text{O})]^{1-}$	-1047	-1004 [18]
04^{c}2^c	2	*cis* $[\text{PtBr}_4(\text{H}_2\text{O})_2]$	*-203* [c]	
04^{t}2^t	2	*trans* $[\text{PtBr}_4(\text{H}_2\text{O})_2]$	*-135* [c]	
03^{f}3^f	3	*fac* $[\text{PtBr}_3(\text{H}_2\text{O})_3]^+$	583	
03^{m}3^m	3	*mer* $[\text{PtBr}_3(\text{H}_2\text{O})_3]^+$	825 [c]	Not reported before
02^{c}4^c	4	*cis* $[\text{PtBr}_2(\text{H2O})_4]^{2+}$	1543	
02^{t}4^t	4	*trans* $[\text{PtBr}_2(\text{H2O})_4]^{2+}$	1612	
015	5	$[\text{PtBr}(\text{H}_2\text{O})_5]^{3+}$	2465	
006	6	$[\text{Pt}(\text{H}_2\text{O})_6]^{4+}$	3312	

[a] Obtained in 6 M HClO$_4$ at 30°C, [b] obtained in water and [c] predicted $\delta(^{195}\text{Pt})$

$[\text{PtBr}_6]^{2-}$ and some minor quantities of $[\text{PtBr}_5(\text{H}_2\text{O})]^-$ are formed immediately after addition of NaBr to tentative $[\text{Pt}(\text{H}_2\text{O})_6]^{4+}$. Since Br$^-$ is a stronger nucleophile than Cl$^-$, Br$^-$ coordination to Pt(IV) is kinetically favourable. Coupled with the fact that Br$^-$ exhibits a stronger *trans* kinetic effect,[36] it may account for the initial quick formation of $[\text{PtBr}_5(\text{H}_2\text{O})]^-$ and $[\text{PtBr}_6]^{2-}$. Formation of new signals after the solution was "aged" indicates formation of thermodynamic more favourable species under these reaction conditions. Due to the fast kinetics and relatively long acquisition times required with ^{195}Pt NMR analysis, it was not possible to quantify the Cl$^-$ and Br$^-$ anation rates in these reaction conditions. It is however clear, that Cl$^-$ and Br$^-$ anation of $[\text{Pt}(\text{OH})_6]^{2-}$ is fast when treated with 6 M HClO$_4$, suggesting protonation and formation of labile H$_2$O, something which is not observed with $[\text{Pt}(\text{OH})_6]^{2-}$ in water.

4.3.4.4 Rationalization of the observed slow water exchange and relative fast halide anation on tentative $[Pt(H_2O)_6]^{4+}$

Detailed water exchange studies on the second- and third-row hexa-aqua metal ions are limit and have only been reported for $[\text{Ru}(\text{H}_2\text{O})_6]^{2+/3+}$, $[\text{Rh}(\text{H}_2\text{O})_6]^{3+}$ and $[\text{Ir}(\text{H}_2\text{O})_6]^{3+}$.[1-3] In the absence of any related quad-valent charged hexa-aqua metal ions a comparison of H$_2$O, Cl$^-$ and Br$^-$ exchange rates on $[\text{Pt}(\text{H}_2\text{O})_6]^{4+}$ is only possible with these divalent and trivalent hexa-aqua metal ions. Kinetic studies revealed that for group 9 low-spin t_{2g}^6 metal ions, the

inertness of the complex towards H_2O exchange increases down a group in the order $[Co(H_2O)_6]^{3+}$ [37] $\rightarrow$ $[Rh(H_2O)_6]^{3+}$ [8] $\rightarrow$ $[Ir(H_2O)_6]^{3+}$ [9] a trend which is in line with a gain in ligand-field stabilization.[36] Slow water exchange rates were also reported for the low-spin t_{2g}^5 complex $[Ru(H_2O)_6]^{3+}$ (3.5 x 10^{-6} s^{-1})[7] and the divalent t_{2g}^6 complex $[Ru(H_2O)_6]^{2+}$ (1.8 x 10^{-2} s^{-1}).[7] For a dissociative activated complex, bond breakage is the rate determining step, so that halide anation rates are independent of the entering ligand, while for an associatively activated complex, bond formation and thus the nature of the entering ligand is important. It was on this bases that ligand exchange studies with Cl^- and Br^- (and I^- in some cases) were carried out in order to determine the exchange mechanism for $[Ru(H_2O)_6]^{2+/3+}$, $[Rh(H_2O)_6]^{3+}$ and $[Ir(H_2O)_6]^{3+}$. Kallen et al.[38] and Aebischer et al.[39] reported similar H_2O exchange and halide (Cl^-, Br^- and I^-) anation rates on $[Ru(H_2O)_6]^{2+}$ so that a dissociative activated intermediate was assigned. Activation volume values close to zero ($\Delta V^{\ddagger}$ = -0.4 cm^3 mol^{-1}) however indicated that both bond breakage and bond formation is equally important so that an I mechanism was assigned.[7] Harris et al.[35, 40] reported similar H_2O exchange and halide (Cl^- and Br^-) anation rates on $[Rh(H_2O)_6]^{3+}$ and an I_d mechanism was assigned. This mechanism was discounted after an $\Delta V^{\ddagger}$ value of -3.3 cm^3mol^{-1} was determined by Laurenzy[8] and an I_a mechanism was assigned. It was confirmed by Galbraith et al.[41] that different rates of anation is obtained with other ligands on $[Rh(H_2O)_6]^{3+}$ and that similar anation rates with Cl^- and Br^- are merely a coincidence and property of $[Rh(H_2O)_6]^{3+}$. No anation of 2.3 x 10^{-3} M $[Ir(H_2O)_6]^{3+}$ was observed in 3.7 M Cl^- or Br^- after 15 days at 313 K and a rate constant of < 10^{-9} $M^{-1}s^{-1}$ was estimated by Castillo-Blum.[42] This result was rationalized by Cusanelli et al.[9] after determining a half-life ~15 years for water exchange at that temperature. Calculations by de Vito[43] indicated an I mechanism for water exchange on $[Ru(H_2O)_6]^{2+}$ and an I_a mechanism for exchange on $[Rh(H_2O)_6]^{3+}$ and $[Ir(H_2O)_6]^{3+}$. This outcome was rationalized in terms of stronger $M^{3+}-OH_2$ bonds due to the 3+ charge, so that a dissociative activated complex is thermodynamically un-favorable.

The extreme inertness of these trivalent t_{2g}^6 complexes towards H_2O exchange or Cl^- and Br^- anation is thus mainly rationalized by the high LFAEs of these complexes while the mechanism seems to depend on variation between the following factors as proposed by

Galbraith[41]: *i)* contribution from strong σ-donating ligands like Cl⁻, Br⁻ or OH⁻; *ii)* the bond strength of the leaving ligand; *iii)* the electrostatic attraction between the entering ligand and metal ion (defined by the cationic charge on the complex) and *iv)* steric effects. Since $[Pt(H_2O)_6]^{4+}$ has a low spin t_{2g}^6 electron configuration and therefore a similar LFAE as the inert metal ions $[Ru(H_2O)_6]^{2+}$, $[Rh(H_2O)_6]^{3+}$ and $[Ir(H_2O)_6]^{3+}$ (according to MO theory), it was anticipated that H_2O exchange on $[Pt(H_2O)_6]^{4+}$ should also be slow.[4, 42] A slow rate of H_2O exchange was confirmed for the tentative $[Pt(H_2O)_6]^{4+}$ complex from Figure 4.9 (after 48 h ~1% change in ^{16}O : ^{18}O isotopologue ratio was observed). In the context of slow anation rates (Cl⁻ and Br⁻) observed for $[Ru(H_2O)_6]^{2+}$, $[Rh(H_2O)_6]^{3+}$ and $[Ir(H_2O)_6]^{3+}$ the fast anation rate of tentative $[Pt(H_2O)_6]^{4+}$ (Figures 4.11 and 4.12) is a surprise. Since an inert complex towards water exchange and halide anation is anticipated from the LFAEs, the relative fast anation rates were evaluated in terms of the factors proposed by Galbraith *(i-iii)* to possibly rationalize the rates.

i)   *Contribution from strong σ-donating ligands: enhanced ligand exchange rate on $[Pt(H_2O)_6]^{4+}$ in terms of the conjugate-base effect*

Due to the rapid acid-base equilibrium 4.9, fractions of the monohydroxido metal ion $[M(H_2O)_5(OH)]^{x-1}$ will always exist in solution, leading to a possible alternative pathway for H_2O exchange or halide anation.[1-3, 7, 9, 35]

$$[M(H_2O)_6]^{x+} \rightleftharpoons [M(H_2O)_5(OH)]^{x-1} + H^+ \qquad (4.9)$$
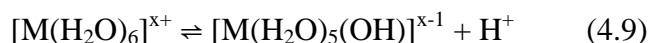
A two term rate law which defines the water exchange rate was found in the kinetic studies involving $[Ru(H_2O)_6]^{2+/3+}$, $[Rh(H_2O)_6]^{3+}$ and $[Ir(H_2O)_6]^{3+}$ when significant quantities of the monohydroxido species were present.[7, 9, 35] The second term in the rate law is inversely proportional to $[H^+]$ as expressed in Equation 4.10, with k_1 and k_2 referring to the rate constants for water exchange on $[M(H_2O)_6]^{x+}$ and $[M(H_2O)_5(OH)]^{x-1}$ respectively.

$$k_{obs} = k_1 + k_2/[H^+] \qquad (4.10)$$

Depending on the pK_a value of $[M(H_2O)_6]^{x+}$ and the acid concentration, the concentration of $[M(H_2O)_5(OH)]^{x-1}$ and contribution to the observed rate varies. Since OH⁻ is a stronger

electron donating ligand than H_2O, it strengthens the M–OH bond whereas the M–OH_2 bond *trans* thereof is weakened. The H_2O ligand thus becomes more labile favouring a dissociative activation mechanism. Volume of activation studies, indicates an I_a mechanism for H_2O exchange on $[Rh(H_2O)_6]^{3+}$ and $[Ir(H_2O)_6]^{3+}$, whereas an I mechanism is indicated for the conjugate-bases $[Rh(H_2O)_5(H_2O)]^{2+}$ and $[Ir(H_2O)_5(H_2O)]^{2+}$.[9, 35] The conjugate-base effect has been credited as the main reason why H_2O exchange may seem that much slower on $[Ir(H_2O)_6]^{3+}$ compared to $[Rh(H_2O)_6]^{3+}$. The conjugate-base $[Rh(H_2O)_5(OH)]^{2+}$ is ~6000 times more reactive than $[Rh(H_2O)_6]^{3+}$ towards H_2O exchange, whereas $[Ir(H_2O)_5(OH)]^{2+}$ is only ~1000 times more reactive than $[Ir(H_2O)_6]^{3+}$.[2, 3] The conjugate base effect is amplified by the lower pK_a value of $[Rh(H_2O)_6]^{3+}$ (pK_a ~ 4) compared to $[Ir(H_2O)_6]^{3+}$ (pK_a ~ 4.45).

The quantity of $[Pt(H_2O)_5(OH)]^{3+}$ with respect to $[Pt(H_2O)_6]^{4+}$ is unknown in the reactions conditions studied here. If a large fraction of $[Pt(H_2O)_5(OH)]^{3+}$ is present in these solutions, it does not increase the overall H_2O exchange rate significantly, since the observed H_2O exchange rate is extremely slow (Figure 4.9). A dissociative mechanism cannot be assumed for the conjugate-base $[Pt(H_2O)_5(OH)]^{3+}$ since the 3+ charge will counteract such a mechanism. On the other hand, if anation takes place *via* an associative mechanism on $[Pt(H_2O)_5(OH)]^{3+}$, fast anation is also difficult to rationalized as such an mechanism is slow as anticipated from anation rates *via* associative activated mechanisms on $[Rh(H_2O)_6]^{3+}$ [41] and $[Ir(H_2O)_6]^{3+}$.[42] The conjugated-base effect therefore does not seem to account successfully for slow H_2O exchange, but relatively fast Cl^- and Br^- anation.

ii-iii)   *Bond strength of the leaving ligand and electrostatic attraction between the entering ligand and metal ion: enhanced anation rate on $[Pt(H_2O)_6]^{4+}$ in terms of Eigen-Wilkins type associations*

An associative activated mechanism for anation on $[Rh(H_2O)_6]^{3+}$ and $[Ir(H_2O)_6]^{3+}$ is favored, mainly due to large contributions from strong M-OH_2 bonds (*ii*) and relative large electrostatic attraction between the metal ion and entering ligand (*iii*). For $[Ru(H_2O)_6]^{2+}$ both these contributing factors are smaller so that dissociative character and activation becomes more important. For $[Pt(H_2O)_6]^{4+}$, contributing factors (*ii*) and (*iii*) are large as a

result of the high 4+ formal charge, and an associative activated intermediate (I_a) seems rational. Kinetic studies on the ligand exchange rate of Ni(H$_2$O)$_6$]$^{2+}$ with various type of ligands L^{x-}, established that the variation in the rate constant mainly depends on the ligand charge x-.[44] It was realized, as stated in a review by Richens:[3] "The interchange of ligands on a complex such as [M(H$_2$O)$_6$]$^{m+}$ takes place within a rapid preformed outer-sphere encounter complex [M(H$_2$O)$_6$]$\cdot$L$^{(m-x)}$, held together by electrostatics". The interchange mechanism I_a, is therefore always associated with a degree of pre-association with any anionic ligand approaching a [M(H$_2$O)$_6$]$^{m+}$ metal centre prior to exchange. Three steps has been identified in this process which is referred to as the Eigen-Wilkins mechanism indicated in reaction 4.11:[45]

$$M^{m+} + L^{x-} \rightleftharpoons M^{\cdot}OH_2^{\cdot}OH_2^{\cdot}L^{(m-x)+} \rightleftharpoons M^{\cdot}OH_2^{\cdot}L^{(m-x)+} \rightleftharpoons ML^{(m-x)+} \qquad (4.11)$$

From this perspective it is possible to distinguish between a dissociative or associative activated complex, since for a dissociative activated mechanism the ligand exchange rate of L^{x-} with the [M(H$_2$O)$_6$]$^{m+}$ metal ion cannot be faster than H$_2$O exchange. For an associative mechanism, the rate can be much slower or faster than H$_2$O exchange. Since ligand exchange on the low-spin t_{2g}^6 [Ru(H$_2$O)$_6$]$^{2+}$ complex takes place *via* an I mechanism[7] compared to a I_a mechanism for the isoelectronic [Rh(H$_2$O)$_6$]$^{3+}$ and [Ir(H$_2$O)$_6$]$^{3+}$ complexes, it was argued by Cusanelli *et al*.[9] that the greater charge on the trivalent complexes seems to be the major driving factor that favors penetration of the entering ligand in forming the transition state.

The charge of both M^{m+} and L^{x-} is thus critical for the I_a mechanism according to Eigen-Wilkins type associations. With regards to ligand exchange on [Pt(H$_2$O)$_6$]$^{4+}$, the quad-valent charged metal ion will favor association with a negatively charged entering ligand such as Cl$^-$ or Br$^-$, forming a [Pt(H$_2$O)$_6$$^{\cdot}$Cl]$^{3+}$ type association prior to Pt–OH$_2$ bond breakage and H$_2$O substitution. The fact that no [Pt(H$_2$O)$_5$Cl]$^{3+}$ is observed in Figure 4.11 is a result of the Cl$^-$ induced *trans* effect, labilizing the *trans* Pt–OH$_2$ bond promoting dissociation of H$_2$O. Since the rate of halide anation cannot be faster than H$_2$O exchange in a dissociative mechanism, the different rates observed for H$_2$O exchange compared to Cl$^-$

and Br^- anation on tentative $[Pt(H_2O)_6]^{4+}$ also supports an associative mechanism. In terms of this argument, an associative interchange (I_a) Eigen-Wilkins type mechanism can account for the slow H_2O exchange rates and much faster Cl^- and Br^- anation rates, on the condition that the fully protonated $[Pt(H_2O)_6]^{4+}$ complex must exist in the solutions studied here ($[HClO_4] \geq {\sim}2.5$ M).

4.4   Conclusions

Three different methods were investigated to obtain the $[Pt(H_2O)_6]^{4+}$ complex. Although precipitation of AgCl drives aquation of $[PtCl_6]^{2-}$, no $[Pt(H_2O)_6]^{4+}$ is formed, only a minor quantity of $[PtCl(H_2O)_5]^{3+}$. The final coordinated chloride could not be removed due to the thermodynamic stability of $[PtCl(H_2O)_5]^{3+}$, and Pt(IV) starts to precipitate if $AgClO_4$ addition is persisted. This method did furnish all the $[PtCl_n(H_2O)_{6-n}]^{4-n}$ ($n = 1\text{-}6$) complexes to allow estimation of the $\delta(^{195}Pt)$ value of $[Pt(H_2O)_6]^{4+}$ in 1 M $HClO_4$ by ^{195}Pt NMR chemical-shift-trend analysis. The direct protonation of coordinated hydroxido ligands of $[Pt(OH)_6]^{2-}$ in strong acidic solution is a potentially favourable method to obtain the $[Pt(H_2O)_6]^{4+}$ complex. A ^{195}Pt NMR titration type experiment indicates an inflection point at ${\sim}2.5$ M $HClO_4$, which implies a countertrend in the downfield shift (observed as a result of electrostatic interaction such as ion-pairing in these strong acidic solutions). Since a protonation reaction is the only factor that contribute towards an up-field shift, the inflection point at ${\sim}2.5$ M $HClO_4$ suggests protonation of $[Pt(OH)(H_2O)_5]^{3+}$ and formation of $[Pt(H_2O)_6]^{4+}$. Oxygen-18 enrichment of the $[Pt(OH)_6]^{2-}$ complex indicates extremely slow H_2O exchange at room temperature, evident from the appearance of $^{16}O/^{18}O$ isotopologues in the ^{195}Pt NMR spectrum. The rate of exchange can be increased by white light so that after 59 h of irradiation, all seven of the $[Pt(^{16}OH)_n(^{18}OH)_{6-n}]^{2-}$ ($n = 0\text{-}6$) isotopologues are observed. Treatment of the $[Pt(^{16}OH)_n(^{18}OH)_{6-n}]^{2-}$ ($n = 0\text{-}6$) solution with concentrated $HClO_4$ (final $[HClO_4] = 5.8$ M) confirmed extremely slow H_2O exchange (coordinated $^{16}O/^{18}O$ ratio change of ${\sim}1$ % during 48 h of acquisition), as anticipated from the t_{2g}^6 electron configuration and related studies on $[Ru(H_2O)_6]^{2+}$, $[Rh(H_2O)_6]^{3+}$ and $[Ir(H_2O)_6]^{3+}$. Oxidation of $[Pt(H_2O)_4]^{2+}$ with both sodium chlorate and sodium bromate in high concentration of perchloric acid (6 M $HClO_4$) also furnishes putative $[Pt(H_2O)_6]^{4+}$,

although significant quantities of $[PtCl(H_2O)_5]^{3+}$ or $[PtBr(H_2O)_5]^{3+}$ (depending on the oxidant) and minor quantities of polynuclear Pt complexes are formed.

The $[Pt(OH)_6]^{2-}$ complex is inert towards substitution with chloride or bromide in water, and no exchange is observed after several hours. In contrast, a $[Pt(OH)_6]^{2-}$ solution treated with 6 M $HClO_4$ results in the relative fast formation of the $[PtCl_n(H_2O)_{6-n}]^{4-n}$ ($n = 0-6$) and $[PtBr_m(H_2O)_{6-m}]^{4-m}$ ($m = 0-6$) complexes when NaCl or NaBr is added to the solution. Slow H_2O exchange and fast Cl^-/Br^- exchange cannot be rationalized in terms of the conjugated-base effect due to $[Pt(H_2O)_5(OH)]^{3+}$. A fast anation rate can be envisaged by the highly charged 4+ complex according to Eigen-Wilkins type associations evident for the I_a mechanism, favouring association of a negatively charged ligand and penetration to the metal ion in activating the transition state.

These results are the first evidence in favour of the existence of $[Pt(H_2O)_6]^{4+}$. Further studies on this topic, especially accurate estimation of the pK_a value of $[Pt(H_2O)_6]^{4+}$ and accurate estimation of rate constants and activation parameters will be fundamental in validating the existence of $[Pt(H_2O)_6]^{4+}$ in the reaction conditions discussed here. Calculation of the activation parameters, especially the activation volume for H_2O exchange on $[Pt(H_2O)_6]^{4+}$ may be challenging, if possible at all, since the apparent extremely slow kinetics necessitates high temperature to realistically measurement the exchange rate. High temperature will also speed-up formation of polynuclear species and precipitation of Pt(IV). Kinetic and mechanistic studies on the Cl^-/Br^- anation of $[Pt(H_2O)_6]^{4+}$ may seem more practical, although such an endeavor will also pose several challenges.

4.5   References

1.   S. F. Lincoln, *Helv. Chim. Acta,* 2005, *88*, 523-545.

2.   L. Helm, A. E. Merbach, *Chem. Rev.,* 2005, *105*, 1923-1959.

3.   D. T. Richens, *Chem. Rev.,* 2005, *105*, 1961-2002.

4.   D. T. Richens, *Chemistry of aqua ions.*, Wiley, Chichester, 1997.

5.   L. Helm, A. E. Merbach, *Coord. Chem. Rev.,* 1999, *187*, 151-181.

6.   L. I. Elding, *Inorg. Chim. Acta,* 1976, *20*, 65-69.

7.   I. Rapaport, L. Helm, A. E. Merbach, P. Bernhard, A. Ludi, *Inorg. Chem.,* 1988, *27*, 873-879.

8.   G. Laurenczy, I. Rapaport, D. Zbinden, A. E. Merbach, *Magn. Reson. Chem.,* 1991, S45.

9.   A. Cusanelli, U. Frey, D. T. Richens, A. E. Merbach, *J. Am. Chem. Soc.,* 1996, *118*, 5265-5271.

10.   L. Z. Tschugajeff, *Z. Anorg. Allg. Chem.,* 1924, *137*,

11.   A. A. Grinberg, V. V. Sibirskaya, *Zh. Neorg. Khim.,* 1967, *12*, 2069-2071.

12.   L. N. Essen, *Inorg. Synth.,* 1974, *15*, 93-96.

13.   V. B. Klein, L. Heck, *Z. Anorg. Allg. Chem.,* 1975, *416*, 269-284.

14.   D. C. Giedt, C. J. Nyman, *Inorg. Synth.,* 1966, *8*, 239-241.

15.   T. M. Gilbert, T. Ziegler, *J. Phys. Chem. A,* 1999, *103*, 7535-7543.

16.   E. Penka Fowe, P. Belser, C. Daul, H. Chermette, *Phys. Chem. Chem. Phys.,* 2005, *7*, 1732-1738.

17.   J. Kramer, K. R. Koch, *Inorg. Chem.,* 2007, *46*, 7466-7476.

18.   A. N. Westra, PhD Thesis, Stellenbosch University., 2005.

19.   S. J. Barton, K. J. Barnham, A. Habtemariam, R. E. Sue, P. J. Sadler, *Inorg. Chim. Acta,* 1998, *273*, 8-13.

20.   C. M. Davidson, R. F. Jameson, *Trans. Faraday Soc,* 1965, *61*, 2462-2467.

21.   S. U. Dunham, E. H. Abbott, *Inorg. Chim. Acta,* 2000, *297*, 72-78.

22.   B. Shelimov, J.-F. Lambert, M. Che, B. Didillon, *J. Am. Chem. Soc.,* 1999, *121*, 545-556.

23.   T. G. Appleton, J. R. Hall, S. F. Ralph, C. S. M. Thompson, *Inorg. Chem.,* 1984, *23*, 3521-3525.

24.   K. Seppelt, *Z. Anorg. Allg. Chem,* 2010, *636*, 2391-2393.

25.   M. Maltese, W. J. Orville-Thomas, *J. Inorg. Nucl. Chem.,* 1967, *29*, 2533-2544.

26.   H. G. Scott, *Acta Crystallogr.,* 1979, *B35*, 3014-3015.

27.   D. Dou, D.-J. Liu, W. B. Williamson, *Appl. Catal., B,* 2001, *30*, 11-24.

28.   B. I. Nabivanets, L. V. Kalabina, L. N. Kudritskaya, *Zh. Neorg. Khim.,* 1971, *16*, 3281-3284.

29.   J. Halperin, H. Taube, *J. Am. Chem. Soc.,* 1952, *74*, 375-380.

30.   J. Halperin, H. Taube, *J. Am. Chem. Soc.,* 1952, *74*, 380-382.

31.   C. H. Langford, H. B. Gray, *Ligand Substitution Processes*, Benjamin: New York, 1965.

32.   J. Burgess, *Metal ions in solution.*, Ellis Horwood Limited, Chichester, UK, 1978.

33.   T. W. Swaddle, *Coord. Chem. Rev.,* 1974, *14*, 217.

34.   O. Groning, T. Drakenberg, L. I. Elding, *Inorg. Chem.,* 1982, *21*, 1820-1824.

35.   K. Swaminathan, G. M. Harris, *J. Am. Chem. Soc.,* 1966, 4411-4414.

36.   F. Basolo, R. G. Pearson, *Mechanisms of Inorganic Reactions*, John Wiley and Son: New York, 1967.

37.   T. J. Conocchioli, G. H. Nancollas, N. Sutin, *Inorg. Chem.,* 1965, *5*, 1-5.

38.   T. W. Kallen, J. E. Earley, *Inorg. Chem.,* 1971, *10*, 1149-1151.

39.   N. Aebischer, G. Laurenczy, A. Ludi, A. E. Merbach, *Inorg. Chem.,* 1993, *32*, 2810-2814.

40.   R. J. Buchacek, G. M. Harris, *Inorg. Chem.,* 2008, *15*, 926-930.

41.   S. C. Galbraith, C. R. Robson, D. T. Richens, *Dalton Trans.,* 2002, 4335-4338.

42.   S. E. Castillo-Blum, A. G. Sykes, H. Gamsjäger, *Polyhedron,* 1987, *6*, 101-103.

43.   D. De Vito, J. Weber, A. E. Merbach, *Inorg. Chem.,* 2008, 858-864.

44.   M. Eigen, R. G. Wilkins, *Adv. Chem. Ser.,* 1965, *49*, 55.

45.   R. G. Wilkins, *Adv. Inorg. Bioinorg. Mech.,* 1983, *2*, 139.

Chapter 5

A ^{195}Pt NMR study of the oxidation of [PtCl$_4$]$^{2-}$, [Pt(CN)$_4$]$^{2-}$ and [Pt(H$_2$O)$_4$]$^{2+}$ with NaClO$_3$, NaBrO$_3$ and H$_2$O$_2$

5 .1   Introduction

Large-scale separation of platinum from other PGMs is dependent, amongst other factors on the efficient oxidation of Pt(II) to Pt(IV). The oxidation states of PGMs in HCl rich process solutions are manipulated to allow separation with modern methods such as gel chromatography, solvent extraction (SX) or ion-exchange methods.[1-5] The solvent-solvent and ion-exchange properties of $[PtCl_6]^{2-}$ for instance, are significantly more favourable than square-planar $[PtCl_4]^{2-}$. Industrial refining/separation of platinum from other precious metals on a large scale is therefore largely dependent on the efficient oxidation of Pt(II). Several studies[6-10] have concluded that the oxidation of square-planar Pt(II) complexes with various oxidants such as $S_2O_8^{2-}$, H_2O_2, MnO_4^-, Cl_2, Br_2 and I_2 yields an octahedral Pt(IV) oxidation product. Chlorate (ClO_3^-) and bromate (BrO_3^-) are strong oxidizing agents and have been used for the oxidation of various inorganic[11-13] complexes. Although the precious metals refining industry makes use of chlorate and bromate as oxidants in the refining of PGMs as shown in various patents,[14-16] there has been no systematic study of the oxidation of Pt(II) square-planar complexes with these oxidants in the literature, and the oxidation kinetics and mechanism of Pt(II) with these oxidants are hitherto unknown. Oxidation of Pt(II) with chlorate from a refining perspective, offers several advantages over the above-mentioned oxidants, since these are either hazardous and/or will introduce unwanted ions into the process stream(s). Preliminary studies have shown that oxidation with bromate increases the oxidation rate of PGMs significantly in acidic solutions, while bromide coordination is minimised by high chloride concentrations in process solutions.

In this chapter, oxidation of $[PtCl_4]^{2-}$ with chlorate and bromate are investigated with ^{195}Pt NMR as a model for other PGMs as may be found in a typical industrial process feed solution. As will be seen, the oxidation mechanism of $[PtCl_4]^{2-}$ with these oxidants are complex and may result in more than 20 different oxidation products! Some aspects of the oxidation mechanism can be concluded from the species distribution after oxidation, for example does oxidation of $[PtCl_4]^{2-}$ yield a Pt(IV) complex with exclusive *trans* stereochemistry, e.g. *trans*-$[PtCl_4(OH)_2]^{2-}$ as concluded previously for oxidation with H_2O_2 in *water*.[17] Although it is reasonable to expect formation of *trans*-$[PtCl_4(H_2O)_2]$ when the

oxidation is carried out in *acidic* solution, initial results indicate formation of all the $[PtCl_n(H_2O)_{6-n}]^{4-n}$ (n = 1-6) species when $[PtCl_4]^{2-}$ is oxidized with H_2O_2 in perchloric acid, contrary to previous findings.[7] The origin of formation of all the $[PtCl_n(H_2O)_{6-n}]^{4-n}$ (n = 1-6) species in *acidic* solution is investigated in a series of experiments. It is illustrated that Pt(II)-Pt(IV) associations accounts for rapid redistribution of the oxidation product(s) and cause formation of the $[PtCl_n(H_2O)_{6-n}]^{4-n}$ (n = 1-6) species in *acidic* solution. Rapid ligand "scrambling" and re-distribution of the oxidation products complicate unravelling of the oxidation mechanism considerably. Oxidation of $[Pt(CN)_4]^{2-}$ was therefore examined with the same oxidants (H_2O_2, ClO_3^- and BrO_3^-) in view of the strong covalent Pt–CN bonds which results in a kinetically inert complex towards ligand exchange and ligand "scrambling" observed in the oxidation of $[PtCl_4]^{2-}$. Cyano ligands coordinated in the square-planar *xy*-plane, are expected to remain bound to Pt(II) and Pt(IV), and may simplify unravelling of the oxidation mechanism by monitoring changes in the *z*-plane. Oxidation of $[Pt(H_2O)_4]^{2+}$ was initially investigated as a means to obtain the elusive $[Pt(H_2O)_6]^{4+}$ complex (*Chapter 4*). Oxidation of $[Pt(H_2O)_4]^{2+}$ is also of interest from a mechanistic point of view as it is not expected to take part in Pt(II)-Pt(IV) associations since H_2O cannot act as the bridging ligand. The labile coordinated water ligands are likely to exchange with chloride or bromide ions in solution, and may reveal properties of the reduced form of ClO_3^- and/or BrO_3^- to assist in the understanding of the oxidation mechanism with these oxidants.

In summary this chapter deals with speciation of the Pt(IV) oxidation products formed in the oxidation of $[PtCl_4]^{2-}$, $[Pt(CN)_4]^{2-}$ and $[Pt(H_2O)_4]^{2+}$ with H_2O_2, $NaClO_3$ and $NaBrO_3$ respectively as studied by ^{195}Pt NMR.

5.2   Experimental

5.2.1   Reagents

The platinum salt potassium tetrachloroplatinate(II) (99.9+ %, K_2PtCl_4, Aldrich) and potassium tetracyanoplatinate(II) (99.9 %, $K_2Pt(CN)_4$, Aldrich) were of reagent grade quality and used without further purification and stored in a desiccator. Tetra-aquaplatinate(II) (*ca.* 0.2 M, $[Pt(H_2O)_4]^{2+}$) solutions were prepared by known methods.[18, 19] Hydrogen peroxide (30% (w/w), H_2O_2, Riedel-de Haën), sodium chlorate (99+ %, Sigma-Aldrich, $NaClO_3$) and sodium bromate (99+ %, Sigma, $NaBrO_3$) were of reagent grade quality and used as is. Perchloric acid (70 % (w/w), $HClO_4$, 1 L = 1.68 kg, MERCK) was used for $HClO_4$ dilutions. Deuterium oxide (99.9 %, D_2O, Aldrich) was used as solvent to obtain a lock signal for all NMR measurements and $Na^{13}CN$ (90 %, Isotec) was used for isotopic enrichment of $[Pt(CN)_4]^{2-}$ solutions. All aqueous solutions were made with ultra pure de-ionised Milli-Q water (MQ > 18 MΩ) and degassed with Ar gas to remove O_2 for at least 1 h prior to use.

5.2.2   Instrumentation

5.2.2.1 ^{195}Pt and ^{13}C NMR spectroscopy

The same ^{195}Pt NMR parameters described in *Chapter 2* were used. ^{195}Pt NMR spectra were recorded at 293 K or 303 K (± 0.1 K) immediately after oxidation and cooling. It typically did not take longer than 30 min. In some cases a correction of ~1 ppm/°C is necessary for comparison of $\delta(^{195}Pt)$ values recorded at different temperature.[20] A line broadening function of 1 Hz was applied to optimize the resolution for $^{35}Cl/^{35}Cl$ isotopic shifts. Where the average $\delta(^{195}Pt)$ value is reported, a line broadening factor of 20 Hz was applied.

^{13}C NMR spectra were recorded at 293 K (± 0.1 K) with a Varian INOVA 600 MHz spectrometer operating at 150 MHz with a 5 mm broad-band probe. Spectra were recorded

at conditions of optimal resolution using an excitation pulse of 2.0 μs, with an acquisition time 1.016 s, and no relaxation delay was applied in order to ensure homogeneous and complete excitation over the full spectral window. Broad band [1]H-decoupling was applied in all measurements. A line-broadening factor of 20 Hz was applied in [195]Pt NMR spectra processing, resulting in an effective line-width at half height.

5.2.2.2 UV-visible spectrophotometry

Preliminary kinetic measurements to study slow reactions (oxidation of $[PtCl_4]^{2-}$ with H_2O_2 and $NaClO_3$) were collected on the integrated ChemStation software on a single beam Agilent 8453E rapid scan UV-visible spectrophotometer (Agilent Technologies). UV-visible spectra were collected between 200-600 nm with 0.5 cm single cell quartz cuvettes, relative to the appropriate solvent at 25°C or 50°C. The solution temperature was regulated with a Julabo heater in a circulating water bath (Julabo LABORTECHNIK GMBH) (± 0.1 °C). Kinetic measurements on fast reactions (oxidation of $[PtCl_4]^{2-}$ with BrO_3^-) were performed on an Applied Photophysics SX 18MV stopped-flow instrument (University of Erlangen-Nürnberg, Germany). Fast reactions at elevated pressure were performed on a laboratory-made high-pressure stopped-flow instrument.[21] The temperature was controlled and maintained in these instruments at 35°C to within ±0.1°C using a circulating water bath (Julabo MP-5).

5.2.2.3 Crystallography and structure refinement

A colourless single crystal was selected and mounted on a thin glass fibre. The data were collected on a Bruker-Nonius SMART Apex diffractometer using graphite monochromatic Mo-Kα radiation (λ = 0.7107 Å). After structural refinement of the crystal data it was found that the crystal is twinned, and a twinned refinement gave two different space groups. The dominant space group was solved in the *P-1* space group and assigned to *trans-*$[Pt(CN)_4(H_2O)_2]^.(18\text{-crown-}6)_2{}^.8H_2O$ with a satisfactory R^2 factor of 3.75 %. A full structural refinement could not be performed on the other space group due to insufficient data points. All non-hydrogen atoms were determined with successive difference Fourier

syntheses and refined by full-matrix least-squares of F^2. The structure was solved using SHELXS-97[22] and refined using SHELXL-97[23] with the aid of the interface program X-SEED.[24] All non-hydrogen atoms were modelled anisotropically at the 50 % probability level, with the hydrogen atoms placed in calculated geometric positions. Two water molecules were found within the crystal lattice, although both positions were severely disordered; no attempt to model these any further was carried out.

5.2.3   Experimental procedure for oxidation of the Pt(II) complexes

5.2.3.1 Oxidation of $[PtCl_4]^{2-}$ by H_2O_2, $NaClO_3$ and $NaBrO_3$

Solutions containing 0.2 M K_2PtCl_4 were prepared in 500 µL water, 1 and 2 M $HClO_4$. Oxidation with H_2O_2 was carried out by adding five mol equivalents of H_2O_2 (30 % v/v) to the $[PtCl_4]^{2-}$ solutions. Oxidation of $[PtCl_4]^{2-}$ by $NaClO_3$ and $NaBrO_3$ were carried out by adding five mol equivalents of the oxidant (with respect to Pt(II)) directly to the Pt(II) solution. Oxidation of a $[PtCl_4]^{2-}$ solution with a mixture of $NaClO_3$ and $NaBrO_3$ were carried out by adding 2.5 mol equivalents of each oxidant directly to the Pt(II) solution. All oxidants were added at room temperature and then heated at 50°C for five min in an oil bath. Oxidation with H_2O_2, $NaClO_3$ and $NaBrO_3$ is evident from the change in solution colour and complete oxidation were confirmed with [195]Pt NMR spectroscopy in the spectral region 200 $\rightarrow$ -1800 ppm which showed no Pt(II) species. [195]Pt NMR data were collected typically 20 min after oxidation and cooling the solutions to the desired temperature.

5.2.3.2 Oxidations of $[Pt(CN)_4]^{2-}$ by H_2O_2, $NaClO_3$ and $NaBrO_3$

Solutions of 0.2 M $[Pt(CN)_4]^{2-}$ were prepared from the $K_2Pt(CN)_4.3H_2O$ salt either in water or 1 M $HClO_4$. Oxidation by H_2O_2 in water was achieved by adding concentrated H_2O_2 (1 mL, 30 % v/v) to the 0.2 M $[Pt(CN)_4]^{2-}$ solution in water to give a 0.0375M Pt(II) solution. The solution was aged for 2 weeks and then preconcentrated to 450 uL *in vacuo* to give a final solution of 0.1 M Pt(II). Oxidation in water is slow and after 2 weeks only *ca.* 30 % of the $[Pt(CN)_4]^{2-}$ was oxidized. White $KClO_4$ precipitates when 0.2 M $[Pt(CN)_4]^{2-}$ is prepared

in 1 M HClO$_4$. The KClO$_4$ was removed with a Millipore filter fitted to a plastic syringe and washed with aliquots of 1 M HClO$_4$. Oxidation with H$_2$O$_2$ in HClO$_4$ is also slow and after 4 days, some [Pt(CN)$_4$]$^{2-}$ is still present in solution. Oxidation of [Pt(CN)$_4$]$^{2-}$ with NaClO$_3$ and NaBrO$_3$ was achieved by adding five mol equivalent of the oxidants (with respect to Pt(II)) directly to the Pt(II) solution respectively. Oxidation with NaClO$_3$ is slow, and even if the solution is heated at 100°C for 1h almost no oxidation is observed. After 'ageing' the solution for seven days at room temperature the ^{195}Pt NMR signal of [Pt(CN)$_4$]$^{2-}$ has disappeared while a white precipitate formed. Oxidation of [Pt(CN)$_4$]$^{2-}$ with NaBrO$_3$ is fast and completed in seconds as evident from a change in the colour of the solution from clear to light brown.

5.2.3.3 Oxidations of [Pt(H$_2$O)$_4$]$^{2+}$ by NaClO$_3$ and NaBrO$_3$

Solutions of 0.2 M [Pt(H$_2$O)$_4$]$^{2+}$ in 1-2 M HClO$_4$ were oxidized by NaClO$_3$ and NaBrO$_3$ respectively with 5 mol equivalent (with respect to Pt(II)) of the oxidant at room temperature. Oxidation with NaClO$_3$ is slow and the [Pt(H$_2$O)$_4$]$^{2+}$ solution was heated to 50°C to increase the oxidation rate. At 50°C oxidation is completed within five minutes as indicated by a change in colour from light yellow to orange. Oxidation with NaBrO$_3$ is fast and completed in seconds as indicated by a change in colour from light yellow to light brown. The [Pt(H$_2$O)$_4$]$^{2+}$ solution was heated and kept at 50°C for five minutes to ensure complete oxidation. Complete oxidation of [Pt(H$_2$O)$_4$]$^{2+}$ was confirmed with ^{195}Pt NMR spectroscopy in the spectral region 1000 → -1000 ppm which showed no evidence of any Pt(II) signals.

5.2.4 Crystallization of [Pt(CN)$_4$(H$_2$O)$_2$]·(18-crown-6)$_2$·6H$_2$O

A 200 μL solution of 0.2 M *trans*-[Pt(CN)$_4$(H$_2$O)$_2$] was prepared by adding 100 μL H$_2$O$_2$ (30 % v/v) to a 0.4 M [Pt(CN)$_4$]$^{2-}$ solution in 1 M HClO$_4$. The solution was "aged" for a week and 10 mol equivalent of 18-crown-6 (with respect to Pt(II)) dissolved in 200 μL water was added to the Pt(II) solution. Small white crystals formed after a few hours. In order to increase the solubility and favour a slow crystallization, 400 μL water and 100 μL

concentrated $HClO_4$ was added to the solution which was stirred for 1 h to re-dissolve the small white crystals that formed. The solution was left in the dark at room temperature to allow slow crystallization. Colourless plates formed in the solution after a few days. These were filtered, dried *in vacuo* and analysed with single crystal X-ray diffraction.

5.3 Results and discussion

5.3.1 ^{195}Pt NMR studies of the oxidation of $[PtCl_4]^{2-}$ by H_2O_2 in water and perchloric acid

From literature it has been suggested that oxidation of $[PtCl_4]^{2-}$ with H_2O_2 in water results in the exclusive formation of the *trans*-$[PtCl_4(OH)_2]^{2-}$ species as inferred from elemental analysis.[25] This oxidation product was later confirmed by ^{195}Pt NMR and H_2^{18}O enrichment which also indicated that coordinated OH^- originate from the H_2O_2 and solvent H_2O respectively which may coordinate in the z-plane *trans* to one another in the resultant *trans*-$[PtCl_4(OH)_2]^{2-}$ species.[17] A kinetic study with UV-visible spectrophotometry of the oxidation of $[PtCl_4]^{2-}$ with H_2O_2 in 1 M $HClO_4$ by Hindmarsh *et al.*[4] reported that the *trans*-$[PtCl_4(H_2O)_2]$ *aqua* complex is formed as the sole oxidation product in *acidic* solution. Since UV-visible spectroscopy does not allow for detailed speciation in such solutions, the reaction was reinvestigated by means of ^{195}Pt NMR.

Solutions of 0.2 M K_2PtCl_4 was freshly prepared in H_2O and 1 M $HClO_4$. When the solution in H_2O is "aged" for one hour at room temperature in ambient light, the species distribution shown in Figure 5.1 is observed. In addition to $[PtCl_4]^{2-}$ (83 %) a large quantity of $[PtCl_3(H_2O)]^-$ (17 %) has formed due to $[PtCl_4]^{2-}$ aquation. Addition of five mol equivalents of H_2O_2 directly to the Pt(II) solution and stirring for five minutes at 50ºC, resulted in complete oxidation evident in the colour change from red-orange to bright yellow. Essentially no Pt(II) remains in solution as established with ^{195}Pt NMR in the spectral window 200 → -1800 ppm.
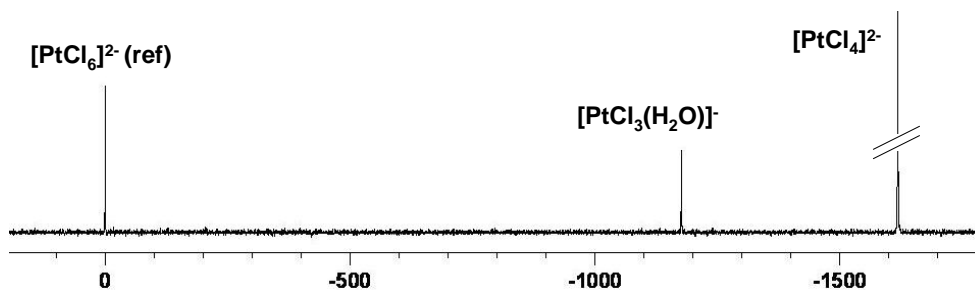
Figure 5.1: [195]Pt NMR spectrum (recorded at 20°C) of a 0.2 M K$_2$PtCl$_4$ solution, 2 h after dissolution in water. The intensity of the [PtCl$_4$]$^{2-}$ peak was adjusted for clarity.

The major oxidation product *trans*-[PtCl$_4$(OH)$_2$]$^{2-}$ is observed at 1232 ppm (Figure 5.2A), and deviates somewhat from the δ([195]Pt) value reported by Dunham *et al.*[17] at 1247 ppm. The small difference in δ([195]Pt) values for this complex may in part be ascribed to the lower temperature at which the [195]Pt NMR spectrum was recorded, and slightly differing reaction conditions, for example, Pt and H$_2$O$_2$ concentration. Assuming the δ([195]Pt) value reported by Dunham *et al.*[17] were recorded at *ca*. 30°C, the δ([195]Pt) at 1232 ppm could be corrected to *ca*. 1240-1244 ppm, given an estimated temperature dependence of (~1 ppm /°C).[20]
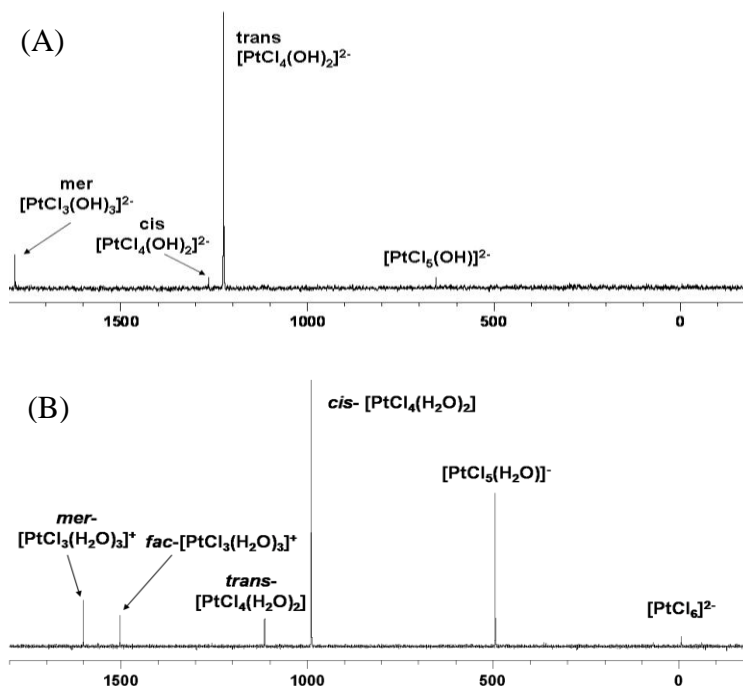
Figure 5.2: (A) The [195]Pt NMR spectrum for the oxidation of 0.2 M [PtCl$_4$]$^{2-}$ with H$_2$O$_2$ in water and **(B)** oxidation of 0.2 M [PtCl$_4$]$^{2-}$ with H$_2$O$_2$ in 1 M HClO$_4$.

In Figure 5.2A some *mer*-$[PtCl_3(OH)_3]^{2-}$ is also observed in the solution which may form *via* concomitant $[PtCl_3(H_2O)]^{2-}$ oxidation. It is significant that the ratio (as percent peak area by integration) of *trans*-$[PtCl_4(OH)_2]^{2-}$ to *mer*-$[PtCl_3(OH)_3]^{2-}$ is 82:14 %, which corresponds well with the Pt(II) ratio of $[PtCl_4]^{2-}$ and $[PtCl_3(H_2O)]^-$ prior to oxidation. Formation of minor concentrations of *cis*-$[PtCl_4(OH)_2]^{2-}$ (2 %) and $[PtCl_5(OH)]^{2-}$ (2 %), probably due to aquation and anation reactions after oxidation is feasible under the reaction conditions used (mixing for five minutes at 50°C).

It is evident that oxidation of $[PtCl_4]^{2-}$ with H_2O_2 in H_2O results in the same major species reported previously.[17, 25] When the oxidation by H_2O_2 is carried out in 1 M $HClO_4$, a completely different species distribution is obtained, resulting in several $[PtCl_n(H_2O)_{6-n}]^{4-n}$ (n = 2–6) *aqua* species (Figure 5.2B). The assignment of complexes in Figure 5.2B was confirmed from the $\delta(^{195}Pt)$ values and least-squares analysis of the isotopologue/isotopomer signals as discussed in *Chapter 2* and *3*. This speciation was unexpected in the light of a previous report, suggesting that only the *trans*-$[PtCl_4(H_2O)_2]$ species is formed.[7] From Figure 5.2B it is clear that only relatively low concentration of *trans*-$[PtCl_4(H_2O)_2]$ is present in the solution (at the time of ^{195}Pt NMR analysis which was ~25 min after oxidation) and that the major species formed are *cis*-$[PtCl_4(H_2O)_2]$ and $[PtCl_5(H_2O)]^-$ in these reaction conditions. To explain the differing species distributions obtained from the oxidation of 0.2 M K_2PtCl_4 with H_2O_2 in the *water* (Figure 5.2A) and *acid* (Figure 5.2B), factors such as 1) perchlorate as possible oxidant; 2) redistribution of Pt(IV) complexes in acidic solution; and 3) Pt(II) assisted ligand exchange mechanisms were considered.

5.3.1.1 Perchlorate as possible oxidant

Given the possibility that the perchlorate anion (ClO_4^-) may act as oxidant, oxidation of 0.2 M $[PtCl_4]^{2-}$ by five mol equivalents H_2O_2 (with respect to Pt(II)) was examined in 2 M $NaClO_4$ (Figure 5.3A); 1.5 M $NaClO_4$ and 0.5 M $HClO_4$ (Figure 5.3B); and 1M trifluoromethanesulfonic acid (Figure 5.3C). Trifluoromethanesulfonic acid (TfOH) is

thermally and chemically stable, and its conjugate base $CF_3SO_3^-$ (triflate) is weakly or non-coordinating, and resists oxidation/reduction reactions.[26]
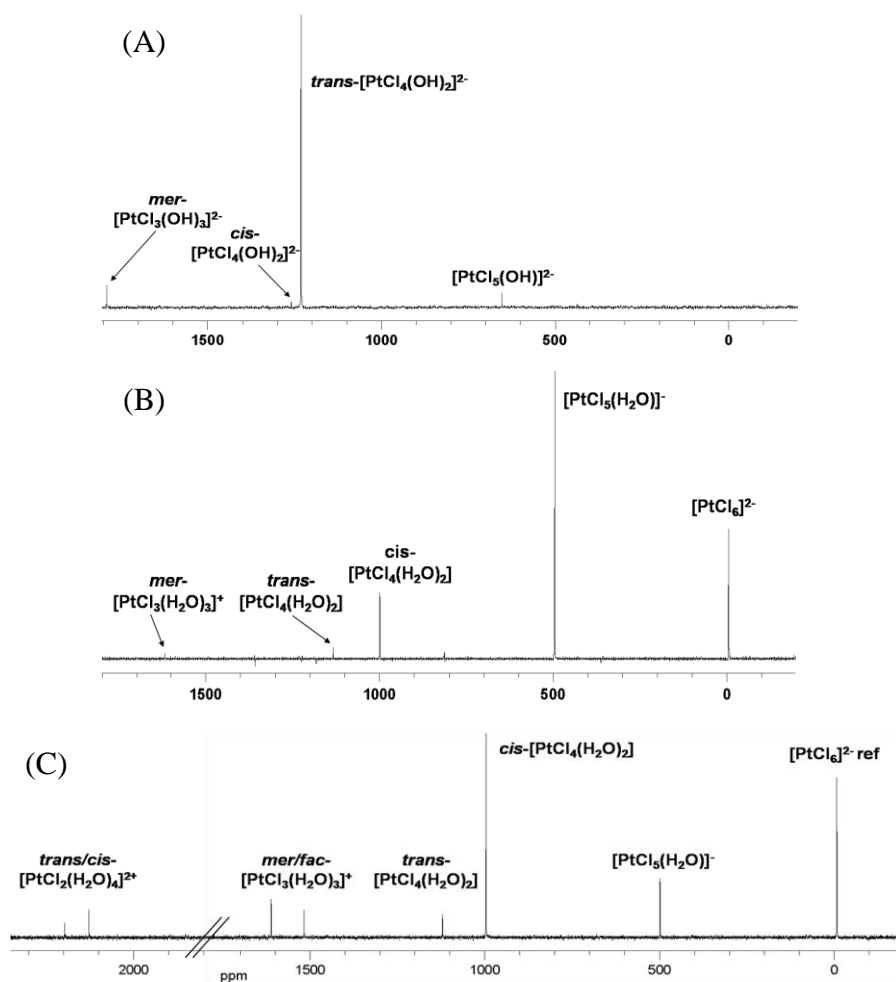
Figure 5.3: 0.2 M K_2PtCl_4 dissolved in **(A)** 2 M $NaClO_4$; **(B)** 1.5 M $NaClO_4$ and 0.5 M $HClO_4$; **(C)** 1 M TfOH and oxidized with five mol equivalents H_2O_2 at 50°C.

There is no qualitative difference in the ^{195}Pt NMR spectra between Figure 5.2A and 5.3A. The *hydroxido* species *trans*-$[PtCl_4(OH)_2]^{2-}$ and *mer*-$[PtCl_3(OH)_3]^{2-}$ are the major oxidation products in both water and 2 M $NaClO_4$, with the *trans*-$[PtCl_4(OH)_2]^{2-}$ species being clearly dominant. The oxidation carried out in an acidic solution (Figure 5.3B; 1.5 M $NaClO_4$ and 0.5 M $HClO_4$), results in the formation of relatively high concentrations of $[PtCl_5(H_2O)]^-$, $[PtCl_6]^{2-}$ and *cis*-$[PtCl_4(H_2O)_2]$, and the oxidation products show a better correlation with that obtained from oxidation of $[PtCl_4]^{2-}$ in 1 M $HClO_4$ (Figure 5.2B) with the exception of the presence of a detectable amount of *fac*-$[PtCl_3(H_2O)_3]^+$ in 1 M $HClO_4$. The concentration

ratio of chloride deficient species $[PtCl_n(H_2O)_{6-n}]^{4-n}$ (n = 2-3), compared to chlorido rich $[PtCl_n(H_2O)_{6-n}]^{4-n}$ (n = 5-6) species is 1:99 % (Figure 5.3B; determined by peak integration), suggesting a re-distribution of the oxidation products to the presumably thermodynamically favoured chlorido rich $[PtCl_n(H_2O)_{6-n}]^{4-n}$ (n = 5-6) products. Since the total Cl^- concentration must clearly be related to the initial $[PtCl_4]^{2-}$ concentration, the possibility of ClO_4^- reduction leading to an increase in Cl^- concentration was considered. Although the ClO_4^- anion is used as a supporting electrolyte in many kinetic and thermodynamic reaction studies, the perchlorate ion is known to be strongly oxidative in acidic media particularly at elevated temperatures and high concentration. Perchlorate reduction may therefore possibly lead to increased Cl^- ion concentration in solution as by-products of ClO_4^- reduction.[27, 28] To examine this possibility, oxidation of $[PtCl_4]^{2-}$ was carried out in trifluoromethanesulfonic acid. Figure 5.3C shows that the corresponding oxidation of 0.2 M K_2PtCl_4 by H_2O_2 in 1 M TfOH results in a qualitatively similar distribution of Pt(IV) species as shown in Figure 5.2B. The ratio of integrated peak areas in the ^{195}Pt NMR spectrum shown in Figure 5.3C of the $[PtCl_n(H_2O)_{6-n}]^{4-n}$ (n = 2-3) species relative to the $[PtCl_n(H_2O)_{6-n}]^{4-n}$ (n = 5-6) species is 55:45 %, as a result of the dominance of cis-$[PtCl_2(H_2O)_4]^{2+}$ under these conditions. It is thus reasonable to conclude that ClO_4^- is unlikely to participate significantly in oxidation in these solutions, and that the variable distribution of species from a quantitative point of view is the result of relatively rapid ligand scrambling reactions during or after the oxidation reactions in the two different acid solutions. The distribution of Pt(IV) oxidation products does not change significantly during the acquisition of the ^{195}Pt NMR spectrum (*ca.* 1 h) since the ^{195}Pt NMR spectra of these solutions obtained after re-acquisition several hours later are very similar. Nevertheless, it is clear that oxidation of $[PtCl_4]^{2-}$ by H_2O_2 in acidic solution do not form a single species as assumed in a previous study,[7] which is largely the case for the oxidation of $[PtCl_4]^{2-}$ by H_2O_2 in water.[17, 25]

5.3.1.2 Redistribution of Pt(IV) complexes in acidic solution

It was considered that analogous to the formation of $trans$-$[PtCl_4(OH)_2]^{2-}$ in the oxidation of $[PtCl_4]^{2-}$ with H_2O_2 in *water*, $trans$-$[PtCl_4(H_2O)_2]$ is formed in *acid*, but subsequently

converts to thermodynamic more stable Pt(IV) species. To illustrate the stability of this possible oxidation product, authentic *trans*-$K_2[PtCl_4(OH)_2]$ was prepared by oxidation of K_2PtCl_4 with 30 % H_2O_2 followed by precipitation of the complex as a pinkish salt with ethanol according to the literature method.[25] The ^{195}Pt NMR spectrum of this salt dissolved in water shows a single peak at $\delta(^{195}Pt) = 1241$ ppm, corresponding to *trans*-$[PtCl_4(OH)_2]^{2-}$ (Figure 5.4A). No Pt(II) species were observed with ^{195}Pt NMR in this solution. The *trans*-$[PtCl_4(OH)_2]^{2-}$ complex is kinetically stable and it persists for several hours at room temperature as the only species, even after keeping the solution at 50ºC for 10 minutes.
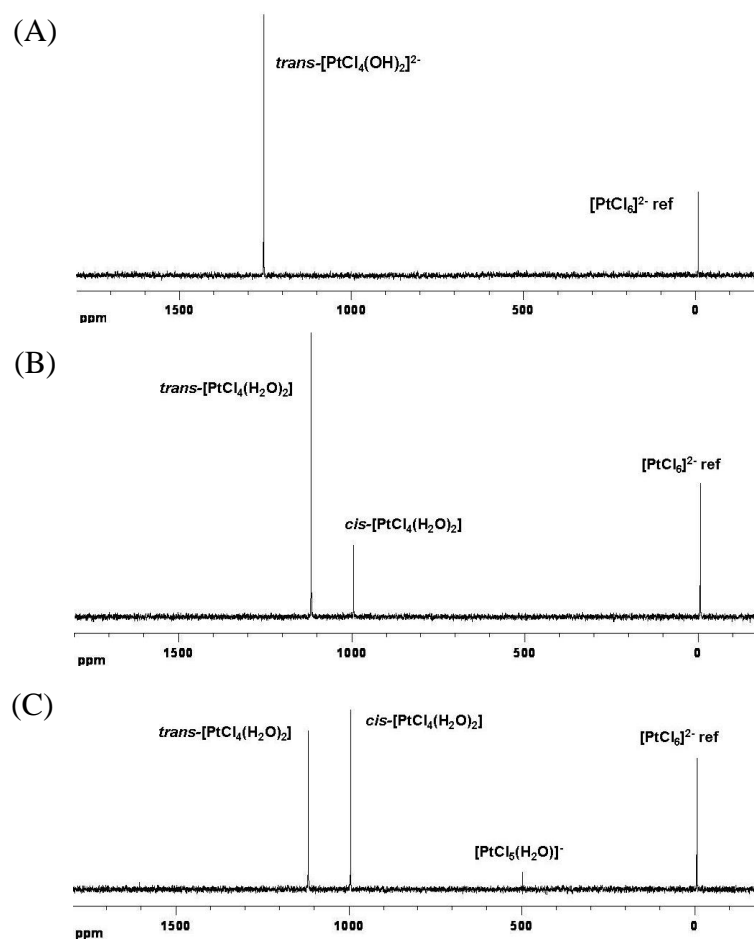
Figure 5.4: (A) ^{195}Pt NMR spectrum of 0.1 M *trans*-$K_2[PtCl_4(OH)_2]$ dissolved in water. **(B)** Addition of $HClO_4$ (final $[H^+] \approx 1.27$ M) to 0.1 M *trans*-$[PtCl_4(OH)_2]^{2-}$. **(C)** After heating the solution for 10 min at 50 ºC.

Addition of concentrated $HClO_4$ (70 % w/w) directly to such a orange coloured solution containing 0.1 M *trans*-$[PtCl_4(OH)_2]^{2-}$ to obtain ~1.3 M $HClO_4$, results in a white precipitate ($KClO_4$) which was removed from solution by filtration, while the colour of the

solution did not change perceptibly. The [195]Pt NMR spectrum of the solution indicates that in addition to the *trans*-[PtCl$_4$(H$_2$O)$_2$] *aqua* complex (δ^{195}Pt = 1117 ppm, 82 %) a peak clearly assigned to *cis*-[PtCl$_4$(H$_2$O)$_2$] (δ^{195}Pt = 993 ppm, 18 %) is present (Figure 5.4B). Heating this solution for 10 minutes at 50ºC shows a clear conversion of *trans*-[PtCl$_4$(H$_2$O)$_2$] to *cis*-[PtCl$_4$(H$_2$O)$_2$] (Figure 5.4C) which becomes the dominant complex, (48 %) in addition to the formation of small quantities of [PtCl$_5$(H$_2$O)]$^-$ (5 %). The conversion of Pt(IV) species essentially illustrates redistribution of *trans*-[PtCl$_4$(H$_2$O)$_2$] to thermodynamic more stable species over time. This observation is in contrast with a report that states only *trans*-[PtCl$_4$(H$_2$O)$_2$] is obtained when *trans*-[PtCl$_4$(OH)$_2$]$^{2-}$ is treated with acid.[29] It is thus clear that the understanding of the distribution of species in acidic solutions is significantly complicated by ligand exchange reactions of Pt(IV) complexes under these conditions, something not observed in neutral to alkaline solutions, in view of the kinetically inert nature of Pt(IV) *hydroxido* complexes.

5.3.1.3 Redistribution of Pt(IV) complexes in acidic solution in the presence of Pt(II): [PtCl$_4$]$^{2-}$ assisted ligand exchange mechanisms

Rapid Pt(II)-Pt(IV) associations resulting in ligand scrambling,[29-31] complicates unravelling of the oxidation mechanism considerably in acidic solutions as relevant here. Such associations may rapidly increase ligand exchange rates of Pt(IV) complexes especially in the presence of high Pt(II) concentration.[30] The presence of [PtCl$_4$]$^{2-}$ in solution undergoing oxidation reactions may result in higher rates of ligand exchange by association reactions between Pt(IV) and Pt(II) in the solutions studied here. To explore such possibilities the [195]Pt NMR spectrum of a mixture containing 0.02 M [PtCl$_4$]$^{2-}$ and 0.2 M *trans*-[PtCl$_4$(OH)$_2$]$^{2-}$ in water is shown in Figure 5.5A. Two peaks assigned to *trans*-[PtCl$_4$(OH)$_2$]$^{2-}$ and [PtCl$_4$]$^{2-}$ (in addition to a [PtCl$_6$]$^{2-}$ reference peak in the external capillary) is observed in Figure 5.5A. No additional Pt(IV) species is observed in the solution if aged overnight at room temperature or heated to 50ºC for 10 minutes; the only other species observed in solution are [PtCl$_3$(OH)]$^{2-}$ due to [PtCl$_4$]$^{2-}$ hydrolysis. Evidently in a fresh solution of the mixture, [PtCl$_4$]$^{2-}$ does not appear to enhance ligand exchange of *trans*-[PtCl$_4$(OH)$_2$]$^{2-}$ at a pH ~ 7-8. Presumably the two *trans* hydroxido ligands in *trans*-[PtCl$_4$(OH)$_2$]$^{2-}$ are poor "bridging" ligands resulting in little or no Pt(II)-Pt(IV) association

of $[PtCl_4]^{2-}$ with *trans*-$[PtCl_4(OH)_2]^{2-}$ as envisaged by Mason.[30] The high kinetic inertness of hydroxido ligands bound to Pt(IV) may also play a role resulting in negligible ligand exchange in the time frame of the oxidation and NMR experiments in non-acidic solution. Essentially the *trans*-$[PtCl_4(OH)_2]^{2-}$ complex under these conditions is quite un-reactive.
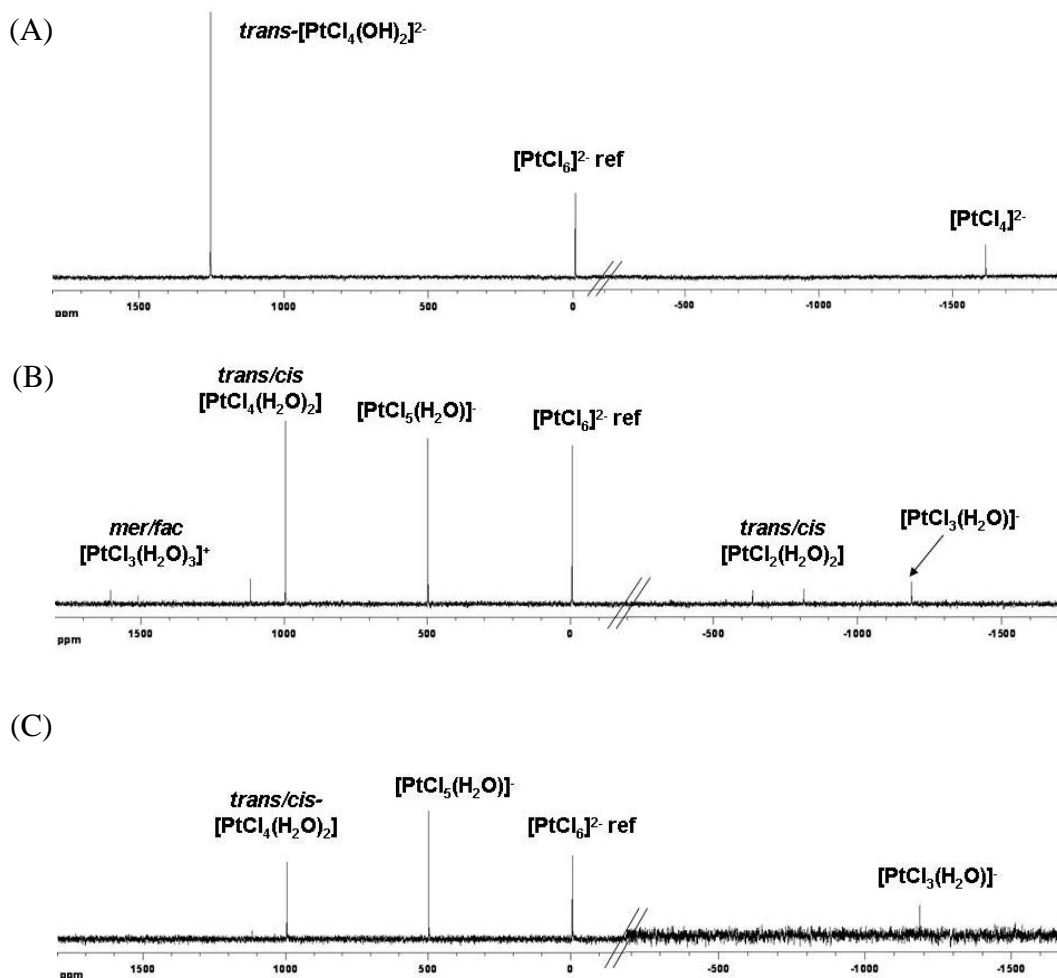
Figure 5.5: (A) ^{195}Pt NMR spectrum obtained from addition of 0.02 M K_2PtCl_4 to 0.2 M *trans*-$[PtCl_4(OH)_2]^{2-}$ in water. **(B)** Protonation ($[H^+] \approx 1.27M$) of an aqueous solution of 0.2 M *trans*-$[PtCl_4(OH)_2]^{2-}$ and 0.02 M $[PtCl_4]^{2-}$ (solution A). **(C)** Addition of 0.02 M $[PtCl_4]^{2-}$ to solution (B).

Treating the 0.02 M $[PtCl_4]^{2-}$ and 0.2 M *trans*-$[PtCl_4(OH)_2]^{2-}$ mixture (solution shown in Figure 5.5A) with a small amount of concentrated $HClO_4$ (final $[HClO_4] \approx 1.3$ M) results in an immediate colour change from orange to bright yellow, and yields the ^{195}Pt NMR spectrum shown in Figure 5.5B. Evidently rapid re-distribution of the Pt(IV) and Pt(II) species takes place, resulting in a species distribution of Pt(IV) complexes very similar to

that obtained in the oxidation of $[PtCl_4]^{2-}$ with H_2O_2 in acidic solution (Figure 5.2B). The rapid redistribution of *trans*-$[PtCl_4(OH)_2]^{2-}$ is only observed in the presence of $[PtCl_4]^{2-}$ and *acidic* solution. Notably, the ^{195}Pt NMR spectrum (Figure 5.5B) reveals the presence of Pt(II) species $[PtCl_3(H_2O)]^-$, *trans*- and *cis*-$[PtCl_2(H_2O)_2]$ in the spectral range -200 $\rightarrow$ -1850 ppm. The relationship between Pt(IV) and Pt(II) is further demonstrated by adding an additional portion of 0.02 M $[PtCl_4]^{2-}$ to the solution in Figure 5.5B. The Pt(IV) species distribution quickly changes again to that shown in Figure 5.5C, while no $[PtCl_4]^{2-}$ is observed, being converted to $[PtCl_3(H_2O)]^-$.

Based on these experiments, it is concluded that oxidation of $[PtCl_4]^{2-}$ with H_2O_2 results in the formation of *trans*-$[PtCl_4(H_2O)_2]$ in acidic solution. The *trans*-$[PtCl_4(H_2O)_2]$ species is then redistributed between the $[PtCl_n(H_2O)_{6-n}]^{4-n}$ (*n* = 2-6) species, *via* rapid ligand exchange reactions assisted by Pt(II)-Pt(IV) associations. Since, the Pt(II) concentration constantly changes during oxidation, the extend of species redistribution reactions assisted by Pt(II)-Pt(IV) will also change as the oxidation reaction progress. Unravelling the oxidation mechanism and calculation of rate limiting parameters in these reaction conditions will be tricky, if practical at all. For this reason a kinetic study was carried out in hydrochloric acid as will be discussed in *Chapter 6*.

5.3.2 Oxidation of $[PtCl_4]^{2-}$ by sodium chlorate and sodium bromate as studied by ^{195}Pt NMR

5.3.2.1 Oxidation of $[PtCl_4]^{2-}$ by sodium chlorate

As previously mentioned, there is almost no available literature that deals with the mechanistic aspects of oxidation of the PGMs with chlorate. In a preliminary experiment, 1 mM $[PtCl_4]^{2-}$ was oxidized with 150 mM ClO_3^- and 40 mM BrO_3^- respectively in 1 M $HClO_4$. The relative rates of $[PtCl_4]^{2-}$ oxidation with chlorate and bromate differs by several orders of magnitude as measured by UV-visible spectroscopy. Oxidation with chlorate is slow (> 3000 s at 35°C) while oxidation with bromate is fast (< 1.5 s at 35°C) as shown in Figure 5.6A and B.

(A)

(B)
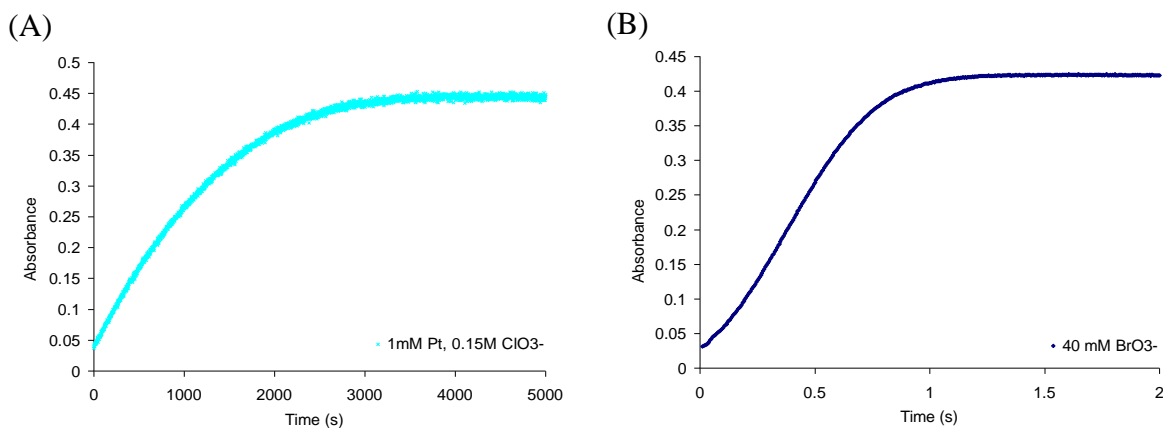
Figure 5.6: UV-visible absorbance change (261 nm) as a function of time for the oxidation of **(A)** 1 mM $[PtCl_4]^{2-}$ with excess ClO_3^- (150 mM) and **(B)** excess BrO_3^- (40 mM) in 1 M $HClO_4$ at 35ºC.

For the purpose of ^{195}Pt NMR analysis, a much higher $[PtCl_4]^{2-}$ concentration is required. Five mol equivalents of $NaClO_3$ (with respect to Pt(II)) was added directly to 0.2 M K_2PtCl_4 in 1 M $HClO_4$. To speed-up the oxidation rate, the solution was stirred at 50°C for five minutes. Oxidation is accompanied by a colour change from red to bright yellow, while a pungent chlorine-like smell is generated at the same time. The ^{195}Pt NMR spectrum of the oxidized solution is shown in Figure 5.7.
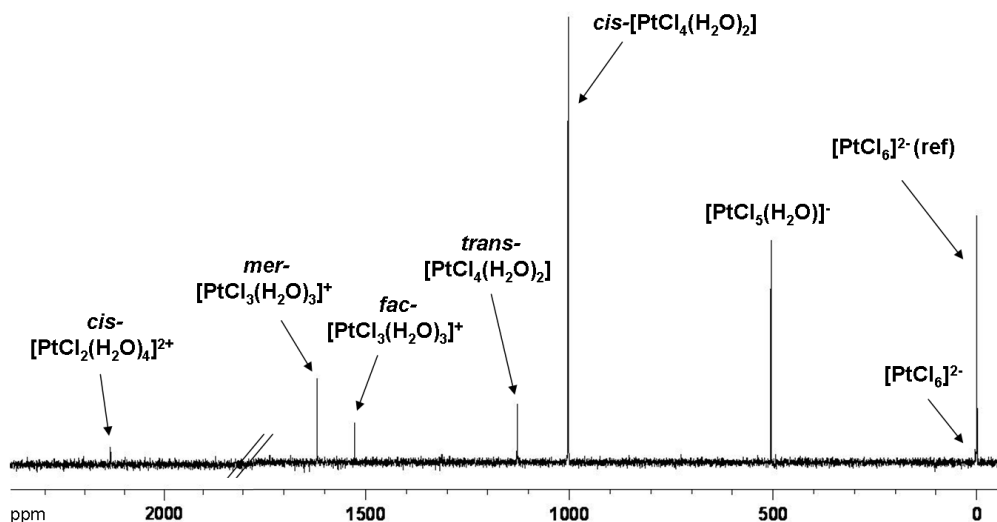
Figure 5.7: ^{195}Pt NMR spectrum (collected at 30°C) of 0.2 M K_2PtCl_4 dissolved in 1 M $HClO_4$ and oxidized with five mol equivalents of $NaClO_3$. The solution was kept at 50°C for five minutes to speed up oxidation.

Oxidation of $[PtCl_4]^{2-}$ with $NaClO_3$ results in the same $\delta(^{195}Pt)$ values obtained from oxidation of $[PtCl_4]^{2-}$ with H_2O_2 (Figure 5.2B), and is assigned to the $[PtCl_n(H_2O)_{6-n}]^{4-n}$ ($n =$

2-6) species. The species intensities are very similar in Figure 5.7 and 5.2B, with the concentration of $[PtCl_5(H_2O)]^-$ and $[PtCl_6]^{2-}$ slightly more abundant in the oxidation with $NaClO_3$, possibly due to ClO_3^- reduction which results in Cl^- formation. The ClO_3^- ion is a six electron oxidant and can be reduced completely in consecutive steps according to the overall reaction $3Pt^{2+} + ClO_3^- + 6H^+ \rightleftharpoons 3Pt^{4+} + Cl^- + 3H_2O$. The higher Cl^- concentration possibly results in a ligand redistribution of the oxidation products to the presumably thermodynamic more stable species such as $[PtCl_5(H_2O)]^-$ and $[PtCl_6]^{2-}$. Alternatively, reduction of ClO_3^-, may form ClO_2^-, ClO^- and Cl_2 or other oxidation states of chlorine which may directly coordinate to Pt(II) in oxidation reactions.

Oxidation of Pt(II) with H_2O_2, [17] $[MnO_4]^-$ [32] and HClO [33] result in an oxygen atom being transferred to the oxidized Pt(IV) product. Experiments by Halperin & Taube[34] involving [18]O tracers have shown that SO_3^- is oxidized by ClO_3^- *via* an ^-O_3S--O–ClO_2^- intermediate. In these experiments it was confirmed that oxygen atoms always coordinated to SO_3^- in the stepwise reduction of $ClO_3^- \rightarrow ClO_2^- \rightarrow ClO^- \rightarrow Cl^-$, except for oxidation with ClO^-, since bond formation may take place *via* either Cl or O. The major oxidation product of $[PtCl_4]^{2-}$ with ClO_3^- prior to ligand scrambling is thus likely to be *trans*-$[PtCl_4(H_2O)_2]$. Similar speciation of the oxidation products from oxidation with ClO_3^- and H_2O_2 in 1 M $HClO_4$ supports this view.

5.3.2.2 Oxidation of $[PtCl_4]^{2-}$ by sodium bromate

Complete oxidation of 0.2 M $[PtCl_4]^{2-}$ in 1 M $HClO_4$ was achieved by adding five mol equivalents of $NaBrO_3$ (with respect to Pt(II)) directly to the Pt(II) solution at room temperature. Oxidation is fast and completed within seconds indicated by the colour change from red to dark yellow-brown while bromine like fumes is generated. The solution kept at 50°C for an additional five minutes to ensure similar reaction conditions used for oxidation with chlorate. The [195]Pt NMR spectrum of the oxidized solution is shown in Figure 5.8.
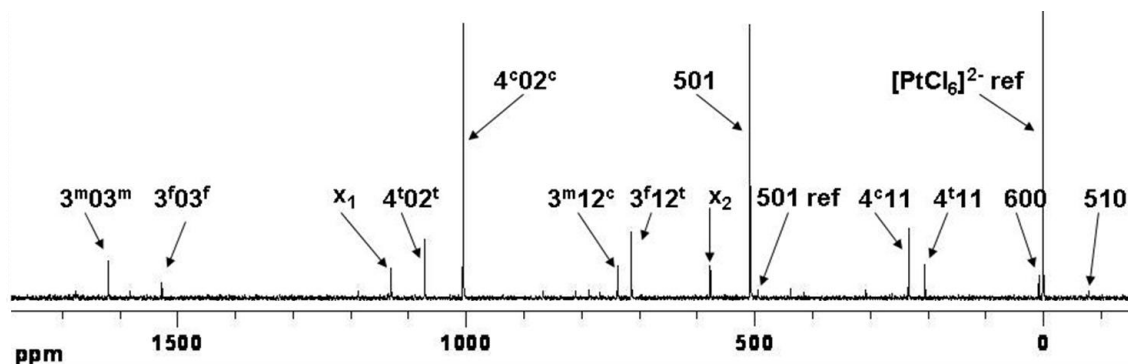
Figure 5.8: ^{195}Pt NMR spectrum (collected at 30°C) of 0.2 M [PtCl$_4$]$^{2-}$ oxidized with NaBrO$_3$ at room temperature. The solution was kept at 50°C for an additional five minutes. The nomenclature code is adopted from Drew and Preetz[18] for better clarity, where the 1st digit = no. coordinated Cl$^-$, 2nd = no. Br$^-$, 3rd = no. H$_2$O, c = *cis* and t = *trans*.

More than 20 different signals can be identified although some of these are present in very low concentration. Chemical-shift-trend analysis (*Chapter 2*) and isotopic effects (*Chapter 3*) were utilized to assist in assigning most of the major species present in the solution. The major oxidation products are once again *cis*-[PtCl$_4$(H$_2$O)$_2$] and [PtCl$_5$(H$_2$O)]$^-$, while the species present at low concentration are assigned to other Pt(IV)-aqua-chlorido or Pt(IV)-aqua-bromido-chlorido species as shown in Figure 5.8. Signals labelled x$_1$ and x$_2$ could not be assigned at this stage with certainty. The low concentration of the *trans*-[PtCl$_4$Br(H$_2$O)]$^-$ species in the solution (4^{t}11) and formation of same major species observed in the oxidation with ClO$_3^-$ support the idea that XO$_3^-$ (X = Cl, Br) binds [PtCl$_4$]$^{2-}$ *via* oxygen in the transition state to form the *trans*-[PtCl$_4$(H$_2$O)$_2$] species initially. It is reasonable to expect that Pt(II)-Pt(IV) assisted ligand exchange mechanisms causes a similar redistribution of *trans*-[PtCl$_4$(H$_2$O)$_2$] species to result in a final speciation similar for chlorate oxidation. The formation of mixed Pt(IV)-aqua-bromido-chlorido species must originate from BrO$_3^-$ since the latter is the only source of bromide ions. It is uncertain whether these species originate from BrO$^-$ (or HBrO) oxidation (*via* bromide coordination), Br$_2$ oxidation or simply Br$^-$ anation. Although Pt(IV) bromide anation is generally regarded to be slow, it has been established that the rate of anation can be greatly increase in the presence of Pt(II).[33, 35]

These results suggests that *trans*-$[PtCl_4(H_2O)_2]$ is most likely to be the major oxidation product when $[PtCl_4]^{2-}$ is oxidized with H_2O_2, ClO_3^- and BrO_3^- respectively in 1 M $HClO_4$. The *trans*-$[PtCl_4(H_2O)_2]$ species is subsequently rapidly converted by Pt(II)-Pt(IV) associations into the various $[PtCl_n(H_2O)_{6-n}]^{4-n}$ (*n* = 2-6) or $[PtCl_nBr_m(H_2O)_{6-n-m}]^{4-n-m}$ (*n*, *m* = 2-6) species. The mechanism by which these associations take place is not clear, although isomerization to the thermodynamic more stable *cis*-$[PtCl_4(H_2O)_2]$ and consequent rapid ligand exchange reactions as envisaged by Mason[30] seems to play an important role. The oxidation mechanism of chlorate and bromate is complicated by the reduced forms of the oxidants and the many possible secondary reactions which may be important.

Since oxidation of $[PtCl_4]^{2-}$ in acidic solution always appear to involve Pt(II)-Pt(IV) associations, it was of interest to investigate the oxidation of a Pt(II) complex which are not susceptible to Pt(II)-Pt(IV) associations. Such a complex should be coordinated to ligands which are unable to act as a bridging ligand (such as $-NH_3$ and $-OH_2$) or consist of strong Pt–L bonds (such as $-NH_3$ and $-CN$), so that bond breakage is not kinetically favoured. Due to ^{195}Pt NMR peak broadening of $[Pt(NH_3)_4]^{2+}$ as a result of ^{14}N quadrupolar relaxation under normal conditions, oxidation of $[Pt(CN)_4]^{2-}$ and $[Pt(H_2O)_4]^{2+}$ were investigated for comparison by H_2O_2, ClO_3^- and BrO_3^-.

5.3.3   Oxidation of tetracyanoplatinate(II) by hydrogen peroxide, sodium chlorate and sodium bromate as studied by ^{195}Pt NMR

Oxidation of $[Pt(CN)_4]^{2-}$ was studied with various oxidants including H_2O_2,[36] ICN,[37] Cl_2,[8] Br_2,[10] I_2,[38] HOCl,[8] and OBr^-[39] amongst others, but not with ClO_3^- and BrO_3^-. The mechanism of oxidation postulated for these reactions are consistent with a *trans* oxidative addition mechanism. Various $[Pt(CN)_4]^{2-}$ oxidation studies were carried out with UV-visible spectrophotometry, but speciation of the oxidation products largely remains unknown from a ^{195}Pt NMR perspective. In this regard no $\delta(^{195}Pt)$ values of any Pt(II) or Pt(IV)-aqua-cyano species are reported in the literature. Since UV-visible spectrophotometry does not allow for detailed speciation, ^{195}Pt NMR is an excellent tool to study the oxidation products. Isotopic effects due to $^{12}C/^{13}C$ were noticed in preliminary ^{195}Pt NMR spectra of the $[Pt(CN)_4]^{2-}$ complex. These effects were seen as an opportunity to

assist in the assignment of Pt(II) and/or Pt(IV) species and is briefly discussed before oxidation of $[Pt(CN)_4]^{2-}$ with H_2O_2, ClO_3^- and BrO_3^- are investigated.

5.3.3.1 Isotopic effects due to natural occurring $^{12}C/^{13}C$ isotopes of tetracyano palatinate(IV) as observed with ^{195}Pt NMR

The proton decoupled ^{13}C NMR spectrum of a 0.2 M $[Pt(CN)_4]^{2-}$ solution prepared in water (from the $K_2[Pt(CN)_4]\cdot3H_2O$ salt), is shown in Figure 5.9A. A ^{13}C signal is observed at 125 ppm, centred between two smaller signals each separated by 515 Hz. The splitting is caused by indirect dipolar coupling (^1J coupling) between the ^{13}C and ^{195}Pt isotopes and give integration values of 0.17 : 0.66 : 0.17 which conforms with the 33.8 % abundance of the ^{195}Pt isotope. The ^{13}C spectrum and $^1J\{^{13}C\text{-}^{195}Pt\}$ coupling value closely resembles that of $[Pt(CN)_4]^{2-}$ reported by Ding.[40]

(A)   (B)
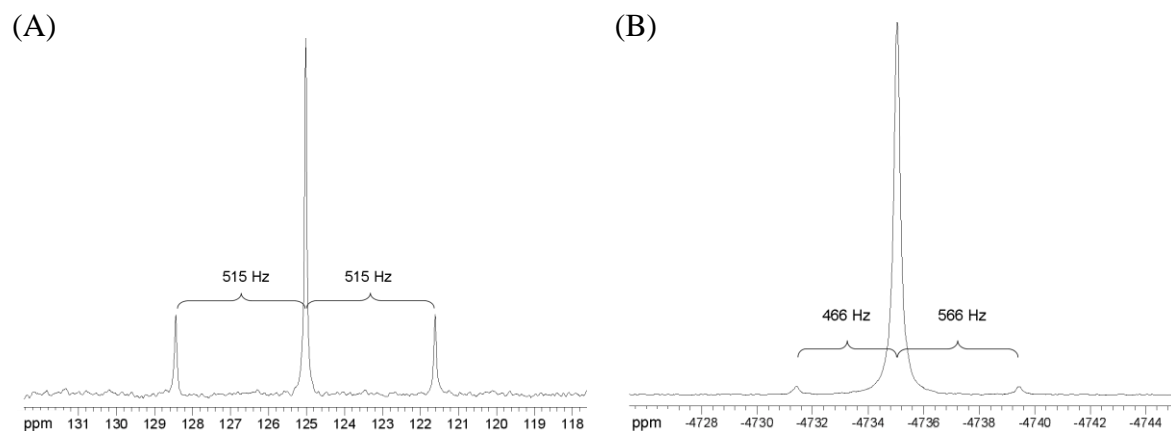
Figure 5.9: (A) $^{13}C\{^1H\}$ NMR spectrum (20°C) of 0.2 M $K_2[Pt(CN)_4]$ in water. **(B)** The ^{195}Pt NMR spectrum of the same solution in (A).

A ^{195}Pt NMR signal is observed at -4735 ppm (Figure 5.9B; 20°C) and is in excellent agreement with the value of -4713 ppm reported by Pesek and Mason[41] (at 40°C) if an adjustment is made for the temperature gradient (~1 ppm/°C is assumed[20]). Two small signals not previously reported are observed either side of the major ^{195}Pt signal. These two signals cannot be the result of ^1J coupling as it resonates 466 and 566 Hz respectively from the major signal. Since the natural abundance of ^{13}C is 1.11%, it may be possible that the small ^{195}Pt signals could originate from the $[Pt(^{12}CN)_3(^{13}CN)]^{2-}$ isotopologue, which is split into a doublet due to $^1J\{^{195}Pt\text{-}^{13}C\}$ coupling. This idea was explored further, by adding four

mol equivalents of Na^{13}CN (with respect to Pt(II)) to the [Pt(CN)$_4$]$^{2-}$ solution. Immediately after Na^{13}CN was added, the two small signals increased to almost the same concentration as the major signal. In addition, seven new signals appeared. Another three mol equivalents Na^{13}CN was added to the solution which resulted in a redistribution of the signal intensity, while an additional eight ^{195}Pt signals appeared as shown in Figure 5.10.
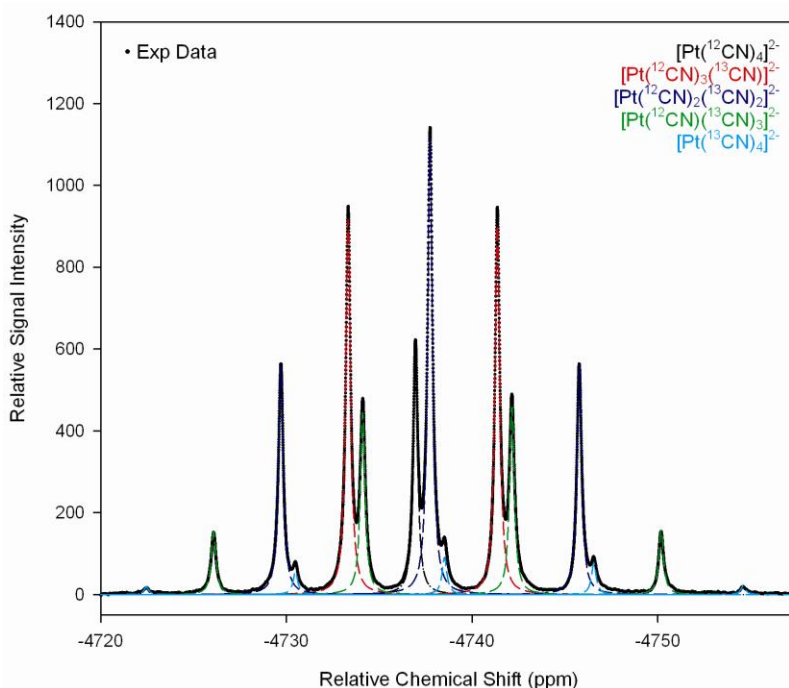
Figure 5.10: ^{195}Pt NMR spectrum of the [Pt(^{12}CN)$_n$(CN)$_{4-n}$]$^{2-}$ (n = 0-4) isotopologues obtained in a 42% ^{13}C enriched [Pt(CN)$_4$]$^{2-}$ solution after adding seven mol equivalents of Na^{13}CN to 0.2 M [Pt(CN)$_4$]$^{2-}$ in water. The sets of ^{12}C/^{13}C isotopologue signals are indicated by the same colour least-square fits.

Five different sets of ^{12}C/^{13}C isotopologues are observed, each set sub-divided according to Pascal's triangle (n + 1; where n = no. ^{13}C isotopes). One ^{195}Pt signal is thus observed for the original [Pt(^{12}CN)$_4$]$^{2-}$ signal, while the [Pt(^{12}CN)$_3$(^{13}CN)]$^{2-}$ isotopologue is split into two signals. The [Pt(^{12}CN)$_2$(^{13}CN)$_2$]$^{2-}$, [Pt(^{12}CN)(^{13}CN)$_3$]$^{2-}$ and [Pt(^{13}CN)$_4$]$^{2-}$ isotopologues are split into three, four and five ^{195}Pt signals respectively according to the same principle. Least-squares analysis of the ^{195}Pt signals reveals that the sum of each set of ^{12}C/^{13}C isotopologues correlates well with the statistical calculated (from Equation 3.1 in *Chapter 3*) ^{12}C : ^{13}C isotope ratio of 58 : 42 %. The experimentally obtained and calculated values are shown in Table 5.1 and were used to plot the different sets of ^{12}C/^{13}C isotopologues shown in Figure 5.10.

Table 5.1: Comparison of the experimental with statistical ^{195}Pt peak intensities of $[Pt(^{12}CN)_n(CN)_{4-n}]^{2-}$ ($n =$ 0-4) isotopologues obtained in a 42 % ^{13}C enriched $[Pt(CN)_4]^{2-}$ solution.

^{12}C/^{13}C isotopologue	Percent ^{12}C/^{13}C isotopologues split by $^1J(^{195}$Pt-^{13}C)		Sum percent ^{12}C/^{13}C isotopologues split by $^1J(^{195}$Pt-^{13}C)	
	Expt.	Statistical	Expt.	Statistical
$[Pt(^{12}CN)_4]^{2-}$	9.12	11.47	9.12	11.47
$[Pt(^{12}CN)_3(^{13}CN)]^{2-}$	15.02	16.48	29.94	32.95
	14.92	16.48		
$[Pt(^{12}CN)_2(^{13}CN)_2]^{2-}$	9.21	8.88	36.65	35.51
	18.26	17.76		
	9.17	8.88		
$[Pt(^{12}CN)(^{13}CN)_3]^{2-}$	2.51	2.13	19.96	17.01
	7.29	6.38		
	7.57	6.38		
	2.58	2.13		
$[Pt(^{13}CN)_4]^{2-}$	0.30	0.19	4.33	3.06
	0.91	0.77		
	1.49	1.15		
	1.27	0.77		
	0.36	0.19		

The hierarchy of ^{12}C/^{13}C isotopologue chemical shifts ($\delta_{itl}(^{195}$Pt)) follows the trend established for ^{35}Cl/^{37}Cl and ^{16}O/^{18}O isotopologues in *Chapter 3*. The heavier isotopologue signals resonate more upfield. To make this comparison it was necessary to take the mean of the ^{12}C/^{13}C isotopologue $\delta_{itl}(^{195}$Pt) value, which results in a constant $\Delta\delta_{itl}(^{195}$Pt) value of 0.39 ppm, presenting a linear correlation ($\delta_{itl}(^{195}$Pt) $= -0.39n - 4737$; $R^2 = 1$) when plotted as a function of coordinated ^{13}C isotopes as shown in Figure 5.11.
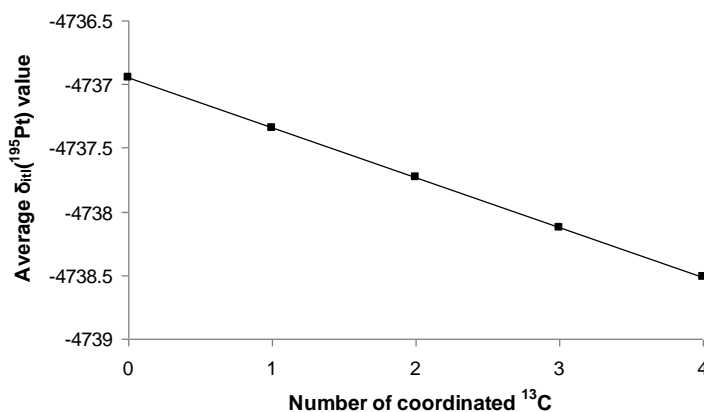
Figure 5.11: Average $\delta_{itl}(^{195}$Pt) value of ^{12}C/^{13}C isotopologues as a function of increased ^{13}C coordination in the $[Pt(^{12}CN)_4(^{13}CN)_{4-n}]^{2-}$ ($n = 0$-4) series of isotopic species.

5.3.3.2 Oxidation of tetracyanoplatinate(II) by hydrogen peroxide in water investigated by means of ^{195}Pt NMR

There are some discrepancies in the literature regarding the oxidation of $[Pt(CN)_4]^{2-}$ with hydrogen peroxide. Many years ago Levy[42] reported that partially oxidized $K_2Pt(CN)_4$ is obtained when a mixture of sulphuric acid and hydrogen peroxide is added to $K_2Pt(CN)_4$ in water. A single crystal X-ray structure of composition $K_{1.74}[Pt(CN)_4]·1.8H_2O$ was solved by Krogmann[43] in 1968. A few years later Atamanov[36] reported that yellow-needle like crystals are formed when H_2O_2 (30 % w/w) is added to $K_2[Pt(CN)_4]$ in water. The crystals were assigned to $K_2[Pt(CN)_4(OH)_2]$ by measuring it's molar conductivity and no single crystal X-ray structure was available. More recently Muehle *et al.*[44] reported that when H_2O_2 is added to the $A_2[Pt(CN)_4]$ (A = K, Rb, Cs) salts in a similar manner described by Levy,[42] yellow crystals of a hydrogen peroxide adduct with the molecular formula $A_2[Pt(CN)_4]·H_2O_2$ (A = K, Rb, Cs), were characterized by single crystal X-ray diffraction. The authors[44] concluded that H_2O_2 do not oxidize $[Pt(CN)_4]^{2-}$ in water. The oxidation of $[Pt(CN)_4]^{2-}$ was reinvestigated here, both in *water* and *acidic* solution.

When concentrated hydrogen peroxide (30% w/w) is added to the $K_2Pt(CN)_4·3H_2O$ salt, no oxidation is observed with ^{195}Pt NMR even after "ageing" the solution for 24 hours. In another reaction 200 µL of 0.1 M $[Pt(CN)_4]^{2-}$ was prepared in water before adding 1 mL concentrated H_2O_2 (30 % w/w). The solution was "aged" for two weeks in the dark at room temperature after which it was concentrated to 450 µL *in vacuo* and stored at 0 ºC. After six days, the solution turned light yellow and small yellow crystals formed in the solution, which visually resembles the crystals described by Atamanov[36] and Muehle.[44] The yellow crystals quickly disintegrate in the solution if removed from the refrigerator, but can be re-crystallized if cooled. The light yellow solution was removed from the refrigerator and ^{195}Pt and ^{13}C NMR spectra were collected, shown here in Figures 5.12A and B.

(A)

(B)
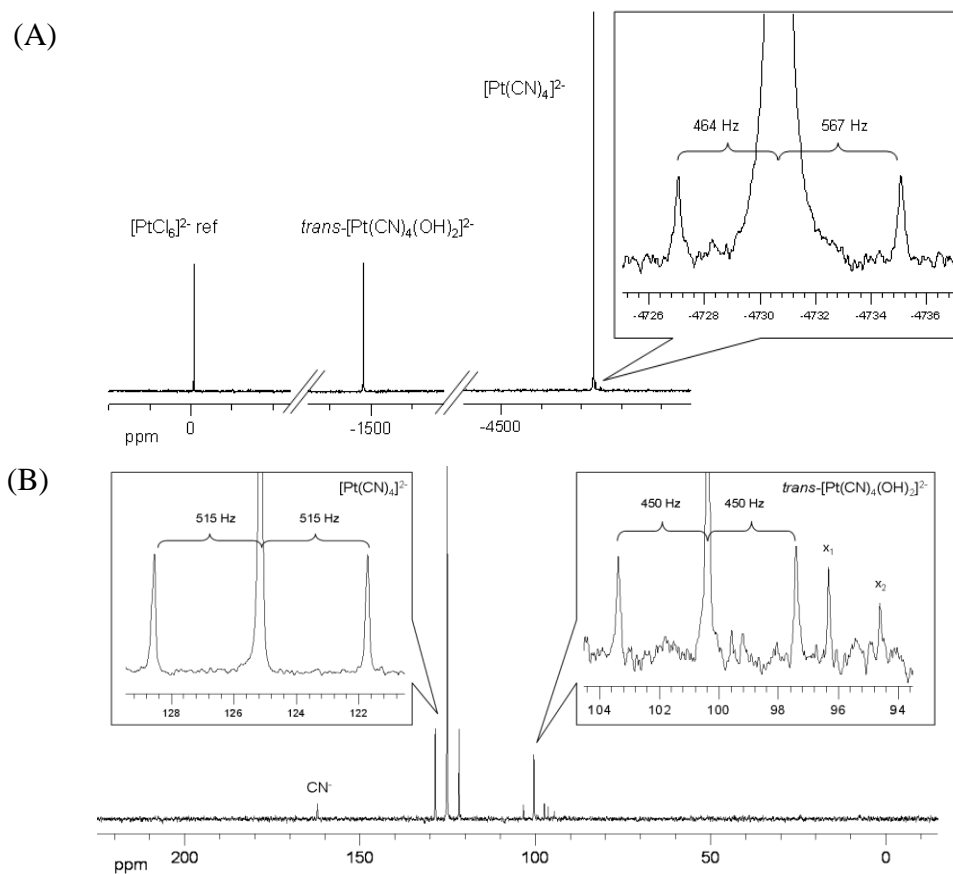
Figure 5.12: (A) ^{195}Pt NMR spectra obtained from the addition of excess H_2O_2 to an aqueous $K_2[Pt(CN)_4]\cdot 3H_2O$ solution. The off-centred $[Pt(^{12}CN)_3(^{13}CN)]^{2-}$ isotopologue split into a doublet   due to $^1J\{^{195}Pt\text{-}^{13}C\}$ coupling is shown in the expansion. **(B)** The $^{13}C\{^1H\}$ NMR spectrum of the same solution. $^1J\{^{13}C\text{-}^{195}Pt\}$ coupling constants of $[Pt(CN)_4]^{2-}$ and *trans*-$[Pt(CN)_4(OH)_2]^{2-}$ are shown in the expansions.

In water, a 0.1 M $[Pt(CN)_4]^{2-}$ solution (obtained from the $K_2Pt(CN)_4\cdot 3H_2O$ salt) shows one major $\delta(^{195}Pt)$ signal at -4735 ppm as previously shown (Figure 5.9A). In addition to the $[Pt(CN)_4]^{2-}$ signal (which shifted to -4731 ppm after addition of H_2O_2) another signal is observed at -1482 ppm as shown in Figure 5.12A. The large $\Delta\delta(^{195}Pt)$ of 3249 ppm between $[Pt(CN)_4]^{2-}$ and the new signal is characteristic of a change in oxidation state and can not be ascribed to the formation of a $K_2[Pt(CN)_4]\cdot H_2O_2$ adduct in solution as found by Muehle[44] in the solid state. According to the *trans* oxidative addition mechanism of $[PtCl_4]^{2-}$ with H_2O_2 it is reasonable to expect formation of *trans*-$[Pt(CN)_4(OH)_2]^{2-}$ as the major oxidation product. Expansion of the signal at -1482 ppm reveals (similarly to the $[Pt(CN)_4]^{2-}$ signal) two small signals on either side of the main peak with an offset of 378 and 526 Hz respectively. Similar signals of $[Pt(CN)_4]^{2-}$ were assigned to the

$[^{195}Pt(^{12}CN)_3(^{13}CN)]^{2-}$ isotopologue which is split into a doublet as a result of $^1J(^{195}Pt-^{13}C)$ coupling. The $^{13}C\{^1H\}$ NMR spectrum in Figure 5.12B shows a similar result. In addition to the triplet of the $[Pt(CN)_4]^{2-}$ species centred at 125.1 ppm, a new triplet centred at 100.4 ppm is observed for the alleged *trans*-$[Pt(CN)_4(OH)_2]^{2-}$ species. The $\delta(^{13}C)$ signal at 100.4 ppm is centred between two smaller signals $^1J\{^{13}C-^{195}Pt\}$ = 450 Hz and integrates to 0.17 : 0.66 : 0.17, according to the 33.8 % natural abundance of the ^{195}Pt isotope. The ^{13}C signal at 162.1 ppm is assigned to cyanide ions in the solution. Two small ^{13}C signals at 96.3 and 94.6 ppm (marked as x_1 and x_2 in Figure 5.12B) remains un-assigned, but it is evident from Figure 5.12A that these species do not include any Pt(II/IV).

Since no $\delta(^{195}Pt)$ or $\delta(^{13}C)$ values of any Pt(IV)-cyano-*hydroxido* or *aqua* species are reported in the literature, the $\delta(^{195}Pt)$ of *trans*-$[Pt(CN)_4(OH)_2]^{2-}$ was estimated from the known $\delta(^{195}Pt)$ values of $[Pt(OH)_6]^{2-}$ (3284 ppm; from *Chapter 4*) and $[Pt(CN)_6]^{2-}$ (-3821 ppm [45]) in water. Although the relation for this series is not necessarily strictly linear, all the Pt(IV) trends discussed so far (*Chapter 3* and *4*) are close to linear. The estimated $\delta(^{195}Pt)$ value is therefore expected to give a good indication of the experimental $\delta(^{195}Pt)$ of *trans*-$[Pt(CN)_4(OH)_2]^{2-}$. If a linear relation is assumed for the $\delta(^{195}Pt)$ values of the $[Pt(CN)_n(OH)_{6-n}]^{2-}$ (*n* = 0-6) series, the average $\delta(^{195}Pt)$ of the *cis*- and *trans*-$[Pt(CN)_4(OH)_2]^{2-}$ isomers is estimated at -1500 ppm (Figure 5.13), which is close to the $\delta(^{195}Pt)$ observed at -1482 ppm in Figure 5.12A.
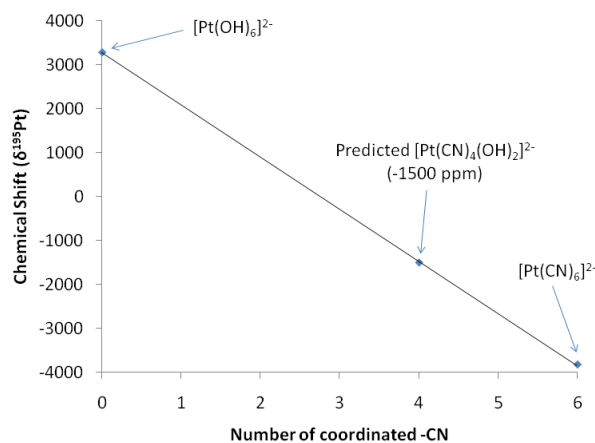
Figure 5.13: Estimated $\delta(^{195}Pt)$ of the average $\delta(^{195}Pt)$ value of *cis/trans*-$[Pt(CN)_4(OH)_2]^{2-}$ in water.

In water, oxidation of 0.1 M $[Pt(CN)_4]^{2-}$ with excess H_2O_2 is slow (after 20 days only a portion of the Pt(II) is oxidized), but oxidation does take place. The ^{195}Pt and ^{13}C NMR data presented in Figures 5.12A and B supports this idea which is consistent with the observations of Atamanov.[36]

5.3.3.3 Oxidation of $[Pt(CN)_4]^{2-}$ by hydrogen peroxide in acidic solution by means of ^{195}Pt NMR

No oxidation of 0.2 M $[Pt(CN)_4]^{2-}$ in water is observed in the presence of excess H_2O_2 after one hour. Heating the solution for one hour at 50ºC still shows no evidence of oxidation as monitored by ^{195}Pt NMR. When concentrated $HClO_4$ is added to the solution (final $[H^+] \sim 1$ M) a bright yellow precipitate is formed immediately. The precipitate quickly dissolves when the solution is shaken and the ^{195}Pt NMR spectrum taken immediately after dissolution shows an additional $\delta(^{195}Pt)$ signal at -1252 ppm. It is reasonable to expect that this ^{195}Pt NMR peak is the *trans*-$[Pt(CN)_4(H_2O)_2]$ species which resonates 230 ppm more downfield relative to the supposed ^{195}Pt signal of *trans*-$[Pt(CN)_4(OH)_2]^{2-}$ at -1482 ppm obtained in water. A ^{195}Pt NMR spectrum taken seven days later shows that the alleged *trans*-$[Pt(CN)_4(H_2O)_2]$ signal has grown relative to the $[PtCl_6]^{2-}$ reference and no more $[Pt(CN)_4]^{2-}$ was detected in the solution (Figure 5.14A).
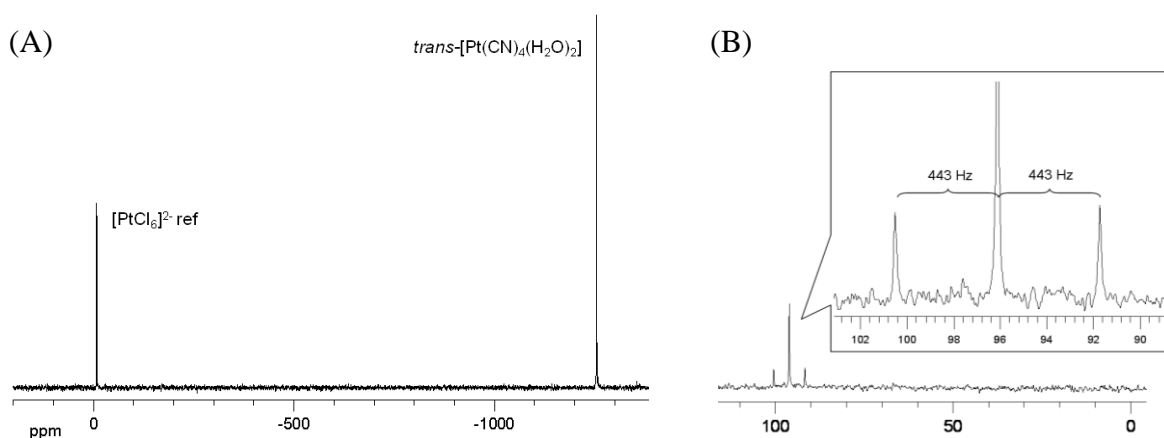
Figure 5.14: (A) ^{195}Pt NMR spectrum of $[Pt(CN)_4]^{2-}$ in 1 M $HClO_4$ oxidized with excess H_2O_2 and aged for a week. **(B)** ^{13}C NMR spectrum of the same solution.

The ^{13}C NMR spectrum confirms only one signal at 96.1 ppm (Figure 5.14B), 4.3 ppm more upfield relative to the $\delta(^{13}C)$ of the supposed *trans*-$[Pt(CN)_4(OH)_2]^{2-}$ species observed

at 100.4 ppm in Figure 5.12B. Two satellites can be observed either side of the major signal with $^1J\{^{13}C\text{-}^{195}Pt\}$ coupling constant of 443 Hz. The small $\Delta\delta(^{195}Pt)$ and $\Delta\delta(^{13}C)$ between these two species is consistent with an effect induced by protonation.

The *trans*-$[Pt(CN)_4(H_2O)_2]$ complex was co-crystallized with 18-crown-6 to confirm the structure. The experimental procedure and twin refinement are discussed in the experimental section. An ORTEP diagram of the refined *trans*-$[Pt(CN)_4(H_2O)_2]^.(18\text{-crown-}6)_2{}^.8H_2O$ crystal structure is shown in Figure 5.15 and displays the numbering scheme for selected bond lengths and angles which is listed in Table 5.2.
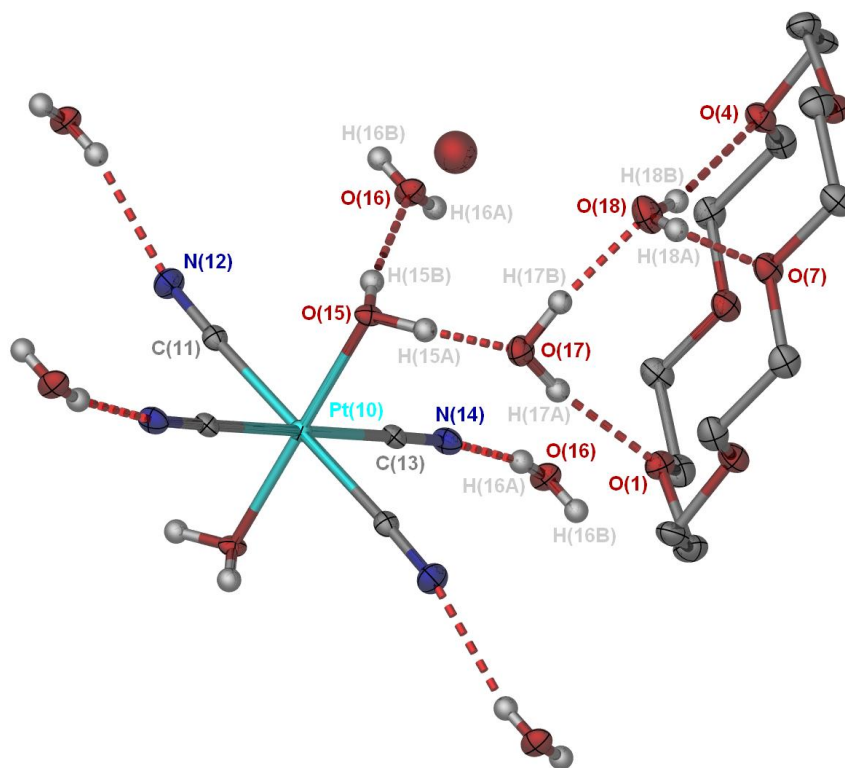
Figure 5.15: ORTEP diagram showing the numbering scheme and crystal structure of *trans*-$[Pt(CN)_4(H_2O)_2]^.(18\text{-crown-}6)_2{}^.8H_2O$. Only one 18-crown-6 molecule is included in the image for simplicity.

The neutrally charged *trans*-$[Pt(CN)_4(H_2O)_2]$ species is sandwiched between two 18-crown-6 ethers, of which the centres of both are perpendicular to the *facial* cavity of *trans*-$[Pt(CN)_4(H_2O)_2]$. These are kept in place by an extensive hydrogen bonded system, favoured by the nature of the water and cyanide ligands. Both Pt–OH$_2$ coordinated water ligands are hydrogen bonded to two other water molecules in the second coordination

sphere. One of these water molecules is hydrogen bonded to the nitrogen atom of an adjacent *trans*-[Pt(CN)$_4$(H$_2$O)$_2$] complex and the other is coordinated to another water molecule and the oxygen atom of an 18-crown-6 ether. Each cyanide ligand is coordinated to a water molecule which connects the respective *trans*-[Pt(CN)$_4$(H$_2$O)$_2$] complexes. A severely disordered water molecule was found between two adjacent 18-crown-6 ethers. It was not modelled further and is modelled in Figure 5.15 as a spherical single atom without coordinated hydrogen atoms. Single crystal X-ray diffraction confirms the ^{195}Pt NMR data that *trans*-[Pt(CN)$_4$(H$_2$O)$_2$] is the exclusive oxidation product when [Pt(CN)$_4$]$^{2-}$ is oxidized with H$_2$O$_2$ in 1 M HClO$_4$.

Table 5.2: Selected bond distances (Å) and bond angles (º) of *trans*-[Pt(CN)$_4$(H$_2$O)$_2$]·(18-cr-6)$_2$·8H$_2$O

Bond distance (Å)	
Pt—O15	2.018
Pt—O15^i	2.018
Pt—C11	2.025
Pt—C11^i	2.025
Pt—C13	2.021
Pt—C13^i	2.021
C11—N12	1.139
C11^i—N12^i	1.139
C13—N14	1.137
C13^i—N14^i	1.137
Bond angles (°)	
O15—Pt—O15^i	180
O15—Pt—C13	91.45
C11—Pt—C13	91.42
O11—Pt—C11^i	180
C13—Pt—C13^i	180

Although the oxidation rate is very different, the oxidation products in water and acid are very similar. Both *trans*-[Pt(CN)$_4$(OH)$_2$]$^{2-}$ and *trans*-[Pt(CN)$_4$(H$_2$O)$_2$] are thermodynamically stable and persist in solution as the only species for weeks. These results were encouraging as it seemed oxidation of [Pt(CN)$_4$]$^{2-}$ could be studied with chlorate and bromate without the complications from Pt(II)–Pt(IV) assisted ligand exchange as observed for the oxidation of [PtCl$_4$]$^{2-}$ in acidic solution. The situation is however different and a single oxidation product is not obtained for oxidation of [Pt(CN)$_4$]$^{2-}$ with NaClO$_3$ and NaBrO$_3$ as will be shown.

5.3.3.4 Oxidation of tetracyanoplatinate(II) by sodium chlorate in acidic solution

Five mol equivalents of $NaClO_3$ was added to a 0.2 M $[Pt(CN)_4]^{2-}$ solution in 1 M $HClO_4$. No oxidation was observed after stirring the Pt(II) solution at 55ºC for 10 minutes. Even after the temperature was increased to 100ºC for one hour no oxidation could be seen with ^{195}Pt NMR. After the solution was "aged" for a week at room temperature in the dark, off-white colloidal like substance formed in the solution. Although the ^{195}Pt signal of $[Pt(CN)_4]^{2-}$ decreased, no new ^{195}Pt signals are observed. The solution was left at room temperature in ambient light for four weeks. After this period no more $[Pt(CN)_4]^{2-}$ was detected in solution with ^{195}Pt NMR and some of the colloidal like substance turned into a flaky off-white precipitate. No additional signals could be detected with ^{195}Pt NMR in solution of the supernatant. Addition of concentrated HCl to the colloidal suspension (final [HCl] ~ 3M) resulted in an immediate colour change to bright yellow and the precipitate dissolved. A ^{195}Pt spectrum of this yellow solution shows one signal at -2600 ppm and the ^{13}C spectrum of the same solution shows one signal at 96.2 ppm. These values compares reasonably well with the $\delta(^{195}$Pt) value of -2575 ppm and $\delta(^{13}$C) value of 98.9 ppm reported by Brown *et al.*[37] for the *trans*-$[Pt(CN)_4Cl_2]^{2-}$ complex in water, considering the different solvents. A correction for temperature can not be made to compare these $\delta(^{195}$Pt) values more accurately since the temperature at which the ^{195}Pt spectra were collected are not reported by Brown *et al.*[37]
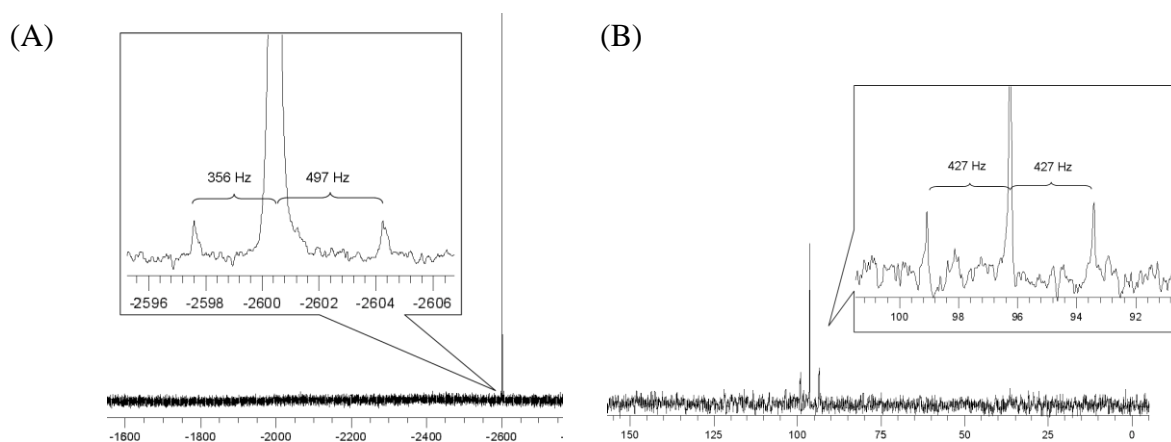
Figure 5.16: **(A)** ^{195}Pt NMR spectrum of 0.2 M $[Pt(CN)_4]^{2-}$ "aged" in the presence of $NaClO_3$ before addition of concentrated HCl (final [HCl] = 3 M). The *trans*-$[Pt(^{12}CN)_4Cl_2$ and *trans*-$[Pt(^{12}CN)_3(^{12}CN)Cl_2$ isotopologues are shown in the expansion. **(B)** ^{13}C NMR spectrum of the same solution, with satellites due to $^1J\{^{13}$C-^{195}Pt$\}$ coupling shown in the expansion.

Expansion of the main signal in Figure 5.16A reveals three closely spaced ^{195}Pt signals which can be deconvoluted by least-squares analysis as illustrated in Figure 5.17. The experimental peak ratios values calculated from a least-squares fit, correlates very well (Table 5.3) with the three statistical ^{35}Cl/^{37}Cl isotopologue ratios expected for *trans*-[Pt(CN)$_4$Cl$_2$]$^{2-}$. These values confirms the assignment of *trans*-[Pt(CN)$_4$Cl$_2$]$^{2-}$ observed at -2600 ppm in Figure 5.16.
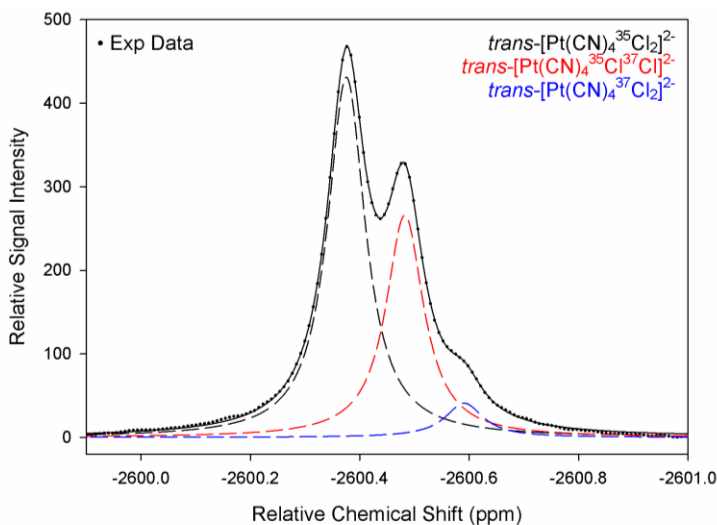
Figure 5.17: ^{195}Pt NMR spectrum of the ^{35}Cl/^{37}Cl isotopologue distribution of *trans*-[Pt(CN)$_4$Cl$_2$]$^{2-}$.

Table 5.3: Experimental ^{35}Cl/^{37}Cl isotopologue ratios of *trans*-[Pt(CN)$_4$^{35}Cl$_2$]$^{2-}$ compared to the statistical calculated values.

^{35}Cl/^{37}Cl isotopologue	Expt.	Statistical
trans-[Pt(CN)$_4$^{35}Cl$_2$]$^{2-}$	58.44	57.41
trans-[Pt(CN)$_4$^{35}Cl^{37}Cl]$^{2-}$	36.01	36.72
trans-[Pt(CN)$_4$^{37}Cl$_2$]$^{2-}$	5.55	5.87

The $\delta(^{195}$Pt) spectrum reveals two small off centred peaks on either side of the major ^{195}Pt signal, shown in the expansion Figure 5.16A. The same proposal suggested for [Pt(CN)$_4$]$^{2-}$ and *trans*-[Pt(CN)$_4$(H$_2$O)$_2$] of a natural occurring ^{12}C/^{13}C isotopologue (^{13}C = 1.11 %) split into a doublet, is valid. The ^{13}C NMR spectrum agrees with these findings, since only one ^{13}C signal is observed at 96.2 ppm, centred between two $^1J\{^{13}$C-^{195}Pt$\}$ coupled satellites (427 Hz; Figure 5.16B).

The composition of the white precipitate obtained is unknown. It is unlikely that the precipitate is still in the Pt(II) oxidation state, considering the fast formation of *trans*-$[Pt(CN)_4Cl_2]^{2-}$ after addition of HCl. Although reaction of HCl with ClO_3^- will form Cl_2, which will rapidly oxidize $[Pt(CN)_4]^{2-}$ (k = (1.08 ± 0.10) x 10^7 $M^{-1}s^{-1}$),[33] the reaction ClO_3^- + H^+ + $2Cl^-$ → $3Cl_2$ + $2H_2O$ is relatively slow. In this regard a Pt(IV) precipitate that quickly reacts with HCl seems more feasible, although further studies are necessary to confirm this speculation. Nevertheless, oxidation of $[Pt(CN)_4]^{2-}$ with $NaClO_3$ is very slow if it takes place and results in an insoluble compound. Oxidation of $[Pt(CN)_4]^{2-}$ is therefore not ideal as substrate for a kinetic study with sodium chlorate. The intimate properties of this reaction remain unknown and further studies are necessary to unravel and fully understand the oxidation mechanism.

5.3.3.5 *Oxidation of tetracyanoplatinate(II) by sodium bromate in acidic solution*

Oxidation of 0.2 M $[Pt(CN)_4]^{2-}$ in 1 M $HClO_4$ with five mol equivalents sodium bromate was investigated by adding the $NaBrO_3$ salt directly to the Pt(II) solution. Oxidation is rapid and complete within seconds as perceived from the colourless solution which changes to a light yellow colour. A relatively small $\delta(^{195}Pt)$ signal at -1263 ppm (Figure 5.18A) is observed, close to the $\delta(^{195}Pt)$ of -1252 ppm observed for *trans*-$[Pt(CN)_4(H_2O)_2]$ in Figure 5.14A.
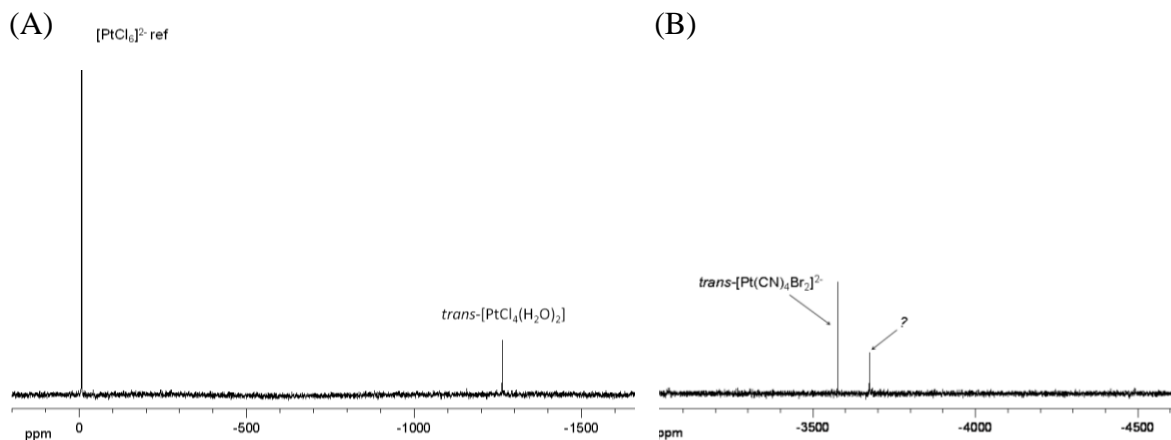
Figure 5.18: (A) ^{195}Pt NMR spectrum of 0.2 M $[Pt(CN)_4]^{2-}$ oxidized with $NaBrO_3$ in 1 M $HClO_4$ **(B)** ^{195}Pt NMR spectrum after addition of concentrated HBr (final [HBr] = 3 M) to the solution in (A).

Although no $[Pt(CN)_4]^{2-}$ is observed after oxidation with $NaBrO_3$ only a small quantity of *trans*-$[Pt(CN)_4(H_2O)_2]$ is observed with [195]Pt NMR with respect to the $[PtCl_6]^{2-}$ reference. No other [195]Pt signals are observed and no precipitate is formed. The ^{13}C NMR spectrum only show very broad low intensity signals in the region 90 - 100 ppm, characteristic of a polynuclear or Pt(III) compound. After the solution was "aged" for a week at room temperature the composition changed to a yellow gel-like substance. The signal at -1263 ppm could still be detected but decreased slightly in intensity. Concentrated HBr was added to the solution (final [HBr] ~ 3 M) in order to try and elucidate the yellow gel-like substance. The yellow gel-like substance dissolved immediately, and resulted in a bright orange-brown solution. The [195]Pt NMR spectrum reveals two signals at -3562 and -3660 ppm respectively (Figure 5.18B). The major [195]Pt signal is relatively close to the -3549 ppm reported by Brown *et al.*[37] for *trans*-$[Pt(CN)_4Br_2]^{2-}$ in water. The more shielded $\delta(^{195}Pt)$ at -3660 ppm could not be assigned to any species reported in the literature before. One possibility is the *cis*-$[Pt(CN)_4Br_2]^{2-}$ stereoisomer, although this species would be unexpected due to the high thermodynamic stability of Pt(II) coordinated cyanide ligands in the *xy*-plane.

Bromate oxidize $[Pt(CN)_4]^{2-}$ rapidly in acidic solution to form *trans*-$[Pt(CN)_4(H_2O)_2]$, although it does not seem to be the major product given the formation of a gel-like substance not amenable to [195]Pt NMR. Formation of *trans*-$[Pt(CN)_4(H_2O)_2]$ confirms formation of a Pt-oxygen bridged intermediate prior to electron transfer. In a UV-visible study, Chandayot *et al.*[39] found that the hypobromite ion (OBr^-) oxidizes $[Pt(CN)_4]^{2-}$ quantitatively to form *trans*-$[Pt(CN)_4Br(OH)]^{2-}$ exclusively ($[OH^-] = 0.01 – 0.1$ M). No evidence could be found in our solution for the formation of this species by [195]Pt NMR. Since there is not a quantitative conversion from $[Pt(CN)_4]^{2-}$ to *trans*-$[Pt(CN)_4(H_2O)_2]$ and no precipitate or any other insoluble substance is observed, the gel-like substance is not amenable to [195]Pt NMR and is possibly paramagnetic in origin. The formation of a gel-like substance prevent a kinetic study of the oxidation of $[Pt(CN)_4]^{2-}$ with $NaBrO_3$ in acidic solution and limits mechanistic interpretations similarly to oxidation with chlorate.

5.3.4 Oxidation of $[Pt(H_2O)_4]^{2+}$ by sodium chlorate and sodium bromate as monitored by ^{195}Pt NMR

No literature is available that deals with the oxidation of $[Pt(H_2O)_4]^{2+}$ with $NaClO_3$ or $NaBrO_3$. Gröning and Elding[46] reported oxidation of $[Pt(H_2O)_4]^{2+}$ with Cl_2 is rapid and results in the exclusive formation of $[PtCl(H_2O)_5]^-$. The $[PtCl(H_2O)_5]^-$ complex is kinetically inert, and additional $\delta(^{195}Pt)$ resonance signals were only observed after "ageing" the solution several months as the $[PtCl(H_2O)_5]^-$ concentration decreased, forming other $[PtCl_n(H_2O)_{6-n}]^{4-n}$ (n = 2-6) complexes. The oxidation of $[Pt(H_2O)_4]^{2+}$ was discussed in *Chapter 4* as a means to the elusive $[Pt(H_2O)_6]^{4+}$ complex, but no mechanistic implications were considered. It was shown in *Chapter 4* that oxidation of $[Pt(H_2O)_4]^{2+}$ with H_2O_2 in 1 M $HClO_4$ results in a long period of effervescence and eventual precipitation of a yellow solid, presumably $H_2[Pt(OH)_6]$. Oxidation of $[Pt(H_2O)_4]^{2+}$ with $NaClO_3$ and $NaBrO_3$ was subsequently carried out in 6 M $HClO_4$ to ensure formation of $[Pt(H_2O)_6]^{4+}$. In these reaction conditions, oxidation resulted in formation of both $[Pt(H_2O)_6]^{4+}$ and $[Pt(H_2O)_5X]^{3+}$ (X = Cl, Br) in addition to various polynuclear Pt(IV) complexes (*Chapter 4*; *Figure 4.6* and *4.7*). Oxidation of $[Pt(H_2O)_4]^{2+}$ with chlorate and bromate was re-investigated here in the context of a mechanistic interpretation.

Three solutions of 0.2 M $[Pt(H_2O)_4]^{2+}$ were oxidized with $NaClO_3$ and $NaBrO_3$ in $HClO_4$. In the first experiment five mol equivalents of $NaClO_3$ was added to the $[Pt(H_2O)_4]^{2+}$ solution in 1 M $HClO_4$. No reaction is observed after 10 minutes at room temperature. When the temperature is increased to 50ºC the colour of the solution change from light yellow to dark yellow-orange, while chlorine-like fumes are generated. At 50ºC the oxidation is completed within five minutes evident from the disappearance of the $\delta(^{195}Pt)$ signal at 30 ppm. Two new signals appeared at 3285 ppm and 2726 ppm respectively as shown in Figure 5.19A. In the second experiment 5 mol equivalents of $NaBrO_3$ was added to 0.2 M $[Pt(H_2O)_4]^{2+}$ in 2 M $HClO_4$. Oxidation is rapid and completed in seconds at room temperature evident from the colour changes from light yellow to dark brown, while bromine-like fumes are generated. The solution was stirred for an additional five minutes at 50°C. Two new signals appear at 3295 ppm and 2482 ppm respectively observed in the ^{195}Pt NMR spectrum shown in Figure 5.19B. In the third experiment a mixture of 2.5 mol

equivalents of $NaClO_3$ and $NaBrO_3$ each was added to a 0.25 M $[Pt(H_2O)_4]^{2+}$ solution in 1 M $HClO_4$. The oxidation is essentially similar to that observed with $NaBrO_3$ and is completed in seconds at room temperature. Three new ^{195}Pt signals appear as shown in Figure 5.19C.
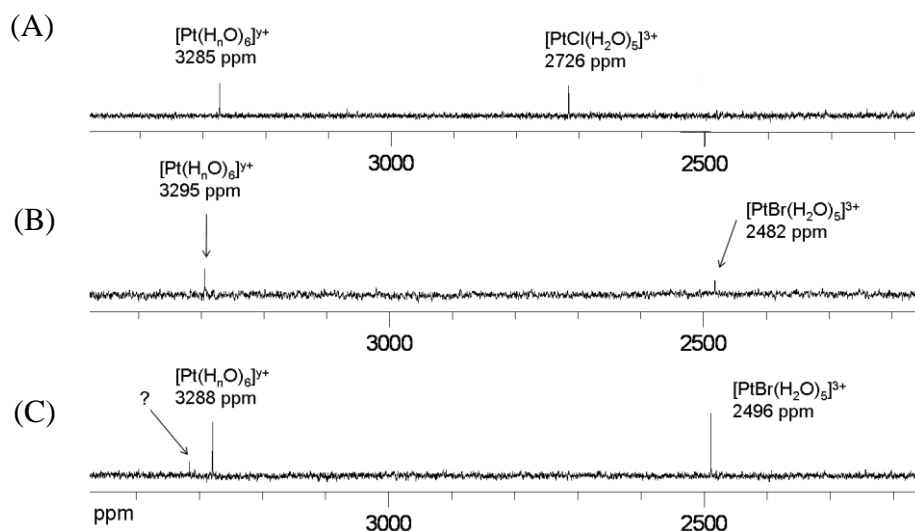
Figure 5.19: Oxidation of $[Pt(H_2O)_4]^{2+}$ with five mol equivalents **(A)** $NaClO_3$ in 1 M $HClO_4$, **(B)** $NaBrO_3$ in 2 M $HClO_4$ and **(C)** a mixture of $NaClO_3/NaBrO_3$ in 1 M $HClO_4$. The ^{195}Pt NMR spectra were collected at 30°C.

Oxidation of $[Pt(H_2O)_4]^{2+}$ with $NaClO_3$ results in two $\delta(^{195}Pt)$ signals close to a 1:1 ratio (by peak integration). The $\delta(^{195}Pt)$ at 2726 ppm is in good agreement (considering the 10°C temperature gradient) with the $\delta(^{195}Pt)$ reported previously for $[PtCl(H_2O)_5]^{3+}$ at 2722 ppm in 6 M $HClO_4$ (*Chapter 4*, *Figure 4.6*) and is assigned accordingly. Since these ^{195}Pt NMR spectra were collected at 30°C, the $\delta(^{195}Pt)$ values can be corrected with ~10 ppm/°C [20] to compare with $\delta(^{195}Pt)$ values collected at 20°C. The $\delta(^{195}Pt)$ at 3285 ppm de-shielded from $[PtCl(H_2O)_5]^{3+}$, is typical in the range observed for $[Pt(OH)_6]^{2-}$ in acidic solution. It is clear from *Chapter 4, Figure 4.5* that the $\delta(^{195}Pt)$ at 3285 ppm in 1 M $HClO_4$ (which can be corrected to ~ 3275 ppm for a more accurate comparison given the temperature gradient) is below the critical concentration of 2.5 M $HClO_4$, so that the species cannot be assigned to a completely protonated $[Pt(H_2O)_6]^{4+}$ species in these reaction conditions. This is supported by the relative large quantity of yellow-orange precipitate that forms after oxidation, which is consistent with $H_2Pt(OH)_6$ formation.[47, 48] For this reason the species in Figure 5.19 are

labelled $[Pt(H_nO)_6]^{y+}$, since the extent of hydrolysis is unknown. Irrespective of the extent of hydrolysis, the $\delta(^{195}Pt)$ value at 3285 ppm certainly points to no coordinated Cl^- ligands and supports the idea that ClO_3^- oxidize Pt(II) by forming a oxygen-bridged intermediate, which is retained after electron transfer. The absence of any Cl^- coordinated ligands for Pt species that resonate at this frequency range was confirmed by the detection of seven $^{16}O/^{18}O$ isotopologue signals in Chapter 4 (Figures 4.8 and 4.9). Likewise, oxidation of $[Pt(H_2O)_4]^{2+}$ with $NaBrO_3$ results in two $\delta(^{195}Pt)$ signals (Figure 5.19B). The $\delta(^{195}Pt)$ at 2482 ppm (which can be adjusted to 2472 ppm) is close to that previously observed for $[PtBr(H_2O)_5]^{3+}$ at 2476 ppm in 6 M $HClO_4$ (*Chapter 4*, *Figure 4.7*) and is assigned accordingly. It was verified in *section 5.3.1.1* that the perchlorate ion is stable and does not take part in the oxidation reaction. Since bromate is the only source of bromide it is clear that the chloride and bromide ligands coordinated to $[PtX(H_2O)_5]^{3+}$ (X = Cl or Br) originates from the oxidant. It was illustrated in *Chapter 4* (*Figure 4.11* and *4.12*) that addition of NaCl or NaBr to $[Pt(H_2O)_6]^{4+}$ results in relative fast anation of $[Pt(H_2O)_6]^{4+}$ and formation of the $[PtCl_n(H_2O)_{6-n}]^{4-n}$ (*n* = 1-6) or $[PtBr_n(H_2O)_{6-n}]^{4-n}$ (*n* = 1-6) species. The absence of $[PtCl_n(H_2O)_{6-n}]^{4-n}$ (*n* = 2-6) or $[PtBr_n(H_2O)_{6-n}]^{4-n}$ (*n* = 2-6) species in Figures 5.19A and B therefore suggests that $[PtX(H_2O)_5]^{3+}$ (X = Cl or Br) is not formed due to XO_3^- (X = Cl or Br) reduction and subsequent Cl^- or Br^- anation, but rather *via* oxidation. Since oxidation of Pt(II) by XO_3^- seems to proceed *via* a Pt–O bonded intermediate, Pt–X (X = Cl or Br) bond formation can be envisaged by oxidation with XO^-, a reduced form of XO_3^-. Another possible route is *via* reduction of ClO_3^- to form Cl^- and subsequent reaction with a second ClO_3^- anion to form Cl_2 according to the reaction $ClO_3^- + H^+ \, 2Cl^- \rightarrow 3Cl_2 + 2H_2O$. Oxidation of $[Pt(H_2O)_4]^{2+}$ with Cl_2 is rapid, and forms $[PtCl(H_2O)_5]^{3+}$.[8] In the same way, Br_2 may be generated to oxidize $[Pt(H_2O)_4]^{2+}$ to form $[PtBr(H_2O)_5]^{3+}$. The chlorine- and bromine-like smell generated in these oxidation reactions supports this idea.

Oxidation of $[Pt(H_2O)_4]^{2+}$ with a ClO_3^-/BrO_3^- mixture emphasize the fast oxidation with BrO_3^-, since only $[PtBr(H_2O)_5]^{3+}$ is observed and no $[PtCl(H_2O)_5]^{3+}$. In addition to the $[Pt(H_nO)_6]^{y+}$ (3288 ppm) and $[PtBr(H_2O)_5]^{3+}$ (2496 ppm) signals a third small ^{195}Pt signal is observed at 3295 ppm in Figure 5.19C. Oxidation of higher concentrations of $[Pt(H_2O)_4]^{2+}$ (0.35 M) in *Chapter 4* revealed several additional signals for oxidation with both chlorate and bromate. These ^{195}Pt signals were assigned to polynuclear Pt(IV) complexes and has

been observed by other authors in similar reaction conditions with different techniques.[19, 48] The slightly higher concentration of 0.25 M $[Pt(H_2O)_4]^{2+}$ oxidized with the $NaClO_3/NaBrO_3$ mixture possible explains the addition ^{195}Pt signal.

5.4   Conclusions

Oxidation of $[PtCl_4]^{2-}$ with H_2O_2 in *water* results in the exclusive formation of *trans*-$[PtCl_4(OH)_2]^{2-}$ which persist in solution for days. In contrast, oxidation of $[PtCl_4]^{2-}$ with H_2O_2 in *acidic* solution (1 M $HClO_4$ or TfOH) results in formation of all the $[PtCl_n(H_2O)_{6-n}]^{4-n}$ (n = 1-6) complexes. Addition, of $[PtCl_4]^{2-}$ to a solution of *trans*-$[PtCl_4(OH)_2]^{2-}$ in *water* has no effect on the speciation, but a rapid redistribution of *trans*-$[PtCl_4(H_2O)_2]$ to the $[PtCl_n(H_2O)_{6-n}]^{4-n}$ (n = 1-6) complexes is observed if the solution is treated with perchloric acid. This ligand "scrambling" effect can be rationalized in terms of Pt(II)-Pt(IV) associations, whereby Pt(II) facilitates ligand exchange on Pt(IV), but only in *acidic* solution when labile H_2O is present and act as leaving ligand. Oxidation of $[Pt(CN)_4]^{2-}$ with H_2O_2 in *water* is slow, but does take place to furnish the *trans*-$[Pt(CN)_4(OH)_2]^{2-}$ complex. Oxidation of $[Pt(CN)_4]^{2-}$ with H_2O_2 in *acidic* solution is faster compared to the reaction in *water*, and furnishes the *trans*-$[Pt(CN)_4(H_2O)_2]$ complex which is thermodynamically stable and persist in solution for weeks. The structure of *trans*-$[Pt(CN)_4(H_2O)_2]$ was confirmed by single crystal X-ray analysis after co-crystallization with 18-crown-6. Oxidation of $[Pt(H_2O)_4]^{2+}$ with H_2O_2 takes place, but a yellow Pt precipitate forms after oxidation in 1 M $HClO_4$, while a small ^{195}Pt NMR signal reminiscent of $[Pt(OH)_6]^{2-}$ is observed. Although oxidation was not carried out under different conditions, it may be possible to form and stabilize $[Pt(H_2O)_6]^{4+}$ under higher concentrations of $HClO_4$. Oxidation of $[PtCl_4]^{2-}$, $[Pt(CN)_4]^{2-}$ and $[Pt(H_2O)_4]^{2+}$ with H_2O_2 in acidic solution therefore conforms with the general observation of a inner-sphere *trans* oxidative addition reaction *via* Pt(II)-oxygen bond formation prior to electron transfer.

Oxidation of $[PtCl_4]^{2-}$ with $NaClO_3$ and $NaBrO_3$ result in similar oxidation products, compared to oxidation with H_2O_2 in acidic solution, and suggest the same major oxidation product *trans*-$[PtCl_4(H_2O)_2]$ prior to ligand re-distribution. This observation also suggests

an inner-sphere one step, two-electron transfer oxidation mechanism *via* a direct Pt(II)–oxygen bond, between the Pt(II) substrate and oxidant. The formation of minor quantities of Pt(IV)-aqua-bromido-chlorido complexes with oxidation by $NaBrO_3$, verify that $NaBrO_3$ donate bromide ions to Pt(IV) either directly *via* oxidation with reduced forms of BrO_3^- or *via* anation after oxidation. Oxidation of $[Pt(CN)_4]^{2-}$ with ClO_3^- is slow and takes several days, and forms an colloidal-like compound that eventually precipitates as an off-white solid. This solid quickly dissolves in hydrochloric acid (~3 M) to form the *trans*-$[Pt(CN)_4Cl_2]^{2-}$ complex. Oxidation of $[Pt(CN)_4]^{2-}$ with BrO_3^- is relative fast and is completed in minutes, forming a yellow gel-like compound and a minor quantity of *trans*-$[Pt(CN)_4(H_2O)_2]$. The gel-like compound quickly dissolves in hydrobromic acid (~3 M), forming mainly *trans*-$[Pt(CN)_4Br_2]^{2-}$. Oxidation of $[Pt(H_2O)_4]^{2+}$ with $NaClO_3$ and $NaBrO_3$ forms two major species in each case. One species conforming to a $[Pt(H_2O)_6]^{4+}$ (likely to be hydrolyzed to some extent in 1-2 M $HClO_4$ as investigated here) and the other $[PtCl(H_2O)_5]^{3+}$ or $[PtBr(H_2O)_5]^{3+}$ depending on the oxidant. Formation of $[Pt(H_2O)_6]^{4+}$ is expected in the context of the *trans* oxidative addition mechanism observed for oxidation of $[PtCl_4]^{2-}$ and $[Pt(CN)_4]^{2-}$ with these oxidants, while formation of $[PtCl(H_2O)_5]^{3+}$ or $[PtBr(H_2O)_5]^{3+}$ is likely to form *via* oxidation of $[Pt(H_2O)_4]^{2+}$ with a reduced form of ClO_3^- or BrO_3^-. Formation of $[PtCl(H_2O)_5]^{3+}$ or $[PtBr(H_2O)_5]^{3+}$ *via* anation seems unlikely in the absence of any $[PtCl_n(H_2O)_{6-n}]^{4-n}$ (n = 2-6) or $[PtBr_m(H_2O)_{6-m}]^{4-m}$ (m = 2-6) species immediately after oxidation. This result support the idea that ClO_3^- and BrO_3^- oxidize Pt(II) *via* a Pt(II)–oxygen bond. That ligand scrambling reactions depends on the nature of the coordinated ligands of both Pt(II) and Pt(IV) is illustrated by the fact that no ligand scrambling is observed for oxidation of $[PtCN)_4]^{2-}$ and $[Pt(H_2O)_4]^{2+}$ as anticipated. Oxidation of Pt(II) with chlorate and bromate is complex and this chapter only serves as a preliminary study for more detailed mechanistic studies.

5.5   References

1.   F. L. Bernardis, R. A. Grant, D. C. Sherrington, *React. Funct. Polym.,* 2005, *65*, 205-217.

2.   G. Schmuckler, Patent No. 4885143, US, 1989.

3.   R. A. Grant, Y. Taylor, Patent No. 756013, EP, 1997.

4.   E. Benguerel, G. P. Demopoulos, G. B. Harris, *Hydrometallurgy,* 1996, *40*, 135-152.

5.   C. S. Smith, 2000-3060161074635, Application: EP, 2001.

6.   T. D. Harrigan, R. C. Johnson, *Inorg. Chem.,* 1977, *16*, 1741-1744.

7.   K. Hindmarsh, D. A. House, R. van Eldik, *Inorg. Chim. Acta,* 1998, *278*, 32-42.

8.   L. Drougge, L. I. Elding, *Inorg. Chem.,* 1988, *27*, 795-798.

9.   L. I. Elding, L. Gustafson, *Inorg. Chim. Acta,* 1976, *19*, 165-171.

10.   W. R. Mason, *Inorg. Chem.,* 1971, *10*, 1914-1917.

11.   M. S. Alam, K. Inoue, K. Yoshizuka, *Hydrometallurgy,* 1998, *49*, 213-227.

12.   Y. Zhang, G. Kshirsagar, J. E. Ellison, J. C. Cannon, *Ind. Eng. Chem. Res.,* 1993, *32*, 2863-2865.

13.   L. Treindl, T. Matsumura-Inoue, P. Ruoff, *J. Phys. Chem. A,* 2002, *106*, 5271-5278.

14.   W. H. Pittie, G. Overbeek, Patent No. 609155, US, 1976.

15.   M. Knothe, E. V. Uebel, R. Wolf, G. Pfrepper, Patent No, 90-4042030, DE, 1992.

16.   J. D. Edwards, D. F. Colton, R. K. Lea, Patent No. 49567, EP, 1982.

17.   S. O. Dunham, R. D. Larsen, E. H. Abbott, *Inorg. Chem.,* 1993, *32*, 2049-2055.

18.   L. I. Elding, *Inorg. Chim. Acta,* 1976, *20*, 65-69.

19.   T. G. Appleton, J. R. Hall, S. F. Ralph, C. S. M. Thompson, *Inorg. Chem.,* 1984, *23*, 3521-3525.

20.   S. M. Cohen, T. H. Brown, *J. Chem. Phys.,* 1974, *61*, 2985-2986.

21.   R. Van Eldik, W. Gaede, S. Wieland, J. Kraft, M. Spitzer, D. A. Palmer, *Rev. Sci. Instrum.,* 1993, *64*, 1355-1357.

22.   G. M. Sheldrick, *Programs for the solution and refinement of crystal structures, University of Goettingen, Germany,* 1997, *1*, 189-191.

23.   L. J. Barbour, *J. Supramol. Chem.,* 2003, *1*, 189-191.

24.   J. L. Atwood, L. J. Barbour, *Cryst. Growth Des.,* 2003, *3*.

25.   L. E. Cox, D. G. Peters, *Inorg. Chem.,* 1970, *9*, 1927-1930.

26.   G. Siegemund, W. Schwertfeger, A. Feiring, B. Smart, F. Behr, H. Vogel, B. McKusiek, *Ullmann's Encyclopedia of Industrial Chemistry*, John Wiley & Sons, New York, 2007.

27.   G. Horanyi, I. Bakos, *J. Electroanal. Chem.,* 1992, *331*, 727-737.

28.   G. Lang, M. Ujvari, G. Horanyi, *Corros. Sci.,* 2002, *45*, 1-5.

29.   L. I. Elding, L. Gustafson, *Inorg. Chim. Acta,* 1976, *19*, 31-38.

30.   W. R. Mason, *Coord. Chem. Rev.,* 1972, *7*, 241-255.

31.   F. Basolo, P. H. Wilks, R. G. Pearson, R. G. Wilkins, *J. Inorg. Nucl. Chem.,* 1958, *6*, 161.

32.   S. V. Zemskov, B. V. Ptitsyn, V. N. Lyubimov, V. F. Malakhov, *Zh. Neorg. Kim.,* 1967, *12*, 1223-1226.

33.   L. Drougge, L. I. Elding, *Inorg. Chem.,* 1985, *24*, 2292-2297.

34.   J. Halperin, H. Taube, *J. Am. Chem. Soc.,* 1952, *74*, 375-380.

35.   L. I. Elding, L. Gustafson, *Inorg. Chim. Acta,* 1977, *24*, 239-246.

36.   D. Atamanov, *Izv. Akad. Nauk Turkm. SSR,. Ser. Fiz.-Tekh., Khim. Geol. Nauk,* 1972, 111-112.

37.   C. Brown, B. T. Heaton, J. Sabounchei, *J. Organomet. Chem.,* 1977, *142*, 413-421.

38.   M. M. Jones, K. A. Morgan, *J. Inorg. Nucl. Chem.,* 1972, *34*, 259-274.

39.   P. Chandayot, Y. T. Fanchiang, *Inorg. Chem.,* 1985, *24*, 3535-3537.

40.   S. Ding, N. D. Jones, C. A. McDowell, *Solid State Nucl. Magn. Reson.,* 1998, *10*, 205-210.

41.   J. J. Pesek, W. R. Mason, *J. Magn. Reson.,* 1977, *25*, 519-529.

42.   L. A. Levy, *J. Am. Chem. Soc.,* 1912, 1081-1101.

43.   K. Krogmann, *Angew. Chem., Int. Ed.,* 1969, *8*, 35-42.

44.   C. Muhle, E.-M. Peters, M. Jansen, *Z. Naturforsch.,* 2009, *64b*, 111-115.

45.   P. S. Pregosin, *Coord. Chem. Rev.,* 1982, *44*, 247-291.

46.   O. Groning, L. I. Elding, *Inorg. Chem.,* 1989, *28*, 3366-3372.

47.   M. Maltese, W. J. Orville-Thomas, *J. Inorg. Nucl. Chem.,* 1967, *29*, 2533-2544.

48.   B. I. Nabivanets, L. V. Kalabina, L. N. Kudritskaya, *Zh. Neorg. Khim.,* 1971, *16*, 3281-3284.

Chapter 6

A preliminary kinetic study on the oxidation of tetrachloroplatinate(II) by hydrogen peroxide in hydrochloric acid solution

6.1   Introduction

Interest in platinum coordination chemistry was sparked by the discovery that *cis*-[Pt(NH$_3$)$_2$Cl$_2$] (*cis*-platin) possesses remarkable anti-cancer properties.[1] Since, more than 30 platinum-based compounds has entered clinical trials[2] including many platinum(IV) complexes. Ligand substitution reactions on the platinum(II) metal centre can be accurately predicted according to established properties such as the order of ligand exchange and *trans* effect.[3-6] For this reason [PtCl$_4$]$^{2-}$ is used in many oxidation reactions as the starting complex of choice in the design of various platinum(IV) complex species. Although ligand exchange on Pt(II) metal centres are arguably one of the best understood reaction mechanisms, oxidation of Pt(II) is not, and only a few kinetic studies has been published on the subject.

Oxidation of [PtCl$_4$]$^{2-}$ with regards to the PGM refining industry is of interest here, and oxidation was carried out mainly in hydrochloric solution to simulate refining process solutions. It is anticipated from the speciation study in *Chapter 5*, that the oxidation mechanism of [PtCl$_4$]$^{2-}$ by H$_2$O$_2$ should be more straightforward compared to oxidation with chlorate and bromate which is also of interest to the refining industry. For this reason, oxidation of [PtCl$_4$]$^{2-}$ by H$_2$O$_2$ was studied first to serve as a benchmark for further studies with other oxidants.

Hydrogen peroxide has been used for the oxidation of various square-planar Pt(II) complexes. These include anionic complexes [Pt(CN)$_4$]$^{2-}$, [PtCl$_2$(ox)]$^{2-}$ (ox = oxalate), cationic complexes [Pt(H$_2$O)$_4$]$^{2+}$, [Pt(NH)$_4$]$^{2+}$ and even dinuclear-Pt(II) compounds *cis*-[Pt(NH$_2$CH$_2$CH$_3$)$_2$(μ-OH)$_2$]$^{2+}$ among others.[7-11] One specific study of interest involves a kinetic study of the oxidation of [PtCl$_4$]$^{2-}$ with H$_2$O$_2$, KMnO$_4$, Na$_2$S$_2$O$_8$ in perchloric acid.[12] In the latter study it was reported that *trans*-[PtCl$_4$(H$_2$O)$_2$] is the only oxidation product in perchloric acid and an outer-sphere one-step two-electron transfer mechanism was proposed. The ^{195}Pt speciation study in *Chapter 5* suggest otherwise and indicates oxidation of [PtCl$_4$]$^{2-}$ with H$_2$O$_2$ in perchloric acid results in the formation of all of the [PtCl$_n$(H$_2$O)$_{6-n}$]$^{4-n}$ (*n* = 2-6) species. It was confirmed in several experiments (*Chapter 5*;

section 5.3.1.3) that $[PtCl_4]^{2-}$ assisted ligand exchange and coinciding "ligand scrambling" effects account for formation of the $[PtCl_n(H_2O)_{6-n}]^{4-n}$ (n = 2-6) species. A review of several studies show that Pt(IV)-Pt(II) associations may be expected under these reaction conditions.[13, 14] Such Pt(II)-Pt(IV) associations were not considered in above mentioned study of the oxidation of $[PtCl_4]^{2-}$ with H_2O_2 in perchloric acid,[12] and complicate unravelling of the oxidation mechanism significantly, so that accurate elucidation of the mechanism is not possible by conventional spectroscopic methods.

In this chapter, the oxidation of $[PtCl_4]^{2-}$ with H_2O_2 in *hydrochloric acid* is of interest, which is expected to simplify interpretation of the mechanism considerably. Aquation of $[PtCl_4]^{2-}$ prior to oxidation due to chloride anation and concomitant Pt(II) assisted ligand exchange reactions are likely to be reduced. In the preceding chapters, various aspects of the oxidation reaction with hydrogen peroxide could be concluded from the speciation, but it did not provide any quantitative data to elucidate the possible fundamental reaction mechanism. A detailed UV-visible and kinetic study on the oxidation of $[PtCl_4]^{2-}$ with H_2O_2 in hydrochloric acid was undertaken to determine the kinetic parameters and rate determining factors, in the process to understand the oxidation mechanism. Due to the high platinum concentrations required for ^{195}Pt NMR analysis, a detailed kinetic study with NMR is not practical. It should be pointed out that oxidation of highly concentrated Pt(II) solutions with hydrogen peroxide causes effervescence for the duration of the reaction, which prevents optimization of the NMR magnetic field homogeneity and spectra acquisition. UV-visible spectroscopy also has the advantage that spectra can be acquired rapidly after the reaction is initiated, which is not possible with conventional NMR techniques.

6.2   Experimental Section

6.2.1   Reagents

The platinum salt of potassium tetrachloroplatinate(II) (99.9+ %, K_2PtCl_4, Aldrich) was of reagent grade quality and used without further purification and stored in a desiccator. Hydrogen peroxide (30% w/w, H_2O_2, Riedel-de Haën) was also of reagent grade quality and used as is. The concentrated hydrogen peroxide solution was kept at -5°C during storage and fresh solutions were always prepared immediately before oxidation reactions were carried out. Sodium chloride (99+%, NaCl, Aldrich) and sodium perchlorate (99+%, $NaClO_4$, Sigma-Aldrich) were of reagent grade quality. Concentrated perchloric acid (70 % w/w, $HClO_4$, 1L = 1.68 kg, MERCK) and hydrochloric acid (HCl, Aldrich) were used for acid dilutions. All aqueous solutions were made with ultra pure de-ionised Milli-Q water (MQ > 18 MΩ).

6.2.2   Apparatus and reaction kinetics

Kinetic experiments performed at the University of Erlangen-Nürnberg and carried out with the following specifically equipped UV-visible spectrophotometers. A Specord S600 (Analytikjena) rapid scan spectrophotometer was used to follow spectral changes in the UV-Visible range 200-600 nm. Slow reactions measured at a single wavelength were performed on a Shimadzu UV-2010PC diode array spectrophotometer. Both instruments were equipped with a thermoelectrically controlled cell holder and 1 cm tandem-cell quartz cuvettes were used. Slow reactions at elevated pressures were also performed on a Shimadzu UV-2010PC diode array spectrophotometer that was equipped with a high pressure cell that housed a capillary-box quartz-cuvette (1.5 cm). Fast reactions at elevated pressure were performed on a laboratory-made high-pressure stopped-flow instrument.[15] The temperature was controlled and maintained in these instruments at 35°C to within ±0.1°C using a circulating water bath (Julabo MP-5). The experimentally obtained rate constants (k_{obs}) for fast reactions were calculated from the average of at least four to five kinetic runs and are reproducible to within ±5%.

Kinetic experiments performed at the University of Stellenbosch to study slow reactions at fixed wavelengths were performed on a GBC Cintra 10e diode array spectrophotometer. Spectra were collected between 200-600 nm on a single beam Agilent 8453E rapid scan (Agilent Technologies) spectrophotometer, regulated and maintained to within ±0.1°C of the selected temperature, using circulating water connected to a Julabo heater (Julabo LABORTECHNIK GMBH). The UV-visible spectra were collected in 0.5 cm single-cell quartz cuvettes.

Stock solutions of 1 mM or 10 mM $[PtCl_4]^{2-}$ were prepared in 1.0 M HCl, from which further dilutions were made. Aquation of $[PtCl_4]^{2-}$ is minimal and in chloride concentrations > 0.1 M, all Pt(II) essentially exists as $[PtCl_4]^{2-}$.[16] The rate of the reaction was followed by measuring the absorbance increase at 261 or 350 nm. Hydrogen peroxide was always present in large excess with regards to the substrate to ensure pseudo-order reaction conditions.

6.3   Results and discussion

6.3.1   UV-visible spectra and species identification

The complexes $[PtCl_6]^{2-}$, $[PtCl_5(H_2O)]^-$ and *trans*-$[PtCl_4(H_2O)_2]$ were all considered as possible oxidation products. The electronic spectra and molar absorptivities (ε) of all these species were previously reported and is used in this study to calculate Pt concentrations from the Beer-Lambert law.[17-20] Five characteristic absorption bands are observed in the UV-visible spectra of $[PtCl_4]^{2-}$. Only the d-d transitions at 331 ($\varepsilon_{331} = 59$ cm^{-1}M^{-1}) and 390 ($\varepsilon_{390} = 56$ cm^{-1}M^{-1}) were used to calculate the concentration (Figure 6.1A). Oxidation of $[PtCl_4]^{2-}$ in hydrochloric acid results in an absorbance increase at all wavelengths (200-600 nm) except for the region between 222 nm and 236 nm, where isosbestic points are observed (Figure 6.1B). Practically no $[PtCl_5(H_2O)]^-$ or *trans*-$[PtCl_4(H_2O)_2]$ was detected by evaluation of the region 200-230 nm (Figure 6.1B), since $[PtCl_6]^{2-}$ has a much lower molar absorptivity at 230 nm ($\varepsilon_{230} = 3300$ cm^{-1}M^{-1})[18] compared to $[PtCl_5(H_2O)^-]$ ($\varepsilon_{230} = 12500$ cm^{-1}M^{-1})[18] and *trans*-$[PtCl_4(H_2O)_2]$ ($\varepsilon_{230} = 22000$ cm^{-1}M^{-1}).[19] Hexachloro-platinum(IV) has maximum absorbance bands at $\varepsilon_{262} = 24500$ cm^{-1}M^{-1}, $\varepsilon_{353} = 490$ cm^{-1}M^{-1}

and $\varepsilon_{453} = 50$ cm^{-1}M^{-1} (Figure 6.1A).[20] For this reason the change in absorbance after oxidation of low concentrations of $[PtCl_4]^{2-}$ (< 0.1 mM) was examined at 262 nm, and for higher concentrations of $[PtCl_4]^{2-}$ (> 0.1 mM) at 350 nm. In some experiments higher hydrogen peroxide concentrations (> 0.05 M) were used relative to Pt(II) (< 0.05 mM), in order to observe specific reaction orders. Evaluation of the 200-230 nm region in such cases was not possible since hydrogen peroxide absorbs strongly in this region and exceeds the useful absorbance range of the UV-visible spectrophotometer. In such cases the concentration was calculated from the change in absorbance at 262 nm compared to the expected (calculated) fraction of $[PtCl_6]^{2-}$. The difference from the total expected $[PtCl_6]^{2-}$ was ascribed to $[PtCl_5(H_2O)]^-$.

(A)

(B)
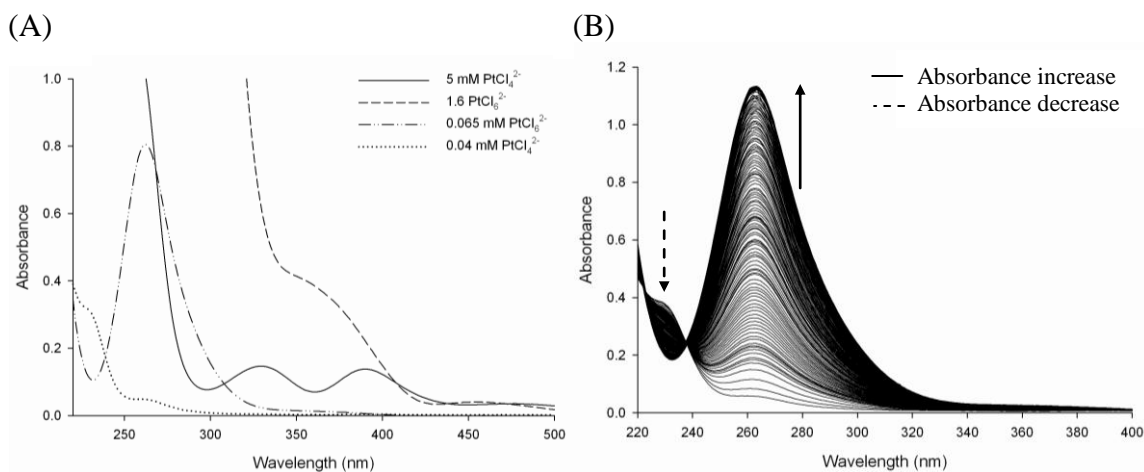
Figure 6.1: **(A)** UV-visible spectra of various concentrations of $[PtCl_4]^{2-}$ and $[PtCl_6]^{2-}$. **(B)** Oxidation of a 0.05 mM $[PtCl_4]^{2-}$ solution with 2.5 mM H_2O_2 in 1 M HCl.

6.3.2 Preliminary oxidation experiments of tetrachloroplatinate(II) with hydrogen peroxide in hydrochloric acid

Oxidation of $[PtCl_4]^{2-}$ with hydrogen peroxide in hydrochloric acid (1 mM [Pt(II)]; 100 mM $[H_2O_2]$; 1 M [HCl]) results in the characteristic spectrum of $[PtCl_6]^{2-}$ in the visible region (300-500 nm) shown in Figure 6.2A, as a result of reaction 6.1.

$$Pt(II) + H_2O_2 \rightarrow Pt(IV) + 2OH^- \qquad (6.1)$$
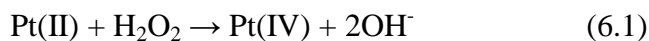
An absorbance versus time plot at 350 nm (Figure 6.2B) resembles that of a first-order reaction, for the duration of the whole reaction but reaches equilibrium abruptly (after ~1300 s) so that a first-order rate law cannot define the kinetics accurately. No isosbestic points were observed and evaluation of the final spectra at 350 nm, correlate with the formation of $[PtCl_6]^{2-}$ exclusively. No evidence for the formation of $[PtCl_5(H_2O)]^-$ or *trans*-$[PtCl_4(H_2O)_2]$ could be found in the UV-visible spectra.

(A) (B)
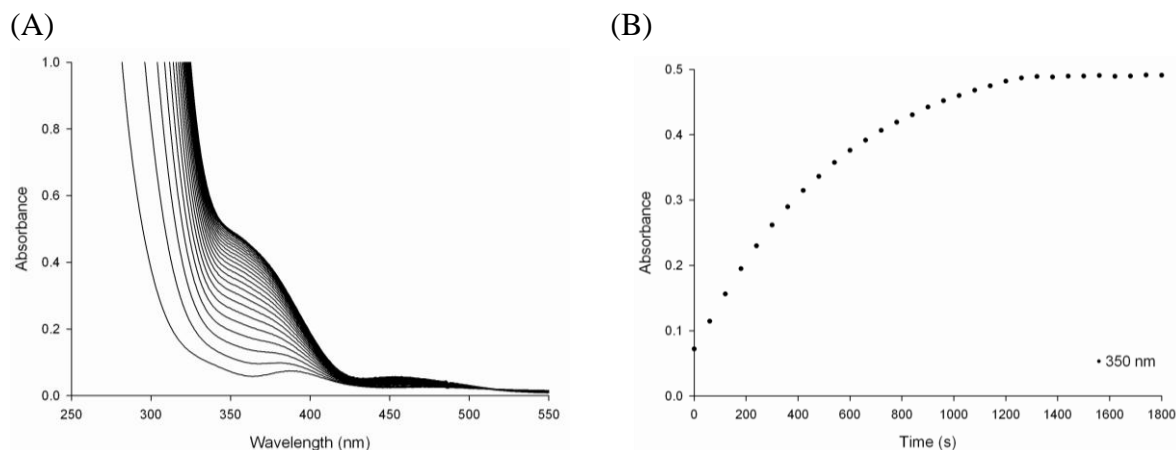
Figure 6.2: (A) UV-visible spectra of 1 mM $[PtCl_4]^{2-}$ oxidized with 100 mM H_2O_2 in 1 M HCl as a function of time. **(B)** Change in absorbance as a function of time at a single wavelength (350 nm).

A systematic study was carried out to determine the rate determining factors and the origin of the unknown reaction order observed in Figure 6.2B. The experimental design used for the kinetic experiments is summarized in Table 6.1.

Table 6.1: Comparison of the Pt(II) and H_2O_2 concentrations used in the UV-visible experiments and the resulting rate constants obtained.

$[PtCl_4]^{2-}$ (mM)	$[H_2O_2]$ (M)	k_{obs} (s^{-1})	$k_1 = k_{obs}/[oxidant]$ (M^{-1}s^{-1})
2	0.100	1.85×10^{-3}	1.85×10^{-2}
1.5	0.100	1.81×10^{-3}	1.81×10^{-2}
1	0.200	3.53×10^{-3}	1.77×10^{-2}
1	0.175	3.09×10^{-3}	1.77×10^{-2}
1	0.150	2.58×10^{-3}	1.72×10^{-2}
1	0.125	2.30×10^{-3}	1.84×10^{-2}
1	0.100	1.75×10^{-3}	1.75×10^{-2}
0.5	0.100	1.95×10^{-3}	1.95×10^{-2}

The reaction order with respect to hydrogen peroxide was determined by oxidizing 1 mM $[PtCl_4]^{2-}$ with five different concentrations of hydrogen peroxide under pseudo first-order conditions (100-200 mM $[H_2O_2]$) (Figure 6.3A). The order with respect to Pt(II) was determined by oxidizing four different concentrations of $[PtCl_4]^{2-}$ (0.5-2.0 mM) with a constant hydrogen peroxide concentration (100 mM H_2O_2) under pseudo first-order conditions (Figures 6.3B). All the kinetic traces obtained, display the unusual reaction order, seemingly first-order but levelling off abruptly. To quantify a comparison between oxidation rates, preliminary rate constants were obtained by fitting a first-order rate law (6.2), to the data points for which a change in absorbance is observed. The pseudo first-order rate constant k_1 was calculated from Equation 6.3. The rate parameters calculated in this manner is listed in Table 6.1. It must be stressed that since, it is obvious that a first-order rate constant does not define the traces observed here entirely, the calculated values only serve as relative rate constants, for comparison of relative reaction rates and not absolute values.

$$d[Pt^{IV}]/dt = -d[Pt^{II}]/dt = k_1[Pt^{II}][H_2O_2] \tag{6.2}$$

$$k_1 = k_{obs}[H_2O_2]^{-1} \tag{6.3}$$

(A)   (B)
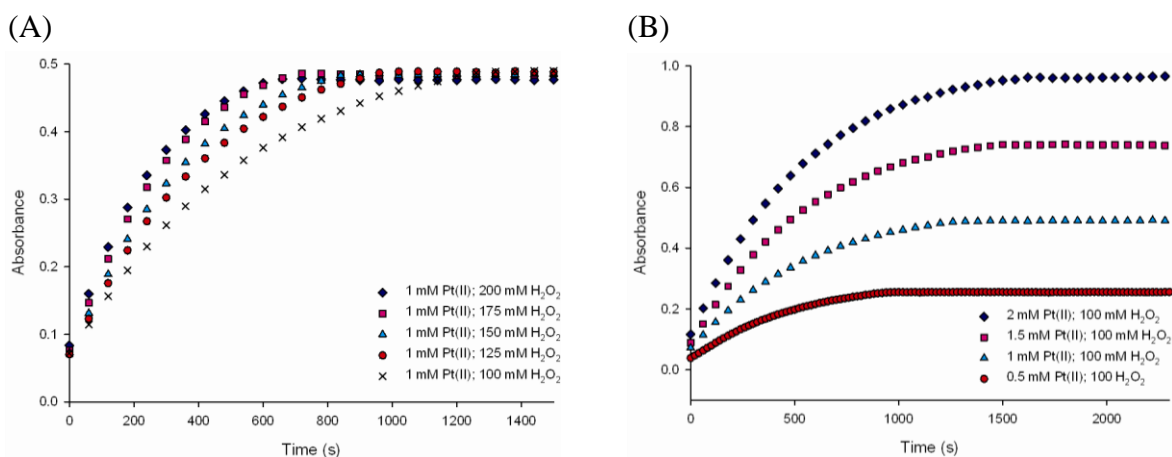
Figure 6.3: Absorbance *vs*. time traces for different concentrations of **(A)** $[H_2O_2]$ and **(B)** $[PtCl_4]^{2-}$ (at 350nm).

A plot of k_{obs} (s^{-1}) as a function of $[H_2O_2]$ is linear with zero intercept, indicating first-order rate dependence with respect to hydrogen peroxide (Figure 6.4). The pseudo first-order rate

constant at a specific concentration of $[H_2O_2]$ may be estimated from expression 6.3 or alternatively the average value $k_1 = (1.77 \pm 0.4) \times 10^{-2}$ $M^{-1}s^{-1}$, was obtained from the slope in Figure 6.4 and relates the rate of the reaction to the reactant concentration in this range. No specific correlation was found between k_{obs} and the Pt(II) concentration.
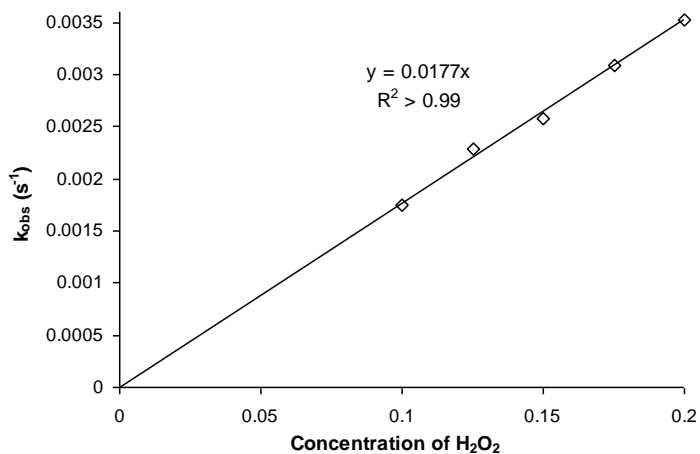
Figure 6.4: A plot of the k_{obs} (s^{-1}) values obtained from oxidation of 1 mM Pt(II) with different hydrogen peroxide concentrations (0.1-0.2 M). The zero intercept indicate first-order rate dependence with respect to the hydrogen peroxide concentration.

In order to get a better understanding of the rate limiting conditions, oxidation of $[PtCl_4]^{2-}$ (0.02 - 0.1 mM) was carried out over a wide range of H_2O_2 concentrations (2 - 200 mM). A perplexing trend emerged from these experiments. If 0.02 mM $[PtCl_4]^{2-}$ is oxidized with 2 mM H_2O_2, the reaction is essentially first-order in character. If the H_2O_2 concentration is increased to 16 mM, the apparent order of the reaction changes and an absorption 'bump' (Figure 6.5A; 16 mM $[H_2O_2]$) is observed before equilibrium is reached. Increasing the H_2O_2 concentration to 50 mM results in an absorbance decrease and the absorbance 'bump' becomes more defined (Figure 6.5A; 50 mM $[H_2O_2]$). With 100 mM $[H_2O_2]$ the order of the reaction changes again, and the kinetic trace is almost perfectly linear (Figure 6.5A; 100 mM $[H_2O_2]$). It is striking that the final absorbance of the respective traces in Figure 6.5A are very different even if the $[PtCl_4]^{2-}$ concentration is kept constant at 0.02 mM. A comparison of the final spectra obtained for the respective reactions is shown in Figure 6.5B.

The electronic UV-visible spectrum of $[PtCl_5(H_2O)]^-$ has been reported before with an absorbance maximum at 230 and 255 nm.[18]. The small hypsochromic shift with respect to the absorbance maximum peak of $[PtCl_6]^{2-}$ is observed with increased concentration of hydrogen peroxide shown in Figure 6.5B. An absorbance increase at 230 nm is also evident suggesting formation of more $[PtCl_5(H_2O)]^-$ in these solutions. Formation of a significant amount of *trans*-$[PtCl_4(H_2O)_2]$ must be excluded due to the large absorbance at $\varepsilon_{230} = 22000$ cm^{-1}M^{-1} of this species.[19] At wavelengths below 250 nm, hydrogen peroxide (> 50 mM) unfortunately absorbs strongly masking all other absorbances in this range. The UV-visible spectra of such solutions is therefore not shown only for values > 250 nm. In such cases the concentration of $[PtCl_6]^{2-}$ were determined at 262 nm, and the deficit with respect to total Pt(IV) concentration were assigned to $[PtCl_5(H_2O)]^-$. The absorbance *versus* time data obtained in this concentration range fluctuated so much smooth traces could not be obtained (Figure 6.5A). The data was also found to be very irregular and the spectra could not be reproduced to within a 5 % error.

(A)   (B)
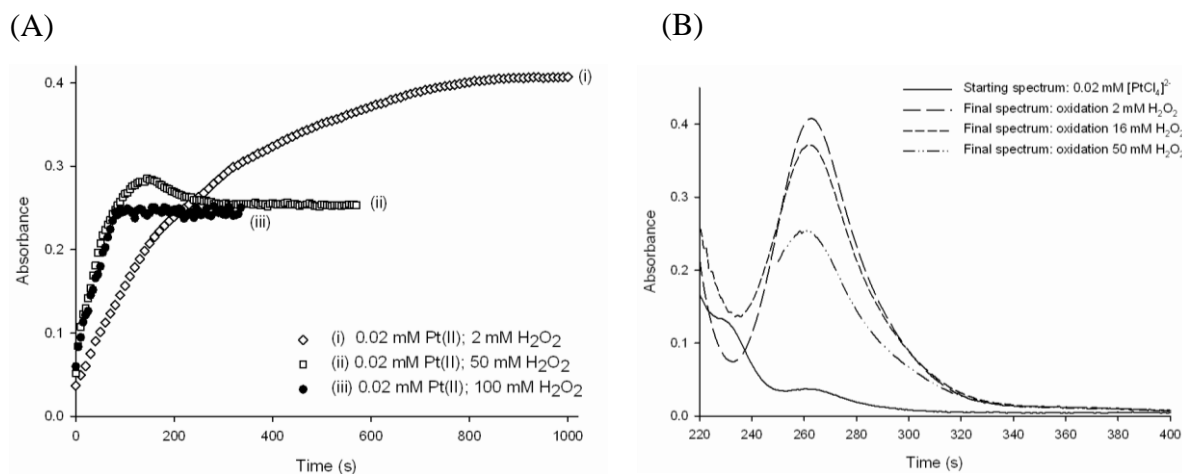
Figure 6.5: (A) The change in reaction order at 262 nm is illustrated by varying the H$_2$O$_2$ concentration between 2 mM and 100 mM while the $[PtCl_4]^{2-}$ concentration is kept constant at 0.02 mM. **(B)** The final UV-visible spectra (220-400 nm) of the kinetic traces shown in (A) are compared.

Pseudo first-order kinetics have been reported by Hindmarsh[12] for the oxidation of $[PtCl_4]^{2-}$ with H$_2$O$_2$ in perchloric acid and a first-order dependence with respect to both Pt(II) and H$_2$O$_2$ were determined. The change-over from pseudo first-order (2 mM H$_2$O$_2$) to pseudo zero-order (100 mM H$_2$O$_2$) kinetics observed here, suggests a similar mechanism of oxidation at low H$_2$O$_2$ concentrations. However, a different mechanism that accounts for

zero-order kinetics is evident at higher H_2O_2 concentrations. The decrease in the formation of $[PtCl_6]^{2-}$ as the result of the formation of more $[PtCl_5(H_2O)]^-$ also suggests at least two different reaction mechanisms depending on the H_2O_2 concentration.

The kinetic 'bump' which forms between first- and zero-order kinetics is quite puzzling (Figure 6.5A). It may indicate formation of an intermediate species which subsequently decomposes to form the final reaction product(s) in a two-step process. In this regard, formation of an intermediate Pt(III) species has been suggested for various oxidation reactions,[12] notably also during irradiation of $[PtCl_6]^{2-}$ with light.[21] Such reactions are often associated with radical formation, and rapid chain-reactions which may account for the unusual kinetic traces observed in this study. It was therefore of interest to determine whether light has an effect on the reaction rates in these solutions, especially since the kinetic traces discussed thus far had been acquired with a rapid scan spectrophotometer, which essentially irradiates the solution with light in the 200-600 nm range each time a measurement is made.

6.3.3   Photo-kinetic effect induced by the spectrophotometer

The kinetic trace of the oxidation of 0.03 mM $[PtCl_4]^{2-}$ by 50 mM H_2O_2 was determined using two different spectrophotometers. In the first case, the change in the UV-visible spectrum was monitored over the wavelength range of 200-600 nm, with a rapid-scan instrument by recording a spectrum every five seconds. The change in absorbance at 262 nm is indicated in Figure 6.6, showing the kinetic 'bump' in the trace (A). In the second case, a measurement was taken every two seconds with a diode-array spectrophotometer fitted with a monochromator that excluded all radiation except for 262 nm from the solution. A perfect zero-order trace (B) was obtained also shown in Figure 6.6. It is clear that very different results are obtained with the respective acquisition methods even though exactly the same experimental conditions were used. This confirms that light plays a significant role in these oxidation reactions.
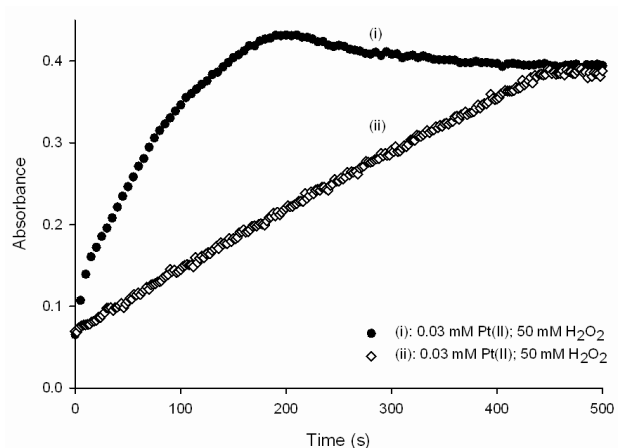
Figure 6.6: Kinetic traces acquired by the full wavelength (200-600 nm) rapid scan method compared to that obtained by scanning a single wavelength (262 nm) for the oxidation of $[PtCl_4]^{2-}$ with H_2O_2 in 1 M HCl.

The rapid scan instrument clearly acts as a light source resulting in photo-excitation of species in solution each time that a spectrum is acquired. The exact mechanism of formation of the 'bump' in the kinetic trace is unclear but possibly relates to (1) light-induced activation of ligand exchange and/or aquation *via* an Pt(III) intermediate and (2) possible $[PtCl_4]^{2-}$ assisted ligand exchange.

It has been shown that both chloride anation of $[PtCl_5(H_2O)]^-$ and aquation of $[PtCl_6]^{2-}$ can be accelerated by light according to reaction 6.4.[14, 22]

$$[PtCl_5(H_2O)]^- + Cl^- \xrightleftharpoons{h\nu} [PtCl_6]^{2-} + H_2O \qquad (6.4)$$
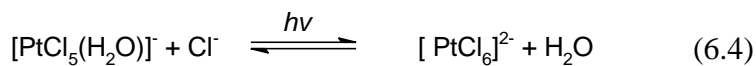
An increase in ligand exchange is also possible *via* Pt(II)–Pt(IV) associations according to the mechanism previously discussed in *Chapter 5*; *Section 5.3.1.*3 as defined by Mason.[13]

As a result of the limited scope of this study, a more in-depth investigation of the interesting light-induced reactions could not be studied further at this time. Nevertheless, it is clear that in the presence of light irradiations the oxidation of $[PtCl_4]^{2-}$ is considerably complicated.

6.3.4 Kinetics of tetrachloroplatinate(II) oxidation under conditions which exclude photo-induced reactions

6.3.4.1 Oxidation of high concentration (0.2-1.0 mM) tetrachloroplatinate(II): first-order kinetics

All the kinetic reactions shown in section 6.3.3 were studied under conditions of light irradiation. In this section photo-induced reactions were excluded, by measuring the change in absorbance at a single wavelength only, keeping the solution effectively in the "dark". Different reaction orders are observed (*vide infra*) for oxidation of high (0.2 – 1.0 mM) and low (0.07 – 0.03 mM) Pt(II) concentration. To avoid confusion the results are discussed separately for conditions of high and low Pt(II) concentration.

The hydrogen peroxide concentration dependence was monitored in the range 15-300 mM to get a better understanding of the rate determining parameters. Hydrogen peroxide was always in excess with respect to the substrate (> 15 time excess). The concentrations of the experimental design are listed in Table 6.2, while the absorption *versus* time traces at 350 nm are shown in Figures 6.7A-C.

Table 6.2: Rate constants for the oxidation of high concentration of $[PtCl_4]^{2-}$ (0.2 - 1.0 mM) in 1 M HCl at 35°C. The concentration ratios of $[PtCl_5(H_2O)]^-/[PtCl_6]^{2-}$ calculated from the final absorbance at 350 nm is also listed.

$[PtCl_4]^{2-}$ (mM)	$[H_2O_2]$ (mM)	$[PtCl_5(H_2O)]^-$ $/[PtCl_6]^{2-}$	k_{obs} (s^{-1})	$k_1 = k_{obs}/[ox]$ (M^{-1}s^{-1})
1.0	300	0.34	3.94×10^{-3}	1.31×10^{-2}
1.0	100	0.21	1.52×10^{-3}	1.52×10^{-2}
1.0	50	0.14	0.81×10^{-3}	1.62×10^{-2}
1.0	15	0.14	0.30×10^{-3}	2.00×10^{-2}
0.6	300	0.24	4.49×10^{-3}	1.50×10^{-2}
0.6	100	0.17	1.57×10^{-3}	1.57×10^{-2}
0.6	50	0.14	0.78×10^{-3}	1.56×10^{-2}
0.6	15	0.14	0.23×10^{-3}	1.53×10^{-2}
0.2	300	0.89	3.84×10^{-3}	1.28×10^{-2}
0.2	100	0.45	1.27×10^{-3}	1.27×10^{-2}
0.2	50	0.33	0.74×10^{-3}	1.48×10^{-2}
0.2	15	0.23	0.23×10^{-3}	1.53×10^{-2}

Since the full absorption spectra were not acquired in these experiments, the concentration of $[PtCl_6]^{2-}$ was estimated from the observed and calculated change in absorbance at 350

nm. The difference between the total expected $[PtCl_6]^{2-}$ concentration is due to the hypsochromic shift at 350 nm (similar to that shown in Figure 6.5B) and is reasonably assumed to be due to formation of $[PtCl_5(H_2O)]^-$. The calculated ratios of $[PtCl_5(H_2O)]^-$ /$[PtCl_6]^{2-}$ to account for the total Pt(IV) concentration are indicated in Table 6.2.
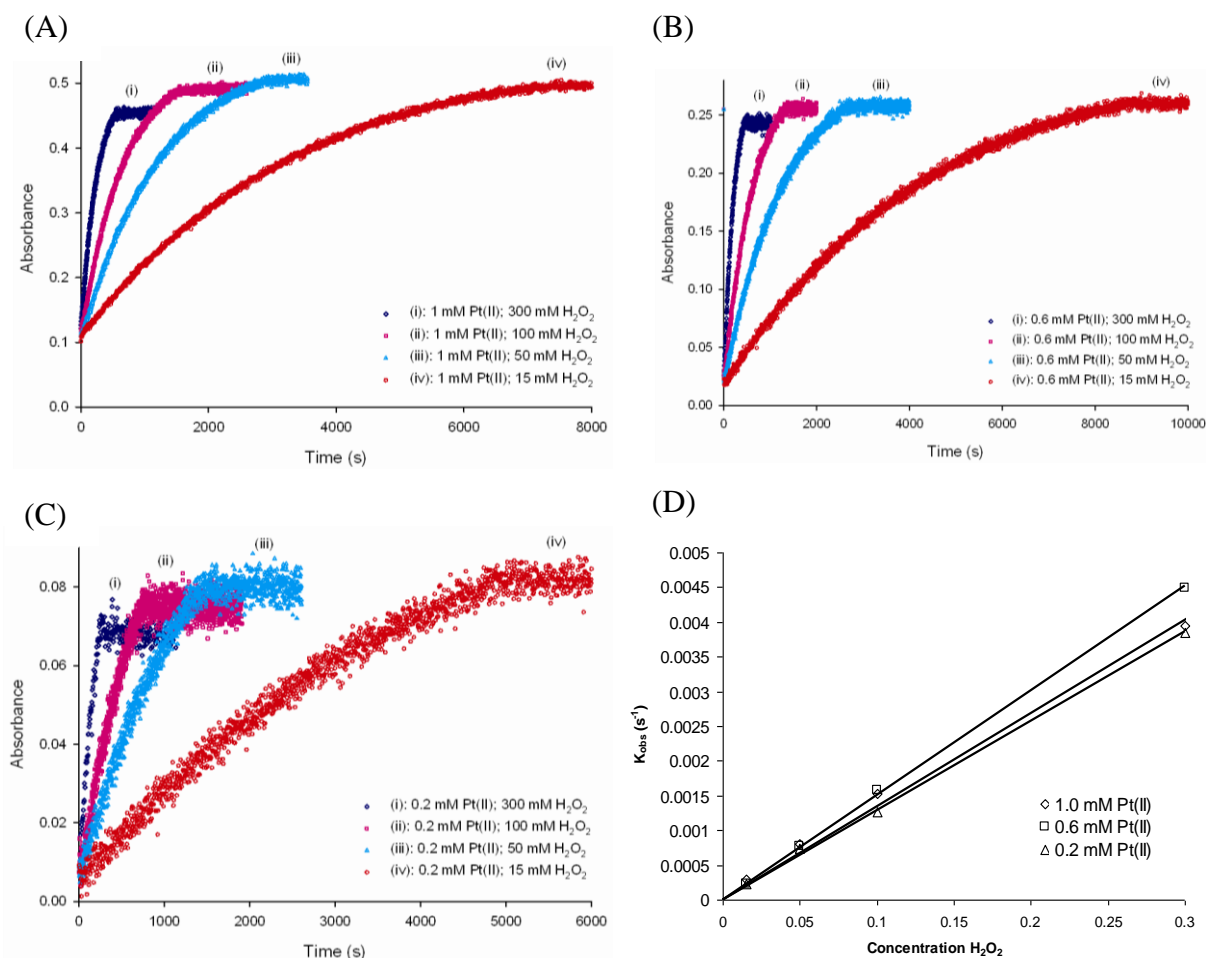
Figure 6.7: (A) Oxidation of 1 mM, **(B)** 0.6 mM and **(C)** 0.2 mM $[PtCl_4]^{2-}$ with H_2O_2 in the concentration range 15-300 mM at 35°C and measured only at 350 nm. **(D)** Plots of k_{obs} (s^{-1}) as a function of H_2O_2 concentration.

Similar to the kinetics observed under conditions of light irradiation, a change in reaction order is observed for oxidation of $[PtCl_4]^{2-}$ in the concentration range 0.2-1.0 mM. The kinetic traces in Figures 6.7 suggest that oxidation is seemingly a first-order kinetic process, but then reaches an abrupt end-point, with the trends levelling off. Rate constants were obtained as before, by applying the first-order rate law 6.2 to data points for which the absorbance change was observed. The first-order rate constants k_{obs} (s^{-1}) obtained in this

manner are listed in Table 6.2. Plots of the k_{obs} values *versus* the H_2O_2 concentration for the various Pt(II) concentrations are linear with a zero intercept, indicating a first-order dependence on oxidant and substrate in this concentration range. The pseudo first-order rate constants k_1 ($M^{-1}s^{-1}$) for a specific Pt(II) concentration were calculated from expression 6.3 and the average values from the slope of the lines for [Pt(II)] = 1 mM, k_1 = (1.3 ± 0.3) x 10^{-2} $M^{-1}s^{-1}$; [Pt(II)] = 0.6 mM, k_1 = (1.51 ± 0.03) x 10^{-2} $M^{-1}s^{-1}$; [Pt(II)] = 0.2 mM, k_1 = (1.3 ± 0.1) x 10^{-2} $M^{-1}s^{-1}$) were obtained. The rate constants determined in this manner are slightly lower i.e. [Pt(II)] = 1 mM, [H_2O_2] = 100 mM, k_1 = 1.75 x 10^{-2} (Table 6.1) *versus* 1.52 x 10^{-2} $M^{-1}s^{-1}$ (Table 6.2), which confirms slower overall oxidation rates in the absence of light.

6.3.4.2 Oxidation of low concentration (0.03-0.07 mM) tetrachloroplatinate(II): zero-order kinetics

Oxidation reactions under these conditions were chosen such that a zero-order kinetic trend was always observed. This can be achieved for the oxidation of $[PtCl_4]^{2-}$ in the concentration range of 0.03-0.07 mM with concentrations of excess H_2O_2 in the range 40-100 mM. The calculated ratios of $[PtCl_5(H_2O)]^-/[PtCl_6]^{2-}$ to account for the total Pt(IV) concentration are indicated in Table 6.3 and were calculated from the final absorbance at 262 nm. The experimental design of the Pt(II) and H_2O_2 concentrations are listed in Table 6.3 and resulting absorbance *versus* time traces are shown in Figures 6.8A-E.

Table 6.3: Pseudo zero-order rate constants, k_0 (s^{-1}) calculated from Figures 6.8A-E for the oxidation of low concentration $[PtCl_4]^{2-}$ (0.03 – 0.07 mM) in 1 M HCl (35°C). The concentration ratios of $[PtCl_5(H_2O)]^-/[PtCl_6]^{2-}$ were calculated from the final absorbance at 262 nm is also listed.

$[PtCl_4]^{2-}$ (mM)	$[H_2O_2]$ (mM)	$[PtCl_5(H_2O)]^-$ $/[PtCl_6]^{2-}$	k_{obs}^0 (Ms^{-1})	$k_0 =$ $k_{obs}^0/[oxidant]$ (s^{-1})
0.07	100	4.70	8.38 x 10^{-8}	8.38 x 10^{-7}
0.07	70	4.27	6.15 x 10^{-8}	8.79 x 10^{-7}
0.07	60	4.16	5.77 x 10^{-8}	9.62 x 10^{-7}
0.07	50	4.04	4.59 x 10^{-8}	9.18 x 10^{-7}

Table 6.3 continued from the previous page.

0.07	40	3.98	4.17×10^{-8}	1.04×10^{-6}
0.06	100	3.70	8.58×10^{-8}	8.58×10^{-7}
0.06	70	3.55	6.50×10^{-8}	9.29×10^{-7}
0.06	60	3.34	5.61×10^{-8}	9.35×10^{-7}
0.06	50	3.17	4.82×10^{-8}	9.64×10^{-7}
0.06	40	3.01	3.92×10^{-8}	9.80×10^{-7}
0.05	100	3.74	7.86×10^{-8}	7.86×10^{-7}
0.05	70	3.58	6.46×10^{-8}	9.23×10^{-7}
0.05	60	3.50	5.44×10^{-8}	9.07×10^{-7}
0.05	50	3.58	4.47×10^{-8}	8.94×10^{-7}
0.05	40	3.50	3.77×10^{-8}	9.43×10^{-7}
0.04	100	4.02	7.42×10^{-8}	$8.38 \times 1 0^{-7}$
0.04	70	3.80	5.41×10^{-8}	8.79×10^{-7}
0.04	60	3.90	4.74×10^{-8}	9.62×10^{-7}
0.04	50	3.77	4.01×10^{-8}	9.18×10^{-7}
0.03	100	4.64	7.10×10^{-8}	7.10×10^{-7}
0.03	70	4.45	5.04×10^{-8}	7.20×10^{-7}
0.03	60	4.17	4.50×10^{-8}	7.50×10^{-7}

The zero-order rate law is expressed by equation 6.5 with the observed zero-order rate constant k_{obs}^{0} (Ms^{-1}) obtained directly from the slope of concentration *versus* time plots (also listed in Table 6.3).

$$-d[Pt(II)]/dt = k_0 [H_2O_2] = k_{obs}^{0} (Ms^{-1}) \qquad (6.5)$$

Plots of k_{obs}^{0} *versus* the H_2O_2 concentration were linear with an intercept close to zero (~1.0 x 10^{-8} Ms^{-1} Figure 6.8F). The pseudo zero-order rate constant k_0 (s^{-1}) was calculated from Expression 6.6.

$$k_0 = k_{obs}^{0} [H_2O_2]^{-1} \qquad (6.6)$$

The average k_0 value at a specific Pt(II) concentration was calculated from the slope of the lines [Pt(II)] = 0.07 mM, $k_0 = (7.1 \pm 0.8) \times 10^{-7}$ s^{-1}; [Pt(II)] = 0.06 mM, $k_0 = (7.7 \pm 0.5) \times 10^{-7}$ s^{-1}; [Pt(II)] = 0.05 mM, $k_0 = (6.9 \pm 0.6) \times 10^{-7}$ s^{-1}; [Pt(II)] = 0.04 mM, $k_0 = (6.8 \pm 0.3) \times 10^{-7}$ s^{-1} and [Pt(II)] =(0.03 mM, $k_0 = (6.6 \pm 0.2) \times 10^{-7}$ s^{-1}. The average value for all the Pt(II) concentrations is $k_0 = (7.0 \pm 0.8) \times 10^{-7}$ s^{-1}. A plot of k_{obs}^{0} *versus* [Pt(II)] shows no

correlation as can be expected. The reaction is therefore first-order with respect to the H_2O_2 concentration and zero-order with respect to the Pt(II) concentration.
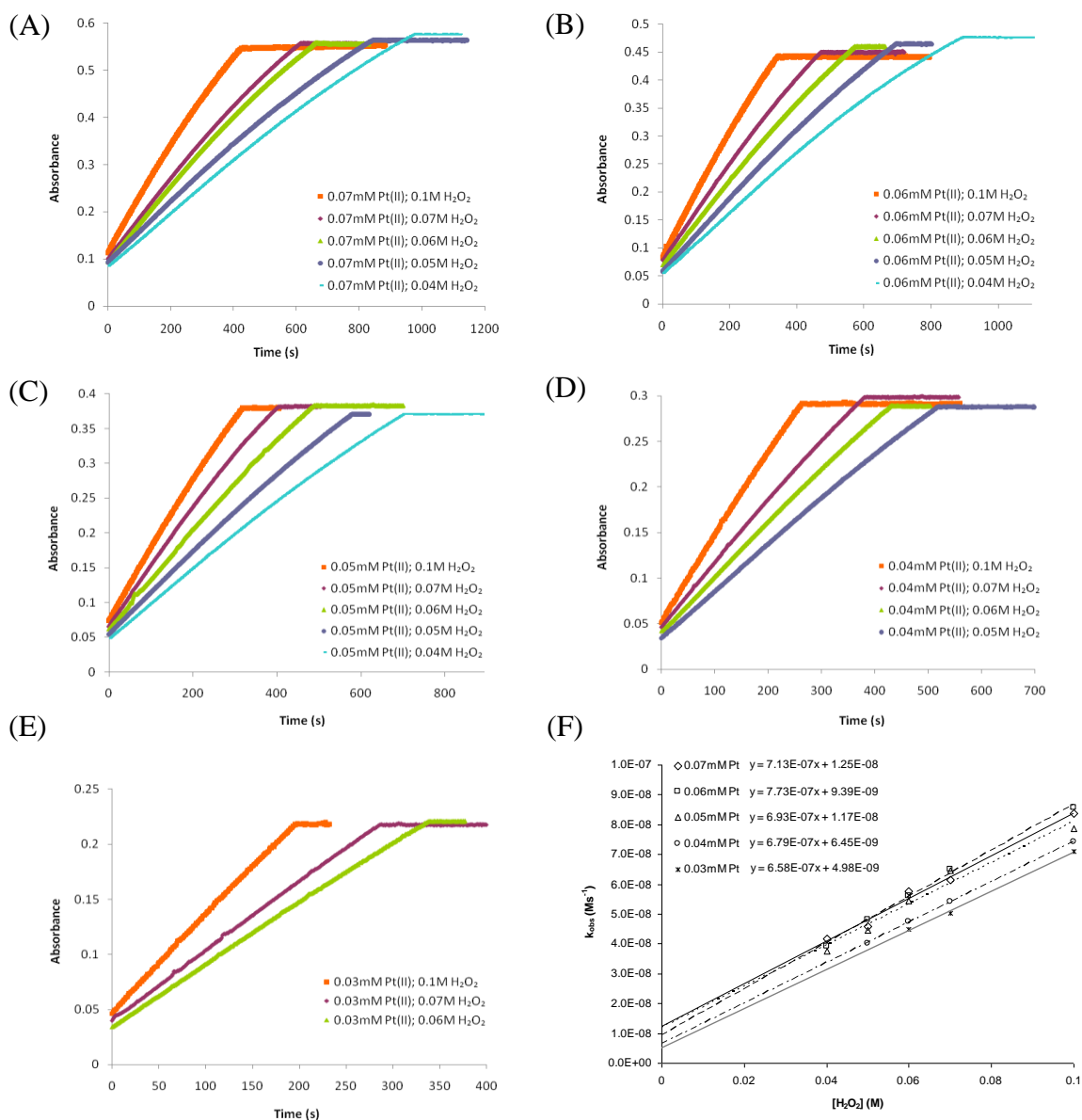
Figure 6.8: Oxidation of **(A)** 0.07 mM **(B)** 0.06 mM **(C)** 0.05 mM **(D)** 0.04 mM and **(E)** 0.03 mM $[PtCl_4]^{2-}$ **(F)** Plots of k_{obs}^{0} as a function of $[H_2O_2]$ showing the linear dependence with respect to $[H_2O_2]$ (35°C; 262 nm).

Oxidation of 0.03-0.07 mM $[PtCl_4]^{2-}$ in 1 M HCl with excess hydrogen peroxide (40-100 mM), exhibit zero-order kinetics exclusively. Reactions which display zero-order kinetics typically indicate the action of a catalyst that remains constant for the duration of the reaction. Formation of hydroxyl radicals has been suggested to account for zero-order

kinetics observed for the oxidation of $[PtCl_4]^{2-}$ with peroxydisulfate $(S_2O_8^-)$.[12] Apparent "catalytic" oxidation of $[PtCl_4]^{2-}$ is also possible *via* formation of other highly oxidative species such as Cl_2 or HOCl which may form during reaction of H_2O_2 with HCl. The idea of formation of a catalyst or catalyst-like species to account for the zero-order kinetics was investigated in more detail by varying the H^+ and Cl^- concentrations in various kinetic experiments.

6.3.4.3 Influence of chloride and acid on the reaction order

The oxidation rate dependence on acid concentration was determined by keeping the $[PtCl_4]^{2-}$, H_2O_2 and Cl^- concentrations constant while varying the acid concentration as a function of different perchloric acid to sodium perchlorate ratios ($HClO_4/NaClO_4$), thereby ensuring a constant ionic strength. Absorbance *versus* time plots (at 350 nm) generated essentially linear slopes (Figure 6.9A) and values of the observed zero-order rate constants (k_{obs}^0) for the acid dependence were obtained from the slope of Pt(IV) concentration *versus* time plots. Pseudo zero-order rate constants (k_0) at specific concentrations were calculated from rate equation 6.6. In order to determine the oxidation rate dependence on chloride, concentrations of $[PtCl_4]^{2-}$, H_2O_2 and H^+ were kept constant, while varying $[Cl^-]$ as a function of different hydrochloric acid to perchloric acid ratios ($HCl:HClO_4$) ensuring that the ionic strength was kept constant at 1 M in all experiments.

For the chloride ion concentration dependence experiments, Pt(IV) concentration *versus* time plots and rate equation 6.6 was also used to estimate values of k_{obs}^0 and k_0 respectively. Since the order of the reaction changes as a function of $[Cl^-]$ (Figure 6.9B), only initial reaction rates (first 500 s) were used for these traces which that exhibit mixed-order kinetics (0.02 and 0.2 M $[Cl^-]$). Both plots of k_{obs}^0 *versus* $[H^+]$ (Figure 6.9C) and k_{obs}^0 *versus* $[Cl^-]$ (Figure 6.9D) are linear ($R^2 > 0.99$) with a small positive intercept, suggesting that k_{obs}^0 varies with $[H^+]$ and $[Cl^-]$ according to equation 6.8.

$$k_{obs}^0 = a + b[Q] \qquad (6.8)$$

where Q = [H^+] or [Cl^-] and a = 3.4 x 10^{-7} Ms^{-1} and b = 8.6 x 10^{-7} s^{-1}. The pseudo zero-order rate constants k^0 (s^{-1}) were obtained from the slope of these plots with [Cl^-] = 0.5 M; k^0 = (8.6 ± 0.2) x 10^{-7} s^{-1} and [H^+] = 1 M; k^0 = (8.2 ± 0.5) x 10^{-8} s^{-1}. This data is summarized in Table 6.4.
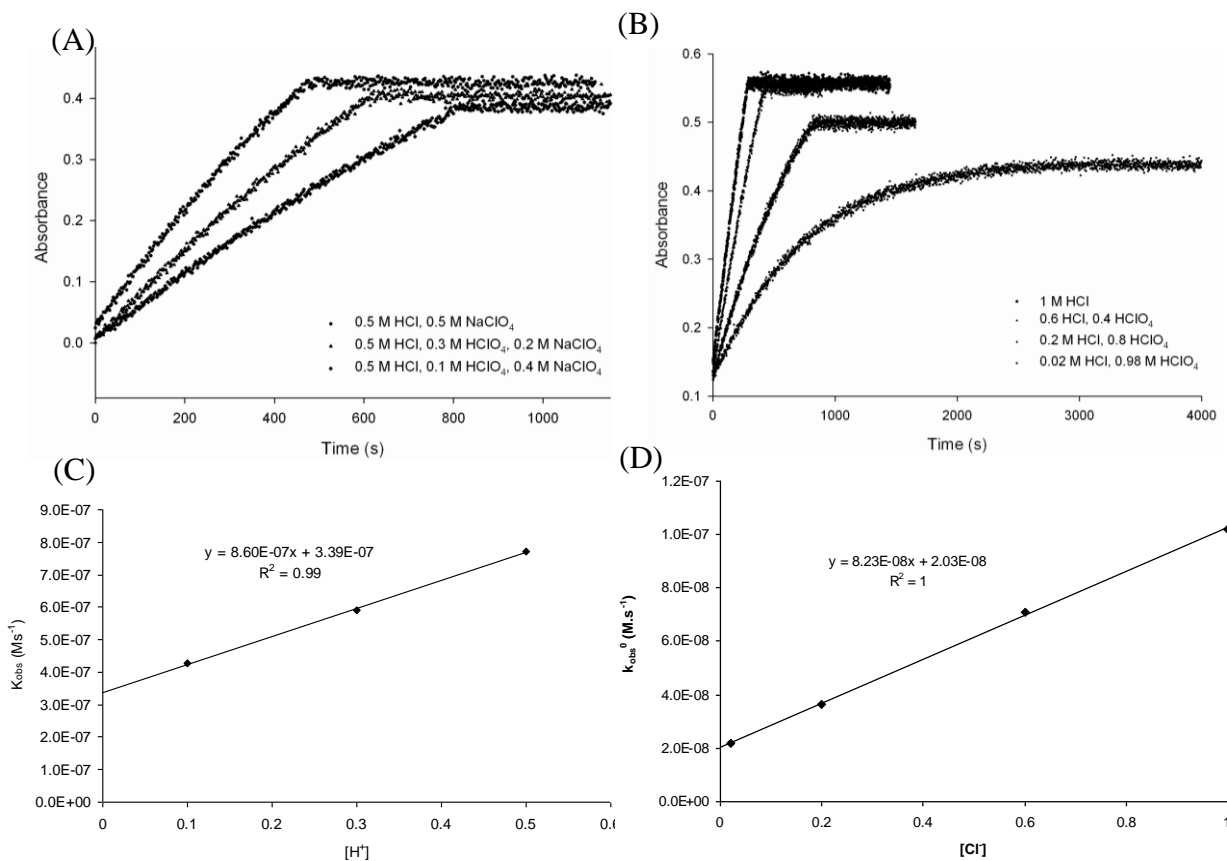
Figure 6.9: Oxidation of 0.04 mM [$PtCl_4$]$^{2-}$ in 0.5 M HCl with 80 mM H_2O_2 and various concentrations of (A) [H^+] and (B) [Cl^-]. (C) Plot of k_{obs}^0 (obtained from the traces in (A)) *versus* [H^+]. (D) Plot of k_{obs}^0 (obtained from the traces in (B)) *versus* [Cl^-].

Table 6.4: Estimated rate constants and activation parameters obtained from oxidation of 0.04 mM [$PtCl_4$]$^{2-}$ with 80 mM H_2O_2 at various concentrations of [H^+] and [Cl^-].

[$PtCl_4$]$^{2-}$ (mM)	[H_2O_2] (mM)	[HCl] (M)	[$HClO_4$] (M)	[$NaClO_4$] (M)	k_{obs}^0 (Ms^{-1})	$k_0 = k_{obs}^0/[H_2O_2]$ (s^{-1})
0.04	80	0.5	0.5	0	7.71 x 10^{-7}	9.64 x 10^{-6}
0.04	80	0.5	0.3	0.2	5.92 x 10^{-7}	7.40 x 10^{-6}
0.04	80	0.5	0.1	0.4	4.27 x 10^{-7}	5.34 x 10^{-6}
0.04	80	1	0	-	1.02 x 10^{-7}	1.28 x 10^{-6}
0.04	80	0.6	0.4	-	7.07 x 10^{-8}	8.84 x 10^{-7}
0.04	80	0.2	0.8	-	3.65 x 10^{-8}	4.56 x 10^{-7}
0.04	80	0.02	0.98	-	2.17 x 10^{-8}	2.71 x 10^{-7}

6.3.4.4 Oxidation as a function of temperature: activation enthalpy and entropy

Reaction conditions were chosen such that a first-order or zero-order reaction mechanism reasonably predominates. Oxidation of 1 mM $[PtCl_4]^{2-}$ with 300 mM H_2O_2, produces a kinetic trace which is essentially first-order in character (Figure 6.10A). A zero-order reaction is observed for the oxidation of 0.04 mM $[PtCl_4]^{2-}$ with 100 mM H_2O_2 (Figure 6.10B). Oxidation of 1 mM and 0.04 mM $[PtCl_4]^{2-}$ were carried out in the temperature range 15-35°C, to enable estimation of the activation parameters for first-order and zero-order kinetics. Both k_{obs} and k_{obs}^0 were estimated as described earlier for pseudo first- and zero-order reactions (from the rate laws 6.2 and 6.5). The associated first- (k_1) and zero-order (k_0) rate constants were subsequently calculated from equations 6.3 and 6.6 and these values are listed in Table 6.5.

(A)   (B)
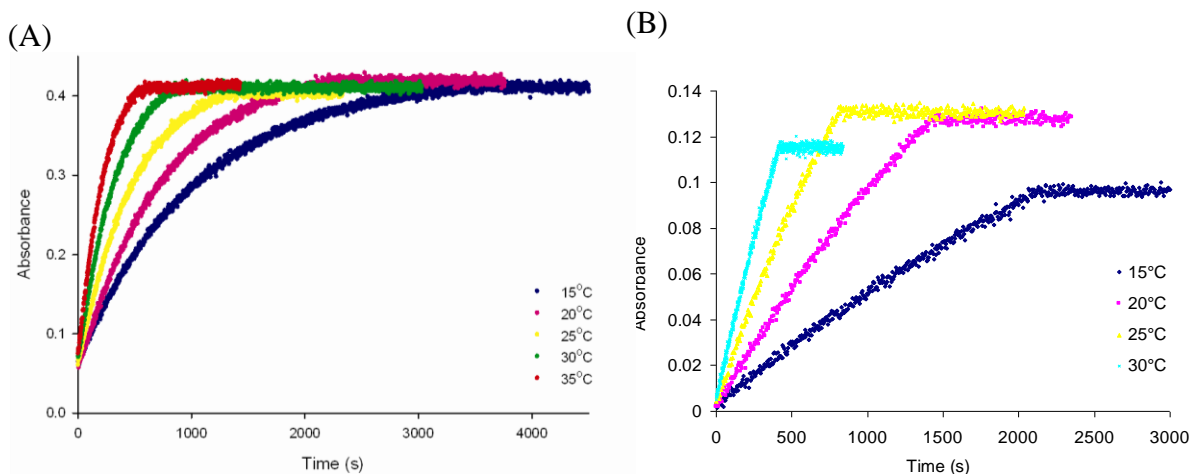
Figure 6.10: (A) Kinetic traces obtained from oxidation of 1 mM $[PtCl_4]^{2-}$ with 300 mM H_2O_2 (measured at 350 nm), and **(B)** 0.04 mM $[PtCl_4]^{2-}$ oxidized with 100 mM H_2O_2 (measured at 262 nm) at various temperatures.

Table 6.5: Estimated rate constants and activation parameters obtained from oxidation of 1 mM and 0.04 mM $[PtCl_4]^{2-}$ with 300 mM and 100 mM H_2O_2 respectively at various temperatures (15-35ºC).

$[PtCl_4]^{2-}$ (mM)	$[H_2O_2]$ (mM)	Temp. (°C)	k_{obs} (s^{-1})	k_1(s^{-1}M^{-1})	$\Delta H^{\ddagger}$ (kJmol^{-1})	$\Delta S^{\ddagger}$ (JK^{-1}mol^{-1})
1	300	15	0.95 x 10^{-5} s^{-1}	0.32 x 10^{-4} s^{-1}M^{-1}		
1	300	20	1.33 x 10^{-5} s^{-1}	4.43 x 10^{-4} s^{-1}M^{-1}		
1	300	25	2.04 x 10^{-5} s^{-1}	6.81 x 10^{-4} s^{-1}M^{-1}	52 ± 1	-121 ± 4
1	300	30	2.87 x 10^{-5} s^{-1}	9.57 x 10^{-4} s^{-1}M^{-1}		
1	300	35	4.15 x 10^{-5} s^{-1}	13.83 x 10^{-4} s^{-1}M^{-1}		

Table 6.5 continued from the previous page.

			k_{obs}^0 (Ms^{-1})	k_0(s^{-1})		
0.04	100	15	1.31 x 10^{-8} Ms^{-1}	1.31 x 10^{-7} s^{-1}		
0.04	100	20	2.63 x 10^{-8} Ms^{-1}	2.63 x 10^{-7} s^{-1}	84 ± 3	-103 ± 12
0.04	100	25	4.73 x 10^{-8} Ms^{-1}	4.73 x 10^{-7} s^{-1}		
0.04	100	30	7.87 x 10^{-8} Ms^{-1}	7.87 x 10^{-7} s^{-1}		

For both concentration ranges of $[PtCl_4]^{2-}$ (1 mM and 0.04 mM) the oxidation rate increases with an increase in temperature, while no change in reaction order is observed. All k_{obs} and k_{obs}^0 values were used to determine the activation parameters from the Eyring equation[23] by plotting $\ln(k/T)$ *versus* $1/T$ in the temperature range 15-35ºC (values of T were converted to Kelvin in the plot Figure 6.11).
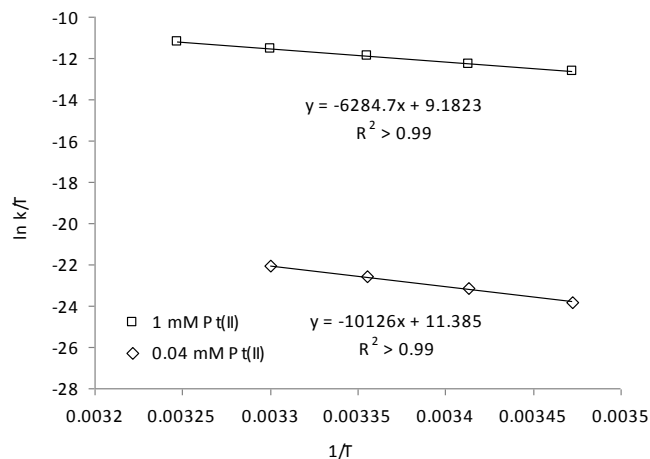
Figure 6.11: Plot of $\ln(k/T)$ *vs*. $1/T$ (values for k obtained from Table 6.5).

A linear correlation for both plots (1 mM and 0.04 mM $[PtCl_4]^{2-}$) is obtained as shown in Figure 6.11. The enthalpy of activation ($\Delta H^{\ddagger}$) was calculated from the slope by setting:

$$\text{Slope} = -\Delta H^{\ddagger}/R \qquad (6.9)$$

The entropy of activation ($\Delta S^{\ddagger}$) was calculated from the intercept by setting:

$$\text{Intercept} = \ln(k_B/h) + \Delta S^{\ddagger}/R \qquad (6.10)$$

Where k_B is Boltzmann's constant and h is Planck's constant. The calculated $\Delta H^{\ddagger}$ and $\Delta S^{\ddagger}$ values are listed in Table 6.5.

The activation enthalpy and entropy values calculated for the first- and zero-order reactions (Table 6.5) are comparable with previously reported[12] values for the oxidation of $[PtCl_4]^{2-}$ with H_2O_2 ($\Delta H^{\ddagger} = 76 \pm 3$ kJmol^{-1}, $\Delta S^{\ddagger} = -35 \pm 9$ JK^{-1}mol^{-1} in 1M HClO$_4$) and points to a similar mechanism.

6.3.4.5 Oxidation as a function of pressure: calculation of the activation volume

Standard kinetic investigation of a reaction involves the study of the dependence of the reaction rate on reactants concentration, pH, ionic strength, temperature and solvent composition. Assessment of only these parameters is often not sufficient to confidently assign the reaction mechanism. Pressure is one of the fundamental physical variables that influences the reaction rate and has become standard procedure to include in mechanistic studies.[23-26] The volume of activation $\Delta V^{\ddagger}$ is defined as the difference between the partial molar volumes of the transition state and the reactants and is related by equation 6.11.

$$[d(\ln k_{obs})/dP]_T = -\Delta V^{\ddagger}/RT \qquad (6.11)$$

The value of $\Delta V^{\ddagger}$ may be either positive or negative depending on whether applied pressure slows the reaction down ($\Delta V^{\ddagger} > 0$) or speeds it up ($\Delta V^{\ddagger} < 0$). Bond stretching as a result of a dissociative step will increase the partial molar volume (decrease in rate constant with increased pressure and a positive $\Delta V^{\ddagger}$ value). Bond formation on the other hand in an associative process will decrease the partial molar volume (increase in rate constant with increased pressure and a negative $\Delta V^{\ddagger}$ value). Electrostriction contributions during ion or dipole formation at the transition role may also have a significant contribution to the $\Delta V^{\ddagger}$ value. The measured $\Delta V^{\ddagger}$ value is therefore usually considered to be the combination of an intrinsic contribution from changes in internuclear distances within the reactants during the formation of the transition state, and from an electrostrictive contribution.

Oxidation of 1 mM $[PtCl_4]^{2-}$ with 15 mM H_2O_2 is slow, and produces a predominately first-order kinetic trace (Figure 6.12A). Oxidation of 0.04 mM $[PtCl_4]^{2-}$ with 100 mM H_2O_2 is relatively fast, and essentially a zero-order kinetic trace is obtained (Figure 6.12B). The

volumes of activation ($\Delta V^{\ddagger}$) were estimated for the first- and zero-order mechanisms by varying the pressure in repetitive oxidation experiments for both 0.04 mM and 100 mM $[PtCl_4]^{2-}$. The slow oxidation reactions (15 mM H_2O_2; oxidation > 6000 s) were measured with a Shimadzu UV-2010PC diode array spectrophotometer equipped with a high pressure cell that housed a capillary box quartz-cuvette in the pressure range 50-1500 ATM. The relative fast oxidation reactions (100 mM H_2O_2; oxidation < 300 s) were measured on a custom made high-pressure stopped-flow instrument[15] in the pressure range 100-1300 atm. The absorbance on the stopped-flow high pressure spectrophotometer is measured as a relative absorbance unit whereas the absorbance values measured on the Shimadzu UV-2010PC are absolute.

(A)   (B)
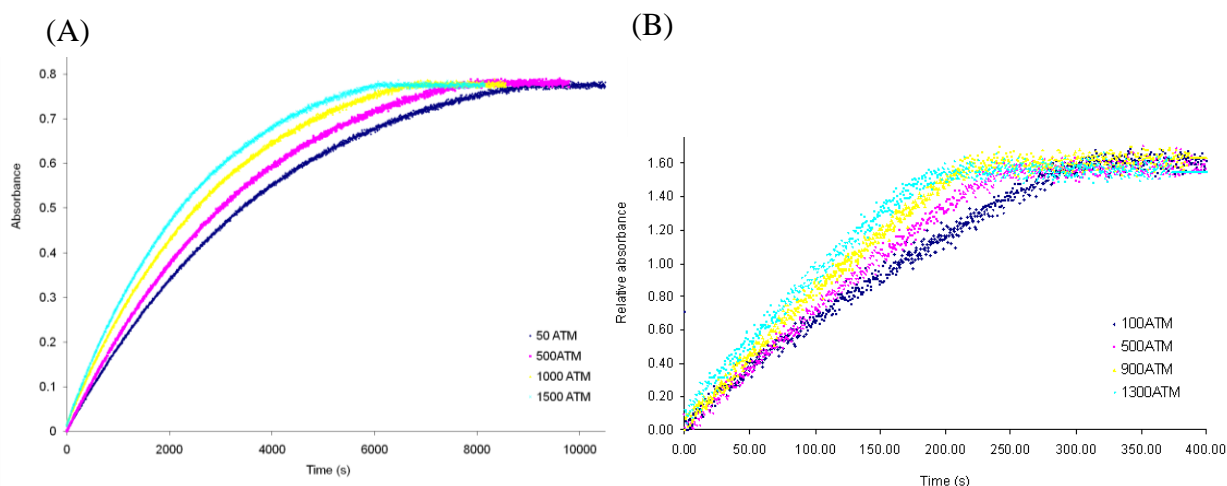
Figure 6.12: Rate dependence of oxidation of **(A)** 1 mM $[PtCl_4]^{2-}$ with 15 mM H_2O_2 in the pressure range 50-1500 atm (350 nm, 35°C) and oxidation of **(B)** 0.04 mM $[PtCl_4]^{2-}$ with 100 mM H_2O_2 in the pressure range 100-1300 atm (300 nm, 35°C).

The observed rate constants k_{obs} (Figure 6.12A) and k_{obs}^0 (Figure 6.12B) were determined from rate laws 6.2 and 6.5 respectively, as previously described for pseudo first- and zero-order mechanisms. The pseudo first- and zero-order rate constants k_1 and k_0 were subsequently derived from equations 6.3 and 6.6 and is listed in Table 6.6.

A plot of ln k_{obs} (Figure 6.12A) and ln k_{obs}^0 (Figure 6.12B) *versus* pressure (MPa) produce a linear correlation. Since $\Delta V^{\ddagger}$ is related to the observed rate constant (k_{obs} or k_{obs}^0) by equation 6.11,[26] the activation volume can be estimated from the slope of ln k_{obs} *versus* pressure (MPa) plot.

(A)

(B)
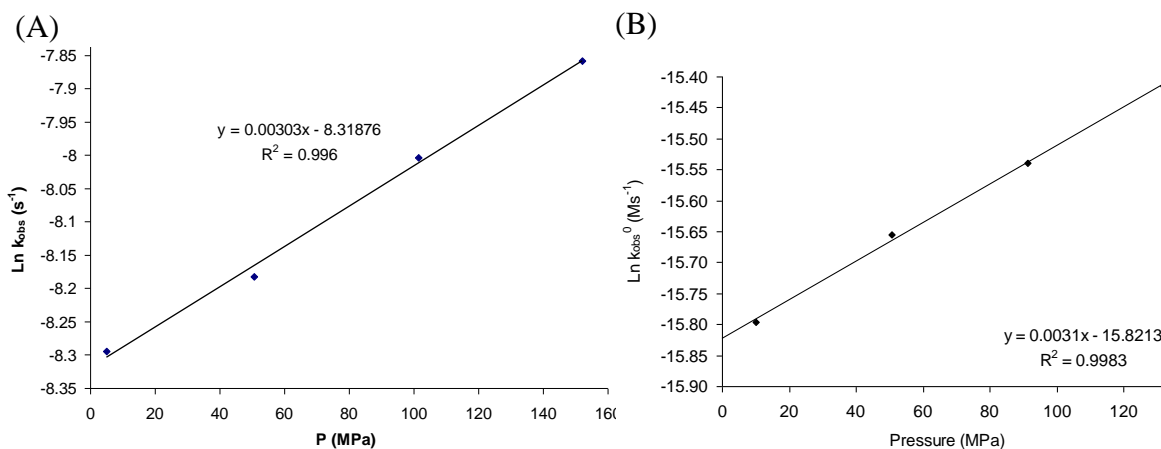
Figure 6.13: Plot of the **(A)** pseudo first-order rate constant (k_{obs}) and **(B)** pseudo zero-order rate constant (k_{obs}^0) as a function of pressure.

Table 6.6: Rate constants and activation volumes calculated for oxidation of 1 mM and 0.04 mM $[PtCl_4]^{2-}$.

$[PtCl_4]^{2-}$ (mM)	$[H_2O_2]$ (mM)	Pressure (MPa)	k_{obs} (s^{-1})	k_1 ($s^{-1}M^{-1}$)	$\Delta V^{\ddagger}$ ($cm^3 mol^{-1}$)
1	15	5	2.50×10^{-4} s^{-1}	1.67×10^{-2} $s^{-1}M^{-1}$	
1	15	51	2.79×10^{-4} s^{-1}	1.86×10^{-2} $s^{-1}M^{-1}$	-7.6 ± 0.4
1	15	101	3.34×10^{-4} s^{-1}	2.23×10^{-2} $s^{-1}M^{-1}$	
1	15	152	3.87×10^{-4} s^{-1}	2.58×10^{-2} $s^{-1}M^{-1}$	
			k_{obs}^0 (Ms^{-1})	k_0 (s^{-1})	
0.04	100	10	1.34×10^{-7} Ms^{-1}	1.34×10^{-6} s^{-1}	
0.04	100	51	1.60×10^{-7} Ms^{-1}	1.60×10^{-6} s^{-1}	-7.9 ± 1.9
0.04	100	91	1.83×10^{-7} Ms^{-1}	1.83×10^{-6} s^{-1}	
0.04	100	132	2.14×10^{-7} Ms^{-1}	2.14×10^{-6} s^{-1}	

A variable pressure kinetic study of the first-order (1 mM $[PtCl_4]^{2-}$) and zero-order mechanisms (0.04 mM $[PtCl_4]^{2-}$) obtained from oxidation with H_2O_2 has very similar activation volumes $\Delta V^{\ddagger} = -7.6 \pm 0.4$ $cm^3 mol^{-1}$; 1 mM $[PtCl_4]^{2-}$ and -7.9 ± 1.9 $cm^3 mol^{-1}$; 0.04 mM $[PtCl_4]^{2-}$ (Table 6.6). Negative $\Delta V^{\ddagger}$ values are typical for oxidative addition reactions i.e. bond formation, and indicates that oxidation takes place *via* a very similar compound.[23, 24]

6.3.5   Possible oxidation mechanism of tetrachloroplatinate(II) with hydrogen peroxide in hydrochloric acid

As previously mentioned, zero-order kinetics usually points towards an active catalytic species which rapidly increases the reaction rate, but is constantly regenerated. A first-order

oxidation rate dependences on both $[H^+]$ and $[Cl^-]$ were established in Figure 6.9, and the order of the reaction changes from first- to zero-order if the concentration of either is increased. Both acid and chloride plays a critical role in maintaining zero-order kinetics, whereas a high Pt(II) concentration inhibits it. Several possible reactions were considered which may produce oxidative species from hydrogen peroxide and hydrogen chloride. A zero-order mechanism may be envisaged by *i*) hydroxyl formation *via* hydrogen peroxide decomposition or *ii*) formation of oxidative species such as chlorine or hypochlorous acid. The mechanistic pathway is discussed in the context of formation of these species to account for the unusual kinetic results shown in section 5.3.4.

6.3.5.1 Possible oxidation via a hydroxyl radical mechanism

Oxidation of various metal complexes with hydrogen peroxide indicates the formation of hydroxyl radicals and successive two-step one-electron transfer reactions. However, both studies concerned with the oxidation mechanism of Pt(II) square-planar complexes indicate an one-step two-electron transfer mechanism.[10, 12] It was reported that oxidation of $[PtCl_4]^{2-}$ with peroxydisulfate $(S_2O_8^-)$ in hydrochloric acid produce linear absorption *versus* time plots and the reaction was found to be zero-order with respect to substrate.[12] The authors[12] proposed that the oxidation proceeds *via* a radical chain mechanism involving a rate-determining steady-state formation of a sulphate radical $(SO_4^-\cdot)$ and a hydroxyl radical $(\cdot OH)$ so that the overall reaction rate is independent of the substrate concentration. This proposal involves two subsequent one-electron oxidation steps and a Pt(III) intermediate.

Several aspects of the zero-order kinetics observed in this study, indicates that a similar two-step one-electron transfer reaction mechanism cannot account for the reaction kinetics observed here. Although the steady-state formation of hydroxyl radicals *via* H_2O_2 disproportionation may account for zero-order kinetics, H_2O_2 is not known to disproportionate spontaneously to form hydroxyl radicals in the way that $S_2O_8^-$ does. Hydroxyl radical formation *via* H_2O_2 reaction with HCl is not possible in these reaction conditions and cannot account for a change in reaction order, observed with an change in H_2O_2 or HCl concentrations. The rate of oxidation is much slower compared to most other

oxidation reactions that involves a hydroxyl radical (that originates from H_2O_2) and one-electron donating metal ion. Hydroxyl formation can be facilitated by a direct one-electron oxidation step of $[PtCl_4]^{2-}$, but if this is the case, the rate will be dependent on the substrate concentration and a zero-order reaction mechanism is not possible. As mentioned earlier, in all previous studies it was found that hydrogen peroxide oxidizes Pt(II) *via* an inner-sphere two-electron transfer mechanism and conclusive evidence was provided that there is bond formation between hydrogen peroxide oxygen and Pt(II), prior to electron (and oxygen) transfer.[8, 10] The activation enthalpy and entropy of $\Delta H^{\ddagger} = (52 \pm 1)$ kJmol^{-1} and $\Delta S^{\ddagger} = (-121 \pm 4)$ JK^{-1}mol^{-1} are also not in line with a disproportionation step but rather points towards an association step prior to electron transfer.

6.3.5.2 Oxidation of tetratchloroplatinate(II) via formation of hypochlorous acid and/or chlorine

The decomposition of hydrogen peroxide takes place spontaneously with time (but is very slow) to form molecular oxygen and water according to equation 6.12, and is extremely sensitive towards catalysis by various substances.[27]

$$2H_2O_2 \rightarrow 2H_2O + O_2 \qquad (6.12)$$
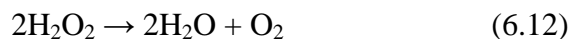
It is long since known, that in the presence of hydrochloric acid the rate of this process increases, since both protons and chlorides catalyzes the decomposition.[28] Catalytic decomposition of hydrogen peroxide in hydrochloric acid has been studied in detail and it was shown to decompose *via* an acid dependent (Equation 6.13) as well as an acid independent pathway (Equation 14).[28-31]

$$H_2O_2 + Cl^- + H^+ \rightleftharpoons HClO + H_2O \qquad (6.13)$$

$$H_2O_2 + Cl^- \rightarrow H_2O + ClO^- \qquad (6.14)$$
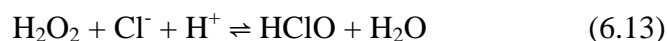
The general rate law 6.15 was established to define the rate of decomposition *via* both pathways 6.13 and 6.14:

$$-d[H_2O_2]/dt = k_1[H_2O_2][Cl^-][H^+] + k_1^0[H_2O_2][Cl^-] \qquad (6.15)$$

Reaction 6.14 is very slow and values of $k_1 = 4.1$ x 10^{-9} $M^{-1}s^{-1}$ (at 50°C with 0.438 M H_2O_2, at pH 6.4 (phosphate buffer) in 1.3 M chloride)[27] and 3.3 x 10^{-8} $M^{-1}s^{-1}$ (at 49.6°C, in 1 M chloride)[29] were determined in two separate studies. This equates to a drop of ~3.4% in the H_2O_2 concentration after 137 hours *via* reaction 6.14. In acidic solution especially, contributions towards hypochlorous acid formation *via* reaction 6.14 will be minimal so that the second term in reaction 6.15 can be neglected and the rate law is simplified to Equation 6.16:

$$-d[H_2O_2]/dt = k_1[H_2O_2][Cl^-][H^+] \qquad (6.16)$$

In this study, hydrogen peroxide and hydrochloric acid were always in excess with regards to $[PtCl_4]^{2-}$. Since, hypochlorous acid is a strong oxidant and rapidly oxidize $[PtCl_4]^{2-}$ quantitatively,[32] decomposition of hydrogen peroxide according to rate law 6.16 will appear to be in the steady-state. It is possible that hypochlorous acid is the oxidant and formation *via* reaction 6.13 the rate determining step.

The mechanism is however more complex due to equilibrium reaction 6.17. Hypochlorous acid may rapidly react with $[H^+]$ and $[Cl^-]$ to form chlorine, another possible oxidant that oxidizes $[PtCl_4]^{2-}$ quantitatively and rapidly.[29]

$$H^+ + Cl^- + HOCl \rightleftharpoons Cl_2 + H_2O \qquad (6.17)$$
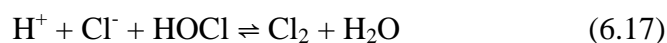
If formation of chlorine according to equilibrium reaction 6.17 and subsequent oxidation of $[PtCl_4]^{2-}$ with chlorine is significantly faster compared to $[PtCl_4]^{2-}$ oxidation with hypochlorous acid, chlorine must also be considered here as an oxidant. Reaction 6.13 therefore becomes the rate determining step, with hypochlorous acid as oxidant if $k_{HOCl}[PtCl_4^{2-}] \gg k[H_2O_2][Cl^-][H^+]$ and with chlorine as oxidant if the two conditions are fulfilled: 1) $k[HOCl][H^+][Cl^-] \gg k_{HOCl}[PtCl_4^{2-}]$ and 2) $k_{Cl2}[PtCl_4^{2-}] \gg k_{HOCl}[PtCl_4^{2-}]$. The rate constants of equilibrium reaction 6.17 and the oxidation rate of hypochlorous acid and chlorine with $[PtCl_4]^{2-}$ were evaluated to determine which of these pathways are possible.

The equilibrium[33, 34] and kinetics[35, 36] of reaction 6.17 were studied in detail over a range of experimental conditions and an equilibrium constant for chlorine hydrolysis of 3.27 x 10^{-4} M^2 at 25°C in a 1 M perchlorate solution was determined. Drougge *et al.*[35] studied equilibrium reaction 6.17 to determine if chlorine or hypochlorous acid is the oxidant of [Pt(CN)$_4$]$^{2-}$ in diluted chlorine solutions and calculated a rate constant 2.66 x 10^4 M^{-2}s^{-1} for chlorine formation. A reaction rate of 2.66 x 10^4 s^{-1} was re-calculated from the reaction conditions used in this study (1 M [H$^+$] and [Cl$^-$]) and is two orders of magnitude faster than the observed rate constants of 18-106 s^{-1} calculated for k$_{HOCl}$[PtCl$_4$$^{2-}$].[35] The equilibrium displacement HOCl $\rightarrow$ Cl$_2$ exceeds the oxidation of [PtCl$_4$]$^{2-}$ with hypochlorous acid in the reaction conditions used here and satisfy the first condition of k[HOCl][H$^+$][Cl$^-$] $\gg$ k$_{HOCl}$[PtCl$_4$$^{2-}$] for chlorine to act as the oxidant.

The oxidation of Pt(II) complexes with chlorine is generally rapid. Previous attempts to determine the oxidation rate of [PtCl$_4$]$^{2-}$ with chlorine have failed, partly due to the fast kinetics and equilibrium reaction 6.13.[14, 37] Preliminary experiments were carried out here to determine the oxidation rate of [PtCl$_4$]$^{2-}$ with chlorine. Problems were encountered with the calculation of a rate constant for oxidation with chlorine, so that accurate values could not be obtained. The results did indicate that the reaction is indeed rapid and was completed within the mixing time and beyond the time scale of the stopped-flow technique that was used. Nevertheless, it did establish that oxidation of [PtCl$_4$]$^{2-}$ with chlorine must be rapid and in the order of k$_{Cl2}$[PtCl$_4$$^{2-}$] > 1 x 10^5 M^{-1}s^{-1} (the detection limit) which is faster than the rate determined for oxidation with hypochlorous acid.[38] A considerable faster oxidation rate of chlorine compared to hypochlorous acid was also confirmed for [Pt(CN)$_4$]$^{2-}$, with second-order rate constant 97.7 M^{-1}s^{-1} for oxidation with HOCl and 1.08 x 10^7 M^{-1}s^{-1} for oxidation with Cl$_2$. These observations satisfy the second condition (k$_{Cl2}$[PtCl$_4$$^{2-}$] $\gg$ k$_{HOCl}$[PtCl$_4$$^{2-}$]) to allow oxidation with chlorine.

Chlorine may also react rapidly with hydrogen peroxide (reaction 6.18) to consume chlorine preventing oxidation of [PtCl$_4$]$^{2-}$.

$$Cl_2 + H_2O_2 \rightarrow 2H^+ + 2Cl^- + O_2 \qquad (6.18)$$

From these considerations, it is not possible to conclude whether hypochlorous acid or chlorine is the major oxidant. Evaluation of the oxidation product(s) may assist to assign the oxidation product. The oxidation product(s) is however complicated by $[PtCl_4]^{2-}$ assisted ligand exchange mechanisms, since $[PtCl_5(H_2O)]^-$ is converted to $[PtCl_6]^{2-}$ *via* $[PtCl_4]^{2-}$ association in hydrochloric acid solution. Elding and Gustafson[14] studied the kinetics of $[PtCl_4]^{2-}$ assisted chloride anation of $[PtCl_5(H_2O)]^-$ in 0.96 M HCl and confirmed that the rate of $[PtCl_6]^{2-}$ formation increases significantly. A rate constant of $(4.6 \pm 1) \times 10^{-4}$ s^{-1} was determined[14] for $[PtCl_6]^{2-}$ formation, which is comparable with the rates constants observed in this study.

From the final absorbance values it seems that at high $[PtCl_4]^{2-}$ concentration (0.2 - 1.0 mM; Table 6.2) the major product is $[PtCl_6]^{2-}$, whereas $[PtCl_5(H_2O)]^-$ is the major product for oxidation of lower concentrations $[PtCl_4]^{2-}$ (0.03-0.07 mM; Table 6.3). Conversion of $[PtCl_5(H_2O)]^-$ to $[PtCl_6]^{2-}$ is dependent on the $[PtCl_4]^{2-}$ concentration so that conversion of $[PtCl_5(H_2O)]^-$ to $[PtCl_6]^{2-}$ is more efficient in high concentrations of $[PtCl_4]^{2-}$. The first-order oxidation reactions are generally slower, and allow more time for ligand exchange to take place. Initial deviations from first-order kinetics may well be rationalized in terms of $[PtCl_4]^{2-}$ assisted ligand exchange. Hypochlorous acid must therefore account for oxidation of $[PtCl_4]^{2-}$ since $[PtCl_5(H_2O)]^-$ is formed as oxidation product in these reaction.

Irrespective of the oxidant, oxidation with both these species will be rapid in comparison to reaction 6.13. If catalytic formation of HOCl (or Cl_2) is true, the observed oxidation rate of the zero-order traces (Figure 6.8) should be similar to the reaction rate defined by rate law 6.16 at the same values for $[H_2O_2]$ and [HCl]. A rate constant of 12.4×10^{-5} $M^{-2}min^{-1}$ was reported for reaction 6.13 (at 32.9°C, with $[H_2O_2]$ = 0.8 M, $[Cl^-]$ = 3.0 M, $[H^+]$ = 7-26 mM) by Mohammad and Liebhafsky[29] and can be adjusted to 2.07×10^{-6} s^{-1} for comparison to the concentrations used in this study ($[Cl^-]$ = 1.0 M, $[H^+]$ = 1.0 M). This value is comparable with the values calculated in Table 6.3 for the observed zero-order oxidation rates and supports formation of catalytic quantities of HOCl (or Cl_2) at the steady-state.

6.3.5.3 Catalytic action of hypochlorous acid: balance between zero- and first-order kinetics

Different reaction orders are observed because two different oxidation pathways are operational. High concentrations of $[H_2O_2]$, $[H^+]$ and $[Cl^-]$ favors formation of hypochlorous acid that rapidly oxidizes $[PtCl_4]^{2-}$ so that the rate seems zero-order in $[PtCl_4]^{2-}$. In high concentrations of $[PtCl_4]^{2-}$ and low concentration of H_2O_2 the rate of hypochlorous acid formation is insufficient so that oxidation takes place mainly *via* H_2O_2 and the reaction is first-order with respect to $[PtCl_4]^{2-}$. Even in conditions that favor mainly one reaction order, evidence of the parallel reaction is seen. This is evident in the abrupt end-point of the pseudo first-order traces or the slight curvature in some of the zero-order traces. The small intercept in k_{obs} versus $[H^+]$ or $[Cl^-]$ plots (Figure 6.9) also suggests that the oxidation reaction occurs *via* two parallel pathways; only one of these depending on H^+ in the first case and only one pathway depends on Cl^- in the second. To account for both reaction pathways, the rate law is therefore expressed as the sum of Equation 6.3 and 6.6 in rate law 6.19:

$$-d[Pt(II)]/dt = k_0[H_2O_2] + k_1[Pt(II)][H_2O_2] \qquad (6.19)$$

To account for the first order dependence of H^+ and Cl^- in the zero-order reaction, rate law 6.19 is modified to 6.20:

$$-d[Pt(II)]/dt = (k_0[Cl^-][H^+] + k_1[Pt(II)])[H_2O_2] \qquad (6.20)$$

Where k_0 and k_1 can be estimated from Equations 2.21 and 2.22:

$$k_0 = k_{obs}{}^0[H_2O_2]^{-1}[Cl^-]^{-1}[H^+]^{-1} \qquad (6.21)$$
$$k_1 = k_{obs}[H_2O_2]^{-1} \qquad (6.22)$$

6.4   Conclusions

Light-induced reactions has a significant influence on the reaction order and oxidation rate of $[PtCl_4]^{2-}$ with H_2O_2 in HCl. This problem is addressed by measuring the oxidation rate at a single UV-visible wavelength. Oxidation of $[PtCl_4]^{2-}$ with hydrogen peroxide in HCl proceed *via* two parallel reaction pathways. In one pathway, the substrate is directly oxidized by H_2O_2, according to a pseudo first-order rate law, first-order with respect to [Pt(II)]. In the second pathway, the substrate is oxidized by HOCl which is formed in reaction $H_2O_2 + Cl^- + H^+ \leftrightharpoons HClO + H_2O$. Oxidation of $[PtCl_4]^{2-}$ with HOCl results in $[PtCl_5(H_2O)]^-$ and possibly some $[PtCl_6]^{2-}$. The $[PtCl_5(H_2O)]^-$ species is converted to $[PtCl_6]^{2-}$ by un-oxidized $[PtCl_4]^{2-}$ in a subsequent second reaction. The efficient conversion depends on high concentrations of $[PtCl_4]^{2-}$ so that conversion of $[PtCl_5(H_2O)]^-$ to $[PtCl_6]^{2-}$ is more efficient at higher Pt(II) concentration (0.2 - 1 mM; first-order reactions). The observed oxidation rate is defined by a two term rate law, one term first-order with respect to the substrate and a second term zero-order with respect to substrate. High Pt(II) concentration (≥ 0.2 mM) and low H_2O_2 concentration (≤ 300 mM) favour a first-order mechanism with pseudo-first order rate constant $k_1 = 1.52 \times 10^{-2}$ M^{-1}s^{-1} due to oxidation with H_2O_2. Low Pt(II) concentration (≤ 0.07 mM) and high H_2O_2 concentration (≥ 40 mM) favour a zero-order mechanism with pseudo-zero order rate constant $k_0 = (7.0 \pm 0.8) \times 10^{-7}$ s^{-1} due to the catalytic steady-state formation of HOCl. Oxidation of $[PtCl_4]^{2-}$ with HOCl is rapid compared to oxidation with H_2O_2, so that HOCl formation is the rate determining step and the reaction appear zero-order with respect to Pt(II).

The results indicate that both H_2O_2 and HOCl oxidize $[PtCl_4]^{2-}$ *via* an inner sphere one-step two electron transfer mechanism. Since it is known that square-planar Pt(II) complexes have a vacant coordination site in the axial plane, formation of an inner-sphere complex (i.e. bond-formation) prior to electron transfer seems reasonable. The positive $\Delta H^{\ddagger}$ and negative $\Delta S^{\ddagger}$ values support the idea of bond formation prior to electron transfer for oxidation with both H_2O_2 and HOCl. The negative $\Delta V^{\ddagger}$ values obtained here are typical for such bond formation processes in Pt(II) complexes, and indicate the activated intermediate is very similar, which is reasonable for oxidation with H_2O_2 and HOCl. A schematic

diagram that illustrates the parallel oxidation mechanisms proposed here is shown in Figure 6.14.
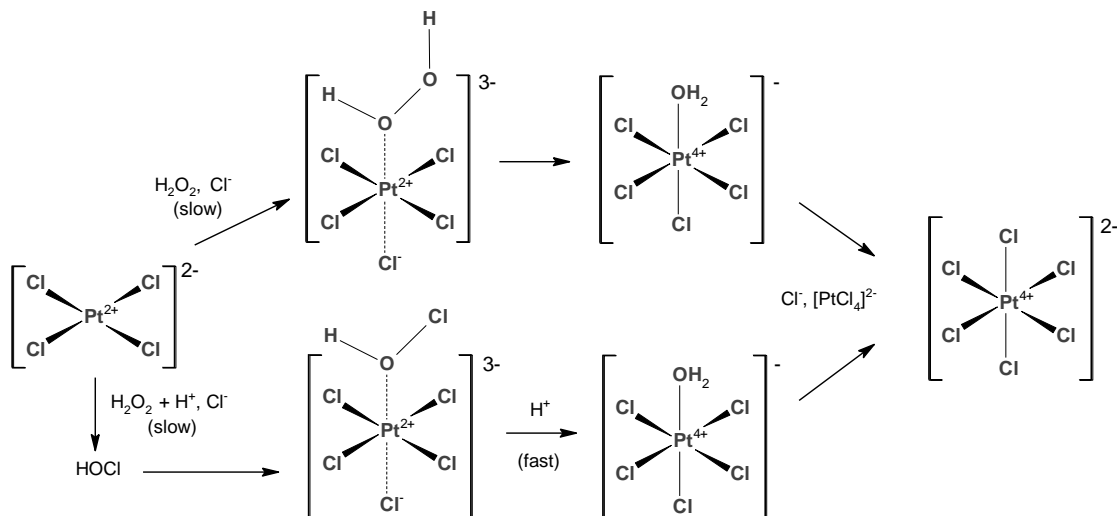

Figure 6.14: Schematic illustration of the parallel oxidation mechanism of $[PtCl_4]^{2-}$ with H_2O_2 in 1 M HCl hydrochloric acid. Hypochlorous acid is formed in a reaction between H_2O_2 and HCl, resulting in the zero-order mechanism.

Similar 'catalytic' side reactions are evident in the oxidation of $[PtCl_4]^{2-}$ with $NaClO_3$ and $NaBrO_3$ in sufficient concentrations of hydrochloric acid (1 M). Preliminary kinetic studies confirmed zero-order kinetics for oxidation of $[PtCl_4]^{2-}$ with ClO_3^- in hydrochloric acid, probably as a result of the steady-state formation of Cl_2 (or other oxidants) that rapidly oxidizes Pt(II). The parallel oxidation mechanism as discussed here for oxidation of $[PtCl_4]^{2-}$ with H_2O_2 has not been reported for the oxidation of other Pt(II) complexes, and is fundamental in the understanding of oxidation of $[PtCl_4]^{2-}$ with $NaClO_3$ and $NaBrO_3$.

6.5   References

1.   B. Rosenberg, L. Van Camp, T. Krigas, *Nature,* 1965, *205*, 698-699.

2.   Y. Jung, S. J. Lippard, *Chem. Rev.,* 2007, *107*, 1387-1407.

3.   J. K. Burdett, T. A. Albright, *Inorg. Chem.,* 1979, *18*, 2112-2120.

4.   J. K. Burdett, *Inorg. Chem.,* 1977, *16*, 3013-3025.

5.   K. M. Anderson, A. G. Orpen, *Chem. Commun.,* 2001, 2682-2683.

6.   L. G. Vanquickenborne, J. Vranckx, C. Goeller-Walrand, *J. Am. Chem. Soc.,* 1974, *96*, 4121-4125.

7.   C. Muhle, E.-M. Peters, M. Jansen, *Z. Naturforsch,* 2009, *64b*, 111-115.

8.   S. O. Dunham, R. D. Larsen, E. H. Abbott, *Inorg. Chem.,* 1993, *32*, 2049-2055.

9.   O. Groning, L. I. Elding, *Inorg. Chem.,* 1989, *28*, 3366-3372.

10.   T. D. Harrigan, R. C. Johnson, *Inorg. Chem.,* 1977, *16*, 1741-1744.

11.   S. Al-Baker, J. C. Dabrowiak, *Inorg. Chem.,* 1987, *26*, 613-617.

12.   K. Hindmarsh, D. A. House, R. van Eldik, *Inorg. Chim. Acta,* 1998, *278*, 32-42.

13.   W. R. Mason, *Coord. Chem. Rev.,* 1972, *7*, 241-255.

14.   L. I. Elding, L. Gustafson, *Inorg. Chim. Acta,* 1976, *19*, 31-38.

15.   R. Van Eldik, W. Gaede, S. Wieland, J. Kraft, M. Spitzer, D. A. Palmer, *Rev. Sci. Instrum.,* 1993, *64*, 1355-1357.

16.   L. I. Elding, *Inorg. Chim. Acta,* 1978, *28*, 255-262.

17.   L. I. Elding, L. F. Olsson, *J. Phys. Chem.,* 1978, *82*, 69-74.

18.   L. E. Cox, D. G. Peters, E. L. Wehry, *J. Inorg. Nucl. Chem.,* 1972, *34*, 297-305.

19.   L. E. Cox, D. G. Peters, *Inorg. Chem.,* 1970, *9*, 1927-1930.

20.   C. K. Jorgensen, *Acta Chem. Scand.,* 1956, *10*, 518-534.

21.   R. L. Rich, H. Taube, *J. Am. Chem. Soc.,* 1954, *76*, 2608-2611.

22.   T. M. Buslaeva, S. A. Simanova, *Russ. J. Coord. Chem.,* 1999, *25*, 151-161.

23.   R. Van Eldik, T. Asano, W. J. Le Noble, *Chem. Rev.,* 1989, *89*, 549-688.

24.   A. E. Merbach, *Pure Appl. Chem.,* 1987, *59*, 161-172.

25.   T. Asano, W. J. Le Noble, *Chem. Rev.,* 1978, *78*, 407-489.

26.   A. Drljaca, C. D. Hubbard, R. Van Eldik, T. Asano, M. V. Basilevsky, W. J. Le Noble, *Chem. Rev.,* 1998, *98*, 2167-2289.

27.   D. F. Evans, M. W. Upton, *Dalton Trans.: Inorg. Chem.,* 1985, 2525-2529.

28.   R. S. Livingston, W. C. Bray, *J. Am. Chem. Soc.,* 1925, 47, 2069-2082.

29.   A. Mohammad, H. A. Liebhafsky, *J. Am. Chem. Soc.,* 1934, *56*, 1680-1685.

30.   E. A. Budge, *J. Am. Chem. Soc.,* 1932, 54, 1769-1778.

31.   C. Bender, H.-D. Brauer, *Perkin Trans. 2,* 1999, 2579-2587.

32.   J. O. Edwards, *Peroxide Reaction Mechanisms*, Interscience, New York, 1962.

33.   G. Zimmerman, F. C. Strong, *J. Am. Chem. Soc.,* 1957, *79*, 2063-2066.

34.   R. E. Connick, Y.-T. Chia, *J. Am. Chem. Soc.,* 1959, *81*, 1280-1284.

35.   L. Drougge, L. I. Elding, *Inorg. Chem.,* 1985, *24*, 2292-2297.

36.   M. Eigen, P. Matthies, *Chem. Ber.,* 1961, *94*, 3309-3317.

37.   M. M. Jones, K. A. Morgan, *J. Inorg. Nucl. Chem.,* 1972, *34*, 259-274.

38.   L. I. Elding, L. Gustafson, *Inorg. Chim. Acta,* 1976, *19*, 165-171.